High-Capacity Multicarrier Electro-Optical Transceivers based on Analogue Signal Processing

Fernando A. Gutiérrez Uruñuela

B.Eng., M.Eng.

A Dissertation submitted in fulfilment of the
requirements for the award of
Doctor of Philosophy (Ph.D.)
to the

Dublin City University

Faculty of Engineering and Computing

School of Electronic Engineering

Principal Supervisor: Prof. Liam Barry

Secondary Internal: Dr. Philip Perry

Secondary External: Prof. Andrew Ellis (Aston University, UK)

September 2016

Declaration

I hereby certify that this material, which I now submit for assessment on the programme of study leading to the award of Doctor of Philosophy is entirely my own work, and that I have exercised reasonable care to ensure that the work is original, and does not to the best of my knowledge breach any law of copyright, and has not been taken from the work of others save and to the extent that such work has been cited and acknowledged within the text of my work.

Signed: Fernando A. Gutiérrez Uruñuela
ID No.: 12211206
Date: 08/09/2016

To my parents, Fernando and Teresa,
for their sacrifice to make my life so easy.

To my wife, Bárbara,
for her support and patience.

A mis padres, Fernando y Teresa,
por su sacrificio para hacer mi vida tan fácil.

A mi mujer, Bárbara,
por su apoyo y paciencia.

Acknowledgements

I would like to thank my supervisor Prof. Liam Barry both for the faith he showed in me by accepting me as his student and for the continual support, guidance and encouragement. I am also grateful to my co-supervisors, Dr. Philip Perry and Prof. Andrew Ellis, for their help and guidance and for their willingness to discuss new ideas at any time.

Additionally, I would also like to acknowledge the enormous help I received from my past and present colleagues at DCU. In particular I am grateful to the following: Eamonn, for his continuous support, especially at the latest stages of my research; Desi, Arsalan, Colm, and Vidak for their help, advice, and friendship; Prince and Sean, for encouraging me and for his generosity with their time; Frank, for his work in the project and his guidance at my early stages at DCU; and Rui, Aravind, Tam, Regan, Tong, Sepideh and Anthony, for inspiring conversations.

Lastly, I would like to thank Dublin City University, Science Foundation Ireland and Enterprise Ireland, for the generous financial support.

Table of Contents

List of Acronyms

ADC	Analogue to Digital Converter
ADSL	Asymmetric Digital Subscriber Line
APD	Avalanche Photo-Diode
ASE	Amplified Spontaneous Emission
ASP	Analogue Signal Processing
ATM	Asynchronous Transfer Mode
BER	Bit Error Rate
BERT	Bit Error Rate Tester
BPF	Bandpass Filter
BPSK	Binary Phase Shift Keying
BTB	Back to Back
CAD	Computer Aided Design
CATV	Cable Television
CNR	Carrier to Noise Ratio
CPRI	Common Public Radio Interface
CPU	Central Processing Units
CSO	Composite Second Order
CSPR	Carrier to Signal Power Ratio
CTB	Composite Triple Beat
DAC	Digital to Analogue Converter
DCF	Dispersion Compensating Fibre
DD	Direct Detection
DD-MZM	Dual-Drive MZM
DFB	Distributed Feedback Laser
DSP	Digital Signal Processing
EAM	Electro-Absorption Modulator
ECL	External Cavity Laser
EDFA	Erbium-Doped Fibre Amplifier
EML	Externally Modulated Laser
ER	Extinction Ratio
FDM	Frequency Division Multiplexing
FEC	Forward Error Correction
FFT	Fast Fourier Transform
FIR	Finite Impulse Response
FPGA	Field Programmable Gate Arrays
FSR	Free Spectral Range
FWM	Four-Wave Mixing
GSL	Gain Switched Laser

HD	Harmonic Distortion
HDTV	High Definition Television
HFC	Hybrid Fibre Coaxial
HT	Hilbert Transform
ICI	Inter Channel interference
IF	Intermedium Frequency
IFFT	Inverse Fast Fourier Transform
IM	Intensity Modulation
IM/DD	Intensity Modulation / Direct Detection
IMD	Intermodulation Distortion
IMP	Intermodulation Products
IP	Internet Protocol
IQ	In-phase Quadrature
ISI	Inter Symbol Interference
ITU	International Telecommunication Union
LAN	Local Area Networks
LED	Light Emitting Diode
LO	Local Oscillator
LPF	Low Pass Filter
MAN	Metropolitan Area Networks
MLL	Mode Locked Lasers
MMF	Multi-Mode Fibres
MMIC	Monolithic Microwave Integrated Circuit
MZM	Mach-Zehnder Modulators
NF	Noise Figure
NIC	Network Interface Card
NLD	Non Linear Distortion
NRZ	Non Return to Zero
ODSB	Optical Double Side Band
OFC	Optical Frequency Comb
OFDM	Orthogonal Frequency Division Multiplexing
OIQM	Optical IQ Modulator
OMI	Optical Modulation Index
OPLL	Optical Phase Locked Loops
OSCM	Orthogonal Subcarrier Multiplexing
OSSB	Optical Single Side Band
OTDM	Optical Time Division Multiplexing
OTN	Optical Transport Networks
PAM	Pulse Amplitude Modulated
PAPR	Peak to Average Power Ratio

PCB	Printed Circuit Board
PCIe	Peripheral Component Interconnect Express
PDM	Polarization Division Multiplexing
PMD	Polarization Mode Dispersion
POTS	Plain Old Telephone Service
PRBS	Pseudo Random Binary Sequence
QAM	Quadrature Amplitude Modulation
RAN	Radio Access Network
RC	Raised Cosine
RE	Radio Equipment
REC	Radio Equipment Control
RF	Radio Frequency
RIN	Relative Intensity Noise
RMS	Root Mean Square
SCM	Subcarrier Multiplexing
SDH	Synchronous Digital Hierarchy
SMF	Single Mode Fibre
SNR	Signal to Noise Ratio
SOA	Semiconductor Optical Amplifier
SONET	Synchronous Optical Networking
SPM	Self-Phase Modulation
SRD	Step Recovery Diode
SRRC	Square Root Raised Cosine
SSMF	Standard Single Mode Fibre
SSR	Sideband Suppression Ratio
TDM	Time Division Multiplexing
TIA	Trans-Impedance Amplifier
VCSEL	Vertical Cavity Surface Emitting Laser
VOA	Variable Optical Attenuator
WDM	Wavelength Division Multiplexing
XPM	Cross-Phase Modulation

List of Figures

List of Tables

Abstract

High-Capacity Multicarrier Electro-Optical Transceivers based on Analogue Signal Processing.

Fernando A. Gutiérrez

Currently, the proliferation of services and applications based on the cloud and the Internet are translating into increasing demand for capacity in data networks. Optical Communications is the only technical field that can address this issue by providing higher performance electro-optical transceivers with enhanced spectral efficiency, power consumption and latency. Many research and implementation efforts are focusing on multicarrier solutions, often referred to as subcarrier multiplexing (SCM), as they are more tolerant to dispersion and allow a higher modulation order per subchannel.

In recent years, the most widespread trend has developed SCM subsystems based on digital signal processing (DSP). They can achieve high spectral efficiencies with complicated algorithms, but also present an important drawback: intensive DSP brings about unwanted high-power consumption and high latency. An alternative consists of developing SCM systems based on analogue signal processing (ASP) as it potentially achieves lower power consumptions and lower latencies.

Several advances on the state of the art of ASP based SCM systems are provided in this thesis. Firstly, the implementation of broadband SCM systems based on optical IQ modulators is thoroughly analysed. These optical modulators achieve simultaneously two important features: direct colourless generation of optical single side band signals (OSSB) and partial optical carrier suppression. These features translate into higher tolerance to dispersion and better sensitivities in the receiver. Secondly, the colourless generation of OSSB signals is leveraged to develop SCM systems consisting of several tightly allocated optical channels. This implementation gives rise to low-cost spectrally-efficient wavelength division multiplexing (WDM) configurations. Thirdly, the main weakness of ASP based SCM systems is overcome. These systems have typically consisted of separated subchannels. It is demonstrated that orthogonally overlapping broadband subchannels can be modulated and demodulated without requiring DSP. The concept is proven in real-time all-analogue SCM and WDM/SCM implementations.

Introduction

Optical communications overcame the limited data rates of electrical systems and made possible the development of the Internet. Currently, all high-capacity networks employ optical systems regardless of their reach and purpose. The devices that carry out the interface between the electrical and optical domains are called electro-optical transceivers. These key components can adopt a number of forms and characteristics depending on the network where they are deployed. The signals, modulations, and processing techniques that they employ, must be carefully selected to meet the requirements of a given subsystem.

The search for solutions based on all-optical signal processing is an active research topic, and some promising techniques like coherent WDM or all-optical OFDM have been demonstrated. However, they rely on complicated implementations with optical components and, consequently, remain as important research topics but still impractical for real deployment. Instead, commercial and practical applications support optical signal generation and detection with electrical signal processing, which can be accomplished with more mature and reliable components. Potentially, the next revolution in the area will rely on the introduction of low-cost optical modulators based on silicon photonics and its combination with mature electronic circuits and processing.

The transmission of multicarrier electrical signals in optical communication links presents several advantages. Firstly, the baseband data rates are lower, reducing the complexity of the electronic circuits in the electrical interfaces. Secondly, due to the narrower subchannels, the overall electro-optical solution is more tolerant to fibre dispersion. Finally, higher modulation orders can be applied in every subchannel increasing the spectral efficiency. The transmission of a multicarrier frequency division multiplexing (FDM) signal in an optical link is referred to as subcarrier multiplexing (SCM). Multiple SCM signals at different optical carriers can also be combined in a wavelength division multiplexing (WDM) optical signal.

SCM can be implemented with digital signal processing (DSP) and with analogue signal processing (ASP). While DSP based techniques provide unique possibilities, their higher power consumption and latency make them prohibitive in some subsystems. Apart from that, when very high-speed processing is required,

analogue to digital converters (ADC) and digital to analogue converters (DAC) are unavoidably expensive. For that reason, research on ASP based systems is necessary in order to exploit the possibilities of low power consumption and low latency processing. Moreover, the development and generalization of monolithic microwave integrated circuit (MMIC) technology currently provides low-cost integrated circuits at microwave frequencies, which reduces drastically the cost of high-speed ASP.

This thesis focuses on ASP based SCM broadband electro-optical transceivers, as they present low cost, high tolerance to dispersion, and real possibilities of spreading the range of applications where they are deployed. All the experiments were conducted emphasizing the feasibility of the proposed solutions. Modern current research often relies on offline processing. It assumes that the desired components can be potentially implemented and can then perform all the processing at the desired speeds. In contrast, this thesis shows experiments running in real-time and, more importantly, relying largely on off-the-shelf components.

Main Contributions

Several key advances in the state of the art were accomplished and are presented in this document:

- A real-time all-analogue SCM electro-optical transceiver, consisting of five broadband subchannels and largely based on MMIC technology, was physically implemented. The setup was employed to experimentally demonstrate all the key contributions studied in the thesis.

- The theory of direct detection SCM links transmitting optical single side band (OSSB) signals is extended for the particular case of optical IQ modulators (OIQM). Unlike other optical modulators, OIQMs achieve simultaneously OSSB generation and partial optical carrier suppression. The complicated trade-off between the nonlinearities generated by the modulator at different bias points and the sensitivity of the system is thoroughly analysed. For any frequency plan, the developed mathematical model can predict the optimum bias point and the best achievable sensitivities for every subchannel. The mathematical model is supported by experimental measurements.

- A WDM/SCM scheme based on OSSB signals is presented. It is shown that a cost and spectrally efficient implementation, consisting of tightly allocated optical channels, is possible with a state of the art OIQM without requiring optical filters in the transmitter. A penalty can occur due to the imperfectly suppressed sideband of the adjacent optical channel.

- The main weakness of traditional all-analogue SCM systems is the spectral efficiency. This thesis theoretically and experimentally demonstrates that this weakness can be overcome by transmitting orthogonally overlapping broadband subchannels. The pulse shaping and demodulation of the broadband baseband signals is accomplished with microwave filters. Mathematical and simulation strategies are provided to predict the behaviour and obtain appropriate microwave orthogonality filters. The technique is referred to as orthogonal subcarrier multiplexing (OSCM) and, due to the multiplexing of orthogonal subchannels, can potentially double the spectral efficiency of traditional all-analogue SCM links.

- A novel technique that achieves subcarrier synchronization employing a lower number of components than previous solutions is demonstrated. The concept can be applied to SCM and OSCM links in which the subcarriers are located at harmonics of the data rate.

- Experimental real-time WDM/OSCM links are presented. Due to the orthogonal subchannels, they achieve substantially higher spectral efficiencies than previous solutions. The experiments make use of optical frequency combs (OFC), based on gain switched lasers (GSL) and mode-locked lasers (MLL), which allow a tighter allocation of optical channels and also enhance the cost efficiency of the implementation. High capacities of up to 400 Gbit/s are obtained.

Thesis Structure

The thesis is structured as follows:

- Chapter 1 provides a general review of optical communications developing on the main concepts that will be employed in the rest of the document. The main focuses are electro-optical transceivers and the key properties that arise due to the different implementation options.

- Chapter 2 discusses SCM from the basics and details the implementation of an all-analogue SCM electro-optical transceiver based on an OIQM and off-the-shelf components. The key electrical components, namely the microwave off-the-shelf IQ mixers, are characterised.

- Chapter 3 develops a theoretical and experimental analysis of the trade-off between carrier suppression and nonlinearities induced by optical IQ modulators in direct-detection subcarrier multiplexing systems. The trade-off is obtained by examining the influence of the bias conditions of the modulator on the transmitted OSSB signal.

- Chapter 4 discusses the implementation of a cost and spectrally efficient WDM/SCM link based on a state-of-the-art OIQM. Tightly allocated OSSB channels are multiplexed without employing optical filters in the transmitter and the penalty associated with the imperfectly suppressed sideband of the adjacent channel is measured.

- Chapter 5 discusses theoretically and experimentally the development of microwave OSCM links consisting of orthogonally overlapping subchannels and based on filter bank multicarrier (FBMC) theory. The implementation of microwave FBMC schemes employing custom and standard filters is analysed. Apart from that, a novel technique for the synchronization of receiver subcarriers in SCM systems is provided.

- Chapter 6 shows experimental implementations that emulate WDM/OSCM links where the optical carriers are obtained with different types of OFCs, namely GSLs and MLLs.

- Chapter 7 provides a brief summary of conclusions which can be drawn from the results presented in this thesis. The potential for future work in the areas discussed throughout the thesis is also outlined.

- Appendix A shows the schematics of a printed circuit board that was developed to distribute the local oscillators necessary in the SCM experiments.

- Appendix B presents the mathematical developments that were used to obtain the frequency components in the electric field and the associated photocurrent at the output of the OIQM.

- Appendix C outlines the mathematics used to demonstrate a simplified technique to achieve the orthogonal phase alignment in a microwave FBMC transmission system.

- Appendix D lists the publications arising from this work.

Chapter 1

1 Optical Communications

Communication is an essential element in our social, cultural and technical evolution. Especially over recent decades, human habits and technology have influenced each other, but always relying on a growing exchange of information. Optical communications have enabled this development and have become the only mature technology that can satisfy the demand of capacity in wired communication links.

This chapter provides an introduction to optical communications following a high-to-low level perspective. Firstly, the relevance of optical communications is addressed comparing with other technologies and in terms of overall capacity. Secondly, the most widespread topologies in optical networks are presented. Finally, the most common physical devices that make optical networks feasible are described, explaining more deeply the elements and concepts over which the following chapters will build up new technical advances.

1.1 Relevance of Optical Communications

This section shows that the introduction of optical devices marked an inflexion point in the performance of communication links. The trends in the capacity of optical networks are also illustrated.

1.1.1 Bit Rate – Distance Product

The Bit Rate – Distance product is a figure of merit of any digital communication link. It is equal to $B{\cdot}L$ where B is the bit rate and L is the repeater spacing. Figure 1.1 illustrates the evolution of this value in deployed links along the period extending from 1850 to 2000 [1]. It can be observed that the value increased exponentially through the introduction of emerging technologies. During the last decades, optical devices have made possible the latest revolutions in the field.

In the 1950s it was theoretically known that the $B{\cdot}L$ product could be increased by several orders of magnitude employing optical waves as carriers [1]. However, suitable sources of lightwaves and a transmission medium were not

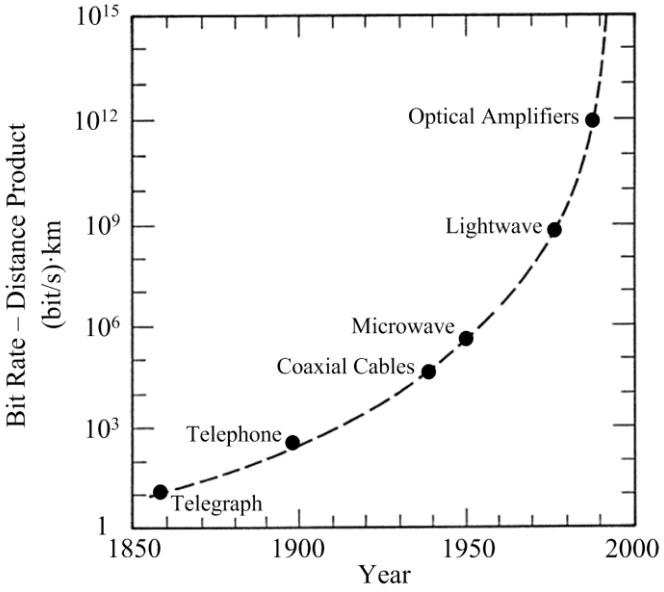

Figure 1.1 Increase of the Bit Rate - Distance product from 1850 to 2000 [1].

available. In 1960, the demonstration of the first functional laser [2] solved the first problem, and, in 1966, optical fibre was proposed as the best choice for guiding light [3]. Those were the first steps that led to the development of modern optical communications. The subsequent breakthroughs proved the feasibility of optical systems. In 1970, semiconductor lasers operating continuously at room temperature were demonstrated [4]. Simultaneously, fibre losses were reduced below 20 dB/km at wavelengths ≈1μm [5]. The first commercial optical links were finally available in 1980 [6], and transmitted 45 Mbit/s at 0.8 μm with a repeater spacing of up to 10 km. The next efforts focused on transmitting at wavelengths ≈1.3 μm, where optical fibre presented losses below 1 dB/km and minimum dispersion. In 1981, such systems were able to transmit 2 Gbit/s over 44 km [7] and, in 1987, similar schemes became commercially available [1]. The subsequent steps attempted to use wavelengths around 1.55 μm, where fibre losses are lower, namely 0.2 dB/km [8]. The introduction of these systems was delayed because fibre dispersion at 1.55 μm was higher. Two compatible solutions were proposed: dispersion shifted fibres and lasers capable of emitting only one longitudinal mode. In 1985, laboratory experiments showed rates of up to 4 Gbit/s over 100 km of fibre [9], but this technology did not become commercially available until 1990 [1].

The next revolution occurred during the 1990s with the advent of optical amplifiers, as it can be observed in Figure 1.1. These devices avoid the necessity of electronic repeaters. In 1991, an experiment demonstrated the transmission of 5 Gbit/s over 14.300 km [10]. By 1995, these systems became commercially available

and were implemented in transoceanic links [11]. Simultaneously, a technique defined as Wavelength Division Multiplexing (WDM) substantially multiplied the achievable capacity. WDM consists of transmitting a number of optical channels in the same optical fibre, each one carried by a different wavelength. Combining these breakthroughs, optical amplifiers and WDM, the *B·L* products increased drastically. In 2001, 300 optical channels operating individually at 11.6 Gbit/s were transmitted over 7380 km [12], resulting in a *B·L* product of more than 25000 (Tb/s)·km.

During the last 15 years, efforts have been focused on the implementation of spectrally efficient modulation formats that can increase the data rate per optical channel. Firstly, traditional modulation schemes were employed using multilevel configurations [13]. Later, more sophisticated modulations, like Orthogonal Frequency Division Multiplexing (OFDM), were proposed [14, 15]. Finally, coherent systems were implemented to reach longer transmission distances. Coherent transmission modulates the phase of the optical carrier reducing the average power of the signal [1]. Lower sensitivities and longer transmission distances are achieved at the expense of requiring complex and expensive receivers [16]. Coherent schemes were well known since the 1980s [16], but they have only become a requisite to increase the *B·L* product in the last decade, as it can be observed in Figure 1.2, taken from [17]. Figure 1.2 shows the evolution of the *B·L* product obtained in optical communication experiments since 1983 [17], classifying them according to the implemented technique: single wavelength, single wavelength with Optical Time Division Multiplexing (OTDM), WDM, OFDM and coherent detection. As an

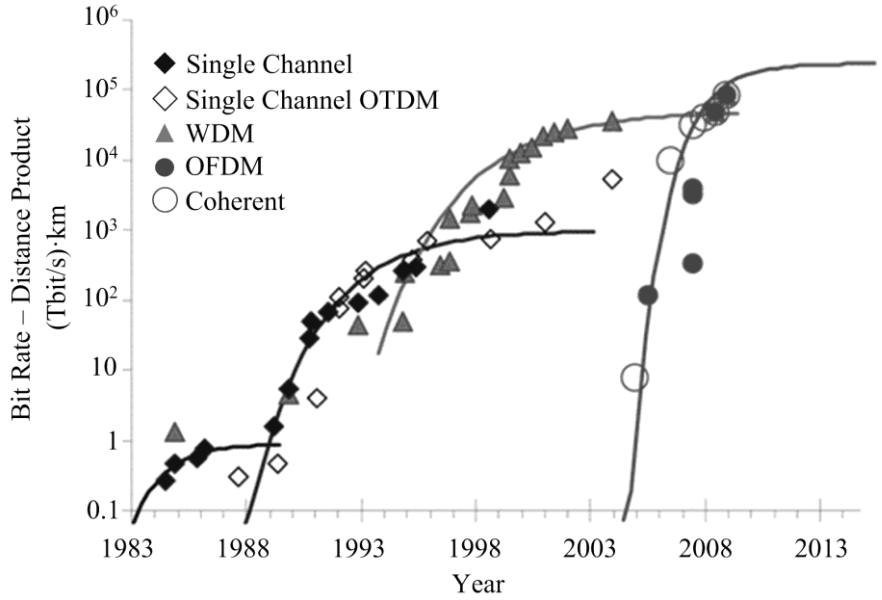

Figure 1.2. Evolution of *B·L* product in optical communication links [17].

example, in 2009, a WDM coherent OFDM experiment achieved a $B{\cdot}L$ product of ≈85000 (Tb/s)·km [18]. Currently, the $B{\cdot}L$ product can be increased beyond 10^6 (Tbit/s)·km by using multicore fibres [19].

1.1.2 Worldwide Data Traffic

The introduction of the Internet and its growth during the last decades [20] brought about the necessity of implementing high speed data networks [21]. To satisfy the ever-increasing demand of capacity, multidisciplinary advances were required in many technical fields like materials, electronics and communications. However, as explained in section 1.1.1, lightwave transmission was and continues to be the only technology that can satisfy the demand of data traffic.

An estimation and forecast of the worldwide Internet Protocol (IP) data traffic since 1990 is illustrated in Figure 1.3, taken from the Cisco´s Virtual Networking Index [22]. During the 1990s Internet access popularised and IP data traffic at least doubled every year. More recently, modern and demanding services, like on-demand High Definition Television (HDTV), are increasing its popularity. World habits are changing towards a situation in which every device can potentially be connected to the Internet [23]. Consequently, the most recent forecasts claim that the increase of IP data traffic per year is around 23% [22]. Although this trend is less pronounced than in the past, some studies have concluded that, currently, the increment of data traffic tends to exceed the capacity of fibre communication systems [24]. While optical communications technology matures, it becomes more difficult to increase the $B{\cdot}L$ product, in line with [17] and Figure 1.2.

It can be concluded that the telecommunications industry is facing important

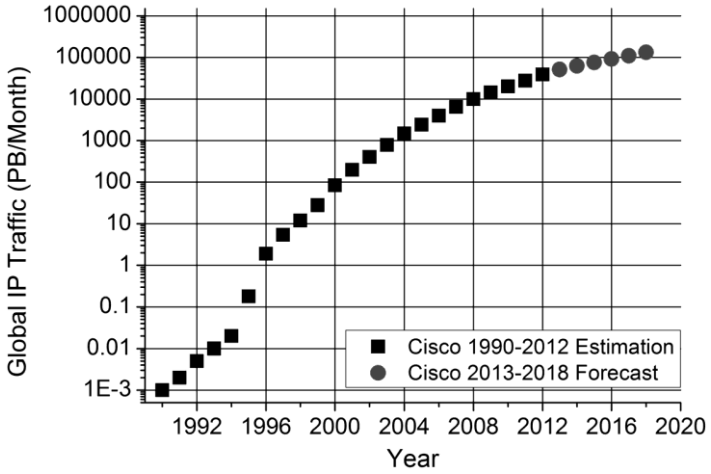

Figure 1.3 Global internet traffic growth for period 1990-2018 [22].

and significant challenges. Research and development of optical technologies is of vital importance to find functional solutions. It should be noted that data traffic must be processed at several stages giving rise to different types of optical networks, as it will be seen in the next section. At every level, the optimal optical transceivers are in reality determined by different parameters like cost, power consumption and/or latency. For example, in an expensive transoceanic link, the priority is to increase the $B{\cdot}L$ product at practically any cost. On the contrary, in a high performance data centre where multiple interfaces are necessary, low power consumption and latency are essential.

1.2 Optical Networks

This section provides a basic classification of optical networks. The overall network is a complicated system that ensures robust communications between exchange information nodes. This high-level system can be divided into typical subnetworks that meet specific geographical and functional requirements: the core network, Metropolitan Area Networks (MAN), access networks and Local Area Networks (LAN). This division is illustrated in Figure 1.4 and each subnetwork is briefly described below.

1.2.1 Core Network

The core network is the backbone of the global optical communications

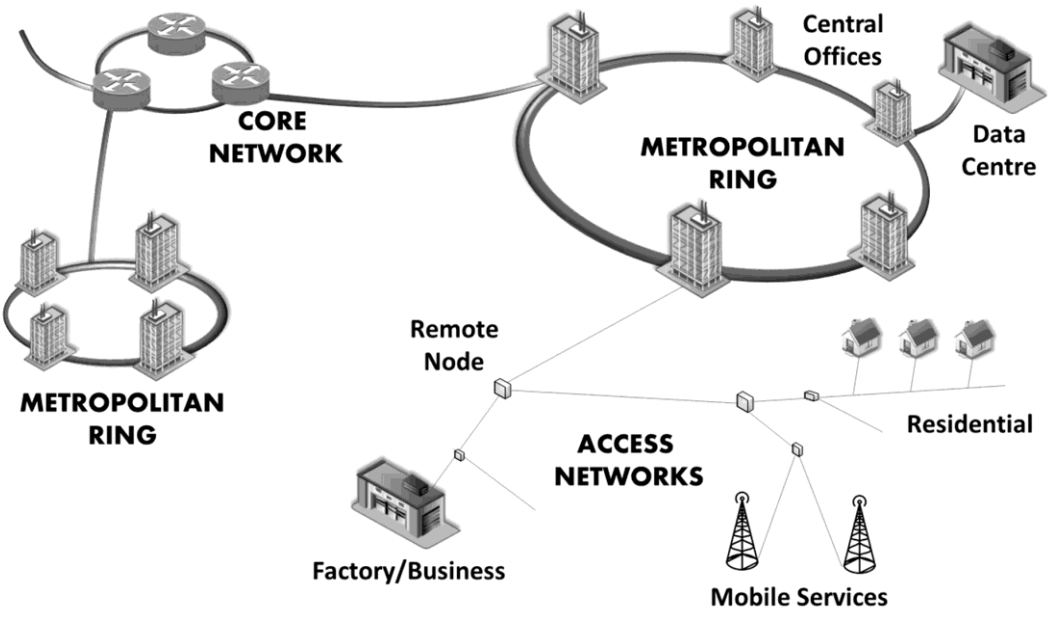

Figure 1.4 Global network topology including core, metropolitan and access networks.

system. It interconnects areas separated by hundreds or thousands of kilometres and, consequently, its longer subsystems are also referred to as long-haul links. It consists of both terrestrial and submarine links that transport aggregated data from MANs located in different cities, countries or continents. This is made possible by combining a number of technologies: distributed optical amplification [25], advanced modulation formats [13], Dispersion Compensating Fibres (DCF) [26], Forward Error Correction (FEC) codes [27] and coherent detection [16, 17].

Legacy core networks [28] employ a Time Division Multiplexing (TDM) scheme, known as Synchronous Digital Hierarchy (SDH) or Synchronous Optical Networking (SONET), to carry voice and data services such as IP or Asynchronous Transfer Mode (ATM). In WDM core networks, every wavelength carries an SDH/SONET service at typical rates of 2.5 or 10 Gbit/s. Modern core networks are transitioning towards a new protocol, Optical Transport Networks (OTN) defined in the International Telecommunication Union (ITU) standard G.709 [29]. OTN accepts a wide variety of client services like IP, Ethernet, ATM or legacy SDH/SONET, and provides transport and management over WDM networks exploiting its multi wavelength capabilities [28]. Data rates up to 40 Git/s and 100 Gbit/s per wavelength are supported [29]. An example of commercially available equipment with 10 Tbit/s capacity (i.e. 100 wavelengths and 100 (Gbit/s)/wavelength) can be found in [30].

1.2.2 Metropolitan Area Networks

MANs provide the connection between Central Offices (CO) in a metropolitan area. COs are the locations where telecommunication operators and Internet Service Providers (ISP) connect their overall network infrastructure to the access networks that serve their subscribers and clients. COs are typically separated by less than 100 kms, which reduces the cost of the deployed technology in comparison with long haul links.

Typical MANs present a ring topology that is served with SDH/SONET in the physical layer [28], similarly to core networks. Due to the recent growth of video services and data centres, it is estimated that metro traffic will increase two times faster than core traffic by 2017 [31]. Until recently, a single wavelength configuration was sufficient. The traffic growth was absorbed increasing the data rate up to the SDH/SONET 10 Gbit/s configuration, once it became affordable for MANs [28]. The transition towards WDM MANs is now in progress [32], using existing

commercially available equipment that can multiplex 10 Gbit/s services in each wavelength [33].

1.2.3 Access Networks

Access networks connect the final customers with a CO in the MAN, usually implementing links of less than 20 kms. Apart from voice and data services for residences and business, access networks also include Cable Television (CATV) systems and Radio Access Networks (RAN). The bitrates involved in access networks are not very high, but they present important technical challenges due to the non-uniform distribution of users.

1.2.3.1 Legacy Networks

Currently, the most common access networks employed for voice and data are based on the legacy Plain Old Telephone Service (POTS). They use a pair of twisted copper wires and were originally designed for transmitting voice. However, a technique called Asymmetric Digital Subscriber Line (ADSL), based on the transmission of multiple subchannels, maximise the potential of these wires reaching potentially 24 Mbit/s in the downlink and 3.3 Mbit/s in the uplink [34]. In contrast, CATV systems required coaxial cables even in the initial implementations, as they multiplexed a number of 8 MHz analogue video channels in the same cable. The main drawback of this method is that it requires amplifiers or regenerators every few hundred meters. For that reason, Hybrid Fibre-Coaxial (HFC) systems were adopted [35]. They transmit the broadband signal from the CO over fibre and a node close to the end users performs the opto-electrical conversion. Finally, the signal is distributed to the customers with coaxial cable in a point to multipoint configuration. These networks have evolved to also offer voice and data services. The standard that rules this technology is the Data Over Cable Service Interface Specification (DOCSIS). The most recent developments employ OFDM to achieve 10 Gbit/s in the downlink and 1 Gbit/s in the uplink [36, 37]. These bitrates are shared and, normally, the highest end user rates are limited to < 1 Gbit/s in the downlink.

1.2.3.2 Passive Optical Networks

The deployment of optical access networks purely based on optical fibre, normally defined as Fibre To The Home (FTTH) solutions in residences, is not widespread. Substituting the installed electrical links based on copper by point to point optical links would be very expensive for network operators. Instead, most

efforts are focused on a cost-efficient tree-like point to multipoint solution defined as Passive Optical Network (PON).

An illustrative diagram of a PON is shown in Figure 1.5, in a TDM implementation. The Optical Line Terminal (OLT) is the unit or the equipment located at a CO or a remote node that controls and manages the connection with the end users, referred to as Optical Network Units (ONU). Only the OLT and the ONUs require active equipment which reduces the cost. For the downlink, the data for all the users is generated and introduced in a single fibre by the OLT. At some point close to the customers, a passive splitter produces multiple replicas of the multiplexed signal and each one is transmitted to a different ONU. When the ONU receives the signal, it decodes the information that was allocated for it. For the uplink, each ONU transmits information and the passive device combines and multiplexes all the incoming signals in a single one that is then received in the OLT.

First generation gigabit PONs [38], often called G-PONs, multiplex the data in time (TDM), typically reaching shared rates of 2.5 and 1.25 Gbit/s in the downstream and the upstream respectively, which translate into 80/40 Mbit/s

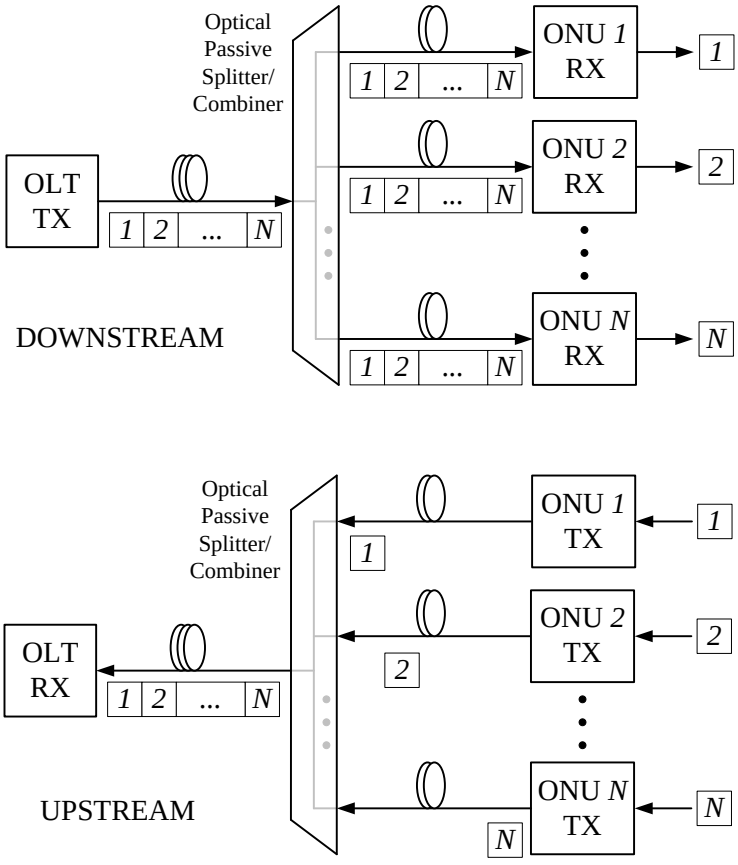

Figure 1.5 TDM point to multipoint optical link in PON.

connections for the end users. The next generation, called 10 Gigabit Passive Optical Network (XG-PON), achieves shared rates of 10/2.5 Gbit/s [39]. Recently, and after the proliferation of vendor-specific PONs based on WDM access [40], a new standard that employs TDM, WDM and sophisticated optical components was defined [41]. It is called Next Generation Passive Optical Networks 2 (NG-PON2) and can provide connections of up to 10 Gbit/s to final subscribers. The general topologies for data (de)/multiplexing in typical applications are explained in detail in section 1.4.2.2.

1.2.3.3 Radio over Fibre

Optical fibres are also employed in access networks to link COs with antennas in radio applications. In general, the term Radio over Fibre (RoF) applies to the cases in which the optical link facilitates the centralisation of several wireless services in one location (the CO) [42]. Theoretically, the high bandwidth of the optical fibre allows the simultaneous transmission of all the conceivable radio bands, even Terahertz applications [43], in the same fibre.

Ideally, an analogue radio signal would be transmitted over fibre from the CO and the base station would be a simple system consisting of a receiver plus an antenna [44]. Commercial applications based on such analogue RoF concepts have been deployed for cellular communications [45]. Currently, most research efforts are focused on such a configuration using the free 60 GHz band for future mobile generations [46], 5G or Internet of Things (IoT). Moreover, an alternative technique called digital RoF [46] is also being implemented and deployed. A functional example of a digital RoF system is the Common Public Radio Interface (CPRI) [47, 48]. It supports most of the current mobile networks standards and employs the following terminology: Radio Equipment Control (REC) in the CO and Radio Equipment (RE) in the antenna. For the downlink, the REC generates the samples of the modulating signal and transmits a bitstream that contains the values of those samples over fibre. The RE uses the samples to perform the digital to analogue conversion, and then it modulates the reconstructed waveform onto the Radio Frequency (RF) carrier that is finally emitted. For the uplink, the RE demodulates the received RF signal. Then it samples the obtained waveform and transmits a bitstream with the values of the samples over fibre. At the other end, the REC receives and processes the samples [48].

1.2.4 Data Centres

The networks that handle the traffic of data in customer and business premises are called Local Area Networks (LAN) and meet the "Ethernet" standard from the Institute of Electrical and Electronics Engineers (IEEE) 802.3 [49]. LANs are composed of multiple users (typically computers) that are interconnected through hubs, switches, point to point links and/or a shared medium [50]. The standard has evolved constantly during more than 30 years and several optical links with different combinations of bit rates, fibres and distances are supported [51]. In general, the technology for these optical systems has to be cheap and appropriate for large scale markets.

Data centres and high performance computing systems can be seen as particular LANs optimised for a continuous exchange of data provided simultaneously by multiple devices (typically servers). The generalisation of Internet applications accessed by thousands or millions of users has translated into the proliferation of high-capacity high-performance data centres. The common data centre structure consists of racks of servers that are connected with top-of-the-rack switches by links shorter than a few meters. Switches situated at different layers route the traffic towards metro or core networks [52]. Several optical interfaces and standards defined by different institutions are typically employed for the connections between switches: Ethernet [49], Infiniband [53] and FibreChannel [54]. In the optical communications industry, multisource agreements define mechanical slots plus the mechanics of their associated pluggable electro-optical transceivers to allow interoperability between manufacturers. For this particular application, the transceivers are usually designed to be compatible with the three previous standards. Due to the constant growth of traffic in data centres, there is a continuous definition of smaller transceivers in order to increase the spatial density of data interfaces in switches. According to some industrial sources, the transceiver that will become predominant is the Quad Small Form-factor Pluggable (QSFP) [55, 56]. This transceiver integrates four lasers to implement four parallel optical channels at 25 Gbit/s, reaching an overall rate of 100 Gbit/s and supporting 100 Gigabit Ethernet (100GbE), IEEE 802.3bm [49]. There are different variants supported: directly modulated lasers to reach 100 m or with integrated silicon photonics modulators to reach 2 km [56].

1.3 Optical Components

This section describes the typical optical components that can be found in optical communications schemes. The main concepts and ideas that will be employed in the following chapters are emphasised and explained more deeply.

1.3.1 Laser

The term laser is used as a noun, but it was originally an acronym for "light amplification by stimulated emission of radiation". A laser is a fundamental part in any optical transmitter, as it is the generator of the optical carrier. In optical communications, the spectral location of a carrier is often stated in wavelengths (typically nm) instead of frequencies.

1.3.1.1 Physics of the Laser

This section briefly describes the physical principles that explain the operation of optical sources [1]. The energy of an electron depends on the position of its orbit with respect to the nucleus. Higher energies are required for orbits farther from the nucleus. If the electron is in an inner orbit with a low energy E_1, it can absorb the energy from a source of light (photon) and move to the orbit with higher energy E_2. This process, called *absorption*, is illustrated in Figure 1.6(a). The energy provided by the photon is equal to $\Delta E=E_2-E_1=h\nu$, where h is the Planck´s constant and ν is the frequency of the incident light.

The opposite process, called *emission*, also occurs. An electron in an external orbit E_2 tends to return to the internal orbit E_1 emitting a photon with energy ΔE, as it can be seen in Figure 1.6(b). When this phenomenon occurs randomly it is called *spontaneous emission*. If multiple photons are generated in this way, they present different and random phases and directions producing incoherent light, as in a Light Emitting Diode (LED). Although all the photons have the same frequency, the sum of multiple tones with arbitrary phases translates into a random modulation that significantly spread the spectrum. As a consequence, the performance of LEDs in communications is greatly limited. An example of a commercial LED spectrum is shown in Figure 1.6.

In contrast, lasers are based on *stimulated emission*. If one electron occupies the excited level E_2 and one photon with energy ΔE enters in the atom, the electron will come back to the level E_1 but releasing a new photon that is in phase and has the

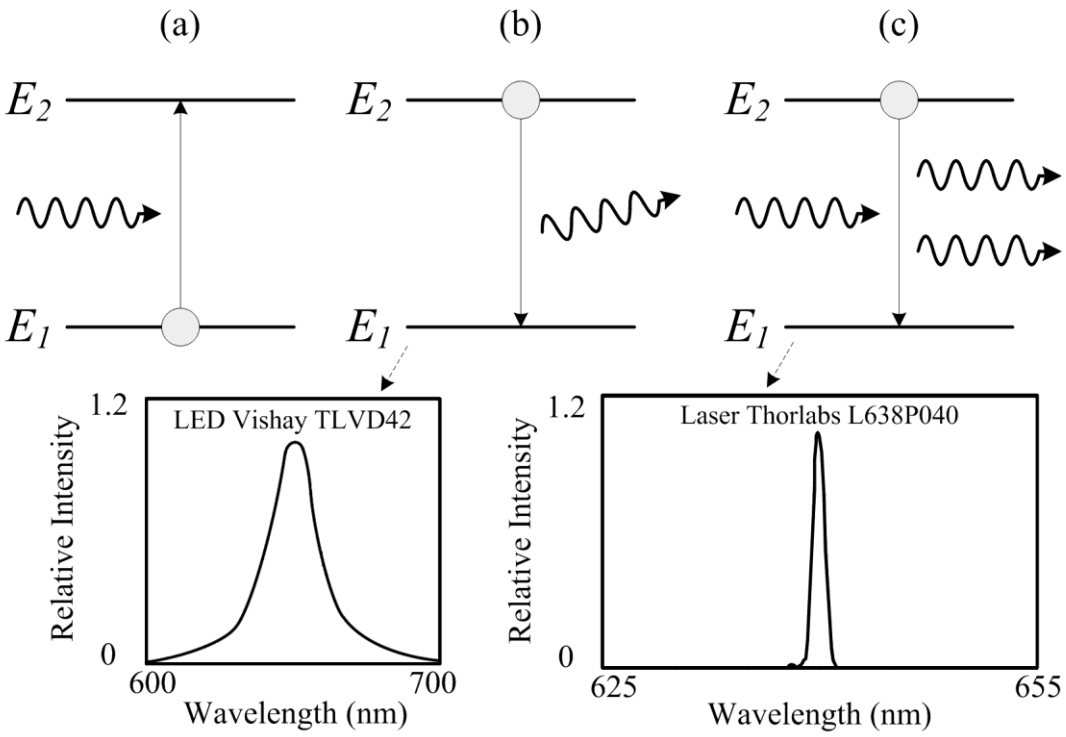

Figure 1.6 Fundamental processes occurring between the energy states of an atom: (a) *absorption*, (b) *spontaneous emission* and (c) *stimulated emission.* Associated spectra for two commercial light sources.

same direction as the incident one, as illustrated in Figure 1.6(c). When multiple photons are generated in this way, a coherent source of light with a narrow spectral range is produced, as it is also shown in Figure 1.6 for a commercial device. A laser is formed of a material whose electrons are continuously excited, by an outside source of light or by an electric field, to occupy higher energy levels in a process known as population inversion. A structure based on mirrors with different reflectivity ensures that multiple photons are travelling repeatedly through the medium, generating more stimulated coherent photons in a chain reaction [1].

Light is an electromagnetic field [57] and lasers are the sources of carriers at optical frequencies. The lasers employed in communications are typically based on semiconductors [58]. Similarly to an electrical oscillator, the spectrum of a laser is not a perfect delta corresponding to a pure tone. As undesired spontaneous emission also occurs inside a laser, random small fields with arbitrary phases are continuously added to the coherent tone. This effect perturbs the amplitude and the phase of the output generating Relative Intensity Noise (RIN) [1] and phase noise [59] respectively. RIN is usually measured in dB_c/Hz and phase noise in terms of spectral

linewidth (Hz). Obviously, both effects can have an impact on the performance of optical communication systems [60].

1.3.1.2 Direct Modulation

Semiconductor lasers can be seen as laser diodes whose output amplitude and power depends on the driving current. Neglecting RIN and phase noise, the electric field at the output of a monochromatic laser can be written as:

$$E(t) = E_p(t)\cos(\omega_c t) \tag{1.1}$$

where $E_p(t)$ is the peak amplitude and ω_c is the frequency of the optical carrier. The term $E_p(t)$ is a function of time reflecting the fact that the amplitude depends on the current that drives the laser diode. Note that $E_p(t)$ can only vary at the rate of an electrical signal and, as a consequence, the frequency of change is several orders of magnitude lower than the optical frequency ω_c. Thus, at the output of the laser, the average power P (also called intensity) with respect to the optical frequencies is:

$$P(t) = \langle E^2(t)\rangle = \langle E_p^2(t)\cos^2(\omega_c t)\rangle = \frac{E_p^2(t)}{2}\langle 1+\cos(2\omega_c t)\rangle = \frac{E_p^2(t)}{2}. \tag{1.2}$$

It can be readily seen that an optical communication link can be established by modulating the power or intensity of the carrier with the information to be transmitted. From the point of view of the signal this process is called Intensity Modulation (IM). From the point of view of the device it is also called direct modulation, in contrast with external modulation which will be explained below. As illustrated in Figure 1.7, the transfer function of a laser diode presents an approximately linear area in which the output power P is proportional to the driving current $i(t)$. This area begins for a current above a given threshold i_{th}, so that the laser must be biased with a higher current i_b that produces a DC power P_b to ensure linear operation. Mathematically, assuming a proportionality factor m:

$$\begin{aligned} P(t) &= P_b + m\cdot i(t). \\ E(t) &= \sqrt{2\left(P_b + m\cdot i(t)\right)}\cos(\omega_c t). \end{aligned} \tag{1.3}$$

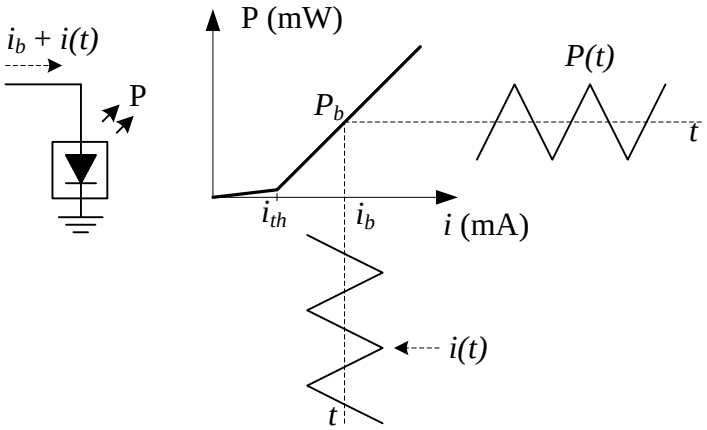

Figure 1.7 Typical transfer function of a laser diode.

Performance of direct modulation is limited by several concepts. Firstly, the RIN degrades the Signal to Noise Ratio (SNR) of the power signal at the output of the laser [1]. Secondly, different optical powers produce a frequency deviation in the output wavelength in a phenomenon known as chirp. Consequently, directly modulated lasers present a broadening in the output spectrum that translates into impairments in the received signals due to fibre dispersion [61]. Thirdly, the bandwidth of the modulation is limited [1] so that broadband lasers are difficult and costly to build [62]. Finally, it is not possible to perform direct modulation of the electric field and the phase of the laser. Phase modulation is required for coherent systems and also to produce Optical Single Side Band (OSSB) signals. While the RIN and linewidth are inherent properties of the laser that cannot be avoided, external modulation can be employed to overcome the rest of the limitations, as explained in section 1.3.2.

1.3.1.3 Classification of Communication Lasers

Three spectral regions are usually employed in optical communications. The first window corresponds to the range of 800-900 nm. The first optical links used these wavelengths because early fibre presented minimum losses in that region. Although the losses in that area are high in current fibre, these wavelengths are still used for short distances due to the low cost of lasers and detectors. The second band of interest is around 1310 nm. This band is attractive because there is zero dispersion fibre available, although sources and detectors are more costly. Finally, the last band of interest is around 1550 nm as fibre losses are the lowest there. Although fibre dispersion is not zero, it can be compensated electronically [63] or optically [26] to achieve longer transmission distances.

Table 1-1 Typical parameters of lasers commonly employed in communications.

Type	*RIN (dB_o/Hz)*	*3dB Linewidth*
DFB	< -140	< 10 MHz
ECL	< -140	< 1000 KHz
VCSEL	> -130	< 100 MHz

According to the internal structure, several types of monochromatic semiconductor lasers are typically employed in communications [1]: Distributed Feedback Lasers (DFB), External Cavity Lasers (ECL), and less costly Vertical Cavity Surface Emitting Lasers (VCSEL). Their typical parameters are shown in Table 1-1.

1.3.2 Optical Modulators

This section introduces the most common optical modulators that are widely employed in optical communications. Optical modulators use electrical signals to modify the physical characteristics of materials in such a way that the propagation conditions of light change. The basic mathematical principles of the electro-optic Mach-Zehnder Modulators (MZM) are emphasized, as they will be employed in the next chapters.

1.3.2.1 Electro-absorption Modulators

Electro-Absorption Modulators (EAM) are based on the Franz–Keldysh effect [64]. An electric field can be applied to a semiconductor modifying the bandgap energy between two bands ΔE. If the incoming lightwave presents photons with a lower energy ($h\nu < \Delta E$), the semiconductor will be transparent. If the incoming energy is higher than the bandgap ($h\nu > \Delta E$), *absorption* will occur as in Figure 1.6(a). With this approach, an electrical signal can be employed to modulate the power of the output lightwave.

EAMs can be integrated in the same package with a laser, in a structure known as Externally Modulated Laser (EML). EMLs achieve low voltage operation, high bandwidth and reduced chirp [65]. The main disadvantage of EAMs is that they cannot perform phase modulation. This limitation impedes not only the use of EAMs in coherent systems, but also the direct generation of OSSB signals.

1.3.2.2 Electro-optic Mach-Zehnder Modulators

The electro-optic effect, also known as Pockels effect, consists of a linear variation in the refractive index of crystals induced by an electric field [64]. A change in the refractive index translates into a change in the propagation speed of

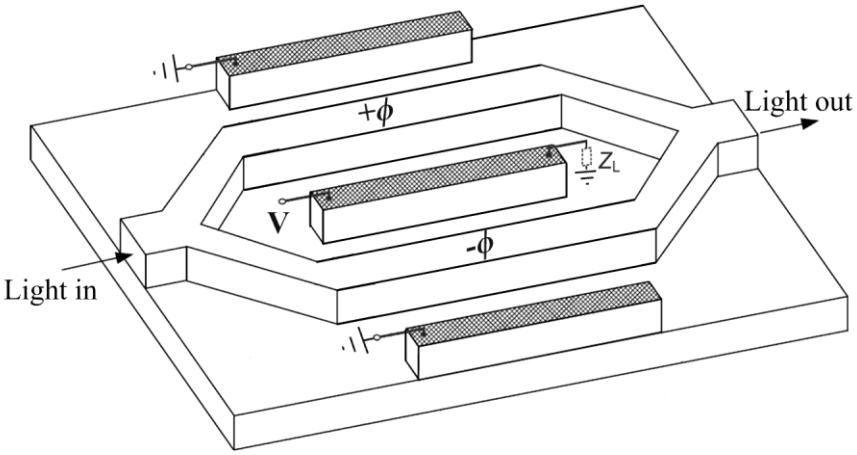

Figure 1.8 Push-pull Mach-Zehnder modulator.

light in the material. A single waveguide in which the speed of light varies according to an electric signal achieves optical phase modulation [66]. Furthermore, this concept is also employed along with Mach-Zehnder interferometers [67] to obtain phase and amplitude modulation of light dependent on an electrical signal [68]. The principle of operation of a MZM can be observed in Figure 1.8. The power of an incident lightwave splits into two equal signals that propagate through waveguides under the effect of a varying electric field. The associated modification of the refractive index produces a relative phase shift between the two lightwaves. When they recombine, any level of interference, from destructive to perfectly constructive, is possible and depends on the applied electrical signal. Figure 1.8 shows a push-pull MZM where the two waveguides suffer opposite phase shifts, $+\phi$ and $-\phi$. This structure is preferred because it can halve the required voltage to obtain any value of relative phase shift [69]. Different configurations of optical modulators exist, but in general they all can be reduced to a combination of phase modulators and/or MZMs.

The transfer function of an ideal MZM will be derived mathematically. The optical incoming signal is a lightwave generated by a laser $E_i \cos(\omega_c t)$. Initially, it is divided into two equal power carriers $E_1(t)$and $E_2(t)$ with a 3dB splitting ratio with respect to the original:

$$E_1(t) = E_2(t) = \frac{E_i}{\sqrt{2}} \cos(\omega_c t). \tag{1.4}$$

The carriers propagate in two different waveguides that suffer an opposite relative phase shift. A figure of merit of any MZM is the half-wave voltage V_π, and it

determines the required voltage to generate an overall relative phase shift equal to π radians. Thus, the phase shift that is produced in any arm of the MZM due to a voltage *V* is:

$$|\phi| = \frac{\pi \cdot V}{2V_\pi}. \tag{1.5}$$

Consequently, once both lightwaves are combined again, the electric field at the output of the MZM can be written as:

$$E_o(t) = \frac{E_i}{2}\cos\left(\omega_c t + \frac{\pi \cdot V}{2V_\pi}\right) + \frac{E_i}{2}\cos\left(\omega_c t - \frac{\pi \cdot V}{2V_\pi}\right). \tag{1.6}$$

Note that each carrier presents an additional 3 dB loss due to the power combiner loss (otherwise there would be more power at the output of the MZM than at the input). Applying the equality $\cos(A)\cos(B) = \frac{1}{2}\left(\cos(A+B)+\cos(A-B)\right)$, the previous equation can be rewritten as:

$$E_o(V,t) = E_i \cos\left(\frac{\pi \cdot V}{2V_\pi}\right)\cos(\omega_c t) = E_p(V)\cos(\omega_c t). \tag{1.7}$$

The peak amplitude of the electric field is also expressed as $E_p(V)$, and depends on *V*. Note that $E_p(V)$ also carries phase information, as it can be positive or negative. The associated power is equal to the average power for the optical frequencies. Similarly to the procedure presented in eq. (1.2):

$$P_o(V) = \left\langle E_o^2(V,t)\right\rangle = \frac{E_p^2(V)}{2} = \frac{E_i^2}{4}\left(1+\cos\left(\frac{\pi \cdot V}{V_\pi}\right)\right). \tag{1.8}$$

The transfer function of the MZM, for $P_o(V)$ and $E_p(V)$, is illustrated in Figure 1.9 normalising E_i=1. It is clear that a MZM is a nonlinear device, although this impairment can be overcome employing the appropriate level in the driving electrical

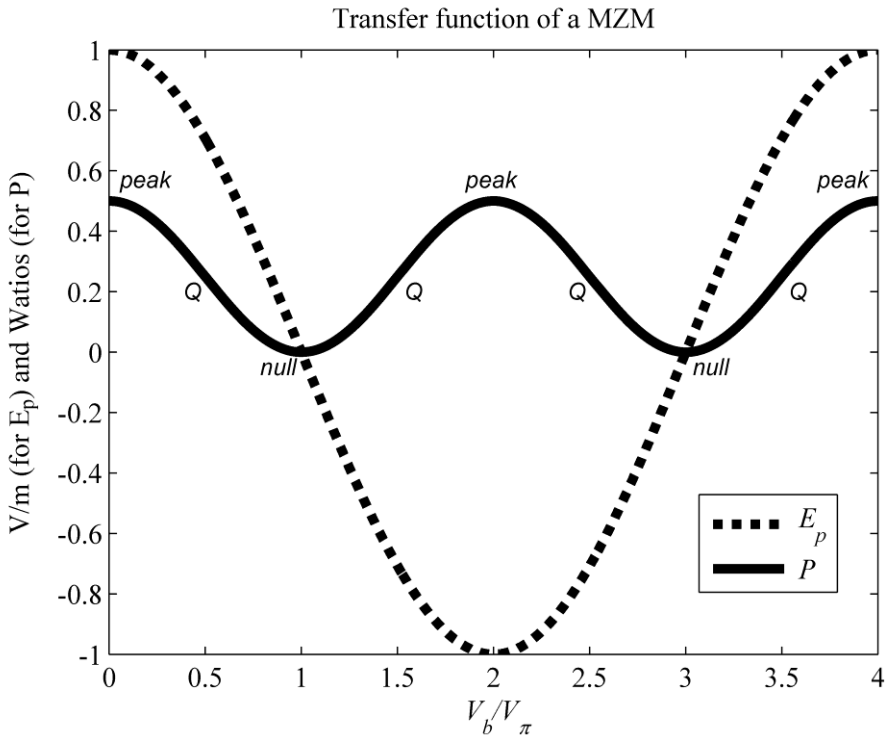

Figure 1.9 Transfer function of a MZM.

signals, as shown below. The applied voltage V can be composed of two elements: a DC component V_b, that defines the bias of the device, plus an AC signal $s(t)$ with the information to transmit:

$$V = V_b + s(t). \tag{1.9}$$

The bias point establishes the initial level from which $P_o(V)$ and $E_p(V)$ will vary according to the modulating signal $s(t)$, similar to Figure 1.7. From the point of view of the output power, there are three types of important bias points that repeat periodically: *peak*, *null* and *quadrature* (Q). These points can be found at $V_b/V_\pi=2n$, $V_b/V_\pi=2n+1$, and $V_b/V_\pi=n+0.5$ respectively, with n being any integer number.

The best bias point depends on the physical parameter that will carry the information and will be detected in the receiver. For intensity modulation, the most linear point is *quadrature*. This can be observed visually in Figure 1.9, and can also be justified mathematically expanding eq. (1.8) with the V provided in eq. (1.9). Considering *quadrature* at $V_b/V_\pi=1.5$, a modulating signal $s(t)$ with a peak amplitude very small in comparison with V_π, and applying $\sin(x)\approx x$ for small values of x, an approximately linear modulation can be achieved:

$$P_o(t) = \frac{1}{4}\left(1+\cos\left(\frac{3\pi}{2}+\frac{\pi\cdot s(t)}{V_\pi}\right)\right) = \frac{1}{4}\left(1+\sin\left(\frac{\pi\cdot s(t)}{V_\pi}\right)\right) \approx \frac{1}{4}\left(1+\frac{\pi\cdot s(t)}{V_\pi}\right). \quad (1.10)$$

Without applying any approximation, the higher the amplitude of *s(t)*, the higher the intermodulation products at the output [70]. Note that in this case, the transmitted power belongs mostly to the optical carrier instead of the information signal. Information can also be transmitted in the phase and/or the amplitude of the electrical field $E_o(t)$. In that case, the optimum bias point is *null*, as it can be deduced from Figure 1.9. Again, a mathematical justification can be provided expanding $E_p(V)$ in eq. (1.7) with eq. (1.9). Considering *null* at V_b/V_π=3 and a peak amplitude of *s(t)* very small in comparison with V_π, the signed peak of the electric field is:

$$E_p(t) = \cos\left(\frac{3\pi}{2}+\frac{\pi\cdot s(t)}{2V_\pi}\right) = \sin\left(\frac{\pi\cdot s(t)}{2V_\pi}\right) \approx \frac{\pi\cdot s(t)}{2V_\pi}. \quad (1.11)$$

Note that in this case there is no power lost in the transmission of the optical carrier. As it will be shown, that benefit is achieved at the expense of requiring a much more complicated receiver.

To summarise, MZMs can achieve phase and intensity modulation of optical carriers. As it will be demonstrated they can generate OSSB signals directly. Moreover, they present higher modulation bandwidths than conventional lasers [45] and can operate free of phase and frequency chirp [71]. The main disadvantage is the nonlinear behaviour, although it can be balanced with a proper analysis on the optimum configuration according to the desired modulating signals.

1.3.3 Optical Fibre

Optical fibres are waveguides typically made of glass (silica). The guiding of light inside the core of the fibre is achieved by employing a higher refractive index than in the cladding [1]. The advantages of optical fibre over traditional copper wire are evident: broader bandwidth, lower attenuation and immunity to electromagnetic interference as the optical fibre is electrically nonconductive. This section briefly reviews three important parameters in optical fibres: attenuation, dispersion and nonlinear behaviour.

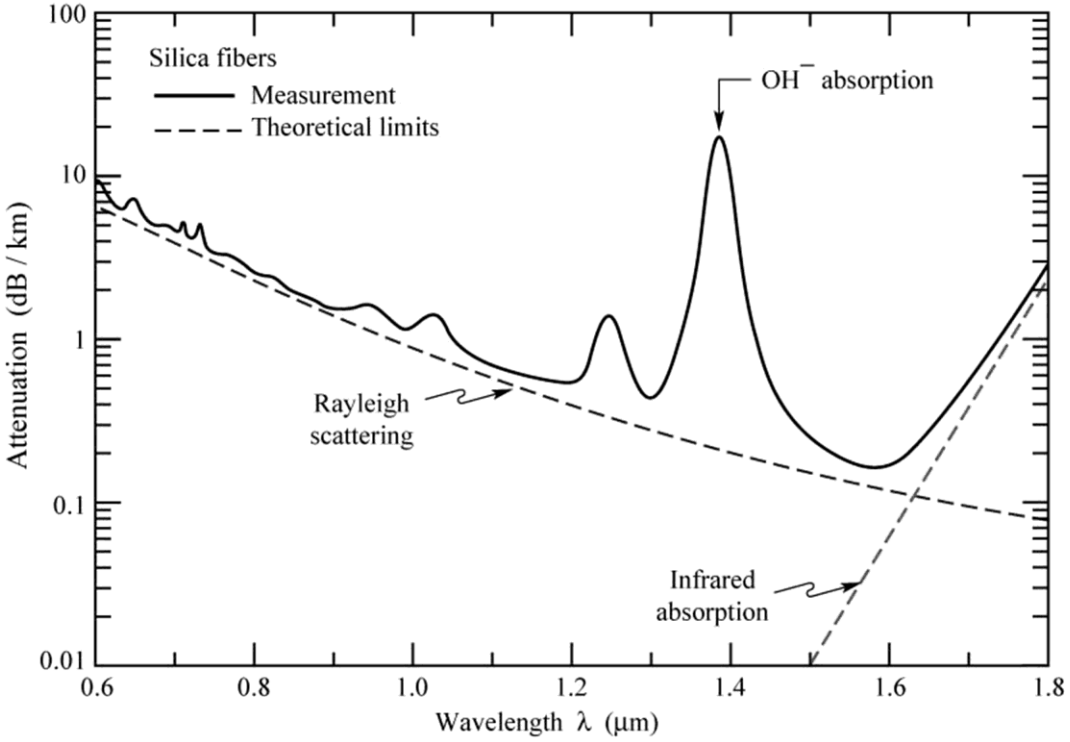

Figure 1.10 Typical attenuation in silica fibre and theoretical limits [72].

1.3.3.1 Attenuation

The typical losses of silica fibre are illustrated in Figure 1.10 [72]. The lowest theoretical limits are given by *Rayleigh scattering* and *material absorption*. Rayleigh scattering is produced by microscopic fluctuations in the refractive index, which are a consequence of the fabrication process [1]. Material absorption is due to the silica itself and to extrinsic impurities as water [1]. Typically, in the bands of interest, losses range from a few dB/km at 800 nm to ≈0.2 dB/km at 1550 nm.

1.3.3.2 Dispersion

The diameter of the fibre core determines the number of electromagnetic modes that can propagate through the fibre. Original fibres allowed the propagation of many modes and are called Multi-Mode Fibres (MMF), in opposition to later fibres that allowed only one and are called Single Mode Fibres (SMF) or Standard Single Mode Fibres (SSMF) [1, 73].

In both cases dispersion is an important impairment that limits the transmission distance. It can be seen as a temporal broadening that any transmitted pulse or signal suffers while propagating through the fibre. In MMFs, it is a consequence of every mode travelling at a different speed and the effect is called *modal dispersion* [1]. In SMFs, there is only one mode and dispersion, although lower, still occurs as a consequence of *material dispersion* and *waveguide dispersion*

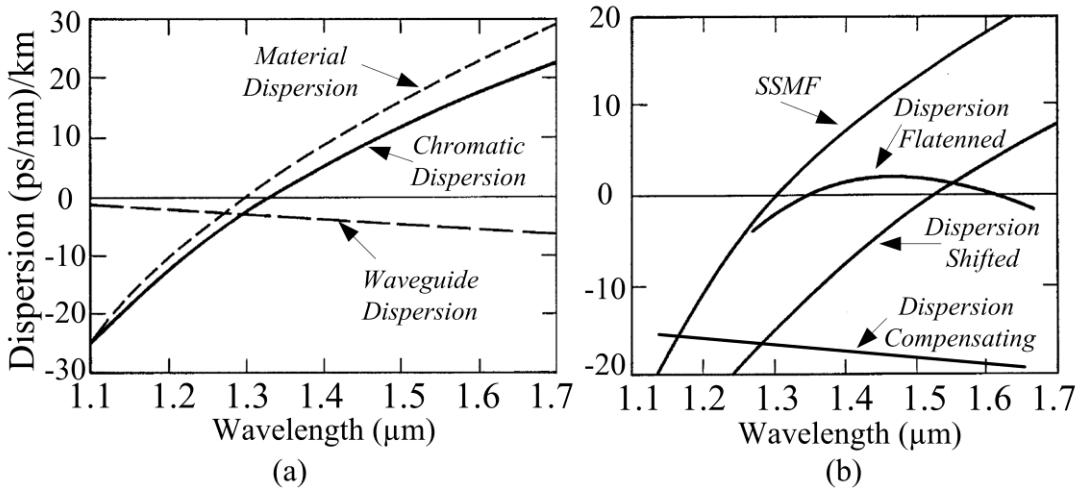

Figure 1.11 (a) Components and chromatic dispersion in SSMF. (b) Chromatic dispersion curves in several types of fibres.

[1, 74]. Any modulated carrier expands its spectrum in a range of frequencies and each frequency propagates with a different refractive index, giving rise to material dispersion. Simultaneously, the energy distribution of the mode while it propagates through the core and the cladding also depends on the wavelength, producing waveguide dispersion. The sum of these sources of dispersion is written as D and called *group velocity dispersion* or *chromatic dispersion*. The dispersion D in SSMFs along with the two individual sources is illustrated in Figure 1.11(a). Typical values are ≈0 (ps/nm)/km at 1300 nm and ≈17 (ps/nm)/km at 1550 nm. Different types of modified SMFs that compensate or shift the curve of dispersion [1, 73] are commercially available and shown in Figure 1.11(b). For a pulse transmission of distance L, at a wavelength λ, with a bandwidth $\Delta\lambda$, over SMF with dispersion $D(\lambda)$, the extent of the pulse temporal broadening is:

$$\Delta T = L|D|\Delta\lambda. \tag{1.12}$$

Another source of dispersion is *Polarization Mode Dispersion* (PMD). A light mode travels at a state of polarization that can be divided into two orthogonal components. Besides, optical fibres present a phenomenon known as birefringence. Due to the differences in the shape of the core and non-uniform stress, there is a continuous power exchange between the two polarization components and light acquires and arbitrary varying state of polarization. Both polarization components present a different refractive index resulting in a time broadening of the transmitted pulses known as PMD [1]. For high rates and long transmission distances, PMD

becomes significant if D is low or has been removed or compensated [75, 76]. Typical modern fibre PMD values are $D_p < 0.1$ ps/(km$^{0.5}$) [1].

To overcome dispersion, one option is to divide the available bandwidth into several subchannels. As each subchannel is narrower in frequency and transports lower bandwidth baseband signals, it is also more tolerant to dispersion. This concept explains the importance of multicarrier techniques and will be emphasized in the next chapter.

1.3.3.3 Nonlinear Behaviour

Intensity inside the core of an optical fibre can be high, especially when multiple WDM channels are transmitted. Due to the Kerr nonlinearity, intensity variations produce a change in the refractive index of the fibre, inducing signal distortions for long transmission distances [77].

This phenomenon can be subdivided into several effects. The intensity variations of one channel modify the refractive index producing a self-induced phase variation that is called *Self-Phase Modulation* (SPM). Similarly, the phase variations associated with the intensity changes of a different channel are called *Cross-Phase Modulation* (XPM). Moreover, this nonlinear behaviour also produces electrical fields at frequencies that are a combination of up to three other frequencies, an effect known as *Four-Wave Mixing* (FWM) [1, 77]. SPM and XPM translate mainly into pulse broadening and jitter while FWM produces amplitude distortion [13]. Note that optical noise can also have an important contribution on the overall intensity, especially in systems where many optical amplifiers are employed. As a consequence, more SPM and XPM induced nonlinear phase noise occurs [13].

The effects of nonlinearities depend on many factors like the type of fibre, channel and subchannel spacing, and the modulation format. Typically, in long reach WDM systems, nonlinearities between different WDM channels (inter-channel) have a higher impact at lower data rates. With higher data rates per WDM channel (> 10 Gbit/s), the nonlinearities produced inside every channel (intra-channel) are dominant [13].

1.3.4 Optical Amplifiers

Optical amplifiers allow the deployment of long distance fibre links without inserting opto-electronic repeaters. The span between amplifiers depends on every particular system and it is usually in the range of several tens of kilometres. A

classification of the optical amplifiers can be made according to their position in the system: after the transmitter they are called *booster amplifiers*, between fibre spans they are referred to as *in-line amplifiers* and, finally, when positioned just before the opto-electronic receiver the employed term is *pre-amplifier*. The dominant optical amplifiers in optical networks are: Semiconductor Optical Amplifiers (SOA), Erbium-Doped Fibre Amplifiers (EDFA) and Raman amplifiers.

SOAs have a structure that is similar to a laser but without the cavity. Population inversion in the medium is achieved by electrical pumping. When the optical signal passes through the semiconductor, amplification is produced by stimulated emission (see section 1.3.1.1) [78]. SOAs can be integrated with lasers, modulators and detectors in the same chip, giving rise to size efficient and economical solutions. Consequently, they are often employed as booster amplifiers or as pre-amplifiers. The main disadvantages with respect to the other technologies are lower gain and saturation power and higher Noise Figure (NF). Other drawbacks that make them impractical to act as in-line amplifiers are polarization sensitivity, inter-channel crosstalk and high coupling losses [1].

EDFAs, a particular type of rare-earth doped fibre amplifier [79], are dominantly used in current optical links. These fibre amplifiers are composed of fibre doped with a rare-earth element in which population inversion is achieved with a coupled optical pumping signal, typically at wavelengths lower than the desired signal. The doped fibre is positioned between isolators that avoid the pumping signal from propagating outside the amplifier. While the desired signal propagates through the doped fibre, it is amplified by stimulated emission [80]. EDFAs can have low NF to act as a pre-amplifiers, but maximum output power is low. In-line and booster EDFAs feature high gain and high saturation power, but at the expense of a higher NF. Low NF EDFAs are typically pumped at 980 nm while boosters are pumped at 1480 nm [81]. EDFAs also present a number of disadvantages: bulky configuration, impossible to integrate and high cost. Finally, due to the optical pumping, EDFAs consume more power than SOAs.

Raman amplifiers are a particular type of distributed amplifiers. These are fibre amplifiers in which the amplification occurs during the transmission over the fibre. SSMFs are suitable for the application of this technique, although certain dopants increase Raman gain. Raman amplification results from the effect of stimulated Raman scattering. The signal is transmitted along a co-propagating or

counter-propagating pumping lightwave located at a higher frequency. Population inversion is achieved allowing stimulated emission at the wavelength of the desired signal. Raman amplifiers have important advantages as in-line amplifiers: the transmission medium amplifies the signal, they exhibit wide gain bandwidth, gain spectrum can be tailored with the pump frequency, and NF can be lower than in EDFAs. On the other hand they require high power pump signals, often exceeding safety limits [25].

1.3.5 Optical Receivers

The role of an optical receiver is to convert the optical signal back into an electrical form, recovering the data that was transmitted through the communication system. This section reviews the physics of typical communications photodetectors and discusses the classification of optical links according to the detection technique.

1.3.5.1 Physics of Photodiodes

A photodetector based on semiconductors, a *p-n* photodiode, can be seen as a reverse biased diode with a middle depletion region free of charged carriers. When photons arrive to the depletion region, absorption occurs (see Figure 1.6(a)) and creates electron-hole pairs. Consequently, a reverse current that is proportional to the incident optical power is generated. The parameter that determines the ratio between the induced photocurrent and the incoming optical power is called *responsivity*, *R*. The depletion region can be increased by inserting a layer of lightly doped semiconductor material, in a configuration that is called a *pin* photodiode and features a higher *R*. Other common devices are Avalanche Photo-Diodes (APD). They present a structure in which an accelerated electron can potentially produce new electron-hole pairs multiplying the photo-detection effect, the *R* and the sensitivity of the device. The main disadvantage is the higher NF [1].

Often, photodetectors are integrated with Trans-Impedance Amplifiers (TIA), a current to voltage converter with an internal amplifier [82]. These structures are usually identified as photo-receivers and achieve a higher equivalent *R*.

1.3.5.2 Direct Detection

As it has been explained in sections 1.3.1.2 and 1.3.2.2, information can be modulated onto the average power or intensity of a lightwave. In the receiver, the modulating signal can be recovered with a photo-detector. The photocurrent *I*

induced in a photo-detector of responsivity R by an incoming optical signal of average power $P(t)$ is:

$$I(t) = RP(t) = R\langle E^2(t)\rangle. \tag{1.13}$$

This technique is defined as Intensity Modulation / Direct Detection (IM/DD).

1.3.5.3 Coherent Detection

By the use of MZMs and phase modulators, complex information can also be modulated onto the amplitude and the phase of a lightwave electric field. A simple photo-detector is not enough to recover the data in these schemes, as average power is independent of the phase of the optical carrier. These applications require more complicated receivers called coherent detectors [83]. This section shows the basic mathematical principle of a coherent receiver. A comparison of IM/DD and coherent systems will be provided in section 1.4.3.

A simple amplitude-phase modulation of an optical carrier was shown in section 1.3.2.2. From eqs. (1.7) and (1.11), neglecting proportionality constants and nonlinear effects, a MZM can be used to modulate a signed AC information signal $s(t)$ onto an optical carrier with arbitrary initial phase φ_c as:

$$E_s(t) = s(t)\cos(\omega_c t + \varphi_c). \tag{1.14}$$

Note that $s(t)$ does not contain a DC term and, consequently, the spectrum of $E_s(t)$ is free of a pure tone at ω_c. That is the main advantage of coherent systems, there is not power wasted in the transmitted signal and a better sensitivity is obtained in the receiver. On the other hand, as $s(t)$ can take positive and negative values, it cannot be recovered with a single square-law direct detection photo-detector.

The simplest ideal coherent receiver can be observed in Figure 1.12(a) and consists of a local laser, a combiner and two balanced photo-detectors. The incoming signal is combined with a laser Local Oscillator (LO) at a frequency ω_{LO}. For simplicity, unit amplitude and arbitrary initial phase φ_{LO} are employed:

$$E_{LO}(t) = \cos(\omega_{LO} t + \varphi_{LO}). \tag{1.15}$$

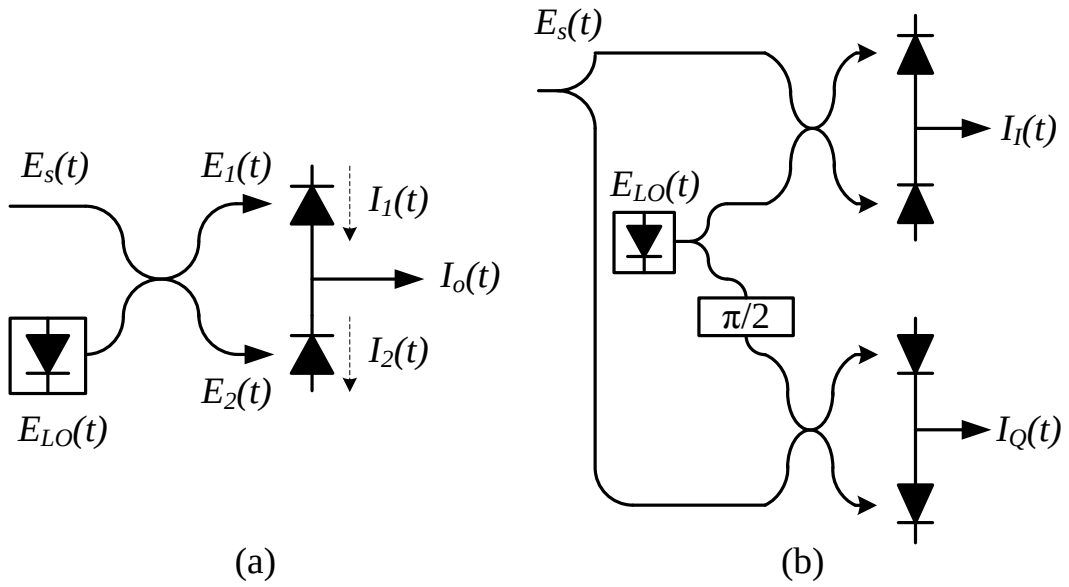

Figure 1.12 Balanced coherent detector (a) and 90º optical hybrid (b).

The combination is performed with a 3 dB loss 180º optical coupler [83] such that:

$$E_1(t) = \frac{1}{\sqrt{2}}\left(E_s(t) + E_{LO}(t)\right).$$
$$E_2(t) = \frac{1}{\sqrt{2}}\left(E_s(t) - E_{LO}(t)\right). \tag{1.16}$$

The detected photocurrents in the photo-diodes, $I_1(t)$ and $I_2(t)$, are calculated as the average optical powers. The terms at frequencies $2\omega_c$, $2\omega_{LO}$ and $(\omega_c+\omega_{LO})$ disappear in the output because their average optical power is zero. For simplicity, considering a responsivity R equal to one:

$$I_1(t) = \left\langle E_1^2(t)\right\rangle = \frac{1}{2}\left(\frac{s^2(t)}{2} + \frac{1}{2} + s(t)\cos\left(\left(\omega_c - \omega_{LO}\right)t + \varphi_c - \varphi_{LO}\right)\right).$$
$$I_2(t) = \left\langle E_2^2(t)\right\rangle = \frac{1}{2}\left(\frac{s^2(t)}{2} + \frac{1}{2} - s(t)\cos\left(\left(\omega_c - \omega_{LO}\right)t + \varphi_c - \varphi_{LO}\right)\right). \tag{1.17}$$

As two detectors in a balanced configuration are used, the final photocurrent $I_o(t)$ is:

$$I_o(t) = I_1(t) - I_2(t) = s(t)\cos\left(\left(\omega_c - \omega_{LO}\right)t + \varphi_c - \varphi_{LO}\right). \tag{1.18}$$

When different ω_c and ω_{LO} are employed, the detection is called *heterodyne* and further electronic down conversion is required. When ω_c and ω_{LO} are the same, detection is *homodyne* [80, 83]. In theory, *s(t)* can be recovered perfectly:

$$I_o(t)\Big|_{\substack{\omega_c=\omega_{LO}\\ \varphi_c=\varphi_{LO}}} = s(t). \tag{1.19}$$

In practice, complicated post processing is required due to major difficulties. Firstly, as there is not a transmitted pilot tone at ω_c, the frequency locking of ω_{LO} is difficult. Secondly, phase noise is also present and independent in the optical carrier and the local oscillator, $\varphi_c(t) \neq \varphi_{LO}(t)$. Optical Phase Locked Loops (OPLL) have been investigated since the 1980s [84], but even with state-of-the-art technology they are not practical for deployment due to frequency drifts and instabilities of semiconductors lasers [83]. Instead, lasers with low linewidth plus high-speed digital signal processing are employed to perform phase and frequency tracking [83].

In the previous example, the electrical signal *s(t)* was modulated onto the in-phase component of the optical carrier. Note that *s(t)* could be both a baseband signal or a multicarrier signal with in-phase and quadrature components. Optical In-phase Quadrature (IQ) modulators also exist. In this case the I and Q signals are recovered with a more sophisticated coherent receiver called a *90º optical hybrid*, shown in Figure 1.12(b) [83]. The principle of operation and the difficulties are the same that have already been explained [83].

1.3.6 Other components

The available bandwidth in an optical fibre is huge; more than 4 THz only in the C band (1530-1565 nm). However, it is not possible to modulate any optical carrier with such a broadband electrical signal directly. WDM maximizes the spectral efficiency of the system by transmitting several optical carriers through the same fibre. In the transmitter it is necessary to couple a number of optical subchannels, while the receiver must separate the optical subchannels before photo detection.

WDM systems need optical couplers and filters to perform these tasks [85]. Arrayed Waveguide Gratings (AWG) split and recombine optical signals in such a way that can multiplex and demultiplex subchannels located at multiple wavelengths

[85]. Devices that can remove and incorporate particular subchannels in WDM signals, called add-drop multiplexers, are also important for flexible networking [28].

1.4 Electro-Optical Transceivers

Inside the network nodes, the electro-optical transceivers are the devices that perform the electrical and optical generation and reception of the information signals that travel through fibre. This section shows the blocks of a generic electro-optical transceiver, the spectra and multiplexing techniques in single carrier and multicarrier systems, and, finally, a comparison between IM/DD and coherent electro-optical transceivers.

Information can be analogue or digital. Analogue information can adopt infinite values inside its margins. In contrast, digital information can always be reduced to binary data: '1's and '0's. In any real communication link, the signals that travel through the transmission medium are always analogue, irrespective of whether the information that they contain is analogue or digital. When analogue information is employed, all the impairments accumulated in the transmission chain are present in the received signal. In contrast, digital links present an important advantage: the information that was transmitted is perfectly recovered if it is possible to discern the '1's and '0's in the receiver, despite the accumulated impairments. For compatibility with the powerful capabilities of digital processors and computers, practically all the information that is exchanged through optical fibre, is digital. An exception would be a legacy HFC CATV system that still transmits analogue video signals, although they tend to be substituted by digital video standards. This document focuses on digital electro-optical transceivers suitable for optical links that transmit digital data.

1.4.1 Block diagram

1.4.1.1 Basic modulation

The blocks that form the simplest digital electro-optical transmitters and receivers in a digital optical link are illustrated in Figure 1.13. A sequence of digital data $b[n]$ inside an electrical digital processor is converted into an analogue signal $s_i(t)$ that carries the digital data. This signal is modulated onto an optical carrier using an electro-optical converter (E/O), which can be composed of a laser or a laser plus an external modulator. The light is an electromagnetic wave, so that the signal at the input of the optical fibre can be represented by an electrical field $E_i(t)$, which is a

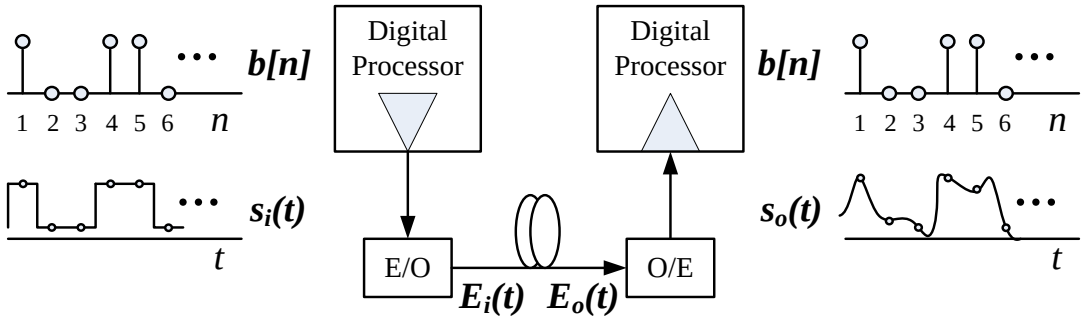

Figure 1.13 Basic digital optical link.

function of $s_i(t)$. After propagation, the electrical field at the other extreme is $E_o(t)$ and includes the impairments associated with the transmission. An opto-electronic converter (O/E), based on photo-detection, obtains $s_o(t)$ from $E_o(t)$. Consequently, $s_o(t)$ is an impaired version of $s_i(t)$. Provided the impairments do not prevent the comparator from discerning the two digital levels correctly, $b[n]$ is recovered free of errors.

1.4.1.2 Advanced modulation formats

To increase the spectral efficiency and the capacity of digital optical links, more sophisticated modulation schemes are required. Consequently, the modulating electrical signal $s_i(t)$ needs to be a more complicated mathematical function of several digital sequences. Depending on the method employed for the electrical processing, the transceivers can be classified into two groups: based on Digital Signal Processing (DSP) and based on Analogue Signal Processing (ASP). In many occasions, DSP plus ASP is performed in the transmitter and ASP plus DSP is performed in the receiver but, for simplicity, this analysis focuses on pure ASP or DSP implementations.

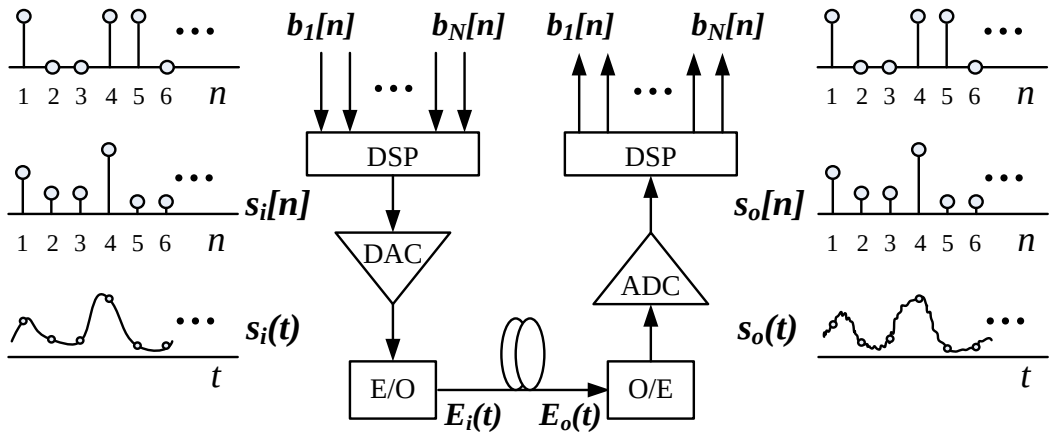

Figure 1.14 DSP based digital optical link.

The DSP based implementation is illustrated in Figure 1.14. N baseband sequences of bits are defined as $b_k[n]$, where k and n are integers that represent the number of the sequence and the position of the bit in the sequence respectively. DSP consists basically of delays, sums and multiplications involving $b_k[n]$, which produce a final sequence $s_i[n]$. A Digital to Analogue Converter (DAC) is required to obtain the analogue signal $s_i(t)$, from $s_i[n]$, that will be transmitted in the electrical field $E_i(t)$. The electrical receiver performs the opposite conversion. $s_o(t)$ is the impaired version of $s_i(t)$ obtained from $E_o(t)$. An Analogue to Digital Converter (ADC) produces the samples $s_o[n]$ that will be processed with DSP in order to recover the transmitted baseband data $b_k[n]$.

An ASP based system, illustrated in Figure 1.15, presents the following differences. The digital sequences $b_k[n]$ are sourced from an analogue interface that generates the equivalent analogue and temporal versions $b_{i,k}(t)$. The processing to generate the modulating signal $s_i(t)$ is performed with analogue devices. In a high frequency system these devices would be filters, phase shifters, combiners and mixers. In the receiver, impaired analogue versions of the digital signals $b_{o,k}(t)$ are obtained from $s_o(t)$ using ASP. Finally, N interfaces recover the original binary sequences $b_k[n]$.

The presented examples have been simplified with the use of only one signal $s(t)$. Note that in some occasions two signals, $s_I(t)$ and $s_Q(t)$, can be required to perform an IQ modulation of the optical carrier. However, the main concepts and ideas discussed earlier remain unaltered.

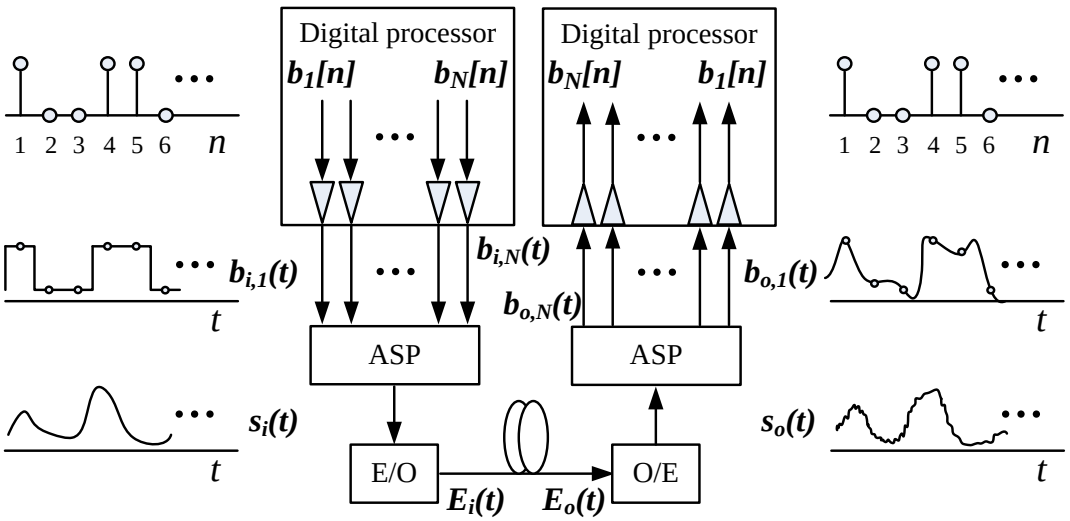

Figure 1.15 ASP based digital optical link.

Complicated mathematical functions can be implemented electronically with DSP or ASP. However, in practice, DSP and ASP configurations translate into major differences in the parameters that measure the performance of an electro-optical transceiver. DSP is powerful for compensating channel impairments and increasing the spectral efficiency, but power consumption increases linearly with the processing frequency [86], and latency is also high when complicated mathematical functions are implemented. On the other hand, for high capacity systems ASP requires broadband linear devices and is less flexible, but two major advantages are obtained: power consumption can be reduced to the amplification stages, and the latency is low. For most applications these two advantages are very important; low power consumption reduces the fixed operational cost of installed equipment, and low latency provides a high quality of service to the final customers. Potentially, ASP is much more power efficient than DSP [87]. For example, in the field of "machine learning", values of up to 1 TOPS/W (10^{12} operations per watt) have been achieved with ASP [88]. In contrast, modern supercomputers and highly-efficient DSP computing platforms present performances in the order of tens of GFLOPS/W (10^{9} floating-point operations per watt) [89, 90]. The previous examples implement massive parallel processing in a fully integrated only-analogue or only-digital solution and, as a consequence, the performance values are not directly applicable to communication schemes.

1.4.2 Single Carrier and Multicarrier Modulations

This section shows the different spectra that are obtained in digital electro-optical transceivers based on single carrier and multicarrier techniques. Then, for the purpose of multiuser applications, the associated (de)multiplexing schemes are discussed.

1.4.2.1 Spectra

All the schemes presented in section 1.4.1 are based on an information electrical signal *s(t)* that consists of digital data and is modulated onto an optical carrier forming an optical signal $E_s(t)$. Several combinations arise depending on the nature of *s(t)* and the modulation to the optical domain. The shapes of the spectra of all the possibilities that will be described are illustrated in Figure 1.16.

Firstly, the case of *s(t)* as a baseband digital AC signal is considered. Thus, *s(t)* can be a multilevel signal following a Pulse Amplitude Modulated (PAM) scheme. In its simplest case it would have two levels (PAM_2). This signal can be modulated onto the power of an optical carrier creating an IM/DD scheme [91]. Another possibility is to employ two baseband digital signals, $s_I(t)$ and $s_Q(t)$, to modulate the phase and the amplitude of the optical carrier with an IQ modulation [83, 92, 93]. Consequently with the phase modulation, a coherent detector is necessary. For both cases, considering standard Non Return to Zero (NRZ) pulses, the electrical spectra $|S(f)|$ and the optical spectra $|E(\lambda)|$ are illustrated in Figure 1.16. These spectra feature a sinc shape, sinc(x) = sin(x)/x, and only the main lobes are plotted in the figure. Note a symbol rate of *B* Gbaud is assumed. The only difference

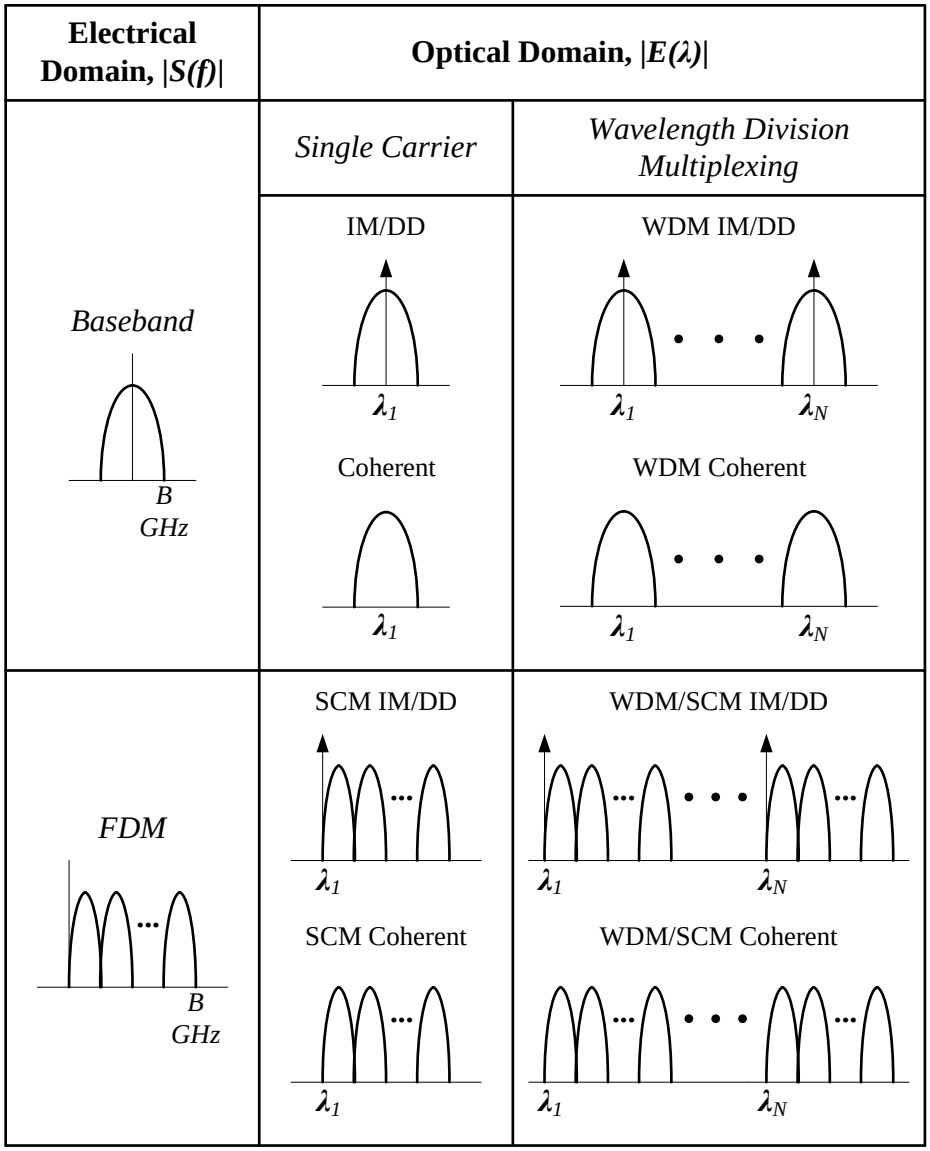

Figure 1.16 Spectra shapes of single carrier and multicarrier implementations.

in the spectra is the presence of the pilot optical tone at ω_c for the IM/DD case while it does not appear for the coherent scheme. In practice, some coherent systems also transmit a low power pilot tone to ease the phase recovery in the receiver [94].

Secondly, *s(t)* can also be an AC multicarrier Frequency Division Multiplexing (FDM) digital signal. When FDM is employed in the electrical domain, the resultant optical technique is referred to as Subcarrier Multiplexing (SCM). Regardless of whether *s(t)* presents IQ electrical subchannels or not, it can be modulated either in the power or in the amplitude-phase of an optical carrier generating an IM/DD [95-98] or a coherent [95, 99, 100] system respectively. Again, the only difference in the resultant spectra is the presence of the optical carrier for the IM/DD case. By default, Optical Double Side Band (ODSB) spectra are generated [101, 102], but OSSB is usually preferred and can be obtained by either optically filtering of one sideband [101, 102] or directly with more advanced configurations of signals and optical modulators [103] (discussed in the subsequent chapter). The spectra illustrated in Figure 1.16 reflect OSSB signals. Apart from the presented cases, there are two particular implementations of SCM that achieve higher spectral efficiency: OFDM, which transmits orthogonally overlapping subchannels [14, 15], and Nyquist SCM, which employs original baseband pulses that occupy a narrower spectrum [104].

Finally, a number of optical carriers can be modulated with any of the options described above, creating a WDM [12] or a WDM/SCM [105] signal. The associated spectra are also illustrated in Figure 1.16. There are also two particular implementations of WDM systems that increase the spectral efficiency by directly generating orthogonal optical WDM subchannels: All-optical OFDM [106] and Coherent WDM [107]. These implementations will be discussed in chapter 5.

All the described implementations can be combined with one technique that doubles the spectral efficiency, Polarization Division Multiplexing (PDM). Inside the fibre, the optical signal travels in a state of polarization or orientation of the electric field. It is possible to transmit two electrical fields in two SOPs orthogonal to each other. This technique is costly, but recently has been introduced in commercially available 100 (Gbit/s)/λ long-haul coherent transceivers [108]. The spectrum of the signal transmitted in every polarization would be equivalent to the ones presented in this section.

1.4.2.2 (De)/multiplexing

All the presented techniques can be applied to point to point links providing different advantages and disadvantages. Single carrier optics is simple but has low tolerance to dispersion and requires high-speed baseband signals. SCM reduces the rate of the baseband signals and is robust against dispersion, but requires more electronic components or processing blocks in the transmitter and the receiver. WDM multiplies the data rate of the link, but at the expense of costly and complicated transceivers. In all the combinations, the difference between IM/DD and coherent detection translates into a trade-off between shorter reach with lower cost and longer reach with higher cost.

For point to multipoint links, access to the medium can be provided with different methods employing single carrier and multicarrier optics. As mentioned in section 1.2.3.2, PONs are a real modern application where these techniques are implemented. Hence, the following examples will be particularised for PONs.

The most straightforward (de)/multiplexing approach is Time Division Multiplexing (TDM), as illustrated in Figure 1.5. In the downlink, the OLT transmits a baseband signal divided in different time slots that carry information for different users. The signal arrives to all the ONUs, and each one reads the data which was allocated for it. In the uplink the opposite procedure happens. The ONUs transmit baseband data in their associated time slots, and all the signals are multiplexed in the passive combiner before reaching the OLT. Although this technique is apparently simple, there are important challenges for the electronics in the uplink. As every ONU can be at a different length from the passive splitter/combiner, accurate synchronization and time guard intervals must be provided to avoid packet collisions. Apart from that, when the multiplexed signal arrives at the ONU, each part of the incoming signal can have a different amplitude so that gain equalization is also required [40, 109].

In standard TDM, data is allocated in time in the electrical domain before electrical-to-optical conversion. As a consequence, the electrical bandwidth is shared and electronic circuits limit the overall performance and the achievable data rate. Optical Time Division Multiplexing (OTDM) is a method that overcomes this electric limitation. An optical short pulse is generated periodically. Then, the optical pulse is replicated in several lines with a splitter and every optical pulse is modulated with different electrical signals. This parallelization allows for the maximization of

the electronic data rate in every subchannel. After the modulation, all the pulses suffer a different optical delay that avoids collisions after recombination. This method can achieve very high data rates but has important synchronization challenges and requires complicated receivers [1]. Currently, OTDM is an active research topic [110] but is not implemented in commercially available systems.

WDM and SCM can also be employed for the (de)/multiplexing of data as shown in Figure 1.17 for a WDM-PON and in Figure 1.18 for a SCM-PON. In this case a spectral optical bandwidth or subchannel is allocated for every ONU. For the downstream, the OLT modulates the data for every ONU at a different subchannel. The multiplex is then replicated in the splitter and every ONU filters and demodulates the data that is allocated in its associated spectrum. For the uplink, each ONU modulates its data in its frequency band and the combiner multiplexes all the optical frequencies in the same signal that travels to the OLT. This technique establishes independent channels between the OLT and the ONUs. Schematically, the application of both WDM and SCM looks similar although the optical and electronic implementation is substantially different. WDM assigns a different

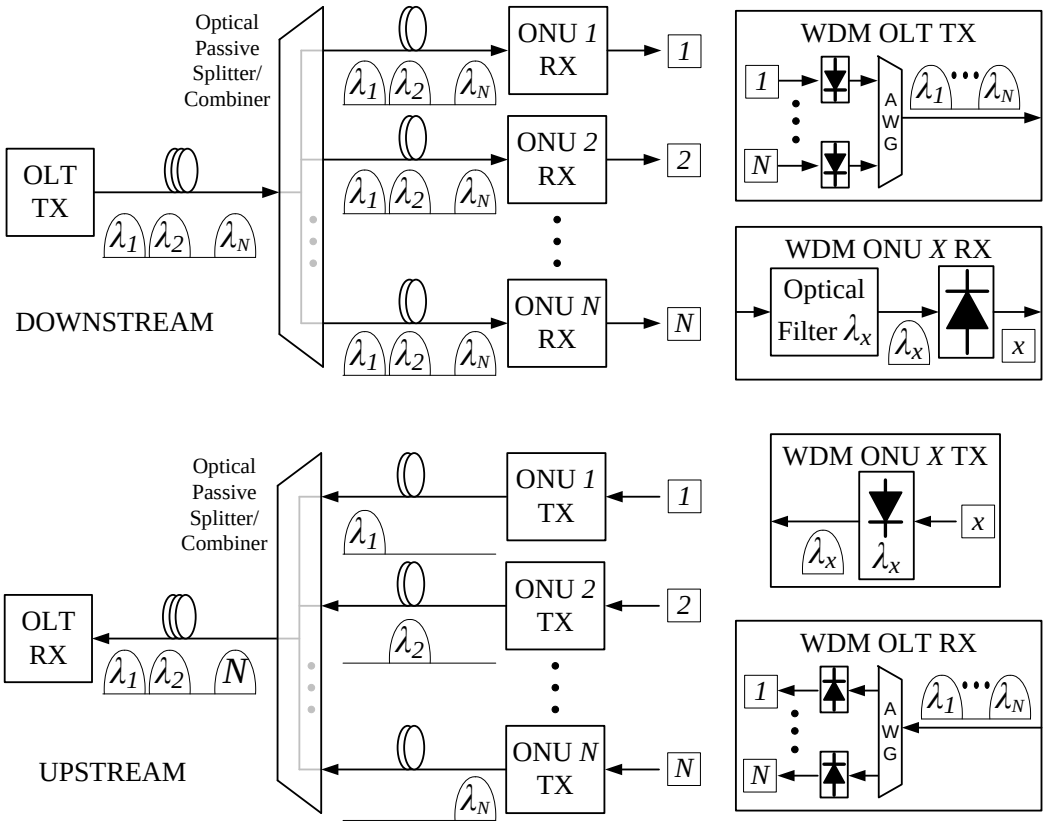

Figure 1.17 WDM PON.

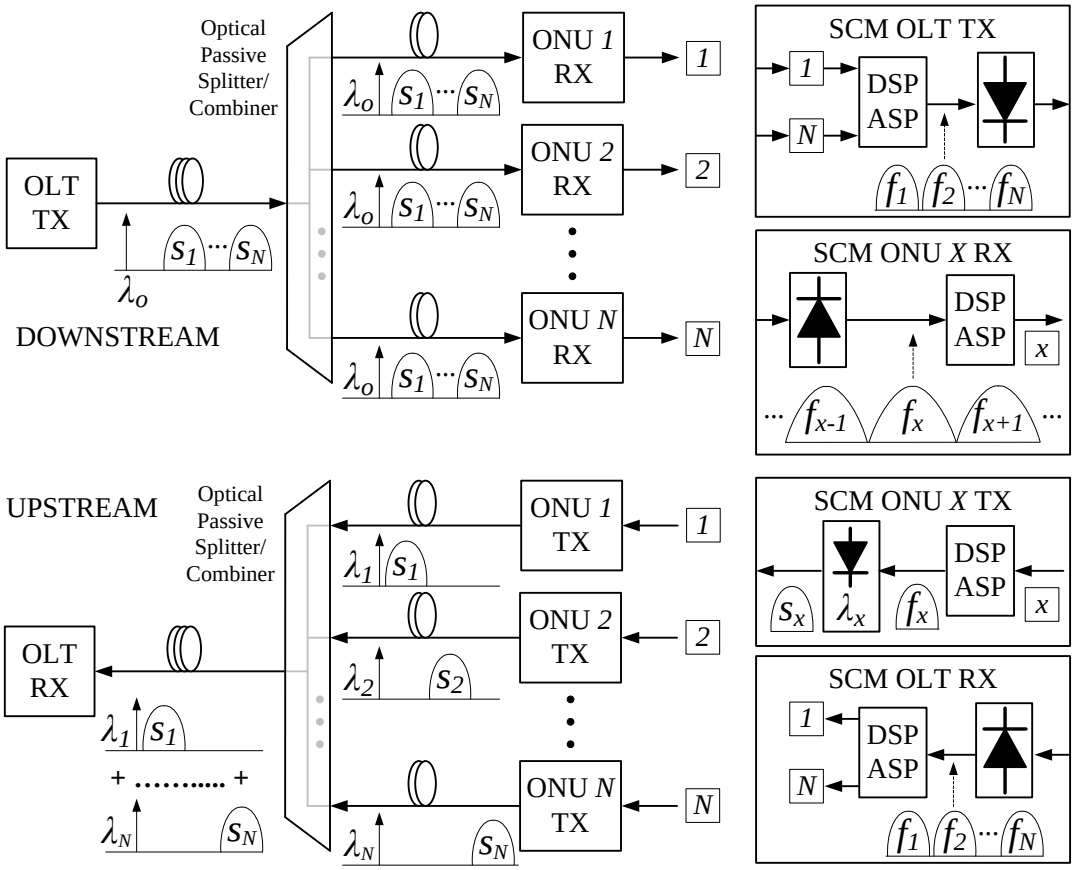

Figure 1.18 SCM PON

wavelength to every subchannel while SCM employs a different subcarrier for every subchannel. Thus, SCM simplifies the optical scheme and avoids the tunable optical filters and AWGs that are necessary for WDM access. However, SCM also presents drawbacks. The main one arises because the *N* independent optical signals that are multiplexed in the uplink are photo-detected simultaneously. As a consequence, the photodetector at the OLT produces increased electrical noise due to the optical beating of the components coming from *N* independent lasers [40, 111]. Finally, it should be remarked that SCM and WDM can be combined in the same PON obtaining a higher number of subchannels with finer granularity [112].

1.4.3 Optical Modulation and Detection

The most relevant figures of merit of digital electro-optical transceivers can be reduced to: data rate, reach or sensitivity, power consumption, latency and cost. All these features are intimately related to the method employed for the modulation and the detection of the optical signal. This section summarizes the main properties of IM/DD and coherent techniques and discusses their implications in electro-optical transceivers.

1.4.3.1 Intensity Modulation / Direct Detection

An AC signal *s(t)* can be modulated onto the power of an optical carrier directly with lasers (section 1.3.1.2) or with external modulators (section 1.3.2). Considering $\varphi_c(t)$ is the phase noise in a laser with frequency ω_c, the transmitted electrical field can be written in the form:

$$E(t) = \sqrt{2\left(P_b + s(t)\right)}\cos\left(\omega_c t + \varphi_c(t)\right) = a(t)\cdot\cos\left(\omega_c t + \varphi_c(t)\right). \qquad (1.20)$$

P_b represents the bias power of the electro-optical converter. *E(t)* can be seen as an envelope signal *a(t)* (with DC and AC components) that multiplies the optical carrier, as it is shown in Figure 1.19. Note that even in high-speed systems, *a(t)* varies much more slowly (GHz) than ω_c (hundreds of THz), so that the relation of cycles shown in the picture is only illustrative. A photodetector obtains the average power of the electrical field for the optical frequencies and, for a responsivity *R*, the detected photocurrent is:

$$I(t) = R\left\langle E^2(t)\right\rangle = 2R\left(P_b + s(t)\right)\left\langle\frac{1+\cos\left(2\omega_c t + 2\varphi_c(t)\right)}{2}\right\rangle = R\left(P_b + s(t)\right). \qquad (1.21)$$

s(t) is recovered and several statements can be made for this technique. The information is transmitted in the envelope of the electric field and, as consequence, *a(t)* cannot change its sign without incurring distortion. Apart from that, power is wasted in the transmission of an unmodulated optical carrier. In contrast, the

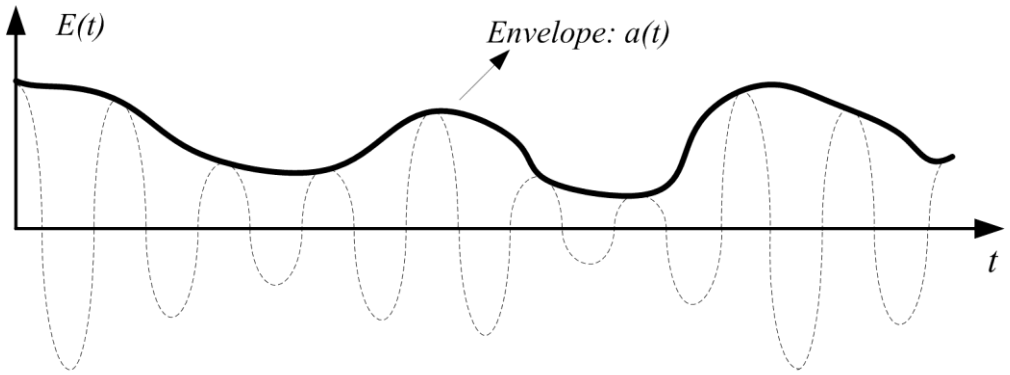

Figure 1.19 Example of the electrical field in a IM/DD system.

presence of this pilot tone eases the demodulation: as the instant phase of the carrier is transmitted, the square law detector obtains the squared envelope independently of the phase noise $\varphi_c(t)$. Hence, lower cost lasers with higher linewidths can be used in IM/DD systems.

1.4.3.2 Phase Modulation / Coherent Detection

The phase and the amplitude of an optical carrier can be modulated with phase modulators or with MZMs (see section 1.3.2.2). The simplest phase modulation scheme, Binary Phase Shift Keying (BPSK), will be employed as an example. A BPSK modulated optical carrier at a frequency ω_c and with a phase noise $\varphi_c(t)$ can be represented in two ways:

$$\begin{aligned} E(t) &= s(t)\cdot\cos\left(\omega_c t+\varphi_c(t)\right). \\ E(t) &= \cos\left(\omega_c t+\theta_s(t)+\varphi_c(t)\right). \end{aligned} \tag{1.22}$$

In the first representation, the transmitted AC signal $s(t)$ can take two values (+1,-1) that in the second representation transform into (0,π) for $\theta_s(t)$. An illustrative example of a possible electrical field for this modulation is presented in Figure 1.20. From section 1.3.5.3, a balanced coherent photodetector is required to recover the data. Using an LO laser at ω_{LO} with a phase noise $\varphi_{LO}(t)$, the detected photocurrent depends on several factors apart from the transmitted phase $\theta_s(t)$:

$$I(t) = f\left(\theta_s(t),(\omega_c-\omega_{LO}),\varphi_c(t),\varphi_{LO}(t)\right). \tag{1.23}$$

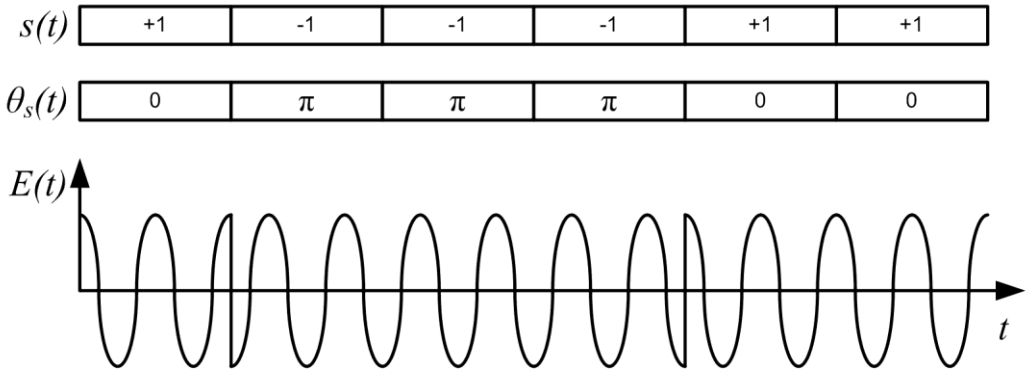

Figure 1.20 Example of the electrical field in a coherent system.

Several statements can also be made for this technique. The transmitted signal does not waste any power in an unmodulated carrier, which translates into lower sensitivity in the receiver or longer reach. As a pilot tone with the phase of the original laser is not transmitted, this phase has to be estimated in the receiver. Expensive lasers with low phase and frequency noise are necessary to guarantee that this estimation is possible. In any case, high-speed signal processing, typically DSP, is required for the phase estimation and correction, translating into higher power consumption and latency.

1.5 Conclusions and Scope

Optical communications surpassed the limited data rates of electrical systems and made possible the development of the Internet. Currently, all high-capacity networks employ optical systems regardless of their reach and purpose.

The devices that carry out the interface between the electrical and optical domains are called electro-optical transceivers. These key components can adopt a number of forms and characteristics depending on the network where they are deployed. The signals, modulations, and processing techniques that they employ, must be carefully selected to meet the requirements of a given subsystem.

Communications industry decisions are fundamentally cost driven. Consequently, IM/DD solutions based on low cost lasers and photodetectors are preferred and widely employed in short range systems, while the use of more expensive MZMs with direct or coherent detection is reserved at the moment for long distances.

New advances suggest that the current trends can be potentially modified. Namely, the advances in silicon optical modulators guarantee the development and future proliferation of low-cost high-performance optical modulators [113]. Some promising optical techniques like coherent WDM or all-optical OFDM rely on complicated implementations with immature optical components and, consequently, remain as important research topics but impractical for real deployment. Unlike them, the presence of low-cost optical MZMs and its combination with mature electronic circuits and processing, advance a revolution in real and practical solutions.

In this foreseen scenario, some techniques can be identified as candidates to offer unique solutions. Namely, IM/DD SCM systems can prove to be relevant for

several applications. SCM had been previously discouraged for low-cost low-range electro-optical transceivers due to the typical higher bandwidth that was required, usually not compatible with low-cost lasers. For these systems, once lower cost MZMs are a reality, SCM can improve the tolerance to dispersion increasing the overall bitrate with respect to single carrier solutions. Moreover, for medium distances, like access or metro networks, IM/DD SCM has always been a competitive solution that now can be emphasized with lower cost optical modulators.

The aforementioned solutions rely mostly on electronic signal processing, like the vast majority of electro-optical transceivers deployed in practical applications. While DSP based techniques provide unique possibilities, their higher power consumption and latency make them prohibitive in some subsystems. Apart from that, when very high-speed processing is required, ADCs and DACs are unavoidably expensive. For that reason, research on ASP based systems is necessary in order to exploit the possibilities of low power consumption and low latency processing. Moreover, the development of Monolithic Microwave Integrated Circuit (MMIC) technology [114] currently provides low-cost integrated circuits at microwave frequencies, which reduces drastically the cost of high-speed ASP.

This thesis focuses on ASP based IM/DD SCM broadband electro-optical transceivers, as they present low cost, high tolerance to dispersion, and real possibilities of spreading the range of applications where they are deployed. Several key advances in the state of the art are presented. Firstly, OSSB implementations based on optical IQ modulators are analysed in detail to obtain the best trade-off between nonlinearities and maximum reach. Secondly, it is proved that OFDM modulation, a popular technique in DSP solutions, can also be applied to broadband ASP systems increasing substantially the spectral efficiency. Finally, the application of the developed techniques in spectrally efficient WDM/SCM systems with tightly allocated OSSB channels is presented. A low-cost approach that does not require an optical filter for every WDM channel in the transmitter is employed.

All the experiments were conducted emphasizing the feasibility of the proposed solutions. Modern current research often relies on offline processing. It assumes that the desired components can be potentially implemented and perform all the processing at the desired speeds. In contrast, this thesis shows experiments running in real-time and, more importantly, relying largely on off-the-shelf components.

1.6 References

[1] G. P. Agrawal, *Fiber-Optic Communication Systems*, 3rd ed.: Wiley, 2002.

[2] T. H. Maiman, "Stimulated Optical Radiation in Ruby," *Nature*, vol. 187, pp. 493-494, 08/06/print 1960.

[3] K. C. Kao and G. A. Hockham, "Dielectric-fibre surface waveguides for optical frequencies," *Electrical Engineers, Proceedings of the Institution of*, vol. 113, pp. 1151-1158, 1966.

[4] I. Hayashi, M. B. Panish, P. W. Foy, and S. Sumski, "Junction Lasers which Operate Continuously at Room Temerature," *Applied Physics Letters*, vol. 17, pp. 109-111, 1970.

[5] F. P. Kapron, D. B. Keck, and R. D. Maurer, "Radiation Losses in Glass Optical Waveguides," *Applied Physics Letters*, vol. 17, pp. 423-425, 1970.

[6] R. J. Sanferrare, "Terrestrial lightwave systems," *AT&T Technical Journal*, vol. 66, pp. 95-107, 1987.

[7] J. I. Yamada, S. Machida, and T. Kimura, "2 Gbit/s optical transmission experiments at 1.3 um with 44 km single-mode fibre," *Electronics Letters*, vol. 17, pp. 479-480, 1981.

[8] T. Miya, Y. Terunuma, T. Hosaka, and T. Miyashita, "Ultimate low-loss single-mode fibre at 1.55 um," *Electronics Letters*, vol. 15, pp. 106-108, 1979.

[9] A. H. Gnauck, B. Kasper, R. A. Linke, R. Dawson, T. L. Koch, T. J. Bridges, *et al.*, "4-Gbit/s transmission over 103 km of optical fiber using a novel electronic multiplexer/demultiplexer," *Lightwave Technology, Journal of*, vol. 3, pp. 1032-1035, 1985.

[10] N. S. Bergano, J. Aspell, C. R. Davidson, P. R. Trischitta, B. M. Nyman, and F. W. Kerfoot, "Bit error rate measurements of 14000 km 5 Gbit/s fibre-amplifier transmission system using circulating loop," *Electronics Letters*, vol. 27, pp. 1889-1890, 1991.

[11] T. Otani, K. Goto, H. Abe, M. Tanaka, H. Yamamoto, and H. Wakabayashi, "5.3 Gbit/s 11300 km data transmission using actual submarine cables and repeaters," *Electronics Letters*, vol. 31, pp. 380-381, 1995.

[12] G. Vareille, F. Pitel, and J. F. Marcerou, "3 Tbit/s (300/spl times/11.6Gbit/s) transmission over 7380 km using C+L band with 25GHz channel spacing and NRZ format," in *Optical Fiber Communication Conference and Exhibit, 2001. OFC 2001*, 2001, pp. PD22-PD22.

[13] P. J. Winzer and R. J. Essiambre, "Advanced Modulation Formats for High-Capacity Optical Transport Networks," *Lightwave Technology, Journal of*, vol. 24, pp. 4711-4728, 2006.

[14] J. Armstrong, "OFDM for Optical Communications," *Lightwave Technology, Journal of*, vol. 27, pp. 189-204, 2009.

[15] W. Shieh, H. Bao, and Y. Tang, "Coherent optical OFDM: theory and design," *Optics Express*, vol. 16, pp. 841-859, 2008/01/21 2008.

[16] R. A. Linke and A. H. Gnauck, "High-capacity coherent lightwave systems," *Lightwave Technology, Journal of*, vol. 6, pp. 1750-1769, 1988.

[17] A. D. Ellis, Z. Jian, and D. Cotter, "Approaching the Non-Linear Shannon Limit," *Lightwave Technology, Journal of*, vol. 28, pp. 423-433, 2010.

[18] H. Masuda, E. Yamazaki, A. Sano, T. Yoshimatsu, T. Kobayashi, E. Yoshida, *et al.*, "13.5-Tb/s (135x111-Gb/s/ch) no-guard-interval coherent OFDM transmission over 6,248 km using SNR maximized second-order DRA in the extended L-band," in *OFC 2009*, 2009, pp. 1-3.

[19] K. Igarashi, T. Tsuritani, I. Morita, and M. Suzuki, "Ultra-Long-Haul High-Capacity Super-Nyquist-WDM Transmission Experiment Using Multi-Core Fibers," *Lightwave Technology, Journal of*, vol. 33, pp. 1027-1036, 2015.

[20] L. Kleinrock, "History of the Internet and its flexible future," *Wireless Communications, IEEE*, vol. 15, pp. 8-18, 2008.
[21] D. Abensour, "High speed networking evolution," in *Distributed Computing Systems, 1990. Proceedings., Second IEEE Workshop on Future Trends of*, 1990, pp. 238-244.
[22] Cisco. *Visual Networking Index*. Available: http://www.cisco.com/c/en/us/solutions/service-provider/visual-networking-index-vni/index.html
[23] R. Khan, S. U. Khan, R. Zaheer, and S. Khan, "Future Internet: The Internet of Things Architecture, Possible Applications and Key Challenges," in *Frontiers of Information Technology (FIT), 2012 10th International Conference on*, 2012, pp. 257-260.
[24] R. Essiambre and R. W. Tkach, "Capacity Trends and Limits of Optical Communication Networks," *Proceedings of the IEEE*, vol. 100, pp. 1035-1055, 2012.
[25] M. N. Islam, "Raman amplifiers for telecommunications," *Selected Topics in Quantum Electronics, IEEE Journal of*, vol. 8, pp. 548-559, 2002.
[26] L. Grüner-Nielsen, S. N. Knudsen, B. Edvold, T. Veng, D. Magnussen, C. C. Larsen, *et al.*, "Dispersion compensating fibers," *Optical Fiber Technology*, vol. 6, pp. 164-180, 2000.
[27] I. Djorjevic, *Coding for Optical Channels*: Springer, 2010.
[28] R. Ramaswami, *Optical Networks: A Practical Perspective*, Third Edition ed.: Morgan Kaufmann, 2010.
[29] ITU, "G.709: Interfaces for the optical transport network," ed.
[30] Telecommunication Cable Solutions: Submarine Systems by NEC Corporation [Online]. Available: http://www.nec.com/en/global/prod/nw/submarine/pdf/submarine-brochure.pdf
[31] (2013). *Metro Network Traffic Growth: An Architecture Impact Study. Strategic White Paper. (Bell Labs ed.)*. Available: http://resources.alcatel-lucent.com/asset/171568
[32] A. Stavdas, *Core and Metro Networks*: Wiley, 2010.
[33] Metro Wavelength Division Multiplexing System. Spectral Wave MW1000 by NEC Corporation [Online]. Available: http://de.nec.com/de_DE/en/global/solutions/nsp/trans_port/wdm/brochures/MW1000.pdf
[34] ITU, "G.992.5 : Asymmetric digital subscriber line 2 transceivers (ADSL2)-Extended bandwidth ADSL2 (ADSL2plus)," ed.
[35] J. A. Vaughan, "The use of fiber optics in cable communications networks," *Lightwave Technology, Journal of*, vol. 11, pp. 154-166, 1993.
[36] CableLabs, "DOCSIS 3.1," ed, 2015.
[37] H. Ibl and C. Klaus. (2015), Application Note 7MH89: DOCSIS 3.1.
[38] ITU, "G.984.1 : Gigabit-capable passive optical networks (GPON): General characteristics," ed.
[39] ITU, "G.987 : 10-Gigabit-capable passive optical network (XG-PON) systems: Definitions, abbreviations and acronyms," ed.
[40] L. Chang-Hee, W. V. Sorin, and K. Byoung Yoon, "Fiber to the Home Using a PON Infrastructure," *Lightwave Technology, Journal of*, vol. 24, pp. 4568-4583, 2006.
[41] ITU, "G.989.1 : 40-Gigabit-capable passive optical networks (NG-PON2): General requirements," ed.
[42] A. Ng'oma, *Radio-over-fibre technology for broadband wireless communication systems*: Technische Universiteit Eindhoven, 2005.
[43] H. Kao-Cheng and W. Zhaocheng, "Terahertz Terabit Wireless Communication," *Microwave Magazine, IEEE*, vol. 12, pp. 108-116, 2011.
[44] C. H. Cox, *Analog optical links: theory and practice*: Cambridge University Press, 2006.

[45] E. I. Ackerman and C. H. Cox, "RF fiber-optic link performance," *Microwave Magazine, IEEE,* vol. 2, pp. 50-58, 2001.
[46] D. Novak, R. B. Waterhouse, A. Nirmalathas, C. Lim, P. A. Gamage, T. R. Clark, *et al.*, "Radio-Over-Fiber Technologies for Emerging Wireless Systems," *Quantum Electronics, IEEE Journal of,* vol. 52, pp. 1-11, 2016.
[47] C.-H. Yao and X. Cheng, "Research of CPRI Protocol Based on High-Speed Fiber Link," in *Information Technology and Computer Science (ITCS), 2010 Second International Conference on*, 2010, pp. 336-339.
[48] A. de la Oliva, J. A. Hernández, D. Larrabeiti, and A. Azcorra, "An overview of the CPRI specification and its application to C-RAN based LTE scenarios," *Communications Magazine, IEEE,* 2015.
[49] IEEE. *IEEE 802.3 Ethernet Working Group*. Available: http://www.ieee802.org/3/
[50] J. E. McNamara, *Local area networks: an introduction to the technology*: Elsevier, 2014.
[51] D. Law, D. Dove, J. D'Ambrosia, M. Hajduczenia, M. Laubach, and S. Carlson, "Evolution of ethernet standards in the IEEE 802.3 working group," *Communications Magazine, IEEE,* vol. 51, pp. 88-96, 2013.
[52] C. Kachris and I. Tomkos, "A Survey on Optical Interconnects for Data Centers," *Communications Surveys & Tutorials, IEEE,* vol. 14, pp. 1021-1036, 2012.
[53] S. K. Coulter and J. E. Martinez, "Introduction to InfiniBand," *Los Alamos National Laboratory,* pp. LA-UR-15-24640, 2015.
[54] *Technical Committee T11 responsible for Fibre Channel Interfaces. (InterNational Committee for Information Technology Standards ed.)*. Available: http://www.t11.org/index.html
[55] E. Mentovich, "Optical Interconnect Technology for Next Generation Servers," in *European Conference on Optical Communications (ECOC)*, Valencia, 2015.
[56] A. Martin, "Overcoming the alphabet soup of form factors with 100G QSFP28," in *The Lightwave Guest Blog*, ed, 2014.
[57] J. C. Maxwell, *A treatise on electricity and magnetism*: Clarendon press, 1881.
[58] W. W. Chow and S. W. Koch, *Semiconductor-laser fundamentals: physics of the gain materials*: Springer Science & Business Media, 2013.
[59] A. L. Schawlow and C. H. Townes, "Infrared and optical masers," *Physical Review,* vol. 112, p. 1940, 1958.
[60] G. P. Agrawal, "Noise in semiconductor lasers and its impact on optical communication systems," in *Boston-DL tentative*, 1991, pp. 224-235.
[61] T. L. Koch and J. E. Bowers, "Nature of wavelength chirping in directly modulated semiconductor lasers," *Electronics Letters,* vol. 20, pp. 1038-1040, 1984.
[62] S. Lindgren, H. Ahlfeldt, L. Backlin, L. Forssen, C. Vieider, H. Elderstig, *et al.*, "24-GHz modulation bandwidth and passive alignment of flip-chip mounted DFB laser diodes," *Photonics Technology Letters, IEEE,* vol. 9, pp. 306-308, 1997.
[63] H. Bulow, F. Buchali, and A. Klekamp, "Electronic Dispersion Compensation," *Journal of Lightwave Technology,* vol. 26, pp. 158-167, 2008.
[64] G. L. Li and P. K. L. Yu, "Optical intensity modulators for digital and analog applications," *Lightwave Technology, Journal of,* vol. 21, pp. 2010-2030, 2003.
[65] Y. Cheng, P. Jiaoqing, W. Yang, F. Zhou, W. Baojun, L. Zhao, *et al.*, "40-Gb/s Low Chirp Electroabsorption Modulator Integrated With DFB Laser," *Photonics Technology Letters, IEEE,* vol. 21, pp. 356-358, 2009.
[66] C. J. Peters, "Gigacycle bandwidth coherent light traveling-wave phase modulator," *Proceedings of the IEEE,* vol. 51, pp. 147-153, 1963.
[67] K. Zetie, S. Adams, and R. Tocknell, "How does a Mach-Zehnder interferometer work?," *Physics Education,* vol. 35, p. 46, 2000.
[68] H. Ito, Y. Ogawa, and H. Inaba, "Integrated bistable optical device using mach-zehnder interferometric optical waveguide," *Electronics Letters,* vol. 15, pp. 283-285, 1979.

[69] W. Wang, Y. Shi, D. J. Olson, W. Lin, and J. H. Bechtel, "Push-pull poled polymer Mach-Zehnder modulators with a single microstrip line electrode," *Photonics Technology Letters, IEEE,* vol. 11, pp. 51-53, 1999.
[70] W. I. Way, *Broadband Hybrid Fiber Coax Access System Technologies*: Academic Press, Inc., 1998.
[71] F. Koyama and K. Iga, "Frequency chirping in external modulators," *Lightwave Technology, Journal of,* vol. 6, pp. 87-93, 1988.
[72] E. F. Schubert, T. Gessmann, and J. K. Kim, *Light emitting diodes*: Wiley Online Library, 2005.
[73] C. A. Ohashi, "Optical fibers: History and future perspectives," in *OptoElectronics and Communications Conference (OECC), 2010 15th*, 2010, pp. 34-35.
[74] T. Kimura, "Single-mode digital transmission technology," *Proceedings of the IEEE,* vol. 68, pp. 1263-1268, 1980.
[75] D. Marcuse and C. Lin, "Low dispersion single-mode fiber transmission - The question of practical versus theoretical maximum transmission bandwidth," *Quantum Electronics, IEEE Journal of,* vol. 17, pp. 869-878, 1981.
[76] S. Ten and M. Edwards, "An Introduction to the Fundamentals of PMD in Fibers," *white paper, avaiable from:< www. corning. com/WorkArea/downloadasset. aspx,* 2006.
[77] G. P. Agrawal, *Nonlinear fiber optics*: Academic press, 2007.
[78] M. J. Connelly, *Semiconductor optical amplifiers*: Springer Science & Business Media, 2007.
[79] M. Norouzi, P. Badeka, P. Chahande, and B. Briley, "A survey on rare earth doped optical fiber amplifiers," in *Electro/Information Technology (EIT), 2013 IEEE International Conference on*, 2013, pp. 1-11.
[80] J. Wilson and J. F. Hawkes, "Optoelectronics-an introduction," 1989.
[81] P. M. Becker, A. A. Olsson, and J. R. Simpson, *Erbium-doped fiber amplifiers: fundamentals and technology*: Academic press, 1999.
[82] S. Parker and P. Shastry, "Transimpedance amplifiers for optoelectronic applications," *IEEE Microwave Magazine,* vol. 2, pp. 52-62, 2001.
[83] K. Kikuchi, "Fundamentals of Coherent Optical Fiber Communications," *Journal of Lightwave Technology,* vol. 34, pp. 157-179, 2016.
[84] S. Norimatsu, K. Iwashita, and K. Sato, "PSK optical homodyne detection using external cavity laser diodes in Costas loop," *IEEE Photonics Technology Letters,* vol. 2, pp. 374-376, 1990.
[85] T. Miki and H. Ishio, "Viabilities of the Wavelength-Division-Multiplexing Transmission System Over an Optical Fiber Cable," *Communications, IEEE Transactions on,* vol. 26, pp. 1082-1087, 1978.
[86] A. P. Chandrakasan and R. W. Brodersen, *Low power digital CMOS design*: Springer Science & Business Media, 2012.
[87] R. Sarpeshkar, "Analog versus digital: extrapolating from electronics to neurobiology," *Neural computation,* vol. 10, pp. 1601-1638, 1998.
[88] L. Junjie, S. Young, I. Arel, and J. Holleman, "A 1 TOPS/W Analog Deep Machine-Learning Engine With Floating-Gate Storage in 0.13 um CMOS," *Solid-State Circuits, IEEE Journal of,* vol. 50, pp. 270-281, 2015.
[89] F. Nielsen, "A Glance at High Performance Computing (HPC)," in *Introduction to HPC with MPI for Data Science*, ed Cham: Springer International Publishing, 2016, pp. 3-20.
[90] A. Olofsson, T. Nordstrom, and Z. Ul-Abdin, "Kickstarting high-performance energy-efficient manycore architectures with Epiphany," in *Signals, Systems and Computers, 2014 48th Asilomar Conference on*, 2014, pp. 1719-1726.
[91] F. Karinou, C. Prodaniuc, N. Stojanovic, M. Ortsiefer, A. Daly, R. Hohenleitner, *et al.*, "Directly PAM-4 Modulated 1530-nm VCSEL Enabling 56 Gb/s/λ Data-Center Interconnects," *IEEE Photonics Technology Letters,* vol. 27, pp. 1872-1875, 2015.

[92] D. S. Ly-Gagnon, S. Tsukamoto, K. Katoh, and K. Kikuchi, "Coherent detection of optical quadrature phase-shift keying signals with carrier phase estimation," *Journal of Lightwave Technology*, vol. 24, pp. 12-21, 2006.

[93] M. Seimetz, "Multi-format transmitters for coherent optical M-PSK and M-QAM transmission," in *Transparent Optical Networks, 2005, Proceedings of 2005 7th International Conference*, 2005, pp. 225-229 Vol. 2.

[94] M. Yoshida, H. Goto, K. Kasai, and M. Nakazawa, "64 and 128 coherent QAM optical transmission over 150 km using frequency-stabilized laser and heterodyne PLL detection," *Optics Express*, vol. 16, pp. 829-840, 2008/01/21 2008.

[95] S. Watanabe, T. Terahara, I. Yokota, T. Naito, T. Chikama, and H. Kuwahara, "Optical coherent broad-band transmission for long-haul and distribution systems using subcarrier multiplexing," *Journal of Lightwave Technology*, vol. 11, pp. 116-127, 1993.

[96] T. E. Darcie and G. E. Bodeep, "Lightwave subcarrier CATV transmission systems," *Microwave Theory and Techniques, IEEE Transactions on*, vol. 38, pp. 524-533, 1990.

[97] J. M. P. Delavaux, G. C. Wilson, C. Hullin, B. Neyret, and C. Bethea, "QAM-PON and super PON for access distribution networks," in *Optical Fiber Communication Conference and Exhibit, 2001. OFC 2001*, 2001, pp. WN2-WN2.

[98] P. Hill and R. Olshansky, "Bandwidth efficient transmission of 4 Gb/s on two microwave QPSK subcarriers over a 48 km optical link," *Photonics Technology Letters, IEEE*, vol. 2, pp. 510-512, 1990.

[99] L. Yang-Han, W. Jingshown, and T. Hen-Wai, "The impact of laser phase noise on the coherent subcarrier multiplexing system," *Journal of Lightwave Technology*, vol. 9, pp. 347-355, 1991.

[100] B. E. Olsson, A. Djupsj, x00F, backa, M. J, x00E, *et al.*, "112 Gbit/s RF assisted dual carrier DP-16-QAM transmitter using optical phase modulator," in *Optical Communication (ECOC), 2011 37th European Conference and Exhibition on*, 2011, pp. 1-3.

[101] B. E. Olsson, A. Kristiansson, and A. Alping, "40 Gbit/s, 16-QAM, transmission utilizing electronic sub-carrier technique and direct detection reception," in *Communications and Photonics Conference and Exhibition (ACP), 2009 Asia*, 2009, pp. 1-2.

[102] B. Olsson, J. Martensson, A. Kristiansson, and A. Alping, "RF-assisted optical dual-carrier 112 Gbit/s polarization-multiplexed 16-QAM transmitter," in *Optical Fiber Communication (OFC), collocated National Fiber Optic Engineers Conference, 2010 Conference on (OFC/NFOEC)*, 2010, pp. 1-3.

[103] R. Hui, Z. Benyuan, H. Renxing, C. T. Allen, K. Demarest, and D. Richards, "Subcarrier multiplexing for high-speed optical transmission," *Lightwave Technology, Journal of*, vol. 20, pp. 417-427, 2002.

[104] A. S. Karar and J. C. Cartledge, "Generation and Detection of a 56 Gb/s Signal Using a DML and Half-Cycle 16-QAM Nyquist-SCM," *IEEE Photonics Technology Letters*, vol. 25, pp. 757-760, 2013.

[105] C. Kottke, K. Habel, M. Eiselt, H. Grie, x00Df, er, *et al.*, "Coherent Subcarrier-WDM-PON system with SSB modulation and wavelength reuse," in *Optical Fiber Communication Conference and Exposition and the National Fiber Optic Engineers Conference (OFC/NFOEC), 2013*, 2013, pp. 1-3.

[106] J. K. K. Rhee, S. J. Lim, and M. Kserawi, "All optical OFDM transmission systems," in *Communications and Photonics Conference and Exhibition, 2011. ACP. Asia*, 2011, pp. 1-6.

[107] A. D. Ellis and F. C. G. Gunning, "Spectral density enhancement using coherent WDM," *IEEE Photonics Technology Letters*, vol. 17, pp. 504-506, 2005.

[108] S. Yamanaka, H. Uzawa, T. Ohara, T. Saida, T. Akashi, K. Mori, *et al.*, "100 Gb/s CFP coherent transceiver enabled by power-optimized DSP," *Proc. OECC, THPDP1-4, Melbourne*, 2014.

[109] X. Z. Qiu, C. Melange, T. D. Ridder, B. Baekelandt, J. Bauwelinck, X. Yin, *et al.*, "Evolution of burst mode receivers," in *Optical Communication, 2009. ECOC '09. 35th European Conference on*, 2009, pp. 1-4.

[110] H. N. Tan, T. Inoue, T. Kurosu, and S. Namiki, "Wavelength Translation of Dual-Polarization Phase-Modulated Nyquist OTDM at Terabit/s," *Journal of Lightwave Technology*, vol. 34, pp. 633-642, 2016/01/15 2016.

[111] H.-D. Jung, Y.-Y. Won, and S.-K. Han, "Optical beat noise reduction in WDM-SCM access networks using modulated optical pulse train," *Photonics Technology Letters, IEEE*, vol. 17, pp. 2215-2217, 2005.

[112] S. B. Weinstein and T. Wang, *Passive Optical Networks: Enhancing the Last Mile Access* vol. 1: John Wiley & Sons, 2010.

[113] G. T. Reed, G. Mashanovich, F. Gardes, and D. Thomson, "Silicon optical modulators," *Nature photonics*, vol. 4, pp. 518-526, 2010.

[114] I. D. Robertson and S. Lucyszyn, *RFIC and MMIC Design and Technology*: Iet, 2001.

Chapter 2

2 Subcarrier Multiplexing

The term subcarrier multiplexing (SCM) refers to a technique usually employed in electro-optical transceivers. It consists of the generation of a multicarrier electrical signal that is modulated onto an optical carrier. In the receiver, after photo-detection, every subchannel must be demodulated independently with electrical processing. This chapter discusses general concepts of SCM: applications, electrical and optical processing, and tolerance to impairments. The context and the main focus of this thesis are emphasized, along with several concepts that are identified as key ideas to advance in the state of the art. Finally, the experimental testbed that was developed implementing these ideas is thoroughly described. This setup represents the starting point that gave rise to the measurements and experiments that will be described in the following chapters.

2.1 Range of Applications

This section briefly reviews the applications where SCM has been implemented with both industrial products and research approaches. According to the main focus of this thesis, a particular implementation based on optical modulators is identified as the established state of the art. Several ideas and concepts will be discussed to upgrade the functionality of that implementation.

2.1.1 SCM in Optical Networks

The applications where SCM is typically implemented are described from a network perspective. In practice, the following classification is not rigid, as the concepts behind different network topologies and technologies can be easily combined. In other words, any of the experiments presented in this thesis could be easily implemented in most of the following applications with minor modifications.

2.1.1.1 Analogue Cable Television (CATV)

One of the first applications of SCM consisted of the transmission of multiple analogue TV channels. In this case, SCM represents a perfect solution as every subcarrier transmits a different channel. Purely optical FTTH [1] and hybrid

fibre/coax HFC [2] systems were employed. Although the direct modulation of lasers was preferred to achieve low cost solutions [1], external optical modulators were also developed and optimised for this application [3]. Analogue video transmission can still be found in legacy access networks, but these solutions are tending to disappear due to the global analogue TV switch-off.

2.1.1.2 Digital Passive Optical Networks (PON)

As with CATV systems, the transmission of voice, video and data services to the final users in access networks can be provided with purely optical FTTH solutions or with HFC systems, but typically employing a point-to-multipoint PON configuration (see section 1.2.3.2).

Due to the point-to-multipoint nature of this implementation, SCM is well suited to accomplish the functions of the network. Each subcarrier/subchannel can be seen as one service, or the data for a particular user or group of users. SCM-PON networks have been reported using directly modulated lasers [4], lasers integrated with electro-absorption modulators (referred to as EMLs) [5] and, finally, MZM electro-optical modulators [6].

2.1.1.3 Local Area Networks (LAN)

SCM is also well-suited for low range networks like LANs and data centres as it can combine a number of lower bandwidth subchannels while obtaining a high overall data rate [7]. As an example, efforts have been made to design integrated circuits capable of reaching 100 Gbit/s SCM optical channels for LANs [8].

2.1.1.4 Radio over Fibre (RoF)

Similarly to the transmission of RF analogue TV channels, SCM is a perfect solution for the transmission of RF signals for wireless applications. A number of services can be transmitted over fibre, using the corresponding subcarrier frequencies, before and after feeding and reception in the antenna.

Many configurations and subcarriers have been employed using directly modulated lasers, EMLs and MZMs [9]. Currently, transmission at 60 GHz is receiving growing attention in the research community for its possibilities in IoT applications [10]. In practice, mobile operators are deploying digital RoF systems based on protocols like the CPRI, which transmits the digital samples of the RF signal instead of the analogue signal [10, 11]. In this case, the system is reduced to a standard digital point to point link and, again, SCM is an interesting alternative

because it improves the tolerance to dispersion reaching longer transmission distances.

2.1.1.5 Metro/Core Networks

Given a fixed bandwidth in a point-to-point link, SCM is an interesting solution as increasing the number of subcarriers reduces the bandwidth per subchannel and improves the tolerance to chromatic dispersion and fibre nonlinearities. For metro and core networks, many SCM experiments have proven the reliability of the technique in links of up to a few hundreds of kms using Direct Detection (DD) [12-14]. Furthermore, SCM has also proven to be powerful for mitigating fibre nonlinearities in coherent long-haul systems [15].

2.1.2 Main Focus

The main focus of this thesis was described in section 1.5, but the key ideas are reviewed here to identify the state of the art over which this document builds up new functionalities and advances.

2.1.2.1 Definition

The high-level context of this thesis is the design of broadband SCM electro-optical transceivers that transmit digital data. Research on this topic is motivated by the following reasons. Firstly, electrical processing is preferred over all-optical processing due to the maturity and reliability of the electrical components with respect to the optical counterparts. In fact, industrial implementations follow the same principle and there is little evidence that this tendency will be reversed. Secondly, as long as higher speed electrical signals are required, there are more difficulties and impairments in the electrical circuits and fibre dispersion compensation becomes more difficult. SCM solves these problems by transmitting a number of subchannels with lower speed baseband signals. Although SCM requires more electrical components than single carrier solutions, low cost can still be guaranteed due to the current capabilities of integration of both digital and analogue components.

Once SCM has been selected, the possible implementations must be analysed in more detail. One key feature is the electrical processing and two options are viable, DSP and ASP. High speed DSP is more flexible and can be easily implemented in integrated semiconductor chips, but it translates into high power consumption and latency. Moreover, the necessity of costly high-speed DACs and

ADCs is unavoidable. In contrast, high-speed ASP potentially achieves lower power consumption and latency and can also make use of low cost integrated microwave circuits. With ASP, higher-speed processing can be achieved at practically no extra cost as DACs and ADCs are not required. The main disadvantage of ASP is its lack of flexibility in the sense that analogue reconfigurable equivalents of Central Processing Units (CPU) and Field Programmable Gate Arrays (FPGA) do not exist. Although this fact promotes and encourages the research in DSP applications, ASP is still a fundamental option that needs to be considered as an alternative for any solution. When any standard is defined for electro-optical transceivers, it is common that digital data rates are fixed or present a static maximum without the need for a dynamic reconfigurable implementation. ASP can be easily implemented for those cases and the disadvantage in the flexibility no longer exists.

Another key issue is the electro-optical conversion. The current necessity for high speed modulation of the optical carriers implies serious difficulties to the direct modulation of standard laser sources. For that reason, EML lasers that integrate electro absorption modulators are receiving a growing interest. However, they present the important limitation of not being able to generate OSSB signals, which are important to enhance the tolerance to chromatic dispersion and to allow a tight allocation of WDM optical channels. The evolution of silicon photonics will translate into the commercial availability of low cost optical modulators, possibly integrating both lasers and MZMs. This is the natural tendency for the following years and will give rise to inexpensive optical devices that can achieve broadband low cost SCM/OSSB electro-optical transceivers.

In summary, this thesis focuses on broadband SCM digital electro-optical transceivers based largely on ASP and capable of a colourless generation of OSSB signals by employing optical modulators. DD is preferred to guarantee the potential low cost of the proposed solutions. Finally, experiments are performed relying largely on off-the-shelf components and with real-time implementations that ensure the feasibility of the proposed ideas. Although the subsequent experiments and discussions will mostly focus on point-to-point links, the techniques presented in this thesis can be easily extended to point-to-multipoint topologies.

2.1.2.2 State of the Art

With the defined focus, the initial state of the art is found in [12] and is illustrated in Figure 2.1. Four 2.5 Gbaud BPSK electrical subchannels were

transmitted in a SCM/OSSB configuration employing only analogue/microwave components, providing an overall real-time data rate of 10 Gbit/s. The high-frequency electrical modulation and demodulation of the subchannels were performed with microwave mixers. The baseband signals at the input and output of the mixers were processed with microwave Low Pass Filters (LPF). The Local Oscillators (LO) that fed the mixers, usually referred to as subcarrier frequencies, were located at 3.6, 8.3, 13 and 18 GHz. The electrical subchannels were combined in the transmitter and replicated in the receiver using a microwave power combiner/splitter. The Hilbert Transform (HT) of the multiplexed FDM electrical signal at the transmitter was generated with a microwave 90º hybrid combiner and was required to achieve OSSB modulation. The OSSB signal was generated with a Dual-Drive MZM (DD-MZM) and optical carrier suppression was applied with an optical circuit at the output of the optical modulator. More details about carrier suppression and the generation of OSSB signals are provided below. EDFAs were used in the optical transmitter, and also in the receiver configuring a "pre-amplified optical receiver". DD was performed employing a single photo-detector.

SCM is a vast topic where many experiments, more recent than [12], have been reported. However, the previous configuration has been selected as it is the one that most closely address the particular target of this work. Focusing on DD systems, higher modulation orders can be achieved. For instance, SCM/QPSK has been reported in [16], where direct modulation of a laser was performed obtaining ODSB, and in [17, 18], where only one electrical subchannel was transmitted. Moreover, SCM/16-QAM solutions have always been based on off-line DSP [19-21].

A testbed was designed and built to advance in the state of the art of real-time broadband SCM/OSSB optical links based on ASP. This testbed will be described in section 2.5. New features can be found with respect to the experiment described above [12]. Off-the-shelf mixers based on monolithic microwave integrated circuit

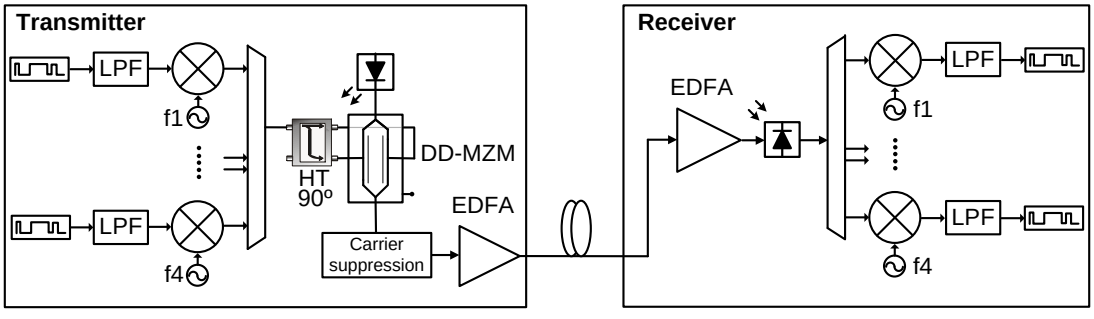

Figure 2.1 SCM/OSSB link with 4 BPSK subchannels based on a DD-MZM and ASP.

(MMIC) technology [22] were employed, proving the immediate feasibility and low cost of the proposed electrical solution. Standard mixers were substituted by IQ mixers, which can achieve a higher modulation order. An Optical IQ Modulator (OIQM) was employed instead of the DD-MZM as it presents the advantage of generating OSSB signals with carrier suppression without requiring additional components (see section 2.3). The use of OIQMs in broadband SCM/OSSB systems in thoroughly analysed in Chapter 3.

2.2 Electrical Processing

This section explains the electrical processing that is found in SCM systems. The electrical (de)modulation is detailed and important implementation concepts are discussed.

2.2.1 Modulation and Demodulation

Broadband SCM systems employ microwave FDM signals in the electrical domain. The generation of N subchannels is achieved by modulating N subcarriers located at f_n (n=1,2..N) with baseband digital signals. Mathematically, the baseband streams that modulate the I and the Q components of the n^{th} subcarrier are denoted as $b_{In}(t)$ and $b_{Qn}(t)$ respectively. The temporal signal of the n^{th} subchannel $s_n(t)$ is:

$$s_n(t) = b_{In}(t)\cos(2\pi f_n t) + b_{Qn}(t)\sin(2\pi f_n t), \qquad n = 1, 2, ..N. \tag{2.1}$$

This is the general expression for a Quadrature Amplitude Modulation (QAM). The modulation order and the bitrate of every subchannel is determined by $b_{In}(t)$ and $b_{Qn}(t)$. In the simplest case, $b_{In}(t)$ is a PAM_2 signal (digital signal with 2 possible levels or symbols) and $b_{Qn}(t)$=0, such that a BPSK subchannel is obtained (two possible symbols). If both $b_{In}(t)$ and $b_{Qn}(t)$ are PAM_M signals (M symbols), a QAM modulation is obtained (M^2 symbols). For a rate of B bauds (symbols/s) in each baseband stream, the bit rate is $R=B\log_2 M$ bit/s per stream and $2R$ per subchannel. The high-frequency content of $b_{In}(t)$ and $b_{Qn}(t)$ is usually removed with a LPF, limiting its bandwidth to B Hz, and the bandwidth of the RF signal $s_n(t)$ to $2B$ Hz.

Once all the subchannels are combined, the resultant FDM signal is:

$$s(t) = \sum_{n=1}^{N} s_n(t). \tag{2.2}$$

The baseband streams $b_{In}(t)$ and $b_{Qn}(t)$ can be demodulated multiplying $s_n(t)$ with the subcarrier components and applying LPFs to eliminate the components at $2f_n$:

$$\begin{aligned} s_n(t)\cos(2\pi f_n t) &= b_{In}(t)\cos^2(2\pi f_n t) + b_{Qn}(t)\sin(2\pi f_n t)\cos(2\pi f_n t) = \\ & b_{In}(t)\frac{1+\cos(2\pi 2 f_n t)}{2} + b_{Qn}(t)\frac{\sin(2\pi 2 f_n t)}{2} \xrightarrow{LPF} b_{In}(t). \end{aligned} \tag{2.3}$$

$$\begin{aligned} s_n(t)\sin(2\pi f_n t) &= b_{In}(t)\cos(2\pi f_n t)\sin(2\pi f_n t) + b_{Qn}(t)\sin^2(2\pi f_n t) = \\ & b_{In}(t)\frac{\sin(2\pi 2 f_n t)}{2} + b_{Qn}(t)\frac{1-\cos(2\pi 2 f_n t)}{2} \xrightarrow{LPF} b_{Qn}(t). \end{aligned} \tag{2.4}$$

The same concept can be applied by multiplying the overall signal $s(t)$ with the subcarrier frequencies (equivalent to Figure 2.1). After the multiplication, extra terms from the adjacent subchannels will be present at adjacent frequencies, but, again, they can be reduced or eliminated with the LPFs. Mathematically:

$$\begin{aligned} s(t)\cos(2\pi f_n t) &= s_n(t)\cos(2\pi f_s t) + \sum_{\substack{i=1 \\ i\neq n}}^{N} s_i(t)\cos(2\pi f_i t) \xrightarrow{LPF} b_{In}(t). \\ s(t)\sin(2\pi f_n t) &= s_n(t)\sin(2\pi f_s t) + \sum_{\substack{i=1 \\ i\neq n}}^{N} s_i(t)\sin(2\pi f_i t) \xrightarrow{LPF} b_{Qn}(t). \end{aligned} \tag{2.5}$$

2.2.2 Implementation

From a practical perspective there are several important concepts to discuss. They are all illustrated in Figure 2.2 with a back to back FDM/BPSK example.

Firstly, it should be noted that the signals $b_{In}(t)$ and $b_{Qn}(t)$, and, consequently, $s_n(t)$ and $s(t)$, should be AC signals. Any DC component would translate into a change in the bias point of the laser or the optical modulator, as it can be concluded from eqs. (1.3) and (1.9). Apart from that, filtering $b_{In}(t)$ and $b_{Qn}(t)$ softens the steepness in their transitions, but also reduces the bandwidth allowing a closer frequency allocation of subchannels.

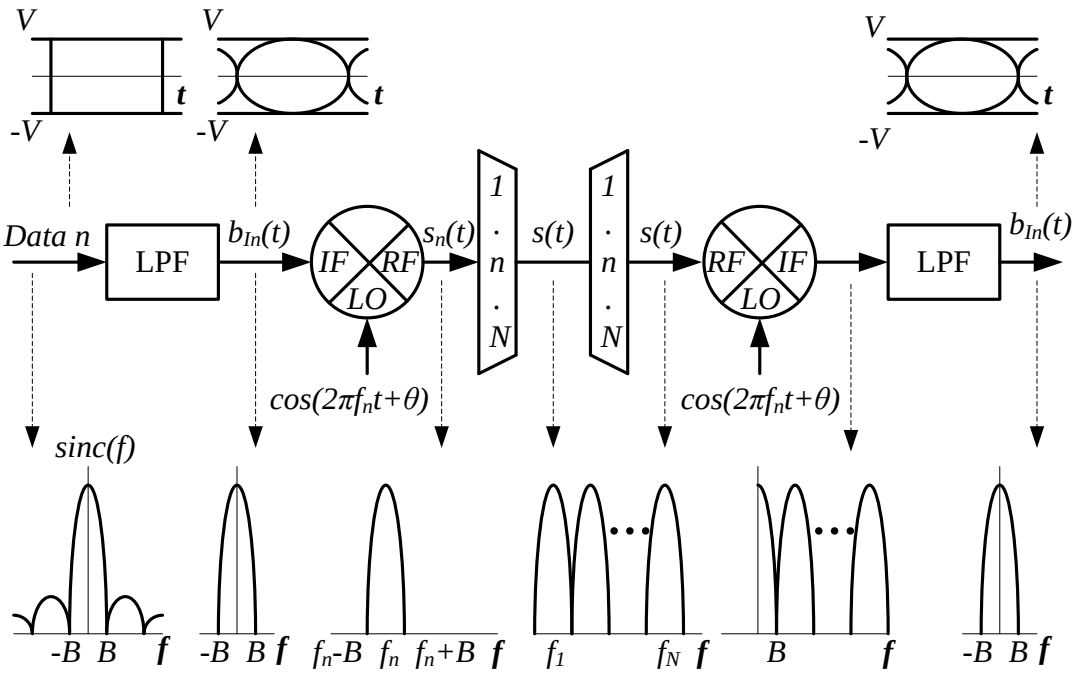

Figure 2.2 Ideal back-to-back FDM/BPSK scheme consisting of *N* subcarriers.

Secondly, the implementation of the FDM (de)modulation can be based on DSP or ASP. In the DSP case the filters and the (de)modulation are performed with digital multiplications of samples. The ADC and DAC need to present a processing rate higher than the highest frequencies of the overall signal *s(t)*. In the analogue case, the LPFs are typically implemented with microwave lumped components. The multiplications are approximated with nonlinear devices, referred to as mixers [23]. To modulate, the baseband or Intermediate Frequency (IF) signal is mixed with the Local Oscillator (LO) to get an RF output. Demodulation consists of the opposite process, the RF signal is mixed with the LO recovering the baseband or the IF data. Every mixer needs to present good amplitude and group delay performance inside the bandwidth of the RF and IF signals. A detailed explanation of the IQ mixers employed in this work is provided in section 2.5.1.

Finally, in the presented example the subcarriers in the receiver are phase and frequency locked to the incoming subchannels $s_n(t)$. Often, this synchronization is achieved by employing the same LOs in the transmitter and the receiver and by using phase shifters to perform the fine phase adjustment [16]. For more practical applications, automatic synchronization is required and Phase Locked Loops (PLL) must be employed [17]. A more detailed discussion on this topic will be provided in Chapter 5.

2.3 Optical Processing

Two main optical processes are involved in the generation of SCM signals: optical carrier suppression and OSSB modulation. Both are described below.

2.3.1 Carrier Suppression

The context of this discussion is the optimisation of DD systems, where the optical carrier is necessary to perform the mixing with the desired signal in the photo-detector. Thus, in this document, the terminology "carrier suppression" implies "partial" carrier suppression, in contrast with coherent systems where full carrier suppression is often desired [24].

2.3.1.1 Relevance

Optical carrier suppression is important because it can achieve lower sensitivities in DD systems. The sensitivity is defined as the minimum average optical power P_{avg} at the input of the optical receiver that is required to meet a level of performance. The average power of an optical signal is equal to the sum of the power of all its frequency components. Considering a photodetector with responsivity equal to 1, the P_{avg} of an optical signal would be the average or DC value of the detected photo-current.

The following analysis is carried out with an OSSB signal for simplicity, but the same conclusions would be obtained employing ODSB. The electric field of an SCM/OSSB signal generated with N subcarriers of equal power located at electrical frequencies Ω_n rad/s (n=1, 2…N) can be expressed as:

$$E(t) = \sqrt{\zeta} E_c \cos(\omega_c t + \theta_c) + \sum_{n=1}^{N} E_s b_n(t) \cos\left((\omega_c + \Omega_n)t + \theta_n\right), \qquad (2.6)$$

where E_c is the amplitude of the optical carrier, E_s is the amplitude of the subcarriers, θ_c and θ_n are arbitrary phases, $b_n(t)$ represents AC binary sequences with amplitude 1 and ζ is the power suppression factor, as explained below. When MZMs are employed, there is a constant relation $E_s = mE_c$ determined by the level of the electrical signal that drives the MZM and its V_π [12]. Besides, the condition $E_s << E_c$ occurs, as the modulating signal is small to reduce the nonlinearities caused by the modulator. With these conditions, the associated photocurrent $I(t)$ and P_{avg} are:

$$I(t) \approx \frac{\zeta}{2} E_c^2 + mE_c^2 \sqrt{\zeta} \sum_{n=1}^{N} b_n(t) \cos(\Omega_n t + \theta_n - \theta_c). \quad (2.7)$$

$$P_{avg} = I_{DC} \approx \frac{\zeta}{2} E_c^2. \quad (2.8)$$

It becomes clear that the term ζ, in the range $0 \leq \zeta \leq 1$, determines the power suppression of the optical carrier. *I(t)* can be rewritten as:

$$I(t) \approx P_{avg} \left(1 + \frac{2m}{\sqrt{\zeta}} \sum_{n=1}^{N} b_n(t) \cos(\Omega_n t + \theta_n - \theta_c) \right). \quad (2.9)$$

The previous equation shows that, for a given value of P_{avg}, higher signal values are obtained when higher levels of carrier suppression (lower ζ) are applied. This procedure present limits, which are explained in the following subsection.

The relevance of carrier suppression can be stated from different perspectives. Firstly, the optical carrier represents the main percentage of the power of the signal but does not contain any information. Consequently, when the carrier is partially suppressed, the same information can be potentially transmitted with a lower average power. Secondly, optical amplifiers saturate with a determined output power. If the optical carrier is partially suppressed, higher power will be obtained in the desired signal at the output of the amplifier. Finally, in the receiver, a lower average power is necessary to receive the required level of the desired signal, which translates into a better (lower) sensitivity.

2.3.1.2 Implementation and Impairments

Carrier suppression consists of reducing the amplitude of the optical carrier with respect to the level of the subchannels. There are two methods to implement carrier suppression. The first one employs an optical filter to reduce the amplitude of the optical carrier after the modulation [12]. Sometimes the same filter is used to produce both carrier suppression and OSSB generation from a ODSB signal [25]. The other alternative relies on biasing the optical modulator closer to the null point, technique often referred to as *low biasing* of the MZM [26, 27]. Both techniques have consequences in the photo-detected signal, as explained below.

When carrier suppression is implemented by filtering a modulated optical signal, increased Intermodulation Products (IMP) will be produced in the received photo-current [28]. The effects of partial carrier suppression in the temporal and spectral shapes of the electric field are illustrated in an example in Figure 2.3. When the level of the optical carrier is reduced, the average value of the temporal signal also reduces, but the shape of the envelope remains. However, the squared envelope obtained by photo-detection would be distorted with respect to the original and desired one (note that the shape of the function $y=x^2$ around two different DC values x_{o1} and x_{o2} changes). As a consequence, the optimum sensitivity is the result of a trade-off between the carrier suppression and the induced nonlinearities [28]. When the level of the carrier suppression is very high, a phenomenon known as *clipping* occurs. It is the result of the envelope attempting to cross the zero value, such that the associated distortion is more severe, as it can also be seen in Figure 2.3.

When biasing a MZM, from Figure 1.9 it is evident that the closer to the null point the bias is, the lower the optical carrier results and the more nonlinear the

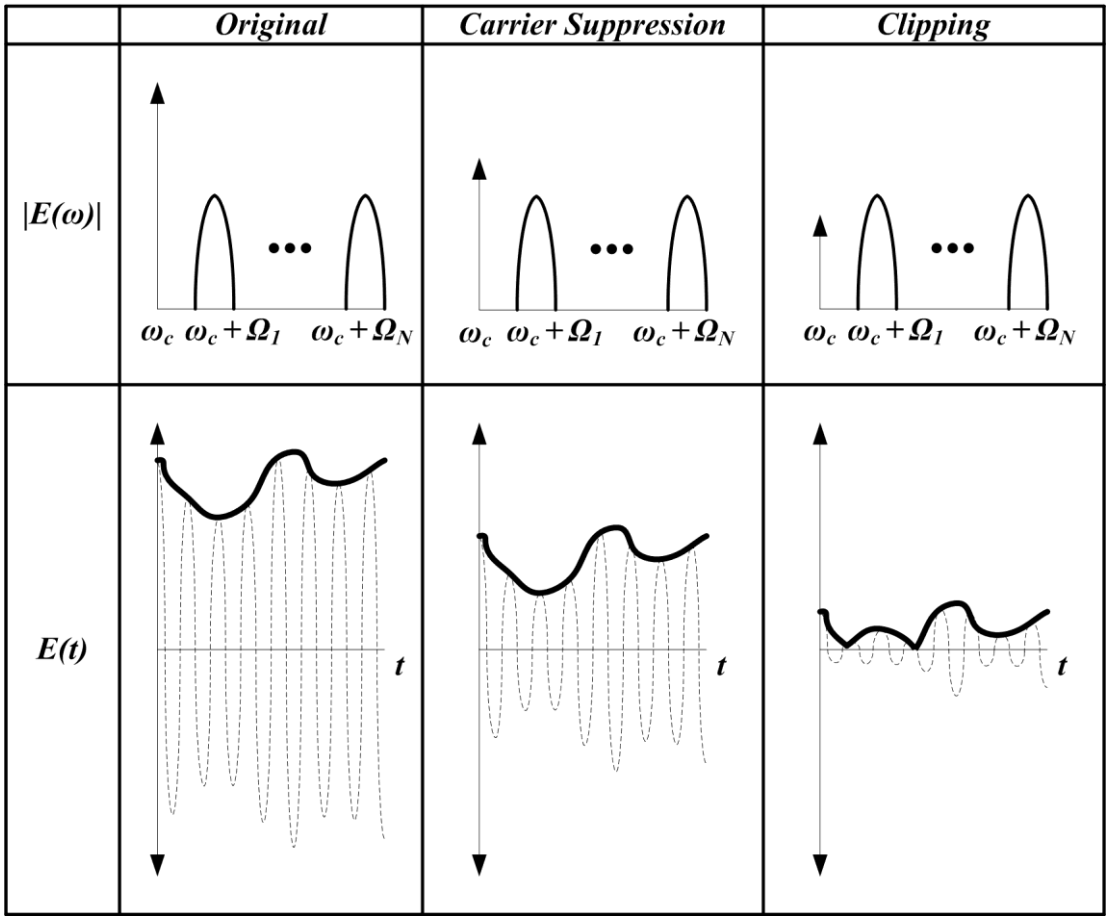

Figure 2.3 Temporal and spectral examples of carrier suppression and clipping.

transfer function of the intensity becomes. As a consequence, the best sensitivity in the receiver is achieved as a trade-off between the carrier suppression and the nonlinearities introduced by the optical modulator [26]. The carrier suppression depends only on the bias point, but the nonlinearities depend on both the bias point and the amplitude of the electrical signal driving the MZM, the Optical Modulation Index (OMI) [29]. Biasing closer to the null increases second order IMPs while higher OMIs translate into higher third-order IMPs [29]. These concepts will be explained in more detail and particularised for optical IQ modulators in Chapter 3.

2.3.2 Single Side Band

When an FDM signal is used to modulate a laser directly or with a MZM, as explained in sections 1.3.1 and 1.3.2, an ODSB spectrum is generated. Filters can be used to remove one sideband generating an OSSB signal [25], but that method requires optical components with an accurate transfer function. For that reason, an OSSB generation produced with optical modulators and lacking external components

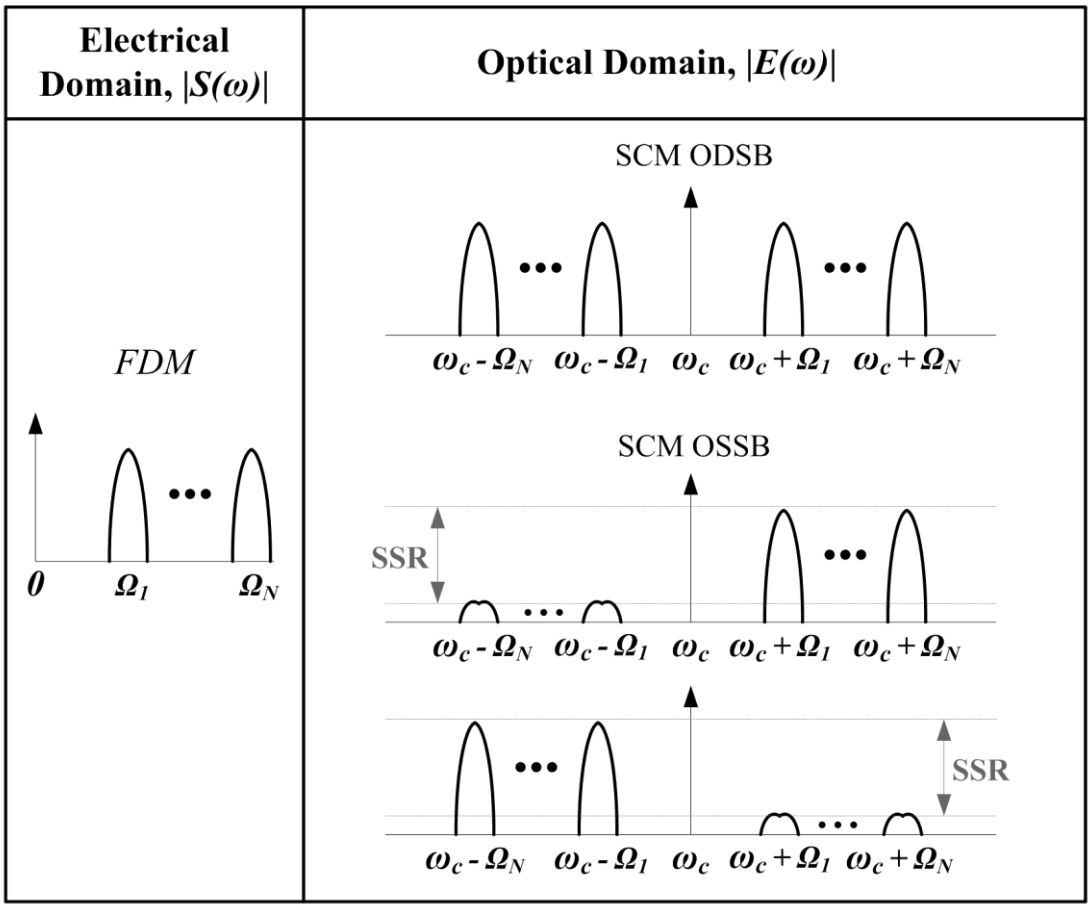

Figure 2.4 Examples of FDM and associated SCM/ODSB and SCM/OSSB spectra.

can be described as colourless. Figure 2.4 shows an FDM electrical spectrum with its associated SCM/ODSB and SCM/OSSB optical spectra. OSSB can be achieved suppressing either of the two sidebands. The Sideband Suppression Ratio (SSR) determines the quality of the OSSB generation. Imperfect SSR is a consequence of non-ideal behaviour of optical filters and optical modulators.

This section firstly emphasizes the relevance of SCM/OSSB signals. The theory of SSB modulation is then developed to prove that two optical modulators, DD-MZMs and OIQMs, achieve a colourless OSSB generation. It will also be shown that only OIQMs can provide OSSB and carrier suppression simultaneously.

2.3.2.1 Relevance

SCM/OSSB signals are relevant for two important reasons. Firstly, an additional spectral bandwidth is gained due to the suppressed sideband. This bandwidth can be occupied by another optical channel achieving WDM configurations with improved spectral efficiency. Secondly, SCM/ODSB signals experience an impairment known as *dispersive fading*. Its associated spectrum presents two sidebands, one on each side of the optical carrier frequency. When such a signal propagates over fibre, complementary frequencies ($\omega_c+\Omega$, $\omega_c-\Omega$) experience a relative phase shift induced by dispersion. During the photo-detection in the receiver, the complimentary frequencies are combined and, depending on the induced phase shift, the combination can be constructive or destructive. In contrast, due to the presence of only one sideband per subcarrier, SCM/OSSB does not present dispersive fading achieving longer transmission distances [30].

For an electrical subcarrier of frequency f_s transmitted on an optical carrier λ_c in an ODSB configuration, the photocurrent recovered after propagation in a fibre of length L and dispersion D is:

$$I_{ODSB}(t) \propto \cos\left(\frac{\pi D \lambda_c^2 f_s^2}{c} L\right) \cos(2\pi f_s t). \tag{2.10}$$

A subcarrier of 10 GHz propagating on SSMF (λ_c=1550nm, D=17ps/(nm·km)) would present a first fading null at ≈37 km. Eq. (2.10) can be calculated studying the propagation over fibre of the temporal tones [31, 32], the complex envelope [33], or with Fourier analysis [34]. If the same subcarrier is transmitted in an OSSB

configuration, dispersion translates only into a phase shift whose sign depends on which sideband is suppressed [34]:

$$I_{OSSB}(t) \propto \cos\left(2\pi f_s t \pm \frac{\pi D \lambda_c^2 f_s^2}{c} L\right). \tag{2.11}$$

2.3.2.2 Colourless Generation

Any component or subcarrier of a signal located at a frequency Ω_s can modulate a higher frequency carrier at ω_c generating a SSB spectrum. This procedure is illustrated for a single tone in Figure 2.5 showing all the involved spectra. First of all, to generate the SSB version of a signal it is necessary to obtain its Hilbert Transform (HT) pair, which is the original signal with all its frequency components shifted 90 degrees. The original signal plus the HT pair are employed to perform an amplitude modulation (AM) of two carriers located at the same frequency but with a relative phase shift of 90 degrees. The resultant high frequency signals are then combined, obtaining upper side band (USB) or lower side band (LSB) depending on the sign of the combination. In the depicted example it can be concluded that the following is a SSB signal:

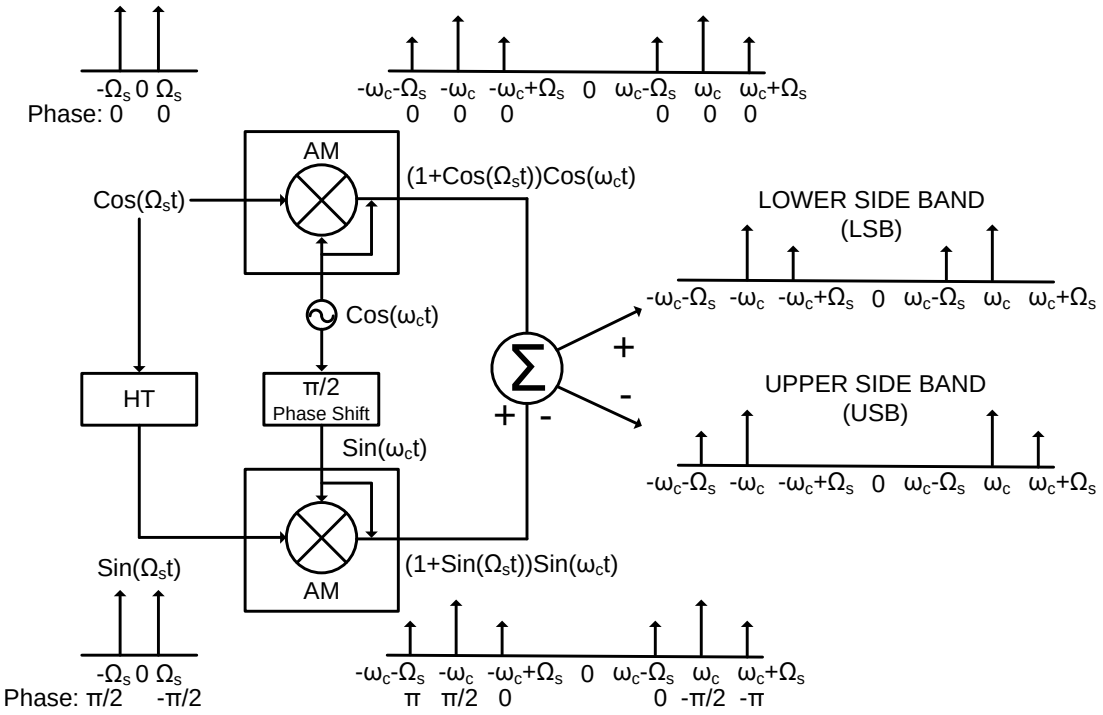

Figure 2.5 Single side band generation.

$$x_{SSB}(t) = (1+\cos(\Omega_s t))\cos(\omega_c t) \pm (1+\sin(\Omega_s t))\sin(\omega_c t). \quad (2.12)$$

The previous procedure can be generalized for any AC signal *s(t)*. Considering HT[*s(t)*]=*ŝ(t)*, the resultant SSB signal would be:

$$s_{SSB}(t) = \left(1+s(t)\right)\cos(\omega_c t) \pm \left(1+\hat{s}(t)\right)\sin(\omega_c t). \quad (2.13)$$

The colourless generation of a SCM/OSSB signal is equivalent to the procedure described above. The FDM signals *s(t)* and *ŝ(t)* consist of electrical frequency components (Ω) that must modulate a higher frequency optical carrier (ω_c). Note that the analysis has been carried out maintaining the unmodulated carrier at ω_c in the resultant signal, as required for DD systems. Next, it is proved that DD-MZMs and OIQMs produce colourless OSSB modulation.

2.3.2.3 Dual-Drive MZM

A DD-MZM is shown in Figure 2.6. It presents a structure similar to a standard MZM. The key difference is that each arm of the MZM can be driven by a different signal. It will be shown that this device can produce colourless OSSB modulation.

Two electrical FDM signals, *s(t)* and its HT *ŝ(t)*, must be the result of the electrical processing. The electrodes of the DD-MZM can be driven such that $V_1(t)=V_b+s(t)$ and $V_2(t)=\hat{s}(t)$. The DC voltage V_b is selected to bias the device at quadrature by introducing a phase shift equal to $-\pi/2$ rad. Being $E_i \cdot \cos(\omega_c t)$ the electric field at the input of a device with half-wave voltage V_π, the output signal is:

$$E_o(t) = \frac{E_i}{2}\cos\left(\omega_c t - \frac{\pi}{2} + \frac{\pi \cdot s(t)}{2V_\pi}\right) + \frac{E_i}{2}\cos\left(\omega_c t - \frac{\pi \cdot \hat{s}(t)}{2V_\pi}\right). \quad (2.14)$$

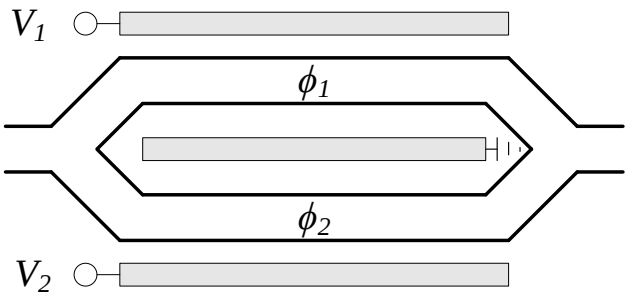

Figure 2.6 Dual-Drive MZM.

Applying the equalities *cos(u+v)=cos(u)cos(v)-sin(u)sin(v)*, *sin(x)=cos(x–π/2)*, *-cos(x)=sin(x–π/2)*, *cos(-x)=cos(x)* and *sin(-x)=-sin(x)*; and after some manipulations, the previous equation becomes:

$$E_o(t)=\frac{E_i}{2}\left(\begin{array}{l}\left(\cos(\omega_c t)\right)\left(\sin\left(\frac{\pi\cdot s(t)}{2V_\pi}\right)+\cos\left(\frac{\pi\cdot \hat{s}(t)}{2V_\pi}\right)\right)+\\ \left(\sin(\omega_c t)\right)\left(\cos\left(\frac{\pi\cdot s(t)}{2V_\pi}\right)+\sin\left(\frac{\pi\cdot \hat{s}(t)}{2V_\pi}\right)\right)\end{array}\right). \qquad (2.15)$$

If the peak amplitude of *s(t)* and *ŝ(t)* is very small in comparison with V_π, and considering *cos(x)≈1* and *sin(x)≈x* for small values of *x*, the final result is:

$$E_o(t)\approx\frac{E_i}{2}\left(\left(1+\frac{\pi\cdot s(t)}{2V_\pi}\right)\cos(\omega_c t)+\left(1+\frac{\pi\cdot \hat{s}(t)}{2V_\pi}\right)\sin(\omega_c t)\right). \qquad (2.16)$$

Comparing with eq. (2.13), it is evident that $E_o(t)$ is an OSSB signal. It is also clear that DD-MZMs cannot generate OSSB and carrier suppression simultaneously, so that external optical filters would be necessary. The higher the peak amplitudes of *s(t)* and *ŝ(t)* are, the higher the nonlinearities in the output. For this particular case, a simple analysis of the nonlinear distortion can be found in [12]. More comprehensive analysis providing the distortion in the final photocurrent are provided in [35] and also in [28] including carrier suppression.

2.3.2.4 Optical IQ Modulator

An OIQM is illustrated in Figure 2.7. It is composed of two parallel MZMs, labelled MZM_I and MZM_Q, plus a third one, labelled MZM_O, which combines the two electrical fields coming from the parallel ones with the required phase difference. A mathematical analysis equivalent to the previous subsection will be developed.

The original FDM signal and its HT, *s(t)* and *ŝ(t)*, drive the MZM_I and MZM_Q respectively. Both parallel MZMs will be biased at the same point such that $V_I(t)=-V_b+s(t)$ and $V_Q(t)=-V_b+\hat{s}(t)$. Without losing generality, the electric field is

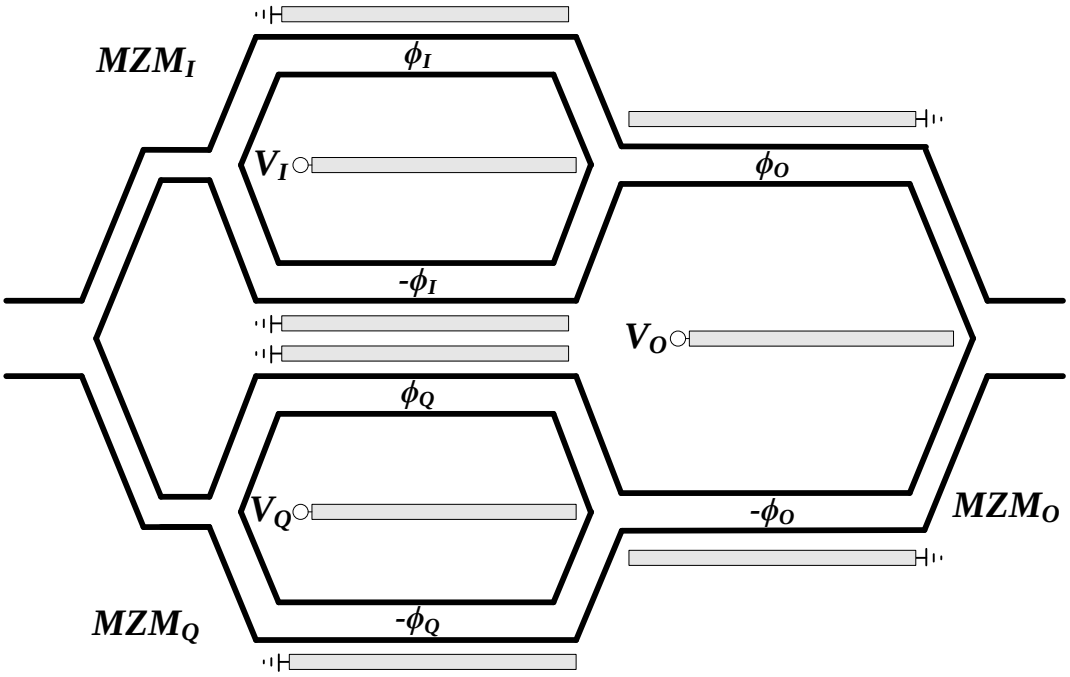

Figure 2.7 Optical IQ Modulator.

$E_i \cdot \cos(\omega_c t - \pi/4)$ at the input of the OIQM, and $(E_i/\sqrt{2}) \cdot \cos(\omega_c t - \pi/4)$ at the input of the parallel MZMs (assuming equal 3dB power splitting). From eq. (1.7), the output of these MZMs considering a half-wave voltage V_π is:

$$E_I(t) = \frac{E_i}{\sqrt{2}} \cos\left(-\frac{\pi \cdot V_b}{2V_\pi} + \frac{\pi \cdot s(t)}{2V_\pi} \right) \cos\left(\omega_c t - \frac{\pi}{4} \right).$$
$$E_Q(t) = \frac{E_i}{\sqrt{2}} \cos\left(-\frac{\pi \cdot V_b}{2V_\pi} + \frac{\pi \cdot \hat{s}(t)}{2V_\pi} \right) \cos\left(\omega_c t - \frac{\pi}{4} \right). \quad (2.17)$$

The function of the MZM_O is to provide a relative 90 degrees phase shift to the outputs of MZM_I and MZM_Q (ϕ_o=+π/4, -ϕ_o=-π/4) and, consequently, is biased at quadrature. With that condition, the electric field at the output of the OIQM can be written as:

$$E_o(t) = \frac{E_i}{2} \left[\cos\left(-\frac{\pi \cdot V_b}{2V_\pi} + \frac{\pi \cdot s(t)}{2V_\pi} \right) \cos(\omega_c t) + \cos\left(-\frac{\pi \cdot V_b}{2V_\pi} + \frac{\pi \cdot \hat{s}(t)}{2V_\pi} \right) \sin(\omega_c t) \right]. \quad (2.18)$$

Using *cos(u-v)=cos(u)cos(v)+sin(u)sin(v)*, the previous equation can be rewritten as:

$$E_o(t)=\frac{E_i}{2}\left\{\begin{array}{l}\left[\cos\left(\frac{\pi\cdot V_b}{2V_\pi}\right)\cos\left(\frac{\pi\cdot s(t)}{2V_\pi}\right)+\sin\left(\frac{\pi\cdot V_b}{2V_\pi}\right)\sin\left(\frac{\pi\cdot s(t)}{2V_\pi}\right)\right]\cos(\omega_c t)+\\ \left[\cos\left(\frac{\pi\cdot V_b}{2V_\pi}\right)\cos\left(\frac{\pi\cdot \hat{s}(t)}{2V_\pi}\right)+\sin\left(\frac{\pi\cdot V_b}{2V_\pi}\right)\sin\left(\frac{\pi\cdot \hat{s}(t)}{2V_\pi}\right)\right]\sin(\omega_c t)\end{array}\right\}. \quad (2.19)$$

If the peak amplitude of *s(t)* and *ŝ(t)* is small in comparison with V_π, and applying *cos(x)=1* and *sin(x)=x* for small values of *x*:

$$E_o(t)\approx\frac{E_i}{2}\left\{\begin{array}{l}\left[\cos\left(\frac{\pi\cdot V_b}{2V_\pi}\right)+\sin\left(\frac{\pi\cdot V_b}{2V_\pi}\right)\cdot\frac{\pi\cdot s(t)}{2V_\pi}\right]\cos(\omega_c t)+\\ \left[\cos\left(\frac{\pi\cdot V_b}{2V_\pi}\right)+\sin\left(\frac{\pi\cdot V_b}{2V_\pi}\right)\cdot\frac{\pi\cdot \hat{s}(t)}{2V_\pi}\right]\sin(\omega_c t)\end{array}\right\}. \quad (2.20)$$

Comparing the expression with eq. (2.13) it is clear that $E_o(t)$ is indeed an OSSB signal. Unlike the DD-MZM, the OIQM achieves OSSB and carrier suppression simultaneously as the bias voltage V_b changes the amplitude relation between the desired signal and the optical carrier. If the parallel MZMs are biased at quadrature (V_b/V_π=n+0.5), both the optical carrier and the signal are present at the output. However, it they are biased at null (V_b/V_π=2n+1), the optical carrier is totally suppressed while the signal is still present. With higher peak values of *s(t)* and *ŝ(t)*, the approximation realized is less accurate and more nonlinear distortion appears. Observing the transfer function of a MZM (see Figure 1.9) it is also clear that, for DD systems, the closer to null the bias point is, the higher the nonlinearities are in the detected photocurrent. It can be concluded that as long as the bias point moves from quadrature to null, the carrier suppression improves and the nonlinear distortion worsens, generating a trade-off in the sensitivity of the system. This trade-off will be thoroughly analysed in Chapter 3.

2.4 Tolerance to Impairments

This section analyses the tolerance to impairments in SCM systems. Firstly, the distortion introduced by fibre transmission is explained. Secondly, the performance of the system is studied as a function of the sources of noise.

2.4.1 Fibre Distortion

2.4.1.1 Chromatic Dispersion

SCM divides a given optical bandwidth into a number of narrower bands occupied by optical subchannels. Intuitively, it can be deduced that SCM is more tolerant to chromatic dispersion than single channel or TDM solutions. On the one hand, every subchannel presents a narrower bandwidth and, additionally, the baseband signals are slower and more robust against impairments. This section mathematically quantifies this enhanced tolerance.

Due to chromatic dispersion, and from eq. (1.12), the temporal pulse broadening of an electrical digital signal of baseband bandwidth Δf, after propagation over a SMF fibre of length L and chromatic dispersion D at a centre wavelength λ_c is:

$$\Delta T = D \cdot \Delta\lambda \cdot L \approx D \frac{\lambda_c^2 \cdot 2\Delta f}{c} L. \tag{2.21}$$

Where the following approximation has been done as the optical frequencies (f_c+Δf and f_c-Δf) are much higher than electrical frequencies (Δf):

$$\Delta\lambda = \lambda_+ - \lambda_- = \frac{c}{f_c - \Delta f} - \frac{c}{f_c + \Delta f} = \frac{2\Delta f \cdot c}{f_c^2 - (\Delta f)^2} \approx \frac{2\Delta f \cdot c}{f_c^2} = \frac{\lambda_c^2 \cdot 2\Delta f}{c}. \tag{2.22}$$

Note that the optical bandwidth is two times the baseband electrical bandwidth. The maximum allowed temporal broadening of a pulse can be defined as a proportion of the bit (or symbol) time ε, such that ε=1 means a pulse broadening equal to one bit (or symbol) time T_b. Considering transmission of NRZ square pulses where the bandwidth Δf is given by the first lobe of the associated sinc spectra:

$$\Delta T < \varepsilon \cdot T_b \xrightarrow{T_b = 1/\Delta f} \Delta f \cdot \Delta T < \varepsilon. \tag{2.23}$$

The spectral comparison between the single channel and the SCM case is illustrated in Figure 2.8. A single channel optical spectrum for a PAM_2 NRZ digital signal of B Gbit/s can be observed on the left, occupying a bandwidth of 2B GHz. The complementary SCM/OSSB spectrum is shown on the right. To present the same

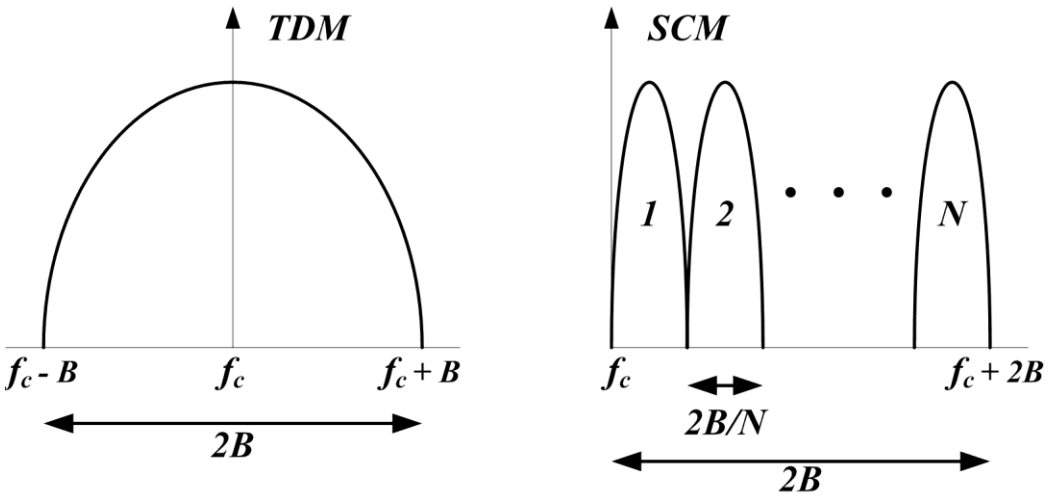

Figure 2.8 Single channel and SCM/OSSB spectra with the same optical bandwidth.

spectral efficiency, the modulation order of the N SCM subchannels must be BPSK with a symbol rate B/N. To calculate the limits of every subchannel, eq. (2.23) can be extended using $\Delta f = B/N$ where N=1 represents the single channel case and N>1 is valid for SCM with N subcarriers:

$$D\frac{\lambda_c^2 \cdot 2B^2}{cN^2}L < \varepsilon \longrightarrow L < \varepsilon \frac{c \cdot N^2}{D \cdot \lambda_c^2 \cdot 2B}. \tag{2.24}$$

It can be concluded that in SCM systems, the tolerance to dispersion is increased by N^2 compared to conventional single channel transmission. Some standards have defined ε=0.306 to obtain maximum power penalties of 1 dB due to dispersion [36]. For a 10 Gbit/s transmission at λ_c 1550 nm and over SSMF with D=17 ps/(nm·km), the single channel case would be limited by L<11.2 km while four SCM subchannels would achieve a distance 16 times longer with the same penalty. With higher modulation orders like PAM_4 in the baseband, ε would be lower due to the reduced tolerance to intersymbol interference.

2.4.1.2 Polarization Mode Dispersion

The propagation of an SCM/OSSB signal over fibre is also affected by PMD. The penalty can be quantified by temporal analysis. For simplicity, the transmission of an optical carrier at ω_c plus one subcarrier at $\omega_c+\Omega$ is considered. Equal power transfer between two orthogonal states of polarization (X and Y) is assumed. The Y axis is usually referred to as the fast axis. If there is a delay τ due to the propagation in the slow X axis, the received electric fields can be written as:

$$E_Y \propto \cos\left(\omega_c t\right) + \cos\left(\left(\omega_c + \Omega\right)t\right).$$
$$E_X \propto \cos\left(\omega_c \left(t-\tau\right)\right) + \cos\left(\left(\omega_c + \Omega\right)\left(t-\tau\right)\right). \quad (2.25)$$

In the receiver there are two contributions in the photo-current. Neglecting the DC components:

$$I\left(t\right) = \left\langle E_Y^2\left(t\right)\right\rangle + \left\langle E_X^2\left(t\right)\right\rangle \propto \frac{1}{2}\left[\cos\left(\Omega t\right) + \cos\left(\Omega\left(t-\tau\right)\right)\right] =$$
$$= \cos\left(\frac{\Omega\tau}{2}\right)\cos\left(\Omega\left(t-\frac{\tau}{2}\right)\right). \quad (2.26)$$

It can be concluded that PMD translates into a fading of the subchannel. The same result can be obtained with frequency domain analysis [12]. As an example, for a subcarrier at Ω=10 GHz, a power penalty of 1 dB in the receiver corresponds with $\tau \approx 15$ ps. For SSMF, PMD is <0.5 ps/km$^{0.5}$ and, consequently, such a penalty would be the result of a transmission over at least 900 km. Thus, PMD is meaningful for SCM/OSSB signals only in long-haul systems.

2.4.1.3 Nonlinearities

SCM transmission over long distances, in configurations with a number of fibre spans and optical amplifiers, is also distorted by the nonlinear Kerr effect. As explained in section 1.3.3.3, this nonlinearity is the result of changes in the refractive index of the fibre due to variations in the optical intensity. Assuming a fixed power in the optical channel, SPM depends on the optical power per subchannel so that SPM decreases with a higher number of subcarriers *N*. Similarly, for a given bandwidth, a higher value of *N* translates into lower XPM, but the higher number of intermodulation products makes FWM dominant [12]. The experiments conducted for this thesis consisted of one fibre span and were mostly focused on short distance links. Consequently, Kerr nonlinear fibre effects could be largely neglected.

Another relevant impairment is chromatic dispersion induced nonlinearity. In an ideal DD configuration, the optical carrier is modulated in such a way that the desired FDM signal would be perfectly recovered squaring the envelope of the electrical field. The last statement means that the envelope of the electrical field includes desired and undesired frequency components that, after photo-detection,

give rise to the desired FDM signal at the same time that the undesired terms cancel out. Due to chromatic dispersion, all the frequency components in the electrical field suffer different delays. This walk-off between components means that the cancelation of undesired terms is not perfect any more, which translates into unwanted nonlinear terms in the photo-detected signal. Consequently, as the optical modulator is a source of nonlinearities itself, transmission over fibre enhances its nonlinear performance. These effects have been thoroughly studied for SCM/OSSB transmission based on DD-MZMs in [28, 35]. Their impact on the system depends on the level and the number of subchannels, but they usually begin to be meaningful at tens of kms [28, 35].

2.4.2 Noise

Noise is a key impairment for any communication scheme. Accordingly, the performance of an optical transmission system largely depends on the accumulated noise. The two parameters that are typically employed to measure performance are the Carrier to Noise Ratio (CNR) and the *Q* value, which is related to the Bit Error Rate (BER). The theoretical calculation of those terms will be particularised for the generic SCM scheme based on a pre-amplified receiver illustrated in Figure 2.9.

2.4.2.1 Carrier to Noise Ratio

From the detected photo-current of the system, the CNR measures the power ratio between a subchannel and the accumulated noise in the bandwidth of that subchannel.

The average photocurrent I_{avg} is equal to $R \cdot P_{PD}$, where R and P_{PD} represent the responsivity and the average optical power at the input of the photo-diode

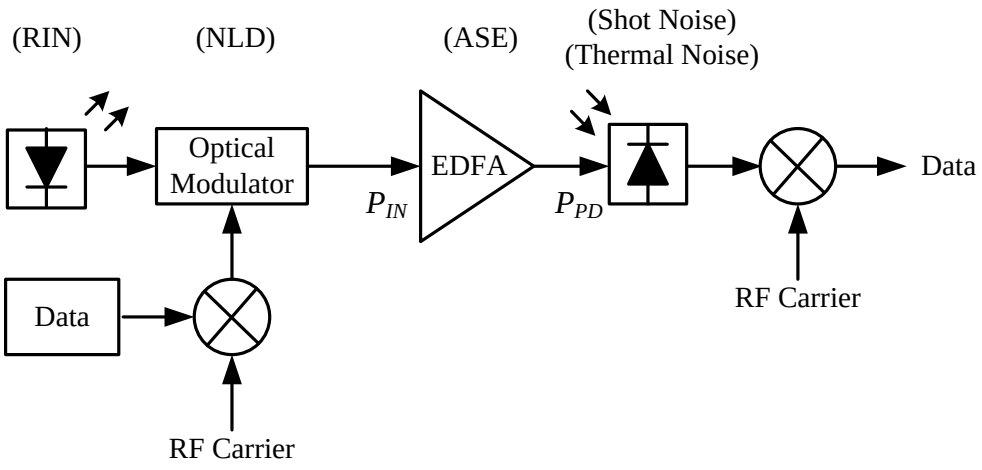

Figure 2.9 SCM scheme with pre-amplified receiver showing the sources of noise.

respectively. The amplitude of one subchannel, I_s, depends on the electrical driving level of the optical modulator [12] and is proportional to I_{avg}, such that $I_s=m\cdot I_{avg}$. Finally, as the subchannel is modulated on a subcarrier, the mean square current is:

$$\left\langle I_s^2 \right\rangle = \frac{\left(mI_{avg}\right)^2}{2}. \tag{2.27}$$

Photo-detected noise has its origin in several sources that will be described individually. The intensity at the output of a laser presents relative fluctuations, *RIN*, which translate into noise in DD systems. For data with a baseband bandwidth *B*, (2*B* in the RF spectrum), the associated photo-detected mean square current is [37]:

$$\left\langle I_{RIN}^2 \right\rangle = I_{avg}^2 \cdot RIN \cdot 2B. \tag{2.28}$$

The next source of noise is given by the Non Linear Distortion (NLD) generated by the optical modulator ($<I^2_{NLD}>$). This noise is proportional to the electrical driving level or *m*. There is a trade-off as a higher *m* increases the power of the desired signal $<I_s^2>$, but also translates into higher $<I^2_{NLD}>$ [29]. This term should also include the fibre induced nonlinearities explained in section 2.4.1.3 if they were meaningful.

The EDFA produces optical noise known as Amplified Spontaneous Emission (ASE). It is a consequence of photons that are generated by spontaneous emission and amplified inside the EDFA. In the photo-current, there are two contributions due to ASE. On the one hand the ASE beats with itself producing spontaneous-spontaneous beat noise. On the other hand, the ASE beats with the desired signal generating signal-spontaneous beat noise. This second contribution is the dominant noise in a pre-amplified receiver and can be expressed as [12]:

$$\left\langle I_{ASE}^2 \right\rangle = 2R^2 P_{IN} F h\nu G\left(G-1\right)B \tag{2.29}$$

where F is the noise figure of the EDFA, h is the Planck´s constant, ν is the frequency of the optical carrier, G is the gain of the EDFA and P_{IN} is the average optical power at the input. Note that $P_{PD}=G\cdot P_{IN}$.

The photo-diode itself is also a source of noise. Shot noise is a quantum effect related with the discreteness of photons as explained next. A photo-detector presents a constant probability of absorption of photons. A probability is in reality a long term average but, on the short term, the distribution of absorptions can vary with time. This non-uniformity is what produces shot noise and can be quantified as [37]:

$$\left\langle I_{shot}^2 \right\rangle = 2q\left(I_{avg} + I_d\right)2B \tag{2.30}$$

where q is the elementary charge and I_d is the dark current of the photo-diode. I_d is a consequence of the random generation of electrons and holes within the depletion area of the photo-diode. As a result, a constant current is produced even in the absence of incoming photons.

Finally, the resistive load R_L inside the photo-receiver is also a source of thermal noise. This noise is a consequence of the thermal agitation of the charged carriers within an electrical conductor. The mean square current is [37]:

$$\left\langle I_{th}^2 \right\rangle = \frac{4kT2B}{R_L} \tag{2.31}$$

where k is the Boltzmann constant and T is the temperature. In this case, the load resistance R_L must be taken into account to ensure the result is consistent with the units in the previous values (A^2).

Thus, the total CNR can be calculated summing all the contributions of noise [38] or as a function of individual CNRs:

$$CNR = \frac{\left\langle I_s^2 \right\rangle}{\left\langle I_{RIN}^2 \right\rangle + \left\langle I_{NLD}^2 \right\rangle + \left\langle I_{ASE}^2 \right\rangle + \left\langle I_{shot}^2 \right\rangle + \left\langle I_{th}^2 \right\rangle} \approx \frac{\left\langle I_s^2 \right\rangle}{\left\langle I_{NLD}^2 \right\rangle + \left\langle I_{ASE}^2 \right\rangle}. \tag{2.32}$$

$$CNR^{-1} = CNR_{RIN}^{-1} + CNR_{NLD}^{-1} + CNR_{ASE}^{-1} + CNR_{shot}^{-1} + CNR_{th}^{-1} \approx CNR_{NLD}^{-1} + CNR_{ASE}^{-1}. \tag{2.33}$$

As reflected in the previous equalities, the noise in pre-amplified receivers is usually dominated by the ASE. This is illustrated in Figure 2.10 showing the noise powers

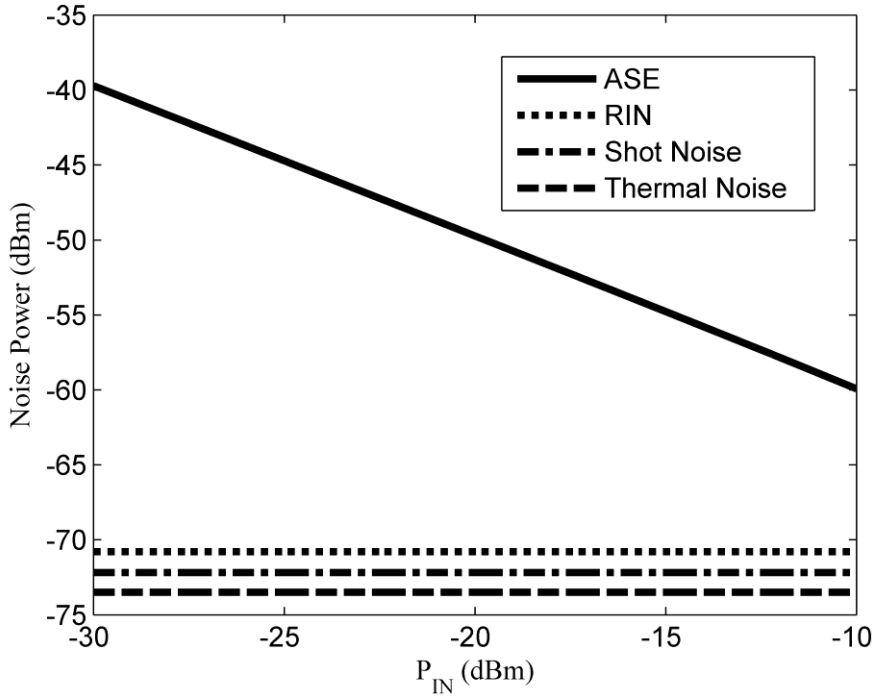

Figure 2.10 Noise power ($<I_i^2>\cdot R_L$) in a pre-amplified SCM system with parameters: R=0.7, P_{PD}=3 dBm, B=1.35 GHz, RIN=-155 dB/Hz, F=5 dB, λ=1550nm, I_d=100nA, T=300ºK, R_L=50 ohm.

obtained in a realistic broadband SCM configuration. The EDFA must ensure a constant output power P_{PD} regardless of the input level P_{IN}, so that the gain and the ASE are higher for lower values of P_{IN}. In the example, the noise from the EDFA is at least 10 dB higher than any other contribution. Apart from ASE, the NLD tends to be meaningful as the electrical driving of the modulator is increased as much as possible in order to reduce the sensitivity in the receiver. The CNR_{NLD} for a MZM can be found in [29], for a DD-MZM in [28, 35], and for an OIQM in Chapter 3.

2.4.2.2 *Q* value

The quality of a digital communication system can be measured with the BER. The higher the noise in the received signal is, the more difficult it is to discern bits giving rise to higher BER. Thus, the quality of the system can also be determined by the relation between signal and noise levels. The *Q* value performs such comparison by a Gaussian approximation of the noise. For a received signal in which I_0 and I_1 represent the amplitude of the associated photo-currents for '0' and '1', both cases under the influence of noise current with mean square value σ^2, the *Q* value is defined as [39]:

$$Q = \frac{I_1 - I_0}{2\sigma}. \tag{2.34}$$

From the previous subsection, the amplitude of the received photocurrent for one subchannel is denoted I_s. Therefore, the photo-current for '1' and '0' in a BPSK subchannel at the electrical subcarrier Ω would be:

$$\begin{aligned} i_1(t) &= I_s \cos(\Omega t). \\ i_0(t) &= -I_s \cos(\Omega t). \end{aligned} \tag{2.35}$$

And the associated Q value:

$$Q_{BPSK} = \frac{I_s - (-I_s)}{2\sigma} = \frac{I_s}{\sigma}. \tag{2.36}$$

In a QPSK subchannel there are four possible combinations:

$$\begin{aligned} i_{11}(t) &= \frac{I_s}{\sqrt{2}}\cos(\Omega t) + \frac{I_s}{\sqrt{2}}\sin(\Omega t) = I_s \cos(\Omega t - \pi/4). \\ i_{10}(t) &= \frac{I_s}{\sqrt{2}}\cos(\Omega t) - \frac{I_s}{\sqrt{2}}\sin(\Omega t) = I_s \cos(\Omega t + \pi/4). \\ i_{01}(t) &= -\frac{I_s}{\sqrt{2}}\cos(\Omega t) + \frac{I_s}{\sqrt{2}}\sin(\Omega t) = I_s \cos(\Omega t - 3\pi/4). \\ i_{00}(t) &= -\frac{I_s}{\sqrt{2}}\cos(\Omega t) - \frac{I_s}{\sqrt{2}}\sin(\Omega t) = I_s \cos(\Omega t + 3\pi/4). \end{aligned} \tag{2.37}$$

With the previous equations, it becomes clear that for a received subchannel amplitude of I_s, the associated baseband '1' and '0' amplitudes for the in-phase and quadrature components are $I_s/\sqrt{2}$ and $-I_s/\sqrt{2}$. Therefore:

$$Q_{QPSK} = \frac{\frac{I_s}{\sqrt{2}} - \left(-\frac{I_s}{\sqrt{2}}\right)}{2\sigma} = \frac{\sqrt{2}I_s}{2\sigma}. \tag{2.38}$$

Under a Gaussian approximation, the individual contributions of noise calculated in the previous subsection become $<I_i^2>= \sigma_i^2$, and assuming that all the sources of noise are uncorrelated, the total mean square current becomes $\sigma^2 = \sum_i \sigma_i^2$.

Finally, the relation between the *Q* factor and the BER is given by [39]:

$$BER = \frac{1}{2} erfc\left(\frac{Q}{\sqrt{2}}\right) \approx \frac{e^{-\frac{Q^2}{2}}}{Q\sqrt{2\pi}}. \qquad (2.39)$$

$$erfc(x) = \frac{2}{\sqrt{\pi}} \int_x^{\infty} e^{-t^2} \cdot dt.$$

2.5 Experimental SCM Scheme

This section details the experimental SCM link that was designed and built to accomplish the developments presented in this work. The section is organised as follows. Firstly, the performance of the key microwave components, namely the IQ mixers, is discussed. Secondly, the full electrical configuration is described. Finally, the electro-optical scheme is presented showing initial results. This setup is the base scheme for the measurements and more advanced configurations demonstrated in the upcoming chapters.

2.5.1 MMIC IQ Mixers

With the focus on ASP, microwave mixers become the key electrical components. These devices perform the modulation/demodulation of the subcarriers/subchannels and are the equivalent of multipliers in DSP systems. Previous SCM schemes have mostly used discrete non-integrated microwave mixers [12] and IQ mixers [16-18, 40]. Integrated MMIC mixers were firstly proposed as an option to transmit a control channel along with baseband information [41]. This section presents a setup that employs MMIC IQ mixers for the design of an SCM link consisting on five QPSK subchannels.

An IQ mixer is a passive device composed of two standard mixers. Figure 2.11 illustrates the schematic of a generic MMIC IQ mixer commercially available from “Hittite Microwave”. These devices can act as modulators or demodulators of

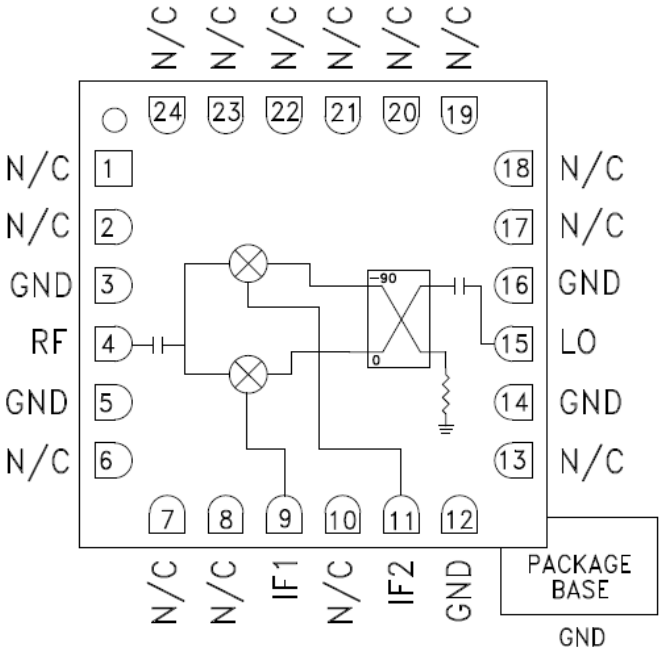

Figure 2.11: Typical schematic of an integrated IQ mixer from Hittite Microwave.

QAM subchannels. When performing a modulation, the IF1 and IF2 pins are the baseband I and Q inputs while the RF pin is an output. The signals flow in the opposite direction in the case of a demodulation. In both cases an incoming LO is passed through a hybrid coupler to create two LOs with a relative phase shift equal to 90 degrees. Each of these LOs feeds a different mixer allowing the IQ (de)modulation. Sometimes these devices present amplifiers in the RF path, becoming unidirectional, and are then referred to as IQ transmitters (Figure 2.12(a)) or IQ receivers (Figure 2.12(b)). For simplicity, during the following chapters, the term IQ mixer will be employed regardless of the presence or absence of additional amplifiers.

2.5.1.1 Frequency Plan

The MMIC IQ mixers were selected to implement the desired FDM signal. Baseband streams with a rate of 1.35 and 2.7 Gbaud were employed during the experiments. For several reasons that will be explained during the following chapters, the subchannels were located at harmonics of the data rate. Namely, five subchannels located at 2.7k GHz ($2 \leq k \leq 6$) were employed. This frequency plan represents a realistic trade-off that gives rise to a feasible industrial implementation. A low number of subchannels would translate into a high baseband data rate, and a more demanding requirement of performance from the IQ mixers. In contrast, a high number of subchannels would translate into too many components.

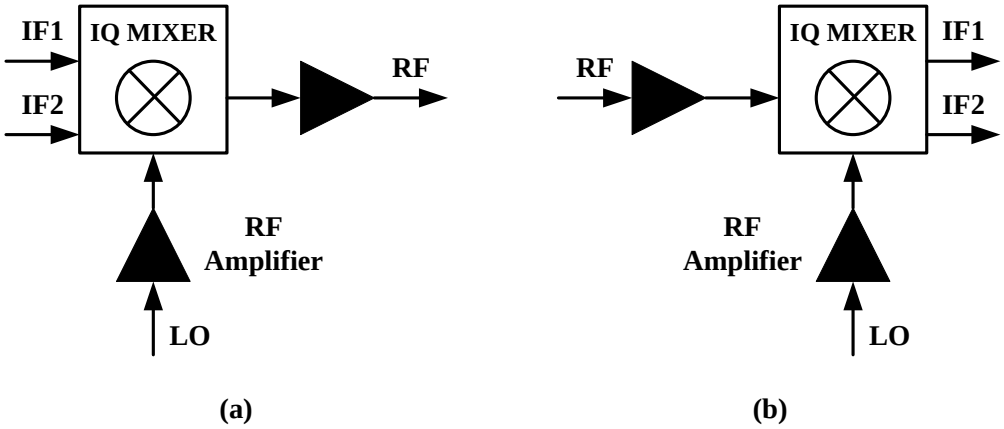

Figure 2.12 (a) IQ Transmitter (IQ_TX) and (b) IQ Receiver (IQ_RX)

Commercially available inexpensive MMIC IQ mixers from Hittite Microwave were used. With the wide range of frequencies required (≈2-20 GHz), Hittite Microwave was the only provider covering approximately the bandwidth of every subchannel with different MMIC IQ mixers. IQ transmitters and IQ receivers were developed combining MMIC IQ mixers and MMIC amplifiers. For every subchannel, the same model of IQ mixer was employed in both the transmitter and the receiver. Table 2-1 shows the part numbers of all the devices employed, including IQ mixers and amplifiers. It also compares the bandwidth requirement of every subchannel, for a baseband rate of 2.7 Gbaud, with the bandwidth specified by the manufacturer for the IQ mixer. The amplifiers are designed to present good performance with broadband signals, so that the IQ mixers are the main source of impairments. The next subsection discusses the suitability of the IQ mixers showing measurements that assess their performance when dealing with broadband signals.

2.5.1.2 Amplitude Response and Group Delay

MMIC mixers are designed for different applications like point to point and point to multipoint radio communications, test equipment, satellite communications and military use. In general, in all those applications, the bandwidth of baseband data is quite low when compared with the traditional rates of high-speed optical

Table 2-1 Bandwidth requirement and IQ mixer specification for every subchannel. Reference of components employed in the IQ transmitters and IQ receivers.

Band	*LO (GHz)*	*Bandwidth (GHz)*	*IQ mixer Reference*	*IQ mixer Specs. (GHz)*	*RF Amplifier Reference*	*LO Amplifier Reference*
1	5.4	2.7-8.1	HMC620	3-7	HMC464	HMC407
2	8.1	5.4-10.8	HMC520	6-10	HMC451	HMC441
3	10.8	8.1-13.5	HMC521	8.5-13.5	HMC451	HMC441
4	13.5	10.8-16.2	HMC522	11-16	HMC451	HMC441
5	16.2	13.5-18.9	HMC523	15-23	HMC451	HMC441

communications. The ratio between the carrier frequency and the modulation bandwidth of traditional radio links can be in the range of 100 – 1000. However, in optical systems like the one presented in this work, this ratio is much lower, in the range of 2 – 6. Consequently, although these mixers can have a wide range of radio frequencies at which they can work, they are not optimized for broadband data communications. This is a known issue that has been pointed out in other independent works in the field [42]. This subsection shows measurements of performance in terms of amplitude response and group delay for the selected family of MMIC IQ mixers.

The evaluation was carried out with the scheme presented in Figure 2.13. An IQ transmitter and an IQ receiver were cascaded to modulate and demodulate a subchannel with an IF tone coming from the network analyser. An attenuator was introduced at the output of the IQ transmitter to ensure the RF amplifier of the IQ receiver worked in the linear region. Extra LPFs were used at the output of the IQ receiver to suppress the LO leakage and the components that can appear at twice the electrical subcarrier frequency. The effect of the LPF in the measured bandwidth was calibrated out with the network analyser. A synthesizer generated the LO which was split to feed the modulator and the demodulator. The LO of the later was phase shifted to ensure phase locking to the input signal. For every subchannel, the frequency of the LO and the employed IQ mixers were the ones defined in Table 2-1. The described configuration characterizes the combined behaviour of one IQ transmitter and one IQ receiver in the complete process of modulation-demodulation. Ideally, perfectly flat amplitude and group delay responses are desired in the measured S-parameter $S_{21}(f)$ for all the baseband frequencies (≤ 2.7 GHz).

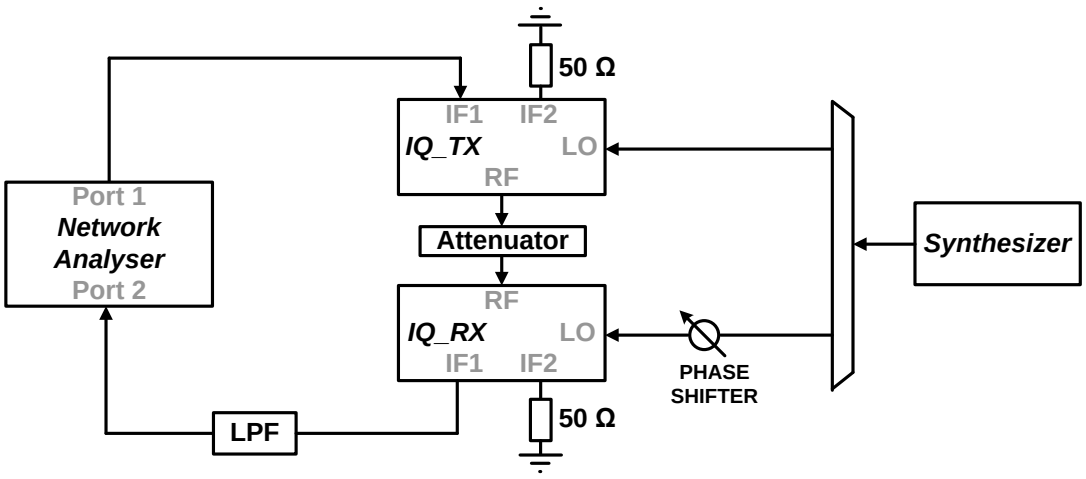

Figure 2.13 Setup for IQ mixer characterization with network analyser.

The characterization is depicted showing the normalised amplitude response (Figure 2.14) and the group delay response (Figure 2.15) measured for the five subchannels. The best performance is obtained in subchannel 3, where there is an almost perfect match between the desired and the specified bandwidth. Equivalently, the worst performance occurs at subchannel 5, as the bandwidth requirement presents a bandwidth of 1.5 GHz out of the specification of the mixers. Focusing now on the second frequency band, a transmission of 2 Gbaud would present a practically perfect match within the specification of the mixers (6-10 GHz). However, in such transmission there would be an amplitude ripple of around 1.5 dB and a group delay ripple of around 160 ps, not negligible for a bit period of 500 ps, which would translate into considerable inter symbol interference. These results confirm that these devices are not optimized for the transmission of broadband data and, as a consequence, it can be difficult to achieve high modulation orders. This concept is discussed with experimental results in the next subsection.

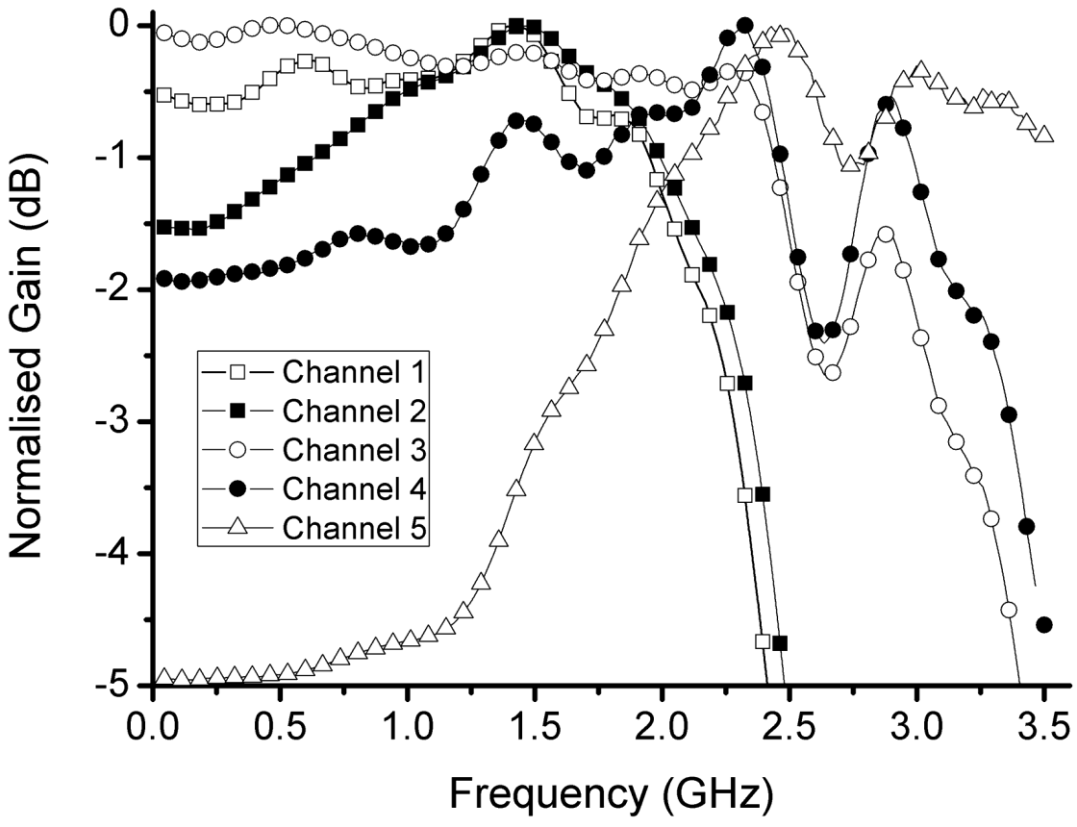

Figure 2.14 Overall amplitude response measured for the five subchannels.

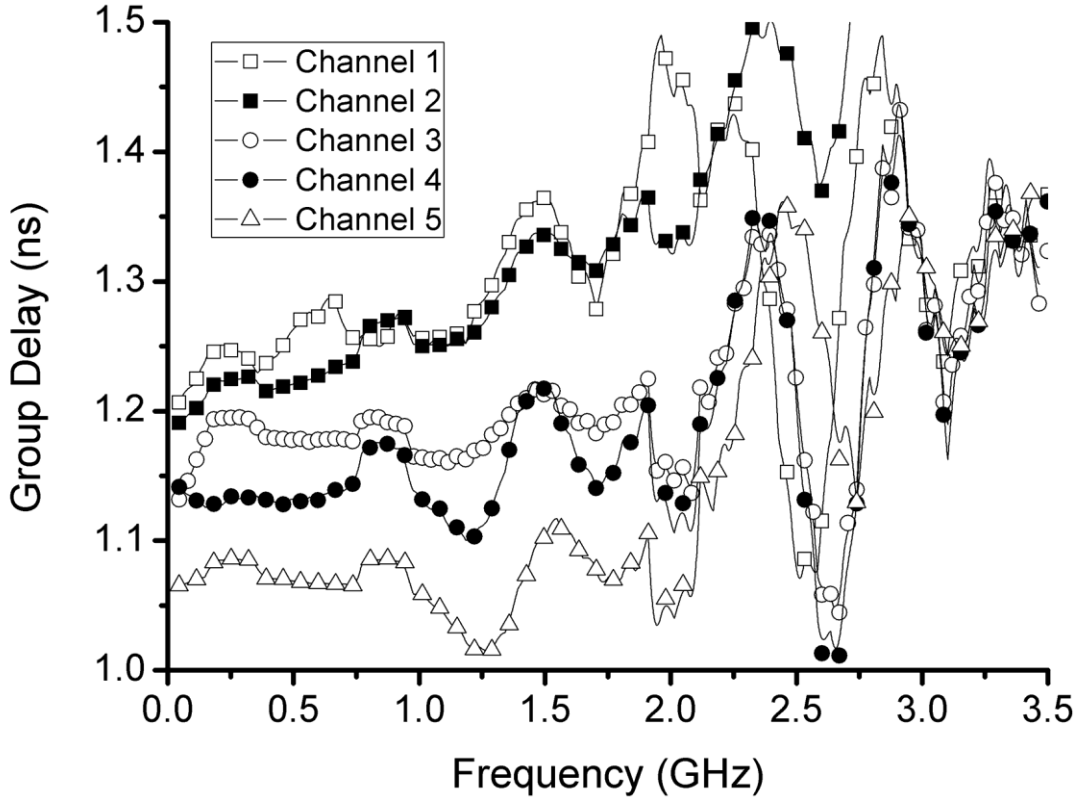

Figure 2.15 Overall group delay response measured for the five subchannels.

2.5.1.3 High Modulation Order

Broadband SCM transmission with 16-QAM subchannels has always relied on DSP [19-21]. The MMIC IQ mixers were evaluated to verify if their specifications could be stretched to obtain reliable 16 QAM transmission with the highest required data rates (≈2.7 Gbaud). The setup employed in these experiments is illustrated in Figure 2.16. The outputs of a digital data generator were filtered with LPFs to limit the sinc spectrum of the generated square signals to the first lobe of the

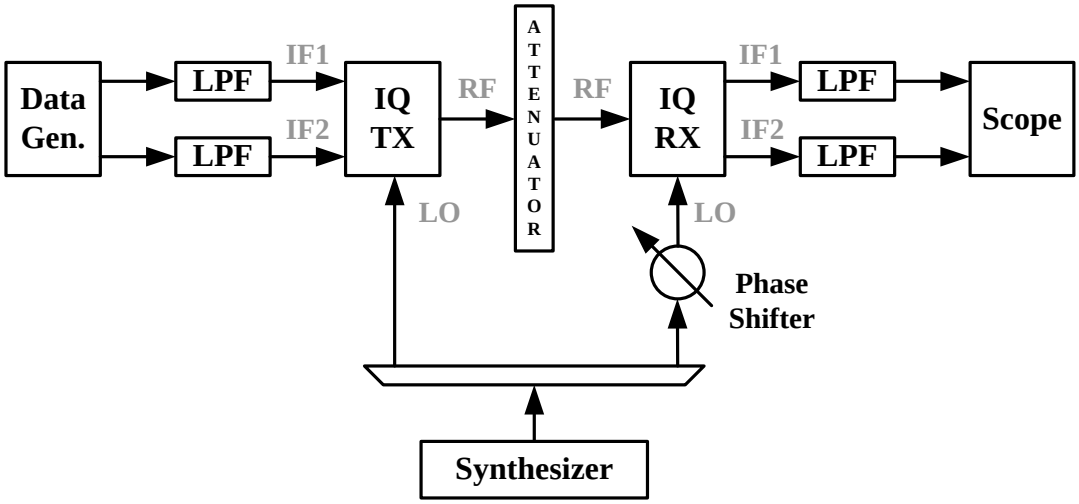

Figure 2.16 Setup for IQ mixer characterization with digital sampling scope.

sinc. These digital signals were fed to the baseband inputs of the IQ transmitter. Its output was attenuated to adapt its power to the input of the IQ receiver. The outputs of the demodulator were filtered with LPFs to remove high frequency components and any leakage coming from the LO. The LOs had the same origin so that frequency locking was guaranteed and phase locking was achieved with a variable phase shifter in the receiver. A digital scope was used to visualize the eye diagrams of the received signals.

The behaviour of any mixer depends on the data rate, the modulation order and the length of the digital pattern, as longer sequences will have more spectral content that will be affected by group delay ripple more severely. The results obtained with the devices of the second subchannel will be analysed. As these IQ mixers present an overall 3 dB loss at 2.4 GHz, a baseband data rate of 2.5 Gbit/s was attempted, with a 16-QAM modulation at a subcarrier frequency of 8.1 GHz. The 16-QAM subchannel was achieved transmitting the PAM_4 baseband signals that can be observed in Figure 2.17(a). Using data locked to the LO and a short pattern (127 bits), the received eye diagram was really poor for both the I and Q components as it can be observed in Figure 2.17(b). This result confirms that amplitude distortion and a group delay ripple comparable with the bit period severely penalises the performance at high modulation orders. Note that additional impairments would be added due to an optical transmission.

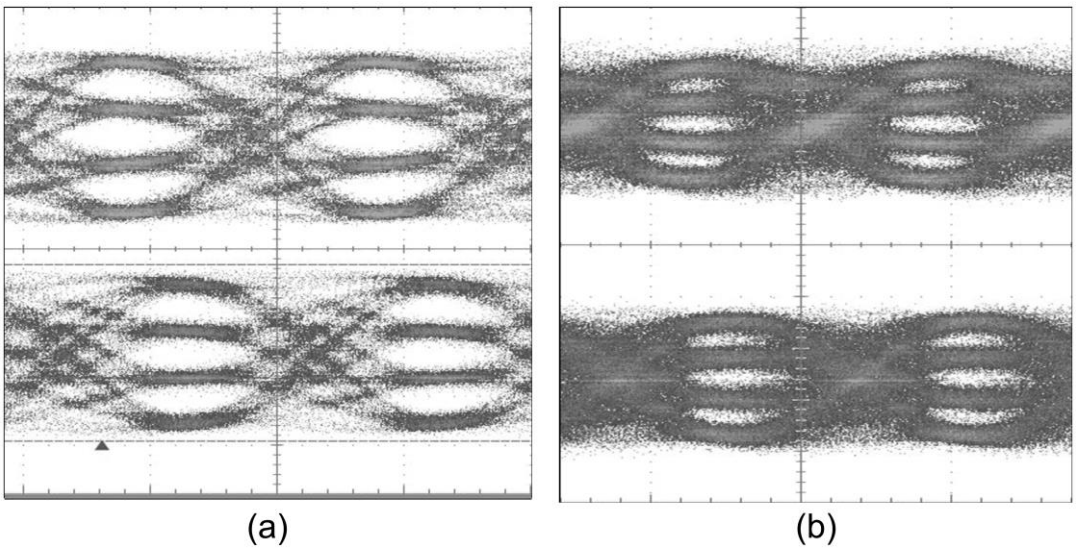

Figure 2.17 Transmitted (a) and received (b) I and Q data for a 2.5 Gbaud 16 QAM modulation and demodulation performed with the IQ mixer HMC520 at 8.1 GHz.

More experiments were conducted with several combinations of mixers, not only MMIC, working as modulators and demodulators. In a few cases, ensuring the RF signal was within the limits of the bandwidth specification and using short patterns, it was possible to achieve good quality with 16-QAM subchannels at rates around 1.25 Gbaud. However, for the design of an SCM link consisting of several subchannels, it is difficult to find off-the-shelf devices with a perfect frequency range match and with amplitude and group delay characteristics that can give rise to reliable performance at 16-QAM. For that reason the experiments performed in this work were conducted with QPSK modulation. Accordingly, some eye diagrams obtained with QPSK subchannels will be shown below. In general, the QPSK modulation is not a limitation in the sense that the relevance of the ideas and studies developed in this document do not depend on the overall transmission rate. 16-QAM subchannels could be made a reality even at higher rates with a custom IC [8].

2.5.2 Electrical implementation

This section details the electrical circuitry and schematics that were designed and implemented for the experiments. The IQ transmitters and receivers have been specified in Table 2-1. The remaining electrical components are defined in Table 2-2.

2.5.2.1 Baseband Data Generation

The use of five QPSK subchannels implies ten digital baseband signals. Ideally, pulse pattern generators with ultra-low output jitter should be used. However, due to the high number of signals required, an FPGA with integrated multi

Table 2-2 Electrical components employed in the experiments

Description	*Provider*	*Model*	*Specifications*	*Other*
FPGA	Xilinx	Virtex-6 XC6VLX240T	Transceivers ≤6.6 Gbit/s	Evaluation Board ML623
LPF	Minicircuits	SBLP-933+	3 dB BW 933 MHz	For 1.35 Gbaud
LPF	BT&D	FLPA2	3 dB BW 2 GHz	For 2.7 Gbaud
Splitter/ Combiner	Sigatek	SP10605	2-18 GHz	6 Way Wilkinson
Broadband Amplifier	Minicircuits	ZVA213+	0.8-21 GHz	
90º Hybrid Coupler	Marki Microwave	QH-0226	2-26.5 GHz	
SRD	Herotek	GCA2700	2.7-21.6 GHz	Comb Generator Input 2.7 GHz

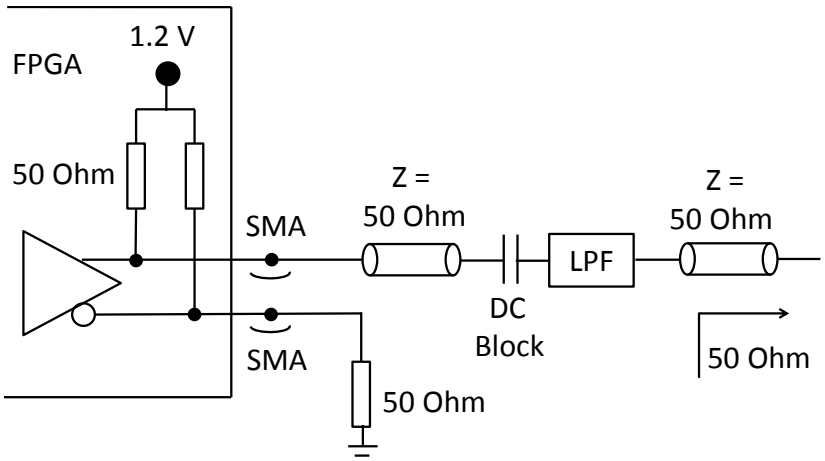

Figure 2.18: Baseband signal generation and conditioning: from DC coupled differential to AC coupled single-ended.

gigabit electrical transceivers was employed [43]. The generation of the baseband signals with a real integrated circuit also reinforces the feasibility of the proposed ideas for practical systems. Output data was uncorrelated due to different track lengths in the Printed Circuit Board (PCB) and different cable lengths. The outputs of the transceivers were square, differential, and had a DC offset. The schematic shown in Figure 2.18 converted the signals to single-ended and AC coupled, and reduced the spectrum to the first lobe of the sinc associated with the square pulse. For the later task, a Bessel LPF with a 3 dB cut-off frequency at 75% of the data rate is usually employed [44]. Accordingly, different LPFs were used for the different rates as specified in Table 2-2.

2.5.2.2 RF Transmitter

The RF transmitter consisted of five QPSK electrical subchannels, as it can be observed in Figure 2.19. With binary streams of 1.35 Gbit/s, the rate per QPSK subchannel was 2.7 Gbit/s and the overall data rate was 13.5 Gbit/s. The subcarriers were located at multiples of 2.7 GHz ensuring that there was no guard band between electrical subchannels. The IQ transmitters specified in Table 2-1 were employed. The outputs of the mixers were attenuated equalizing the power level per subchannel. Then, all the subchannels were combined in a single signal using a 6 way Wilkinson power combiner. The resultant broadband signal was amplified and, finally, a 90º hybrid coupler obtained the HT pair with a relative phase shift of 90 degrees required to perform a SSB modulation. The minimum attenuation at the output of every IQ transmitter was 3 dB. Apart from equalization, the attenuation reduces the effects of impedance mismatches. Similarly, the attenuation between the wideband components compensates mismatches and adjusts the power that will drive the optical modulator.

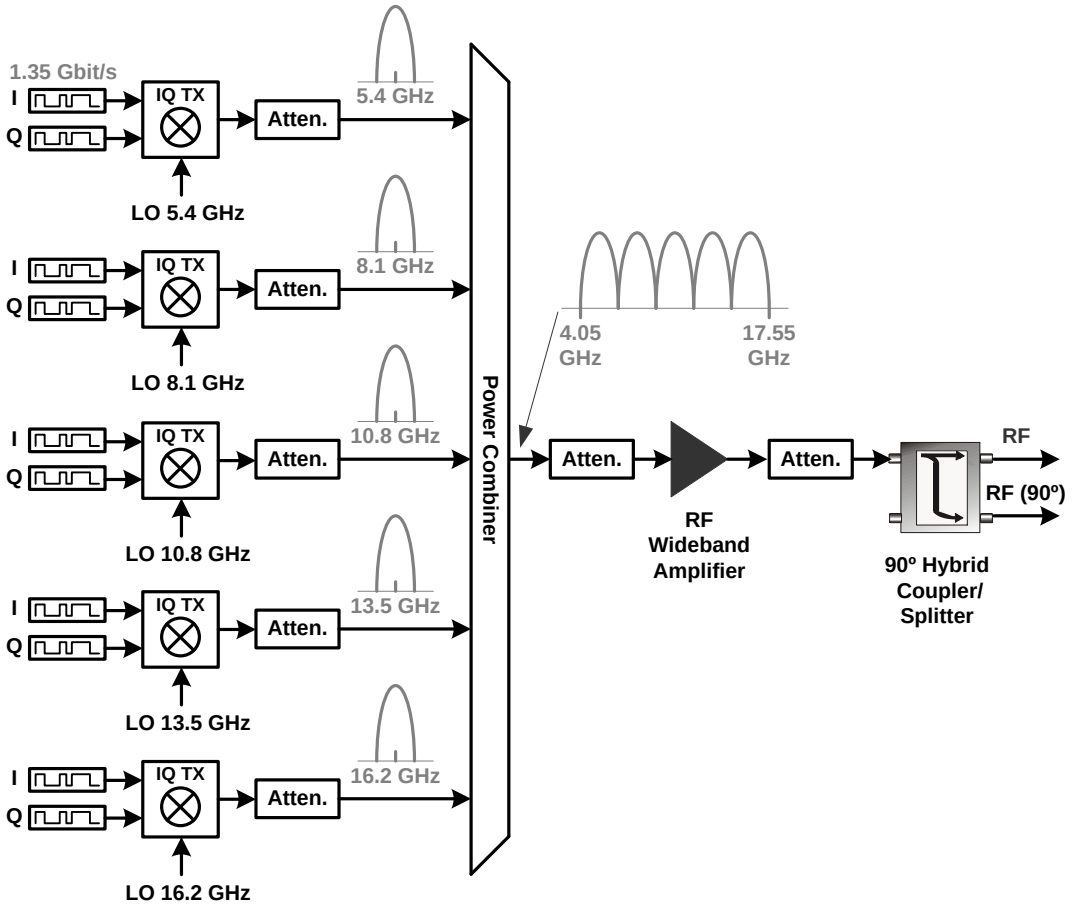

Figure 2.19 RF Transmitter illustrating spectra for 1.35 Gbaud QPSK subchannels.

Due to the imperfect behaviour of IQ mixers, low power replicas of the subchannels can be created at harmonics of the subcarrier frequencies. This unwanted nonlinearity is a potential source of cross-talk once the subchannels are combined. The undesired replicas can be eliminated using a Bandpass Filter (BPF) at the output of every mixer. For this application each of the BPFs should present a different passband with a constant group delay. This solution was also implemented with custom BPFs, but the mismatches and imperfections introduced by the filters translated into a penalty with respect to the original case. For that reason, the experiment was conducted without BPFs as illustrated in Figure 2.19. As will be shown below, good performance with clearly open eye diagrams was achieved with the QPSK subchannels.

2.5.2.3 RF Receiver

The RF receiver performed the equivalent demodulation, as can be seen in Figure 2.20. The received broadband signal was amplified and split. The wideband amplifier and the power combiner were the same model used in the RF transmitter. Attenuators were employed to reduce the effects of the distortion associated with the

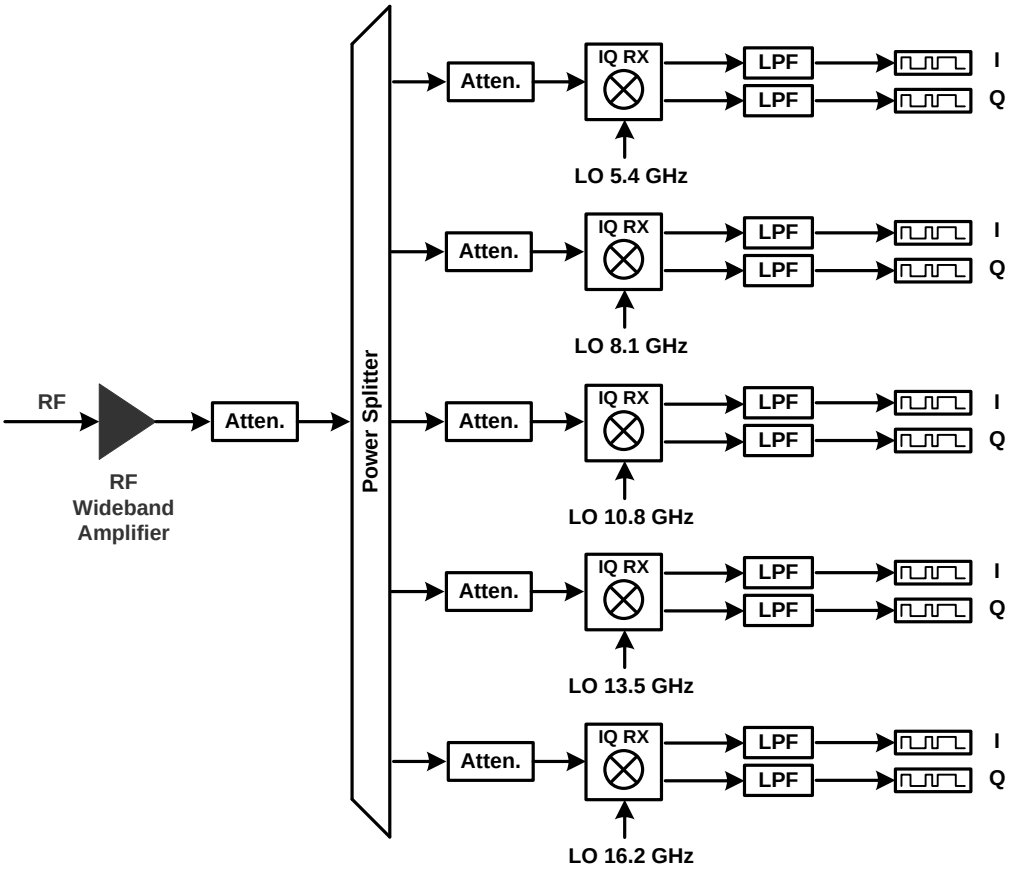

Figure 2.20 RF Receiver.

impedance mismatches. The LOs were phase and frequency locked to the incoming subchannels with the scheme explained in the next subsection. The outputs of the IQ mixers were filtered to suppress the high frequency components and any possible leakage coming from the LOs. To accomplish that task, the LPF reported in Table 2-2 was cascaded with an additional Bessel LPF of higher cut-off frequency, achieving higher high-frequency attenuation without affecting the desired portion of the spectrum. In the experiments, the performance of the received baseband digital signals was evaluated with a Bit Error Rate Tester (BERT).

2.5.2.4 LO Generation and Distribution

The use of subcarriers located at harmonics of the data rate allowed a simplified generation of the LOs. An electrical comb or Step Recovery Diode (SRD) was fed with a 2.7 GHz tone coming from a synthesizer. The 10 MHz output reference of the synthesizer was also used to lock the FPGA clocks, ensuring data and LOs were frequency locked. The outputs of the electrical comb were filtered with a microwave quintplexer that presented one input and five outputs, obtaining every LO in a separated line. Each LO was handled with a custom design PCB that split, amplified and phase shifted them, allowing a variable management of phases

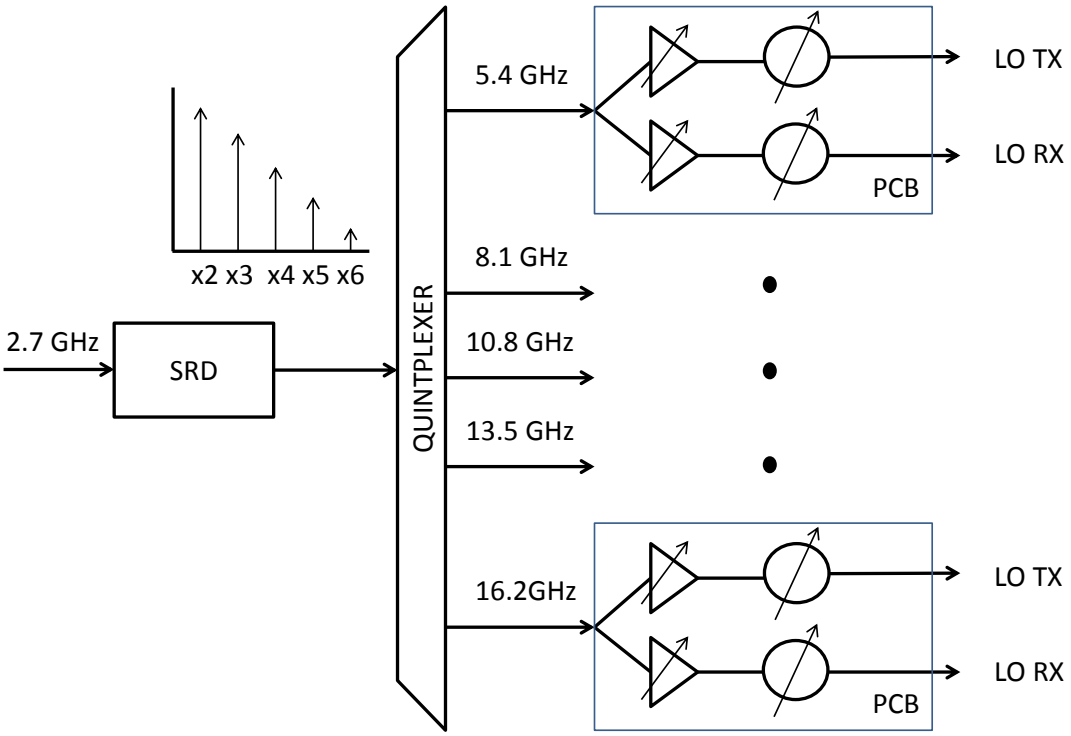

Figure 2.21 LO generation and distribution.

and amplitudes of the LOs for both the RF transmitter and RF receiver. A block diagram of that scheme is illustrated in Figure 2.21. The detailed schematics of the PCB with all the components can be found in Appendix A.

With the described setup, frequency locking at the receiver is guaranteed, as the employed LO has exactly the same origin as the transmitter. For the phase locking, variable phase shifters are employed and can be easily adjusted manually. This is the approach that is traditionally used to avoid synchronization circuitry [12, 16]. In a practical real system the phase locking would be achieved with a phase locked loop (PLL) [17] or with a carrier recovery circuit [40]. A novel synchronization scheme will be demonstrated in Chapter 5.

2.5.3 Electro-Optical Scheme

Combined with the previous RF transmitter and receiver, the optical link was established using the components defined in Table 2-3. The global setup is illustrated in Figure 2.22 simplifying the electronic circuitry. For versatility, full C band tunable ECL lasers were employed. For the optical modulation, a thin film polymer OIQM was selected owing to its high BW, low V_π and good bias point stability [45]. For the optical detection, a photo-receiver with the same bandwidth as the optical modulator, 20 GHz, was employed. EDFAs were used in both the transmitter and the receiver. The transmitter EDFA amplified the output of the OIQM and established the power

Table 2-3 Optical components employed in the experiments

Description	*Provider*	*Model*	*Specifications*	*Other*
Laser	ID Photonics	CBDX4-2-C-H01	ECL	C Band Tunable
OIQM	Gigoptix	LX-8220	BW 20 GHz V_π = 2.5 V	
Photo-Receiver	Discovery Semiconductor	DSC-R401HG	BW 20 GHz R = 0.7 A/W	
EDFA	IPG	EAD-50-C-30	NF=5dB	TX
EDFA	Alnair	LNA-100	NF=4dB	RX
VOA	Eigen Light	410		

launched into the fibre. In the receiver end, the EDFA acted as a pre-amplifier that provided a constant power to the photodetector regardless of the incoming optical power. Optical filters with a bandpass bandwidth of 2 nm were used at the output of every EDFA to remove ASE. A Variable Optical Attenuator (VOA) was introduced to emulate fibre losses changing the average optical power at the input of the pre-amplified receiver.

Examples of electrical and optical spectra are illustrated in Figure 2.23 for 1.35 Gbaud QPSK subchannels. The FDM electrical spectrum is obtained at the output of the wideband amplifier in the transmitter. It can be seen that there is no guard band between subchannels. The illustrated SCM/OSSB optical spectrum is obtained at the output of the transmitter EDFA. In this case the OIQM is biased at quadrature and the optical carrier, necessary to perform direct detection, is present in the output.

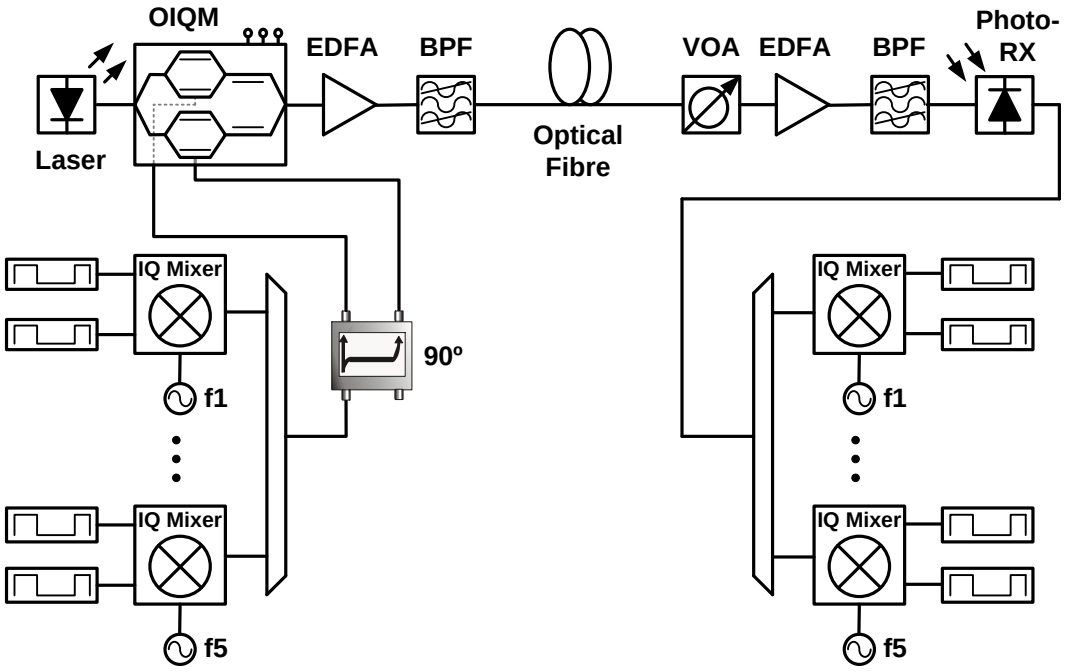

Figure 2.22 SCM/OSSB scheme consisting of 5 QPSK subcarriers and one OIQM.

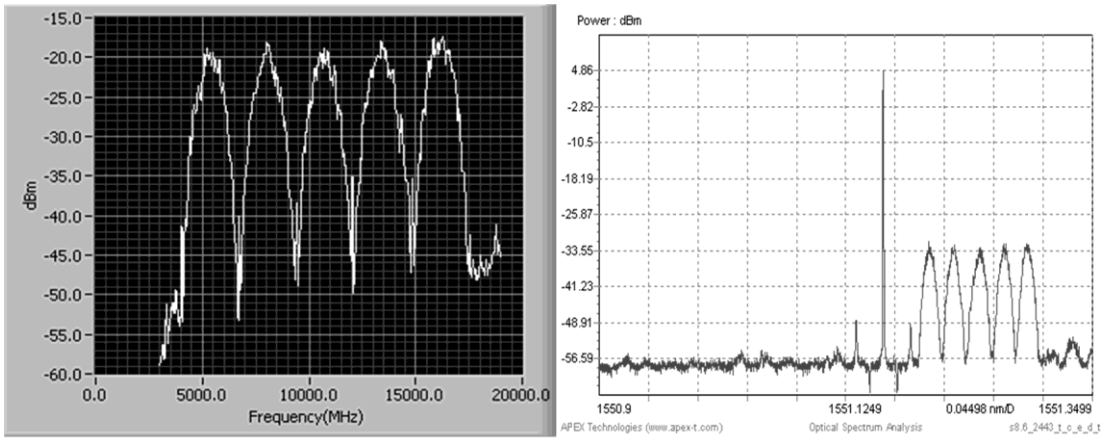

(a) **(b)**

Figure 2.23 Examples of (a) electrical spectrum at the output of the RF amplifier in the transmitter and (b) OSSB optical spectrum at the output of the transmitter EDFA.

Examples of received eye diagrams for the I and Q components of the five subchannels are illustrated in Figure 2.24. These particular results were obtained with a transmitted optical power of 5 dBm in a back to back configuration. The input level of the receiver EDFA was -10 dBm and the power at the input of the photodetector was 3 dBm. The length of the baseband Pseudo Random Binary Sequences (PRBS) was 2^{15}-1 bits. Different amplitudes were a consequence of the different conversion gains of the IQ receivers in each frequency band. Despite this asymmetry, open eye diagrams with BER<10^{-9} were obtained in all the cases. These results prove that broadband SCM/OSSB electro-optical transceivers based on MMIC technology are feasible. The next chapters will show measurements of performance in different situations and configurations.

2.6 Conclusions

SCM divides the available bandwidth into narrower subchannels obtaining high-speed transmission with relevant advantages: increased tolerance to dispersion and baseband signals with reduced bit rate.

Best SCM performance is achieved when it is combined with two techniques: OSSB and carrier suppression. OSSB avoids dispersive fading and allows a closer allocation of WDM channels. Carrier suppression potentially achieves better sensitivities in the receiver. SCM/OSSB and carrier suppression can only be achieved simultaneously with OIQMs.

From an electronic perspective, ASP is preferred to ensure low power consumption and low latency, but a practical industrial implementation would only be possible employing MMIC technology.

An SCM/OSSB electro-optical transceiver consisting of an OIQM and relying on off-the-shelf MMIC technology has been presented. The key electrical components, IQ mixers, have been characterized. Initial results have shown five QPSK subchannels at a symbol rate of 1.35 Gbaud, achieving an overall data rate of 13.5 Gbit/s. This setup is the base for the rest of studies that will be developed in the subsequent chapters.

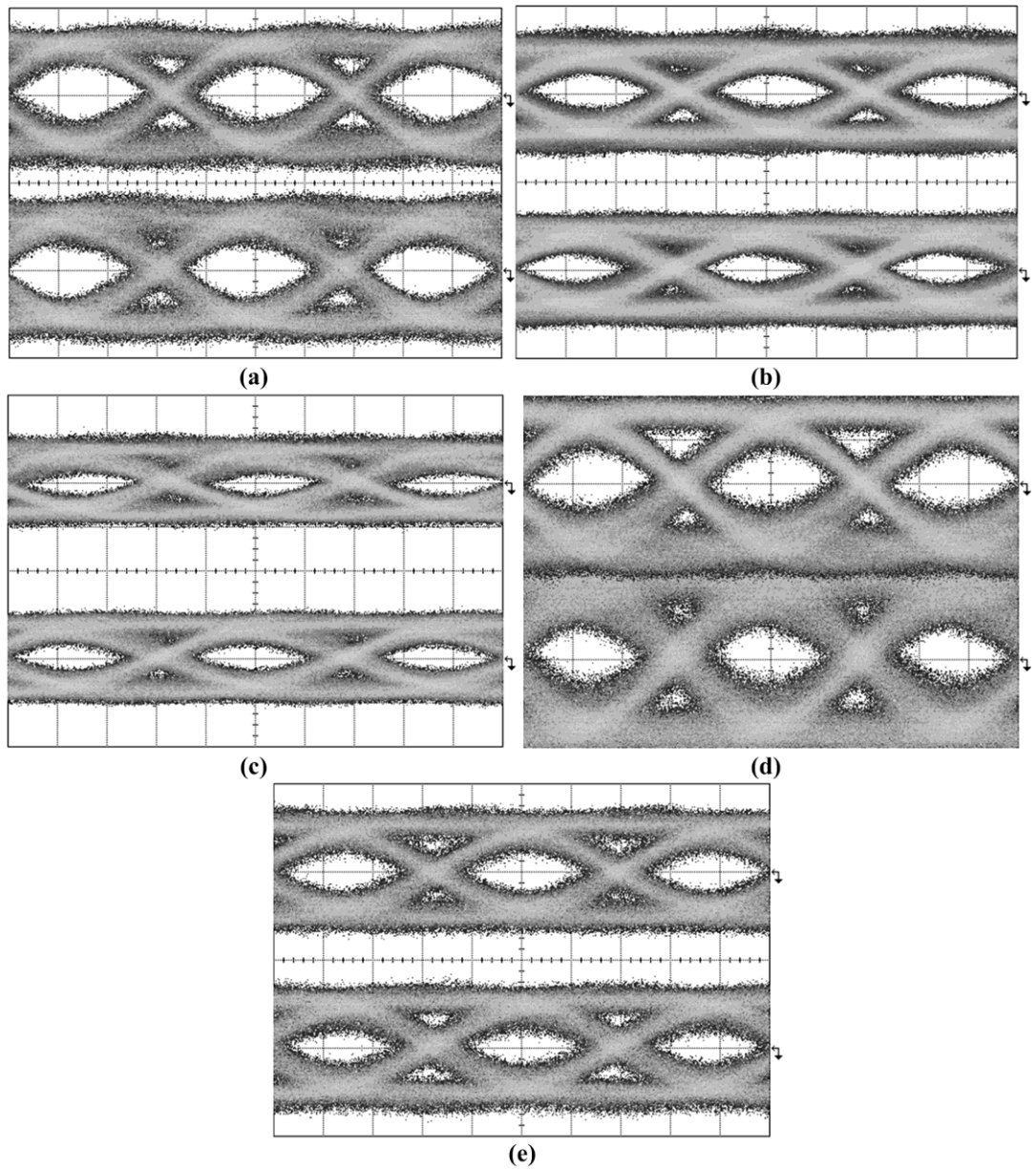

Figure 2.24 (a)-(e) Examples of eye diagrams for the five 1.35 Gbaud subchannels

2.7 References

[1] T. E. Darcie and G. E. Bodeep, "Lightwave subcarrier CATV transmission systems," *Microwave Theory and Techniques, IEEE Transactions on*, vol. 38, pp. 524-533, 1990.

[2] C. Bisdikian, B. McNeil, R. Norman, and R. Zeisz, "MLAP: a MAC level access protocol for the HFC 802.14 network," *Communications Magazine, IEEE*, vol. 34, pp. 114-121, 1996.

[3] E. L. Wooten, K. M. Kissa, A. Yi-Yan, E. J. Murphy, D. A. Lafaw, P. F. Hallemeier, *et al.*, "A review of lithium niobate modulators for fiber-optic communications systems," *IEEE Journal of Selected Topics in Quantum Electronics*, vol. 6, pp. 69-82, 2000.

[4] J.-S. Baik and C.-H. Lee, "Hybrid WDM/SCMA-PON using wavelength-locked fabry-Perot laser diodes," *Photonics Technology Letters, IEEE*, vol. 18, pp. 1585-1587, 2006.

[5] J. M. P. Delavaux, G. C. Wilson, C. Hullin, B. Neyret, and C. Bethea, "QAM-PON and super PON for access distribution networks," in *Optical Fiber Communication Conference and Exhibit, 2001. OFC 2001*, 2001, pp. WN2-WN2.

[6] A. Lebreton, B. Charbonnier, G. B. de Farias, P. Chanclou, D. Rongping, J. Le Masson, *et al.*, "Low complexity FDM/FDMA approach for future PON," in *Optical Fiber Communication Conference and Exposition and the National Fiber Optic Engineers Conference (OFC/NFOEC), 2013*, 2013, pp. 1-3.

[7] K. Chen-Ken and K. Sy-Yen, "Multiaccess processor interconnection using subcarrier and wavelength division multiplexing," *Lightwave Technology, Journal of*, vol. 15, pp. 228-241, 1997.

[8] M. Salter, D. Platt, L. Pettersson, L. Aspemyr, and B. Mingquan, "Circuits and system simulations for 100Gb/s optical SCM transmission," in *Electronics, Circuits, and Systems, 2009. ICECS 2009. 16th IEEE International Conference on*, 2009, pp. 960-963.

[9] E. I. Ackerman and C. H. Cox, "RF fiber-optic link performance," *Microwave Magazine, IEEE*, vol. 2, pp. 50-58, 2001.

[10] D. Novak, R. B. Waterhouse, A. Nirmalathas, C. Lim, P. A. Gamage, T. R. Clark, *et al.*, "Radio-Over-Fiber Technologies for Emerging Wireless Systems," *Quantum Electronics, IEEE Journal of*, vol. 52, pp. 1-11, 2016.

[11] A. de la Oliva, J. A. Hernández, D. Larrabeiti, and A. Azcorra, "An overview of the CPRI specification and its application to C-RAN based LTE scenarios," *Communications Magazine, IEEE*, 2015.

[12] R. Hui, Z. Benyuan, H. Renxing, C. T. Allen, K. Demarest, and D. Richards, "Subcarrier multiplexing for high-speed optical transmission," *Lightwave Technology, Journal of*, vol. 20, pp. 417-427, 2002.

[13] M. C. Wu, J. K. Wong, K. T. Tsai, Y. L. Chen, and W. I. Way, "740-km transmission of 78-channel 64-QAM signals (2.34 Gb/s) without dispersion compensation using a recirculating loop," *IEEE Photonics Technology Letters*, vol. 12, pp. 1255-1257, 2000.

[14] T. Fujiwara and K. Kikushima, "140 Carrier, 20GHz SCM Signal Transmission across 200km SMF by Two-step Sideband Suppression Scheme in Optical SSB Modulation," in *Optical Fiber Communication and the National Fiber Optic Engineers Conference, 2007. OFC/NFOEC 2007. Conference on*, 2007, pp. 1-3.

[15] M. Qiu, Q. Zhuge, X. Xu, M. Chagnon, M. Morsy-Osman, and D. V. Plant, "Subcarrier multiplexing using DACs for fiber nonlinearity mitigation in coherent optical communication systems," in *Optical Fiber Communications Conference and Exhibition (OFC), 2014*, 2014, pp. 1-3.

[16] J. Y. Ha, A. Wonfor, R. V. Penty, I. H. White, and P. Ghiggino, "Spectrally Efficient 10x1 Gb/s QPSK Multi-User Optical Network Architecture," in *Optical Fiber*

Communication and the National Fiber Optic Engineers Conference, 2007. OFC/NFOEC 2007. Conference on, 2007, pp. 1-3.

[17] P. Kourtessis and S. D. Walker, "A Complete 8-GHz QPSK-MODEM Featuring Novel Subcarrier and Data Synchronization for Optical Communications," *IEEE Transactions on Communications*, vol. 55, pp. 987-995, 2007.

[18] P. M. Anandarajah, Z. Rui, V. Vujicic, M. Deseada Gutierrez Pascual, E. Martin, and L. P. Barry, "Long reach UDWDM PON with SCM-QPSK modulation and direct detection," in *Optical Fiber Communications Conference and Exhibition (OFC), 2014*, 2014, pp. 1-3.

[19] F. A. Flood, "A 20 Gb/s per wavelength subcarrier multiplexed optical transmission system," in *Optical Fiber Communication Conference and Exhibit, 2002. OFC 2002*, 2002, pp. 145-146.

[20] L. Giorgi, F. Cavaliere, P. Ghiggino, F. Ponzini, A. Bianchi, and A. D'Errico, "Characterization of a High Capacity Multi-User Optical Access Network Using 1 Gb/s 16 QAM Subcarrier Multiplexing," *Lightwave Technology, Journal of*, vol. 27, pp. 1203-1211, 2009.

[21] B. E. Olsson, A. Kristiansson, and A. Alping, "40 Gbit/s, 16-QAM, transmission utilizing electronic sub-carrier technique and direct detection reception," in *Communications and Photonics Conference and Exhibition (ACP), 2009 Asia*, 2009, pp. 1-2.

[22] I. D. Robertson and S. Lucyszyn, *RFIC and MMIC Design and Technology*: Iet, 2001.

[23] F. Marki and C. Marki, "Mixer Basics Primer," *Marki Microwave. USA.[Online]. Available: www. mar imicrowave. com/menus/appnotes/mixer_basics_primer. pdf*, 2010.

[24] G. E. Betts, "High dynamic range coherent analog links using AM-SSB," in *Lasers and Electro-Optics Society, 2004. LEOS 2004. The 17th Annual Meeting of the IEEE*, 2004, pp. 130-131 Vol.1.

[25] X. Shijun and A. M. Weiner, "Optical carrier-suppressed single sideband (O-CS-SSB) Modulation using a hyperfine blocking filter based on a virtually imaged phased-array (VIPA)," *IEEE Photonics Technology Letters*, vol. 17, pp. 1522-1524, 2005.

[26] M. L. Farwell, W. S. C. Chang, and D. R. Huber, "Increased linear dynamic range by low biasing the Mach-Zehnder modulator," *IEEE Photonics Technology Letters*, vol. 5, pp. 779-782, 1993.

[27] V. J. Urick, M. E. Godinez, P. Devgan, J. D. McKinney, and F. Bucholtz, "Analysis of an Analog Fiber-Optic Link Employing a Low-Biased Mach–Zehnder Modulator Followed by an Erbium-Doped Fiber Amplifier," *Journal of Lightwave Technology*, vol. 27, pp. 2013-2019, 2009/06/15 2009.

[28] P. Laurencio, S. O. Simoes, and M. C. R. Medeiros, "Impact of the Combined Effect of RIN and Intermodulation Distortion on OSSB/SCM Systems," *Lightwave Technology, Journal of*, vol. 24, pp. 4250-4262, 2006.

[29] W. I. Way, *Broadband Hybrid Fiber Coax Access System Technologies*: Academic Press, Inc., 1998.

[30] G. H. Smith, D. Novak, and Z. Ahmed, "Overcoming chromatic-dispersion effects in fiber-wireless systems incorporating external modulators," *Microwave Theory and Techniques, IEEE Transactions on*, vol. 45, pp. 1410-1415, 1997.

[31] F. Devaux, Y. Sorel, and J. F. Kerdiles, "Simple measurement of fiber dispersion and of chirp parameter of intensity modulated light emitter," *Journal of Lightwave Technology*, vol. 11, pp. 1937-1940, 1993.

[32] H. Schmuck, "Comparison of optical millimetre-wave system concepts with regard to chromatic dispersion," *Electronics Letters*, vol. 31, pp. 1848-1849, 1995.

[33] J. Maeda, T. Katoh, and S. Ebisawa, "Effect of Fiber Dispersion on Subcarrier QAM Signal in Radio-Over-Fiber Transmission," *Lightwave Technology, Journal of*, vol. 30, pp. 2625-2632, 2012.

[34] J. Conradi, "Bandwidth-efficient modulation formats for digital fiber transmission systems," *Optical fiber telecommunications IV B*, pp. 862-901, 2002.
[35] W. H. Chen and W. I. Way, "Multichannel single-sideband SCM/DWDM transmission systems," *Lightwave Technology, Journal of*, vol. 22, pp. 1679-1693, 2004.
[36] J. Gibson, "Synchronous optical network (SONET) transport systems: Common generic criteria," GR-1377-CORE.
[37] G. Keiser, "Optical fiber communication," *NY: McGraw-Hill*, 2000.
[38] X. Lu and O. Sniezko, "The evolution of Cable TV networks," *Optical Fiber Telecommunications IV-B: Systems and Impairments*, vol. 2, p. 404, 2002.
[39] G. P. Agrawal, *Fiber-Optic Communication Systems*, 3rd ed.: Wiley, 2002.
[40] P. Hill and R. Olshansky, "Bandwidth efficient transmission of 4 Gb/s on two microwave QPSK subcarriers over a 48 km optical link," *Photonics Technology Letters, IEEE*, vol. 2, pp. 510-512, 1990.
[41] D. J. Blumenthal, J. Laskar, R. Gaudino, H. Sangwoo, M. D. Shell, and M. D. Vaughn, "Fiber-optic links supporting baseband data and subcarrier-multiplexed control channels and the impact of MMIC photonic/microwave interfaces," *Microwave Theory and Techniques, IEEE Transactions on*, vol. 45, pp. 1443-1452, 1997.
[42] B. Olsson, J. Martensson, A. Kristiansson, and A. Alping, "RF-assisted optical dual-carrier 112 Gbit/s polarization-multiplexed 16-QAM transmitter," in *Optical Fiber Communication (OFC), collocated National Fiber Optic Engineers Conference, 2010 Conference on (OFC/NFOEC)*, 2010, pp. 1-3.
[43] Xilinx. (2011), Virtex-6 FPGA GTX Transceivers User Guide UG366. Available: http://www.xilinx.com/support/documentation/user_guides/ug366.pdf
[44] J. R. Andrews, "Low-pass risetime filters for time domain applications," *Picosecond Pulse Labs, Application Note AN-7a*, 1999.
[45] Y. Guomin, E. Miller, J. Mallari, W. Cailin, C. Baoquan, C. Hui, *et al.*, "Small form factor thin film polymer modulators for telecom applications," in *Optical Fiber Communication Conference and Exposition (OFC/NFOEC), 2012 and the National Fiber Optic Engineers Conference*, 2012, pp. 1-3.

Chapter 3

3 SCM based on Optical IQ Modulators

This chapter develops a theoretical analysis of the trade-off between carrier suppression and nonlinearities induced by optical IQ modulators in direct-detection subcarrier multiplexing systems. The trade-off is obtained by examining the influence of the bias conditions of the modulator on the transmitted optical single side band signal. The frequency components in the electric field and the associated photocurrent at the output of the IQ modulator are derived mathematically. For any frequency plan, the optimum bias point can be identified by calculating the sensitivity gain for every subchannel. A setup composed of subcarriers located at multiples of the data rate ensures that the effects of intermodulation distortion are studied in the most suitable conditions. Experimental tests with up to five QPSK electrical subchannels are performed to verify the mathematical model and validate the predicted gains in sensitivity. Note that due to the extension of the required mathematical analysis, they are developed in Appendix B.

3.1 Introduction

This section briefly reviews the relevance of SCM and emphasizes its implementation with optical IQ modulators (OIQM). The key concepts in the generation of OSSB and Carrier Suppression (CS) are reviewed and, finally, the content of the chapter is summarized.

3.1.1 Application

SCM relies on the excellent stability and low phase noise of microwave oscillators to generate one or more digitally modulated RF signals that are then intensity modulated onto an optical wavelength before transmission over fibre. SCM can be combined with WDM to increase the flexibility of the network. Analogue and digital SCM approaches have been used in many applications, including cable television (CATV) [1], radio over fibre [2] (also focusing on the increasingly important digital radio over fibre solutions [3]), broadband point to point links [4], access networks [5] and 100 Gbit/s local area networks [6]. In such a system it is

desired to guarantee the following features: OSSB to increase the spectral efficiency and eliminate dispersive fading [7], low inter channel distortion, and an appropriate level of the optical carrier to optimize the sensitivity at the receiver. The interrelations of these concepts have been explained in section 2.3.

3.1.2 Suitability of Optical IQ Modulators

Focusing on optical modulators, there are three possibilities to generate SCM/OSSB signals with partial CS, as illustrated in Figure 3.1. If a standard MZM is employed for the electro-optic conversion, an optical double side band signal is obtained, and an optical filter is required to suppress the undesired sideband and produce OSSB. The most linear performance of this system is achieved by biasing the device at *quadrature*. As the level of the electrical driving, referred to as optical modulation index (OMI), must be small to minimize nonlinear distortion (NLD), the Carrier to Signal Power Ratio (CSPR) is high and significant energy is wasted in the optical carrier. Consequently, the power efficiency of the transmission and the sensitivity in the receiver can be improved by applying CS. A direct method to achieve CS involves biasing the device at a point different to *quadrature* (Figure 3.1(a)), although NLD will increase presenting a trade-off with the sensitivity of the link [8]. It is also possible to use the same optical filter to remove one sideband and apply partial CS [9].

A conventional approach to generate SCM/OSSB without optical filters employs a DD-MZM whose RF ports are driven by signals with a relative phase shift of 90 degrees [10]. As explained in section 2.3.2.3, in this case the device can only

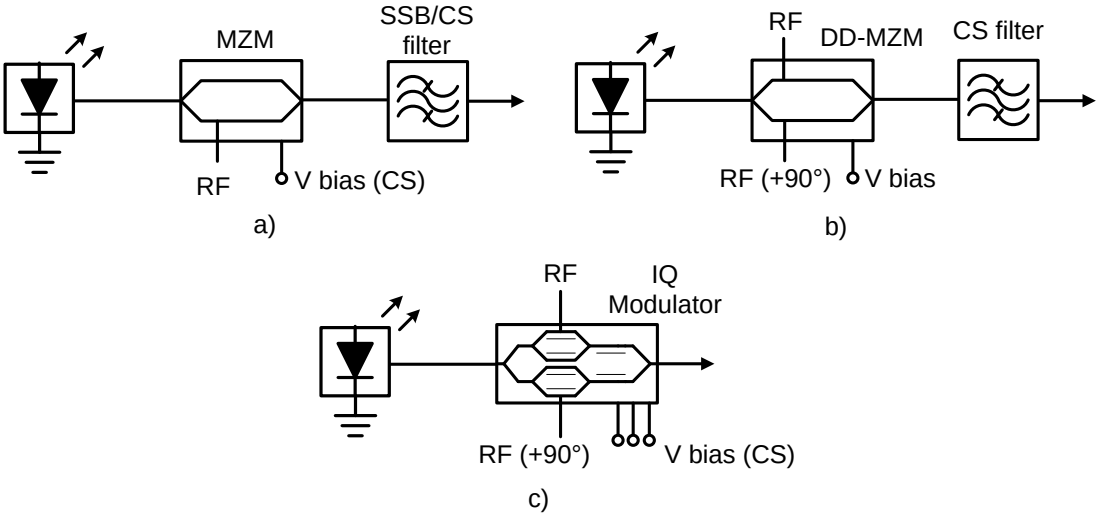

Figure 3.1: Three alternatives to generate SCM/OSSB/CS.

be biased at *quadrature* so that the optical carrier cannot be suppressed in the modulator. Therefore, a costly optical filter or CS block must be included [4] to increase power efficiency (Figure 3.1(b)). For this technique, different studies have presented comprehensive mathematical analysis of the NLD [11] and its trade-off with CS and the sensitivity of the link [12].

An OIQM is a relevant device because it can generate OSSB and partial CS without requiring additional components. This idea has been mathematically proved in section 2.3.2.4., where it has been shown that the CSPR can be modified by adjusting the bias levels (Figure 3.1(c)). A theoretical and experimental demonstration of this concept was also provided in [13]. However, no detailed investigation of NLD was carried out. As NLD increases while CSPR is reduced, a deeper analysis is required.

3.1.3 Content

It can be concluded that SCM and OIQMs are technologies that can be combined to achieve specific system requirements such as colourless OSSB transmitters, received signals free of dispersive fading and, finally, partial optical CS. While the bias point of the modulators moves from *quadrature* to *null*, the CSPR improves and the NLD worsens, generating a trade-off with the sensitivity of the system.

This chapter studies analytically and experimentally the NLD and the CSPR that are generated simultaneously by an OIQM as a function of the bias point. The analysis developed by [13] is largely extended to obtain accurate CSPR and NLD for any number of RF subchannels. An optimum bias point is identified, optimizing the trade-off between NLD and CSPR in the presence of optical noise, where overall system performance is maximized. The analysis and results presented can be used to achieve efficient transmission in any multicarrier SCM link, analogue or digital, without the need for a CS block.

Experimental results were obtained employing the 13.5 Gbit/s SCM/OSSB system presented in section 2.5. It was designed with subcarriers located at multiples of the data rate so that the distortion due to in-band intermodulation products falls in the centre of other subchannels. Measurements show CSPR and NLD, their impact on the performance of channels and real gains in sensitivity. The experimental results show good agreement with theory.

3.2 Theory

A generic SCM/OSSB scheme based on OIQMs is shown in Figure 3.2. In one optical wavelength, *N* QPSK electrical subchannels are multiplexed and transmitted. In this section, the main frequency components at the output of the OIQM will be derived. CSPR and NLD will be generalized for any frequency plan. The analytical study is based on continuous waves instead of real data as this approach has been widely used and its validity proven [14], producing good agreement with experimental data using independently modulated subcarriers.

3.2.1 Definitions

Initially, some basic concepts that will be employed through this chapter are reviewed. They cover the mathematical definitions for MZMs and the theoretical concepts required for an accurate analysis of NLD.

3.2.1.1 MZM: Bias Point and Optical Modulation Index

The bias point of a MZM is determined by the total relative phase shift that is applied to the optical wavelength in the modulator arms before recombination. With a push-pull configuration a total relative phase shift equal to 2ϕ is obtained by producing opposite delays (ϕ and $-\phi$) in each arm. Thus the bias point is defined as the absolute value of the phase shift ϕ introduced in each arm by the bias voltage V_b:

$$\phi = \frac{\pi \cdot V_b}{2V_\pi} \tag{3.1}$$

where $V\pi$ is the half-wave voltage of the MZM. When ϕ=0 the MZM is biased at

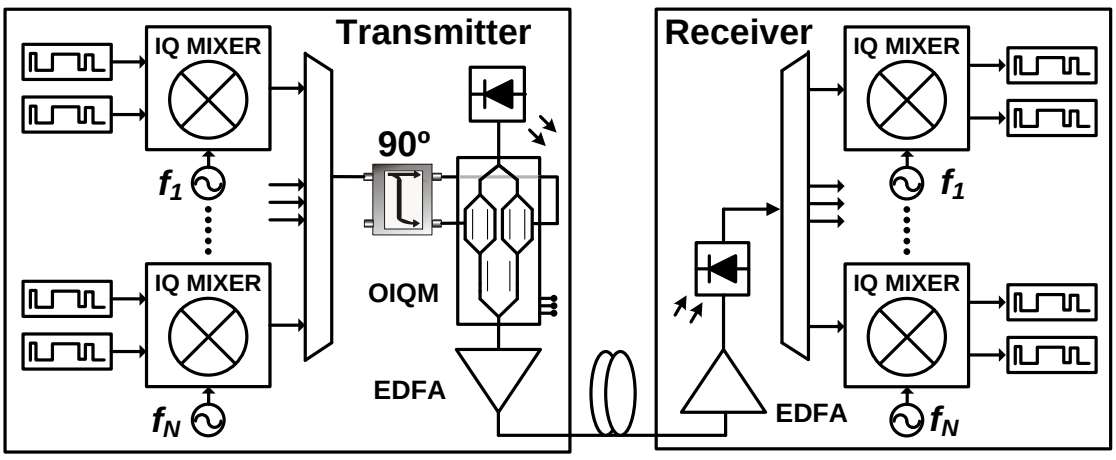

Figure 3.2: SCM/OSSB system consisting of an optical IQ modulator and *N* QPSK electrical subchannels.

peak, when $\phi=\pi/4$ the device is biased at *quadrature* and finally when $\phi=\pi/2$ the modulator is biased at *null*. More details can be found in section 1.3.2.2.

The amplitude of the signal at the RF port of the MZM determines the optical modulation index (OMI). The Root Mean Square (rms) OMI of a modulating signal composed of one subcarrier of amplitude V_{AC} is given by [11]:

$$m = \frac{\pi \cdot V_{AC}}{2V_{\pi}}. \tag{3.2}$$

3.2.1.2 Nonlinear Distortion

Consider a signal x composed of a sum of tones located at different frequencies Ω_i. A nonlinear characteristic can be expressed as a Taylor-series expansion where a_n represents the weight associated to the nonlinearity of order n [15]:

$$y = \sum_{n\geq 2} a_n x^n. \tag{3.3}$$

NLD can be divided into two groups: Harmonic Distortion (HD) and Intermodulation Distortion (IMD). Both HD and IMD can be further subdivided into different contributions that are classified according to the order of the distortion. This order is given by the exponent n in eq. (3.3) and represents the number of tones (two or more) that must be mixed to generate such distortion. HD is a consequence of cross-talk produced by harmonic products. Thus, given a tone at a frequency Ω_i that is affected by a nonlinearity of order n, HD_n falls at the frequency $n\Omega_i$, distorting the desired tone located at that frequency. Equivalently, IMD is a consequence of cross-talk produced by intermodulation products (IMP). Given N ($\geq$2) tones located at different frequencies Ω_i, (i=1,..,N), an IMP of order n would fall at a frequency $\Omega_{IMP}=k_1\Omega_1\pm\ldots..\pm k_N\Omega_N$ where k_i are natural numbers that sum to n. Therefore, two or more original tones can give rise to any IMP of order n, and the associated distortion can be denoted as IMD_n.

The most significant contributions are usually the distortions of second and third order. In this document the following notation is used: HD_2 (distortion at $2\Omega_i$), HD_3 (distortion at $3\Omega_i$), IMD_2 (distortion at $\Omega_{IMP}=\Omega_i\pm\Omega_j$), IMD_3 (distortion at $\Omega_{IMP}=2\Omega_i\pm\Omega_j$) and IMD_{3B} (distortion at $\Omega_{IMP}=\Omega_i\pm\Omega_j\pm\Omega_k$, also called triple-beat).

These terms show the power of an individual distortion normalized to the power of a desired tone. For the application under analysis, different IMDs and HDs will be obtained in the electric field and in the associated photocurrent. Mathematically, focusing on the electric field, $E_{IMD(\Omega)}$ denotes the peak amplitude for an individual IMP that falls at $\omega_c+\Omega$, where a desired tone with peak amplitude E_Ω is located. Obtaining the time averaged powers, $P_{E\_IMD(\Omega)}$ and P_{E_Ω}, the individual IMD for the electric field is expressed as:

$$IMD_{(E)} = \frac{P_{E\_IMD(\Omega)}}{P_{E\_\Omega}} = \frac{E^2_{IMD(\Omega)}/2}{E^2_{\Omega}/2} = \frac{E^2_{IMD(\Omega)}}{E^2_{\Omega}}. \tag{3.4}$$

Equivalently, focusing now on the photo-current, $I_{IMD(\Omega)}$ denotes the peak amplitude for an individual IMP that falls at Ω, where a desired tone with peak amplitude I_Ω is located. Obtaining the time averaged photo-current powers [16, 17], $P_{I\_IMD(\Omega)}$ and P_{I_Ω}, the individual IMD for the photo-current is expressed as:

$$IMD_{(I)} = \frac{P_{I\_IMD(\Omega)}}{P_{I\_\Omega}} = \frac{I^2_{IMD(\Omega)}/2}{I^2_{\Omega}/2} = \frac{I^2_{IMD(\Omega)}}{I^2_{\Omega}}. \tag{3.5}$$

Note that, under a Gaussian approximation, the mean square current of the individual distortion is $\sigma^2_{IMD(\Omega)}=P_{IMD(\Omega)}$. Typically, the values of individual IMD are generalized for a given nonlinearity, and the power of the distortion can be obtained for any value of the desired tone. Substituting and resolving $\sigma^2_{IMD(\Omega)}$ in the previous equation:

$$\sigma^2_{IMD(\Omega)} = IMD_{(I)} \cdot P_{I\_\Omega} = \frac{IMD_{(I)}}{2} I^2_{\Omega}. \tag{3.6}$$

A similar analysis can be done with harmonic products and HD.

In the previous paragraph, the effects of an individual distortion coming from one IMP have been shown. In practice, for a frequency plan composed of several subcarriers, every subchannel is interfered by a different number of individual intermodulation products of each kind. Focusing on the photo-current, for a given

subchannel centred at Ω, N_{CSO} denotes the number of IMPs that fall at Ω generating IMD_2. Equivalently, N_{CTB} represents the number of IMPs that fall at Ω generating IMD_{3B}. For both cases, the associated overall distortion is referred to as Composite Second Order (CSO) and Composite Triple Beat (CTB) respectively. From eq. (3.6) and assuming uncorrelated sources of Gaussian noise [12]:

$$\begin{aligned} CSO &\xrightarrow{\Omega} \sigma_{CSO}^2 = N_{CSO} \cdot \frac{IMD_2}{2} \cdot I_\Omega^2. \\ CTB &\xrightarrow{\Omega} \sigma_{CTB}^2 = N_{CTB} \cdot \frac{IMD_{3B}}{2} \cdot I_\Omega^2. \end{aligned} \tag{3.7}$$

CSO and CTB are the most limiting distortions in direct detection (DD) systems [11, 18]. In general N_{CSO} is higher for the lowest frequency subchannels and N_{CTB} is higher for the channels in the middle of the frequency plan [18].

The setup described in the previous chapter (section 2.5) will be employed as a reference frequency plan. The general theoretical results will be particularized for this case so that theory and experiments can be linked. This plan consists of five electrical subcarriers located at the second, third, fourth, fifth and sixth harmonic of a

Table 3-1 Intermodulation products count for the reference frequency plan.

Centre (GHz)	N_{CSO}	*Mixing IMD_2 (GHz)*	N_{CTB}	*Mixing IMD_{3B} (GHz)*	N_{IMD3}	*Mixing IMD_3 (GHz)*
2.7 (No data)	4	8.1-5.4 10.8-8.1 13.5-10.8 16.2-13.5	5	5.4+8.1–10.8 5.4+13.5–16.2 5.4+8.1–16.2 5.4+10.8–13.5 8.1+10.8–16.2	3	2·5.4–8.1 2·5.4–13.5 2·8.1–13.5
5.4 (Subchannel 1)	3	10.8-5.4 13.5-8.1 16.2-10.8	2	8.1+10.8–13.5 8.1+13.5–16.2	3	2·5.4–16.2 2·8.1–10.8 2·10.8–16.2
8.1 (Subchannel 2)	2	13.5-5.4 16.2-8.1	4	5.4–8.1+10.8 5.4–13.5+16.2 5.4–10.8+13.5 10.8+13.5–16.2	1	2·10.8–13.5
10.8 (Subchannel 3)	1	16.2-5.4	4	5.4–8.1+13.5 5.4–10.8+16.2 8.1–10.8+13.5 8.1–13.5+16.2	2	2·8.1–5.4 2·13.5–16.2
13.5 (Subchannel 4)	0	-	4	5.4–8.1-10.8 5.4–8.1+16.2 8.1–10.8+16.2 10.8–13.5+16.2	1	2·10.8–8.1
16.2 (Subchannel 5)	0	-	2	5.4–8.1–13.5 8.1–10.8–13.5	0	-

fundamental frequency (2.7 GHz in the case of the experimental results). The values of N_{CSO} and N_{CTB} are derived in Table 3-1 for every subchannel. The first subcarrier is the most affected by CSO (N_{CSO}=3, N_{CTB}=2) while the fourth subcarrier is only affected by CTB (N_{CSO}=0, N_{CTB}=4). For completeness, Table 3-1 also shows the number of intermodulation products that give rise to IMD_3, N_{IMD3}.

Note that the previous values of N_{CSO} and N_{CTB} are obtained focusing on the photo-current. Any IMP at a frequency $|\Omega|$ is the result of a combination of subcarrier frequencies that can be positive or negative, e.g. $\pm|\Omega|=\Omega_1-\Omega_2+\Omega_3$. If the sign of all the subcarriers involved in the mixing changes, an IMP at the opposite frequency is obtained, e.g. $\mp|\Omega|=-\Omega_1+\Omega_2-\Omega_3$. The negative realization has in reality a positive equivalent as $\cos(-\Omega t+\varphi)=-\cos(\Omega t-\varphi)$. For a signal x composed of a sum of tones, when expanding eq. (3.3) it can be easily derived that only one of the two potential realizations ($+|\Omega|$ or $-|\Omega|$) occurs. For that reason, the calculation of N_{CSO} and N_{CTB} in Table 3-1 only considers one of the realizations of every pair of potential IMPs. This is compatible with the mathematical derivation of the NLD presented in Appendix B.

3.2.2 Multicarrier Analysis

As shown in Figure 3.1(c) an OIQM consists of three MZMs: two parallel sub-MZMs are modulated by electrical data and the third one establishes a phase shift between the optical outputs of the two parallel sub-MZMs before recombination. Provided that the electrical inputs present a relative phase shift of 90 degrees, OSSB is achieved by biasing the third MZM to produce an optical relative phase shift of 90 degrees, and the two parallel sub-MZMs at the same bias point ϕ. These are operating conditions that are employed in the following analysis.

3.2.2.1 Electric Field

The study of the CSPR requires the derivation of the mathematical expression of the electrical field E at the output of the OIQM. An analysis based on phasors and Bessel expansions can be used to obtain all the frequency components of E for any number of RF subcarriers N. Due to the length of the mathematical development, it is presented in Appendix B.

The following results were obtained with the phases configured to produce optical lower side band (with respect to the optical carrier frequency) and with equal values of OMI per subcarrier m. The frequency of the optical carrier is denoted as ω_c.

The frequencies and phases of the N subcarriers are written as Ω_1, Ω_2,…,Ω_N and θ_1, θ_2,…,θ_N respectively. A single expression can be used to calculate the amplitude and phase of any fundamental tone, harmonic or intermodulation product $E_{k1,k2...kN}$ whose frequency is $(\omega_c+k_1\Omega_1+k_2\Omega_2+\ldots+k_N\Omega_N)$, where $k_1,k_2,\ldots,k_N$ are arbitrary integer numbers reflecting the nature of the signal in question. This contribution in the electrical field is given by:

$$E_{k_1,k_2,\ldots,k_n} = E_i \cdot \left(\prod_{i=1}^{N} J_{k_i}(m) \right) \cdot \cos\left(\frac{\pi}{4}\left(1+\sum_{i=1}^{N} k_i\right)\right) \cdot \cos\left(\phi + \frac{\pi}{2}\left(\sum_{i=1}^{N} k_i\right)\right) \cdot \prod_{i=1}^{N} e^{jk_i\left(\theta_i - \frac{\pi}{4}\right)} \quad (3.8)$$

where $J_n(m)$ stands for the nth order Bessel function of the first kind and E_i is the amplitude of the optical carrier at the input of the OIQM (an ideal lossless OIQM has been considered). To calculate the total contribution at a desired frequency it is necessary to add all the components that fall on it. For the reference frequency plan studied here, the contribution of the first fundamental tone at $(\omega_c-\Omega_1)$ would be $E_{-1,0,0,0,0}$. While the contribution produced by $(\omega_c+\Omega_3-\Omega_5)$, which would fall on $(\omega_c-\Omega_1)$, would be given by $E_{0,0,1,0,-1}$. Proceeding in that way, the individual nonlinear distortions can be calculated and are shown in Table 3-2.

Table 3-2 Normalized NLD power in the electrical field at the output of an optical IQ modulator that is configured to generate an optical single side band signal. Ω_i, Ω_j, and Ω_k are three arbitrary subcarrier frequencies.

Distortion type	*Distortion frequency*	*Formula*
Second harmonic (HD_2)	$\omega_c \pm 2\Omega_i$	$\left[\frac{J_2(m)}{\sqrt{2}\cdot J_1(m)}\cot\phi\right]^2$
Third harmonic (HD_3)	$\omega_c + 3\Omega_i$	$\left[\frac{J_3(m)}{J_1(m)}\right]^2$
	$\omega_c - 3\Omega_i$	0
2nd order IM (IMD_2)	$\omega_c \pm \Omega_i \pm \Omega_j$	$\left[\frac{J_1(m)}{\sqrt{2}\cdot J_0(m)}\cot\phi\right]^2$
3rd order IM (IMD_3)	$\omega_c + \Omega_i \pm 2\Omega_j$	$\left[\frac{J_2(m)}{J_0(m)}\right]^2$
	$\omega_c - \Omega_i \pm 2\Omega_j$	0
Triple beat (IMD_{3B})	$\omega_c + \Omega_i + \Omega_j + \Omega_k$ $\omega_c + \Omega_i - \Omega_j - \Omega_k$	$\left[\frac{J_1(m)}{J_0(m)}\right]^4$
	$\omega_c - \Omega_i - \Omega_j - \Omega_k$ $\omega_c - \Omega_i + \Omega_j + \Omega_k$	0

Most meaningful NLD when m << 1

Table 3-3 Normalized NLD power in the associated photocurrent at the output of an optical IQ modulator configured to generate an optical single side band signal. Ω_i, Ω_j, and Ω_k are three arbitrary subcarrier frequencies.

Distortion type	*Distortion frequency*	*Formula*
Second harmonic (HD_2)	$2\Omega_i$	0
Third harmonic (HD_3)	$3\Omega_i$	$\left[\frac{J_3(2m))}{J_1(2m)}\right]^2$
2nd order IM (IMD_2)	$+\Omega_i - \Omega_j$	$\left[\sqrt{2}\,\frac{J_1(2m)}{J_0(2m)}\cot 2\phi\right]^2$
	$+\Omega_i + \Omega_j$	0
3rd order IM (IMD_3)	$\Omega_i \pm 2\Omega_j$	$\left[\frac{J_2(2m)}{J_0(2m)}\right]^2$
Triple beat (IMD_{3B})	$\Omega_i \pm \Omega_j \pm \Omega_k$	$\left[\frac{J_1(2m)}{J_0(2m)}\right]^4$

Most meaningful NLD when m << 1

3.2.2.2 Photo-current

For the DD scheme envisaged here it is necessary to obtain the distortion in the detected photocurrent *I*, which is proportional to the square of the envelope of the electrical field and, as demonstrated in Appendix B, is given by:

$$I = \frac{E_i^2}{8}\left(1+\frac{1}{2}\left(\cos\left(2m\cdot s(t)+2\phi\right)+\cos\left(2m\cdot \hat{s}(t)+2\phi\right)\right)\right) \tag{3.9}$$

where *s(t)* is equal to the sum of all the subcarriers (normalized with amplitude 1) that are applied to one RF port and *ŝ(t)* is its Hilbert-transformed pair (*s(t)* shifted 90 degrees) that is applied to the other RF port. Again, Bessel expansions can be used to obtain all the frequency components and deduce the nonlinear distortions. They are shown in Table 3-3 and the mathematical demonstration can be found in the Appendix B. Due to the nonlinearity of the photodiode, HD_2 disappears while certain IMD_{3B} appears balancing the combinations of subcarriers that give rise to triple beat.

3.2.3 CSPR as a Function of the Bias Point

3.2.3.1 Accurate versus Approximated

In any direct detection SCM system, the CSPR will depend on the number of electrical subchannels *N* and the OMI. From eq. (3.8), CSPR can be calculated including all the significant contributions from the fundamental tones and distortions. The accurate CSPR was obtained for the reference frequency plan and is shown in Figure 3.3 for two different values of *m*.

A simplified model, neglecting NLD, can be used to obtain an approximate value considering only fundamental tones:

$$CSPR \approx \frac{E_C^2}{NE_S^2} = \frac{1}{2N}\left[\frac{J_0(m)}{J_1(m)}\cot(\phi)\right]^2 \tag{3.10}$$

where E_C is the amplitude of the electric field in the optical carrier and E_S is the amplitude of the electric field in any fundamental tone. This approximation has been employed previously [13] but its accuracy was not analysed.

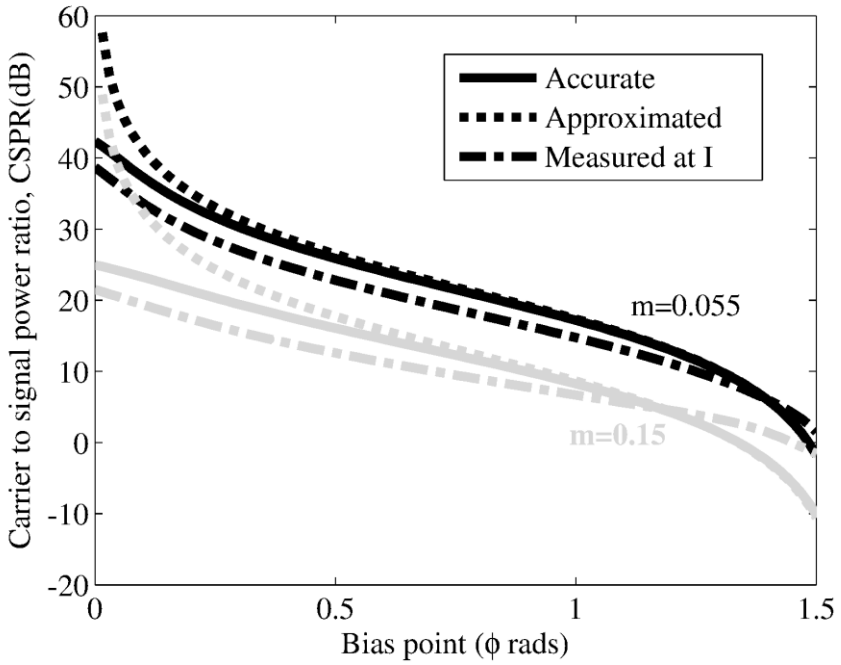

Figure 3.3: Accurate and approximated CSPR for an SCM/OSSB system composed of an optical IQ modulator and five subcarriers for two different values of subchannel OMI (*m*=0.055 and *m*=0.15).

From Table 3-2 it can be concluded that the main contributions of NLD in the electric field E come from HD_2 and IMD_2. The previous statement can be deduced with the following approximations [19]:

$$m << 1,\ \ 1 \le \alpha \le 2,\ \ 2 \le \beta \le 3:$$
$$J_z(m) \approx \frac{1}{z!}\left(\frac{m}{2}\right)^z \quad \left.\begin{array}{l} \longrightarrow \dfrac{J_\alpha(m)}{J_{\alpha-1}(m)} \approx \dfrac{1}{\alpha}\left(\dfrac{m}{2}\right) \\ \longrightarrow \dfrac{J_\beta(m)}{J_{\beta-2}(m)} \approx \dfrac{1}{\beta(\beta-1)}\left(\dfrac{m}{2}\right)^2 \end{array}\right\} \frac{J_\alpha(m)}{J_{\alpha-1}(m)} >> \frac{J_\beta(m)}{J_{\beta-2}(m)}. \quad (3.11)$$

HD_2 and IMD_2 present their maximum at the *peak* bias point and tend to cancel while approaching the *null*. For that reason the approximated CSPR, which is also shown in Figure 3.3, diverges clearly around the *peak*. However, for the bias points of interest in DD systems, between *quadrature* and *null*, the approximation is valid, especially for low values of m (error less than 0.3 dB from *quadrature* in this example).

3.2.3.2 Measurement

The curves in Figure 3.3 also show the CSPR that is obtained with the most significant terms of the photo-current I obtained from eq. (3.9) and its Bessel expansion derived in Appendix B. Apart from the area around the *null* point, CSPR can be approximated by measuring it in the detected photocurrent and adding 3 dB. As a direct measurement of CSPR from the electric field E is not possible, this technique will be used to measure CSPR in the experimental section.

In certain conditions, this behaviour can be easily justified mathematically. Continuing with the same notation and neglecting phases, the associated photo-current can be written as:

$$I \propto \frac{E_C^2}{2} + N\frac{E_S^2}{2} + E_C E_S \sum_{i=1}^{N} \cos(\Omega_i t) + NLD. \quad (3.12)$$

In the next subsection (3.2.4) it becomes clear that the NLD in the photocurrent is small only far from *peak* and *null*. For this region of small NLD, the $CSPR_I$ in the photo-current is calculated and compared with the approximated CSPR of eq. (3.10):

$$CSPR_I = \frac{\left(\frac{E_C^2}{2} + N\frac{E_S^2}{2}\right)^2}{N\frac{E_C^2 E_S^2}{2}} = \frac{E_C^2}{2NE_S^2} + 1 + \frac{NE_S^2}{2E_C^2} \xrightarrow{E_C^2 >> 2NE_S^2} CSPR_I \approx \frac{E_C^2}{2NE_S^2} = \frac{CSPR}{2}. \quad (3.13)$$

In the described region, and while the power of the optical carrier is much higher than the powers of the fundamental tones, the 3dB relation between $CSPR_I$ and the desired CSPR becomes apparent. From the results shown in Figure 3.3, which include all the significant contributions of NLD in *E* and *I*, it can be readily seen that this relation can be extended to the region around *peak*.

3.2.3.3 Conclusion

It can be concluded that, as expected, CSPR decreases when the bias point moves towards *null*. Lower bias points achieve higher optical carrier suppression while the relative power of the transmitted tones increases. Thus, decreasing the CSPR, and neglecting NLD, the subchannels could be received with the same quality with a lower received average optical power, thereby improving sensitivity. However, as it is explained in the next section, some subchannels can be severely impaired due to NLD when the bias point changes.

3.2.4 NLD as a Function of the Bias Point

From Table 3-3 it can be confirmed that the most limiting NLD in the detected photocurrent *I* are the second order intermodulation, IMD_2, and the triple beat, IMD_{3B}. Note that, using eq. (3.11), it can be deduced that $IMD_{3B}=4\cdot IMD_3$. As explained before, IMD_2 and IMD_{3B} become CSO and CTB respectively when all the intermodulation products are considered. Figure 3.4 shows both individual distortions for two values of OMI. Whereas IMD_{3B} depends only on *m*, IMD_2 varies with the bias point cancelling at *quadrature* and worsening sharply if the bias point changes. In both cases higher values of *m* give rise to higher distortions.

The previous results have illustrated the combined behaviour of CSPR and NLD as a function of the bias point. Both terms present a relationship that can be manifested in two different ways depending on the nature of the IMD. All the cases

can be divided into two groups: systems where the desired tones are only interfered by CTB and systems where at least one of the subchannels is interfered by CSO.

The first case happens when the frequency plan ensures that CSO is not interfering (N_{CSO}=0 for all the electrical subcarriers), thus NLD is composed only of CTB and is constant irrespective of the bias point. This is achieved when there is a guard band between the optical carrier and the first subchannel equal to at least half of the total spectrum, as in DD/OFDM [20] or some CATV schemes [21]. Clipping can appear in the optical signal but it does not have a detrimental effect because its associated distortion translates into CSO and falls in the part of the spectrum where no desired subcarriers are present. This particular case is typically simplified and the optimum bias point is supposed to produce a CSPR equal to one [22]. However, in practice, due to the presence of NLD, the optimum CSPR can be different to one [23]. A deeper analysis, like the one presented in the next subsection is required to accurately find the optimum CSPR, bias point and OMI.

The second case happens when there are low frequency subchannels as in broadband SCM [4] or in the reference example. In this case there is a trade-off between CSPR and NLD: biasing closer to *null* improves CSPR but at the same time CSO increases sharply. A mathematical analysis of the system is required to obtain the sensitivity at the receiver as a function of the bias point to find the optimum.

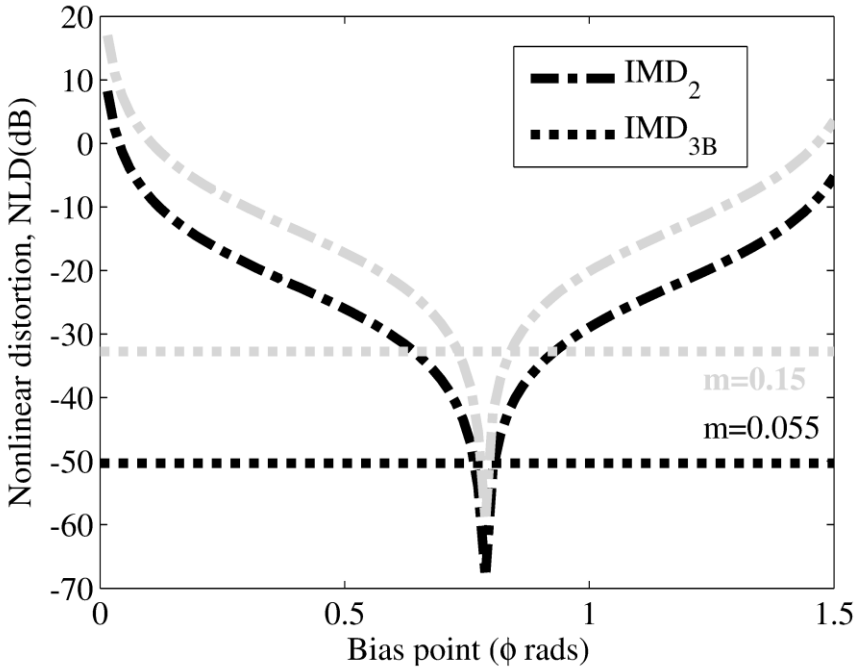

Figure 3.4: Individual NLD (IMD_2 and IMD_{3B}) at the detected photocurrent of an SCM/OSSB system using an optical IQ modulator for two values of OMI.

3.2.5 Optimum Bias Point

3.2.5.1 Mathematical Expression

The study was based on an SCM link composed of *N* subcarriers and with a pre-amplified receiver as shown in Figure 3.5. This receiver consists of an EDFA, a photo-detector and an RF demodulator.

The average optical power P_{IN} at the input of the receiver required for a given quality factor Q_F is mathematically derived in the Appendix B:

$$P_{IN} = \frac{4Q_F^2 FhvB_e}{I_\phi^2\left(1-Q_F^2\left(N_{CSO}IMD_2 + N_{CTB}IMD_{3B}\right)\right)} \tag{3.14}$$

where F is the noise figure of the EDFA, h is the Planck's constant, v is the optical frequency and B_e is the electrical bandwidth of the baseband channels at the receiver. I_ϕ represents the dependency of the amplitude of the subcarrier on the bias point:

$$I_\phi = \frac{\sqrt{2}J_0^{N-1}(2m)J_1(2m)\sin(2\phi)}{1+J_0^N(2m)\cos(2\phi)}. \tag{3.15}$$

As the only sources of noise and distortion considered are amplified spontaneous emission (ASE) and NLD, P_{IN} in equation (3.14) represents the minimum sensitivity that is theoretically achievable in a QPSK SCM/OSSB link implemented with an OIQM and a pre-amplified receiver. According to Figure 2.10, these sensitivities must be achievable values with realistic optical components. In practice, when electronic devices introduce distortion that is not negligible, the obtained sensitivities will be higher.

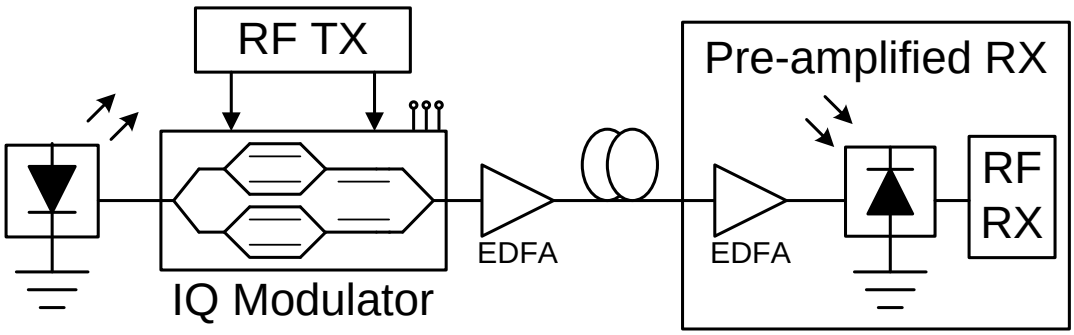

Figure 3.5: SCM/OSSB scheme with a pre-amplified optical receiver.

The gains in sensitivity that can be achieved by varying the bias point depend on NLD. This distortion is different for every subchannel because it is determined by different values of N_{CSO} and N_{CTB}. Therefore, depending on the nature of the link, the optimum bias point is given by either the average BER, or the BER of the worst case channel. The second condition is the strictest and is used in this analysis.

3.2.5.2 Discussion and Example

These results will be particularized for the reference design considering only subcarrier 1, as it is the most affected by CSO (N_{CSO}=3 and N_{CTB}=2), and subcarrier 4, as it is the most interfered of the subchannels affected only by CTB (N_{CSO}=0 and N_{CTB}=4).

Considering *quadrature* and a low value of m as the initial operating point, Figure 3.6 shows the gains in sensitivity (for Q_F=6, BER=10^{-9}) that can be achieved by changing the settings for subchannel 1. Moving the bias point towards *null*, the sensitivity improves notably until CSO is comparable to the ASE induced noise floor. For a value of m=0.055, there is an optimum bias point (ϕ=1.1 rad), where a sensitivity gain of almost 4 dB with respect to *quadrature* is achieved. This gain is very sensitive to changes in ϕ (it is reduced to 3 dB at ϕ=1.175) and m (3.5 dB with m=0.06). From that point sensitivity improves while m increases and the bias point

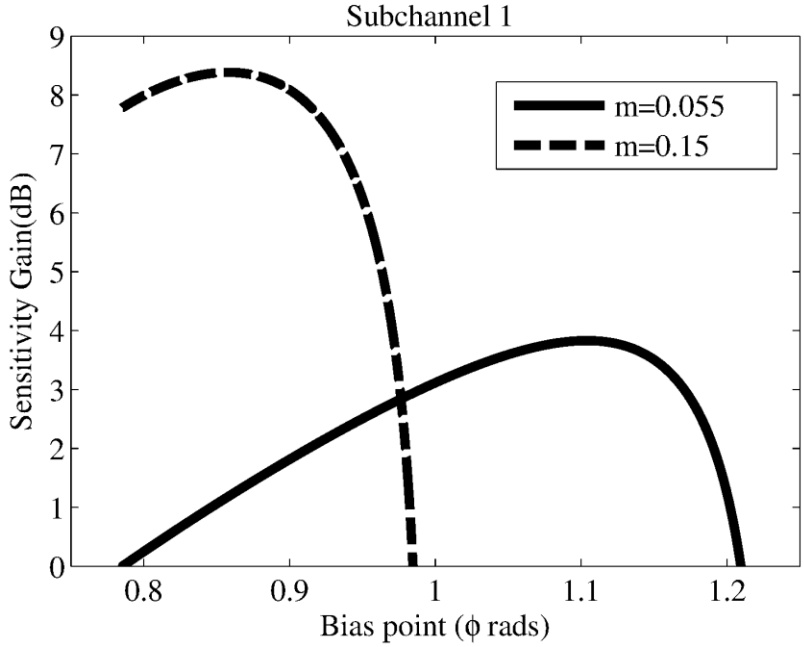

Figure 3.6: Gains in sensitivity for Q_F=6 with respect to quadrature and m=0.055 for a subchannel distorted by NLD (N_{CSO}=3 and N_{CTB}=2) in a five subcarrier QPSK SCM/OSSB link consisting on an optical IQ modulator and a pre-amplified receiver (F=5dB, ν=193.4 THz, B_e=2.7 GHz).

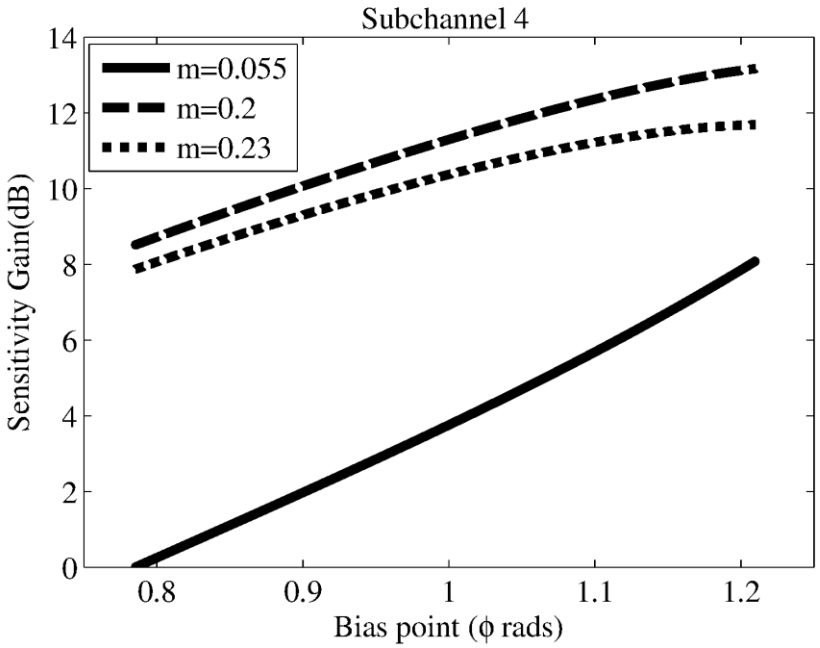

Figure 3.7: Gains in sensitivity for Q_F=6 with respect to quadrature and m=0.055 for a subchannel distorted by NLD (N_{CSO}=0 and N_{CTB}=4) in a five subcarrier QPSK SCM/OSSB link consisting on an optical IQ modulator and a pre-amplified receiver (F=5dB, v=193.4 THz, B_e=2.7 GHz).

moves towards *quadrature*. This effect occurs because CSPR improves with a higher OMI and CSO tends to cancel when close to *quadrature*. A gain in sensitivity of 8 dB is observed for m=0.15 with respect to m=0.055 at *quadrature*.

However, while m increases, the impact of CTB on subchannel 4 also increases, as shown in Figure 3.7. For that channel, as CTB is constant regardless of the bias point, a gain in sensitivity is always achieved when moving the bias from *quadrature* towards *null*. For m=0.055, the gain in sensitivity at the optimum bias point of subchannel 1, ϕ=1.1 rad, is 6 dB with respect to *quadrature*. When m increases, CSPR reduces and CTB increases, resulting in better sensitivity until the level of CTB is comparable with the ASE induced noise floor, as it happens at m=0.2. From that value, further increments of m result in a loss in sensitivity.

3.2.5.3 Practical Conclusions

The previous analysis can be applied to achieve optimum sensitivity in any SCM link using an OIQM. The influence of the bias point can be summarized with two effects. Firstly, for a given OMI, it is possible to find a bias point different to *quadrature* and closer to *null* where overall sensitivity improves. Secondly, as the OMI increases, this optimum bias point will be closer to *quadrature*. In the following section a real scheme is used to validate the predicted gains in sensitivity and to show the described trends.

In general, the overall link performance is determined by the combined behaviour of, among others, the OMI, the bias point, and the performance of the optical and RF components in the bands of use. For different system design level objectives, different individual parameters may be required. On many occasions OMI is maintained small to guarantee low intermodulation distortion but this behaviour can cause a loss in sensitivity. This effect can be overcome with an increase in the OMI of the signal, but that requires a higher power consumption of the RF components. As power consumption is usually a major issue, a lower value of OMI can be used accompanied with a bias closer to *null* to achieve equivalent sensitivity.

3.3 Experimental Results

The experimental setup was based on a SCM/OSSB system with five QPSK subchannels equivalent to Figure 3.2. The components employed were largely the ones detailed in section 2.5, and a brief description will be provided here. The IQ mixers were off-the-shelf devices based on MMIC technology. The symbol rate per subchannel was 1.35 Gbaud, making an overall data rate of 13.5 Gbit/s for the optical channel. An FPGA was used to generate the ten baseband binary signals, each one carrying a PRBS of 2^{15}-1 bits, which were uncorrelated with different delays. The data streams were low pass filtered to reduce the spectrum of the signal to the first lobe of a sinc function. Imitating the reference design that has been studied in the previous subsections, the electrical LOs were even harmonics of the data rate (from 5.4 to 16.2 GHz), obtained using an electrical comb and appropriate demultiplexing filters. Thus no guard band was introduced between subchannels and the total energy of any intermodulation product distorted only one subchannel. No DSP algorithms were employed to compensate the impairments of the analogue components. The electrical signal was applied to a thin film polymer OIQM [24] with a bandwidth of 20 GHz and V_π of 2.5 Volts. The setup was completed in two different configurations depending on the parameter to be measured. Both configurations will be described in the next sections.

3.3.1 Experimental OMI

To make the experimental results comparable with theory, *m* has to be redefined for the case of real data. When a modulated electrical subchannel presents an rms voltage of V_{RMS} the experimental rms OMI of the subchannel is:

$$m = \frac{\pi \cdot V_{RMS}}{2V_{\pi}}. \tag{3.16}$$

Note that the overall OMI, *M*, considering *N* subchannels of the same level is:

$$M = \frac{\pi \cdot \sqrt{N \cdot V_{RMS}^2}}{2V_{\pi}} = \frac{\pi \cdot V_{RMS}}{2V_{\pi}} \sqrt{N} = m\sqrt{N}. \tag{3.17}$$

In some occasions in the following chapters, the OMI will also be provided as a percentage with respect to V_{π} such that:

$$\begin{aligned} m_{\%} &= \frac{V_{RMS}}{V_{\pi}} \cdot 100. \\ M_{\%} &= \frac{V_{RMS}}{V_{\pi}} \sqrt{N} \cdot 100. \end{aligned} \tag{3.18}$$

The Peak to Average Power Ratio (PAPR) of the final electrical signal will depend on the OMI, number of subchannels, and the particular relative phases of the subcarriers when they combine. However, theoretically, system performance will be determined by the rms power or the rms OMI of the final signal, regardless of the individual phases and the PAPR that arises [11]. Obviously it has to be ensured that the rest of the components in the system can handle that PAPR value without including additional nonlinearities.

3.3.2 Bias Points

The system characterization was carried out by biasing the two parallel sub-MZMs of the OIQM to get equal intensity from them, and then varying these bias levels between *peak* and *null*. Sixteen levels of intensity were selected. For each bias setting of these sub-MZMs, the bias point of the third MZM (that combines the optical outputs of the parallel ones) was adjusted to achieve the best sideband suppression ratio (SSR). The optical spectrum of one of these realizations is shown in Figure 3.8, where an SSR of 20 dB can be observed.

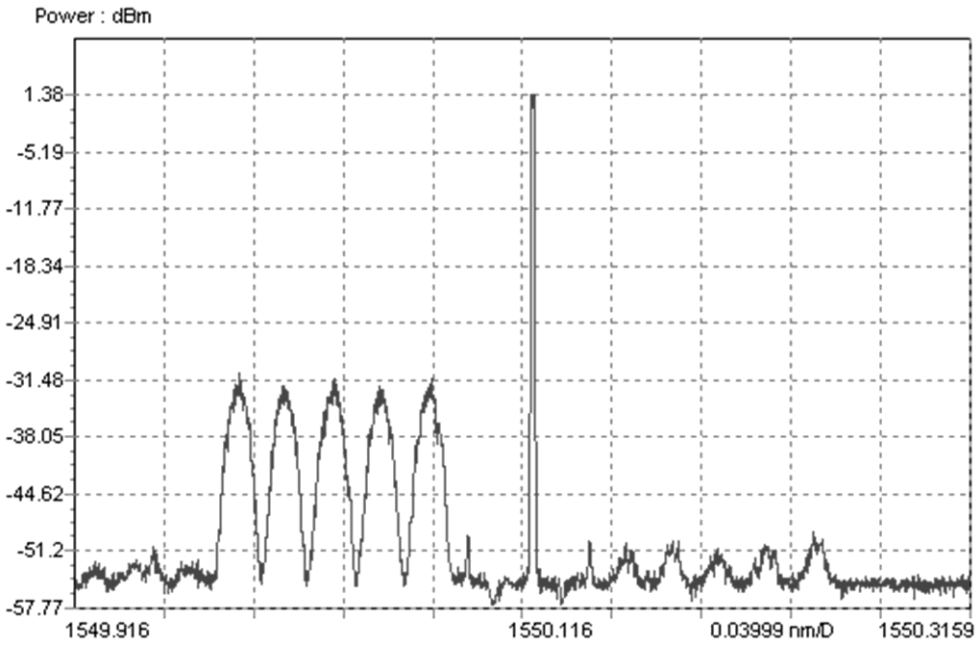

Figure 3.8: Optical spectrum obtained with *m*=0.055 at a one of the sixteen bias points analysed. OSSB with an SSR of 20 dB is achieved. CSPR = 15.7 dB.

3.3.3 Agreement with Model

The theoretical analysis concluded that CSPR and IMD_2 are the two key parameters to determine the optimum bias point in an SCM link implemented with an OIQM. These parameters were measured experimentally to verify the agreement with the model obtained with the employed OIQM. For this particular device the bias is established with constant current instead of voltage, thus the measurements will be presented as a function of bias current. The tests were performed with the configuration shown in Figure 3.9. At the output of the OIQM a variable optical attenuator (VOA) was included prior to an EDFA. The gain of the EDFA was maintained constant and the VOA attenuation was modified to ensure the same optical power at the input of the EDFA for all the bias points that were analysed. With this method the measurements at different bias points were taken under the same conditions.

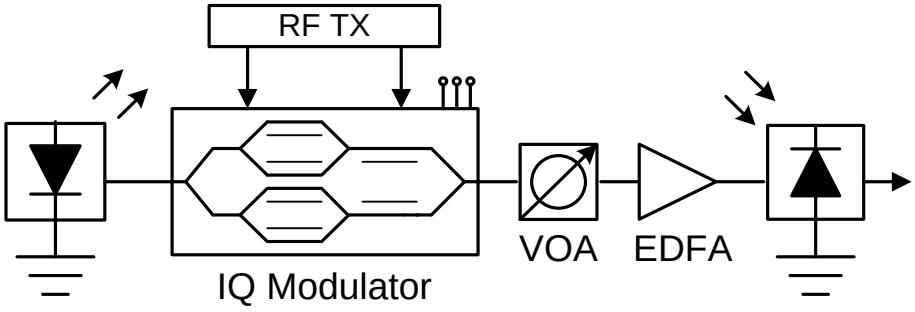

Figure 3.9: Setup employed in the characterization of the optical modulator.

3.3.3.1 Measured IMD_2

To investigate IMD_2, a discrete photo-detector with a bandwidth of 20 GHz was employed. Its output was connected to a spectrum analyser. In the transmitter only the first (5.4 GHz) and the fifth (16.2 GHz) electrical subcarriers were activated such that the second order intermodulation product for this frequency plan falls at 10.8 GHz. Figure 3.10 illustrates the measured and theoretical IMD_2 that were obtained for a modulation index m=0.15 for the different bias points. A trace from the spectrum analyser after the photo receiver is also shown. A good agreement between theory and measurements is observed. The discrepancy with the peak of the theoretical value is due to the fact that the minimum distortion that could be measured was limited by the noise floor. With lower values of OMI this limitation is present in more bias points and for that reason those measurements are not shown.

The previous result confirms that biasing at a point different to *quadrature* translates into a meaningful increase of CSO. In the next sections it will become clear that this impairment can be balanced with the associated improvement in CSPR that gives rise to a better overall sensitivity.

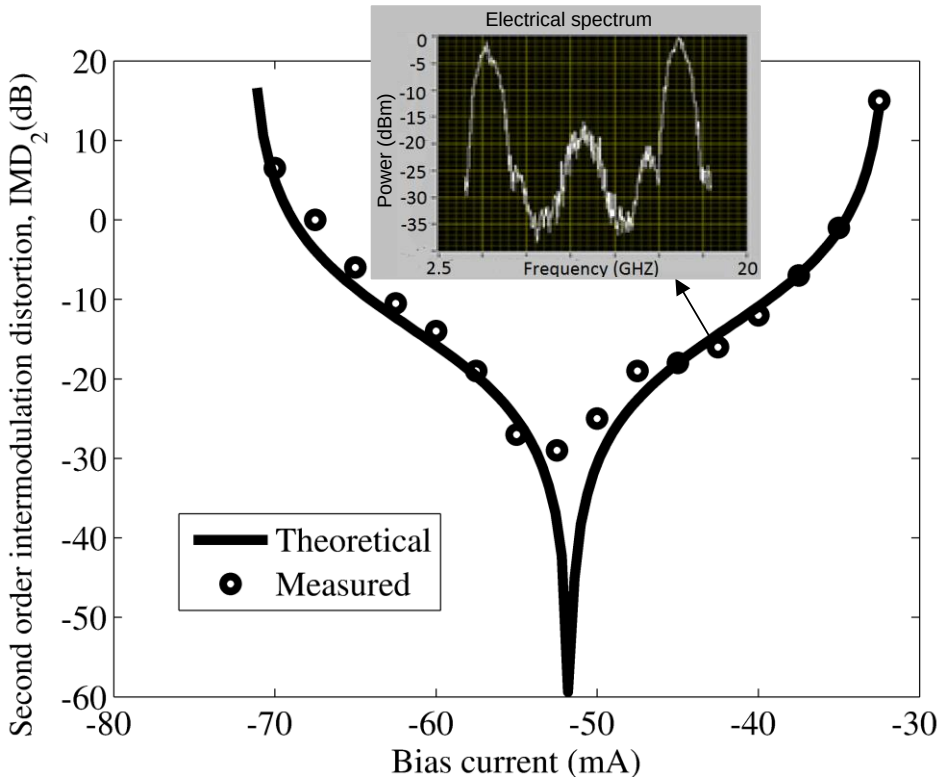

Figure 3.10: Second order intermodulation distortion. Measurements performed activating only the first and the fifth subcarriers and measuring the distortion at the third one. *m*=0.15. Insets show the electrical spectrum at one of the measurements.

3.3.3.2 Measured CSPR

For the measurement of the CSPR, the photo-detector of a digital oscilloscope module was used. CSPR was obtained for the detected photocurrent as the square of the ratio between the DC component and the rms value of the AC signal. Figure 3.3 showed that a good approximation of the optical CSPR could be obtained by adding 3 dB to the value obtained with the detected photocurrent (excluding the area around *null*). Figure 3.11 illustrates the accurate theoretical value and the measurements for *m*=0.055 and *m*=0.15. A good agreement between theory and the experiment is observed.

For the case of lower OMI, the picture also shows the photocurrent at two bias points: *quadrature* (Q in the figure), where IMD_2 presented its lowest value, and point B, the closest to the optimum that was identified in the theoretical section for *m*=0.055. The improvement in CSPR at point B is 5 dB relative to Q, and the optical peak to peak modulation depth approaches unity (roughly from 2/4 to 4/5), making this point more suitable for an efficient transmission.

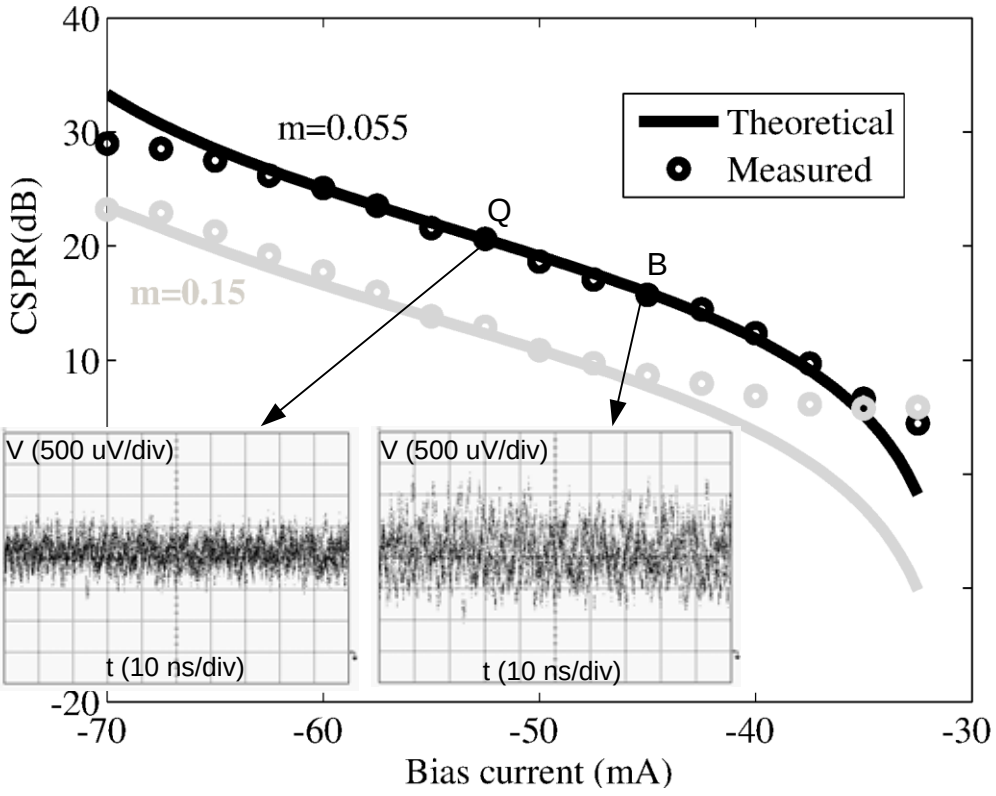

Figure 3.11: CSPR: theoretical and measured. Five subchannels. *m*=0.055 and 0.15. Photocurrent at two different bias points: *quadrature* and point B.

3.3.4 Channel Performance

3.3.4.1 Effects of CSPR and NLD

This section shows how the CSPR and NLD induced by the OIQM influences the performance of electrical subchannels in the communications system. The results were taken with a setup similar to that shown in Figure 3.5, but simulating the losses in the fibre with a VOA so that dispersion effects were removed. The components employed presented the parameters used in the generation of Figure 2.10, so that it can be concluded that ASE induced noise is dominant over RIN, shot noise and thermal noise. Consequently, from the point of view of the optical devices, a good agreement with the theoretical model presented in section 3.2.5 was expected. A low noise EDFA was used in the transmitter and its gain was fixed to obtain 10 dBm at the output. The gain of the EDFA at the receiver was regulated to guarantee the sensitivity in the baseband electrical receivers irrespective of the incoming optical power. Note that the low noise EDFA was used in the transmitter to ensure the dominant ASE was produced by the receiver EDFA, as in the mathematical model.

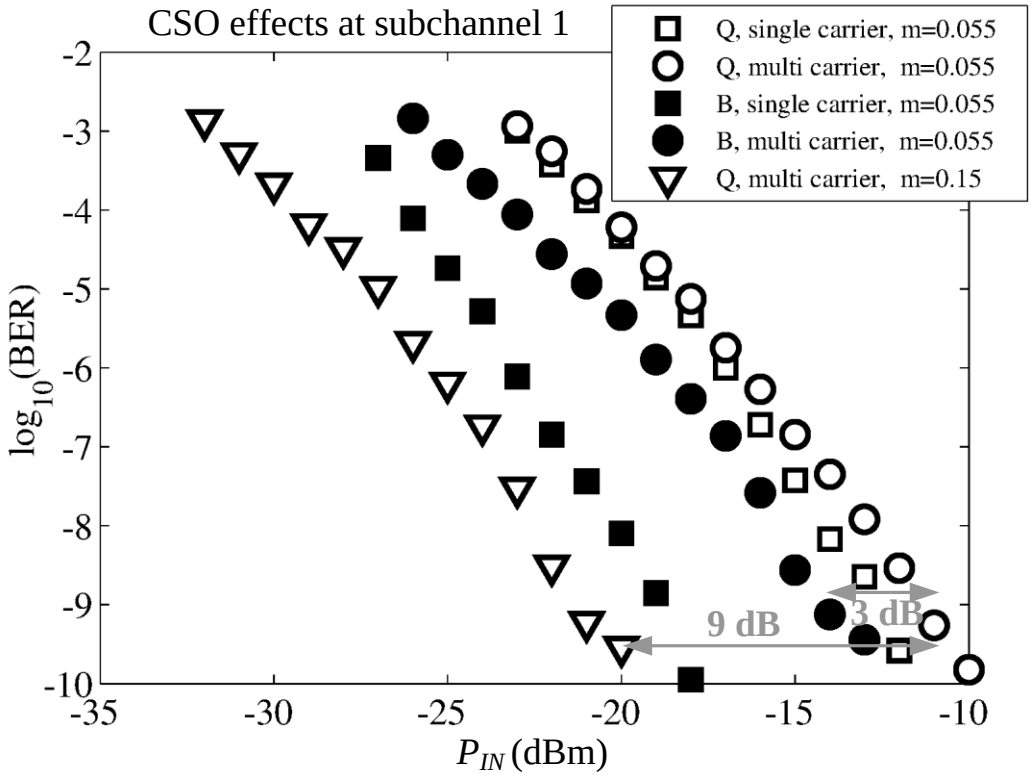

Figure 3.12: BER vs. Optical input power at the receiver for the first electrical subchannel. Two different bias points, Q and B. Measurements obtained with one or five active subcarriers. *m*=0.055 and 0.15.

The measurements were focused on two subcarriers, subchannel 1 to observe the effects of CSO and subchannel 4 to analyse the effects of CTB. The modulation index was *m*=0.055 and two bias points were studied: Q and B. BER versus received optical power at the input of the EDFA, P_{IN}, were obtained in two different situations: activating only one electrical subcarrier so that no IMD was produced, and with all the subcarriers on and NLD present in the system.

The performance of the first subchannel can be observed in Figure 3.12. As expected, the influence of the intermodulation products is more severe when biasing closer to *null* at point B. At Q, CSO is cancelled, so there is only a minor difference in performance when all the channels are active (less than 1 dB). However, when biasing at B, the NLD coming from CSO causes a penalty in performance of up to 5 dB. Despite the higher penalty due to NLD, a sensitivity gain of 3 dB can be observed at point B with respect to Q, for a BER=10^{-9}, in agreement with the theoretical prediction.

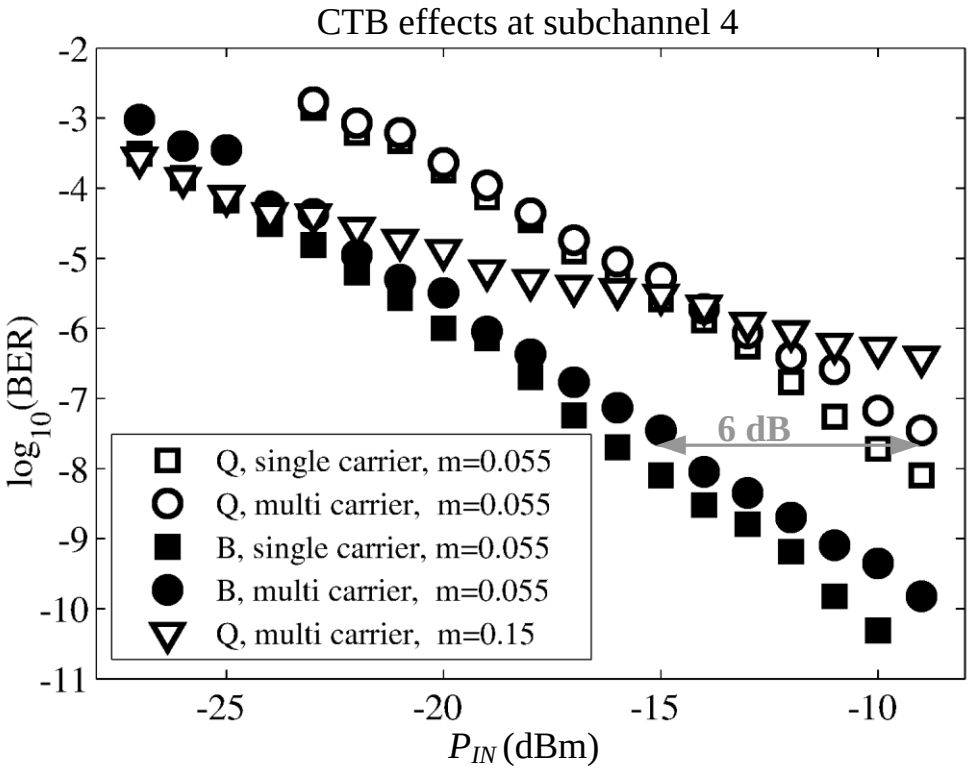

Figure 3.13: BER vs. Optical input power at the receiver for the fourth electrical subchannel. Two different bias points, Q and B. Measurements obtained with one or five active subcarriers. *m*=0.055 and 0.15.

A similar analysis was done for the fourth subchannel and is shown in Figure 3.13. CTB is independent of the bias point, as has been illustrated in Figure 3.4. Due to the low value of CTB for this OMI, the difference that can be observed between the single and multicarrier cases is small and, as expected, is similar at both bias points. The gain in sensitivity due to the better CSPR at point B is 6 dB with respect to Q, as predicted by theory for a BER=10^{-7} (similar to the prediction for BER=10^{-9}).

3.3.4.2 Effects of increased OMI

According to the theoretical study for OIQM-based SCM systems, the behaviour of the sensitivity can be summarized with two trends. For a given OMI, there can be an optimum bias point different to *quadrature*, where the channel most affected by CSO determines the gain in sensitivity of the link. This effect has been verified experimentally in the previous subsection. The second trend shows that it is possible to improve sensitivity by increasing OMI and biasing closer to quadrature, but at some point this process will have a detrimental effect for the channels affected by CTB. This behaviour is shown in this subsection.

The effects of CSO on subchannel 1 shown in Figure 3.12 also include the performance for the case of increased OMI with m=0.15 biasing at *quadrature*. The higher value of m induces a better CSPR and the bias at *quadrature* cancels CSO, resulting in a gain in sensitivity of 9 dB with respect to the lower OMI, consistent with the 8 dB predicted by theory. On the other hand, the behaviour of subchannel 4 shown in Figure 3.13 includes the same case of increased OMI while biasing at *quadrature*. It can be seen that the increment in CTB associated to the higher OMI resulted in a loss of sensitivity with respect to the case of lower OMI for all BER below 10^{-5}. This penalty occurred with an OMI lower than that expected from the theoretical prediction (m=0.20). This is due to the fact that the model considered ideal electrical components and IQ mixers. However, in practice, as it has been demonstrated in section 2.5.1, these components are designed for lower bandwidth signals. As a result, the high rates employed in this experiment can translate into a significant eye closure that is equivalent to an increased NLD.

3.4 Conclusions

SCM is a reliable multicarrier technique that is employed in multiple schemes, usually combined with OSSB to obtain increased tolerance to dispersive fading. The mathematical study of SCM has been extended by analysing the OIQM, an ideal

choice in the transmitter because, unlike other alternatives, both OSSB and carrier suppression can be obtained directly without external components by adjusting the bias points.

When the frequency plan ensures that the subchannels are only affected by CTB, CSPR can be modified without adding any additional impairment in the subchannels. When at least one of the subchannels is interfered by CSO, a trade-off between CSPR and NLD is present. The developed mathematical model can be used to determine the optimum bias point and predict the gains in sensitivity that can be achieved for every subchannel.

Experiments have been conducted with a scheme and components that ensure subcarriers are located at multiples of the data rate, which makes it ideal for an accurate study of the effects of intermodulation distortion. The theoretical predictions have been validated measuring CSPR, NLD, and their effect on the performance of channels. The sensitivity gains that can be directly achieved with OIQMs prove the suitability of this device to improve the power budget of SCM/OSSB links without incurring additional costs.

3.5 References

[1] P. M. Hill and R. Olshansky, "A 20-channel optical communication system using subcarrier multiplexing for the transmission of digital video signals," *Lightwave Technology, Journal of,* vol. 8, pp. 554-560, 1990.

[2] G. H. Smith and D. Novak, "Broad-band millimeter-wave (38 GHz) fiber-wireless transmission system using electrical and optical SSB modulation to overcome dispersion effects," *Photonics Technology Letters, IEEE,* vol. 10, pp. 141-143, 1998.

[3] R. P. Almeida, R. S. Oliveira, N. S. Moritsuka, C. R. L. Frances, A. Teixeira, and J. C. W. A. Costa, "Digital radio over fiber transmission based on SCM and WDM system for C-RAN architecture," in *Telecommunications Symposium (ITS), 2014 International*, 2014, pp. 1-5.

[4] R. Hui, Z. Benyuan, H. Renxing, C. T. Allen, K. Demarest, and D. Richards, "Subcarrier multiplexing for high-speed optical transmission," *Lightwave Technology, Journal of,* vol. 20, pp. 417-427, 2002.

[5] B. Charbonnier, S. Menezo, P. O'Brien, A. Lebreton, J. M. Fedeli, and B. Ben Bakir, "Silicon photonics for next generation FDM/FDMA PON," *Optical Communications and Networking, IEEE/OSA Journal of,* vol. 4, pp. A29-A37, 2012.

[6] M. Salter, D. Platt, L. Pettersson, L. Aspemyr, and B. Mingquan, "Circuits and system simulations for 100Gb/s optical SCM transmission," in *Electronics, Circuits, and Systems, 2009. ICECS 2009. 16th IEEE International Conference on*, 2009, pp. 960-963.

[7] J. Maeda, T. Katoh, and S. Ebisawa, "Effect of Fiber Dispersion on Subcarrier QAM Signal in Radio-Over-Fiber Transmission," *Lightwave Technology, Journal of,* vol. 30, pp. 2625-2632, 2012.

[8] J. Leibrich, A. Ali, and W. Rosenkranz, "OFDM transceiver design for optimizing sensitivity and long-haul performance," in *IEEE/LEOS Summer Topical Meetings, 2008 Digest of the*, 2008, pp. 249-250.

[9] X. Shijun and A. M. Weiner, "Optical carrier-suppressed single sideband (O-CS-SSB) Modulation using a hyperfine blocking filter based on a virtually imaged phased-array (VIPA)," *IEEE Photonics Technology Letters,* vol. 17, pp. 1522-1524, 2005.

[10] G. H. Smith, D. Novak, and Z. Ahmed, "Overcoming chromatic-dispersion effects in fiber-wireless systems incorporating external modulators," *Microwave Theory and Techniques, IEEE Transactions on,* vol. 45, pp. 1410-1415, 1997.

[11] W. H. Chen and W. I. Way, "Multichannel single-sideband SCM/DWDM transmission systems," *Lightwave Technology, Journal of,* vol. 22, pp. 1679-1693, 2004.

[12] P. Laurencio, S. O. Simoes, and M. C. R. Medeiros, "Impact of the Combined Effect of RIN and Intermodulation Distortion on OSSB/SCM Systems," *Lightwave Technology, Journal of,* vol. 24, pp. 4250-4262, 2006.

[13] T. Nakatogawa, M. Maeda, and K. Oyamada, "Optical single sideband modulator for distribution of digital broadcasting signals on millimetre-wave band based on self-heterodyne," *Electronics Letters,* vol. 40, pp. 1369-1370, 2004.

[14] W. Ming-Chia, C. Pi-Yang, and W. I. Way, "On the validity of using CW tones to test the linearity of multichannel M-QAM subcarrier multiplexed lightwave systems," *Photonics Technology Letters, IEEE,* vol. 12, pp. 413-415, 2000.

[15] X. Lu and O. Sniezko, "The evolution of Cable TV networks," *Optical Fiber Telecommunications IV-B: Systems and Impairments,* vol. 2, p. 404, 2002.

[16] F. Ramos and J. Marti, "Compensation for fiber-induced composite second-order distortion in externally modulated lightwave AM-SCM systems using optical-phase conjugation," *Journal of Lightwave Technology,* vol. 16, pp. 1387-1392, 1998.

[17] R. Olshansky, "Optimal design of subcarrier multiplexed lightwave systems employing linearized external modulators," *Journal of Lightwave Technology,* vol. 10, pp. 378-382, 1992.

[18] W. I. Way, *Broadband Hybrid Fiber Coax Access System Technologies*: Academic Press, Inc., 1998.

[19] H. Cohen, *Mathematics for scientists and engineers*: Prentice-Hall, 1992.

[20] B. Schmidt, A. J. Lowery, and J. Armstrong, "Experimental Demonstrations of Electronic Dispersion Compensation for Long-Haul Transmission Using Direct-Detection Optical OFDM," *Lightwave Technology, Journal of,* vol. 26, pp. 196-203, 2008.

[21] T. Nakatogawa, M. Maeda, and K. Oyamada, "A Novel Millimeter Wave Receiver Using Self-heterodyne Detection for a Digital Broadcasting ROF System," in *Microwave Photonics, 2006. MWP '06. International Topical Meeting on*, 2006, pp. 1-4.

[22] A. Lowery and J. Armstrong, "Orthogonal-frequency-division multiplexing for dispersion compensation of long-haul optical systems," *Optics Express,* vol. 14, pp. 2079-2084, 2006/03/20 2006.

[23] I. N. Cano, M. C. Santos, and J. Prat, "Optimum carrier to signal power ratio for remote heterodyne DD-OFDM in PONs," *IEEE Photonics Technology Letters,* vol. 13, pp. 1242-1245, 2013.

[24] Y. Guomin, E. Miller, J. Mallari, W. Cailin, C. Baoquan, C. Hui, *et al.*, "Small form factor thin film polymer modulators for telecom applications," in *Optical Fiber Communication Conference and Exposition (OFC/NFOEC), 2012 and the National Fiber Optic Engineers Conference*, 2012, pp. 1-3.

Chapter 4

4 Cost and Spectrally Efficient WDM/SCM

This section explores experimentally the impairments in performance that are generated when multiple SCM/OSSB signals are closely allocated in frequency to establish a spectrally efficient WDM link. The performance of cost effective WDM/SCM/OSSB implementations, without optical filters in the transmitter, presents a strong dependency on the imperfect sideband suppression ratio (SSR) that can be directly achieved with the electro-optical modulator. Based on the scheme described in chapter 2, a direct detection broadband multichannel SCM link composed of a state of the art optical IQ modulator and five QPSK subcarriers per optical channel was implemented. Performance measurements showed that a suppression ratio of 20 dB obtained directly with the modulator produced a penalty of 2 dB in overall performance, due to interference between adjacent optical channels.

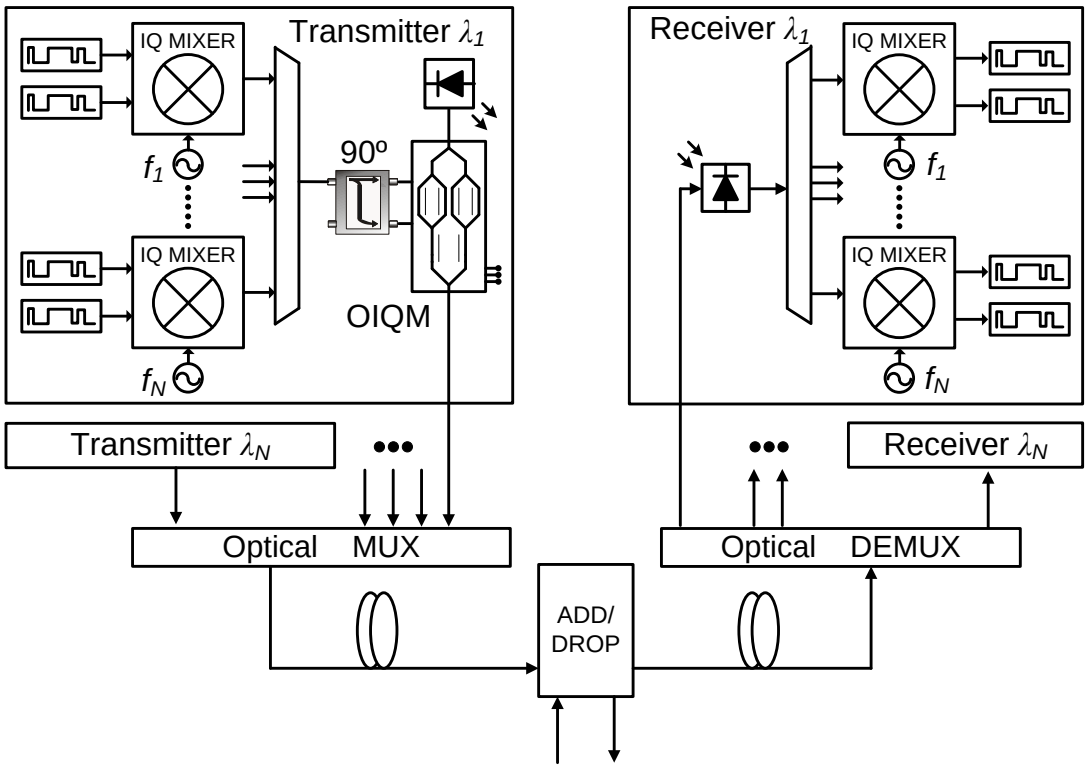

Figure 4.1 WDM/SCM/OSSB network scheme based on optical IQ modulators

4.1 WDM/SCM/OSSB

4.1.1 Generic Scheme

Microwave components present several advantages with respect to their optical counterparts like stability, low phase noise and frequency selectivity. SCM leverages these properties to generate one or more digitally modulated RF signals that are then transmitted on an optical wavelength. Many SCM solutions have been developed addressing different applications like cable television (CATV) [1], radio over fibre [2], broadband point to point links [3], access networks [4] or local area networks [5].

In all these applications, multiple optical SCM channels can be potentially combined in a WDM scheme increasing the capacity and the flexibility of the network [6]. Usually, an OSSB implementation of each optical channel is performed (either with dual drive Mach Zehnder modulators (DD-MZM) [7] or with optical IQ modulators (OIQM) [8]), as a method to eliminate dispersive fading [9]. A generic direct detection WDM/SCM/OSSB network scheme where optical channels can be added, removed and interchanged by optical add drop multiplexers is illustrated in Figure 4.1.

4.1.2 Advanced Implementation

Using the generic scheme as a starting point, increased spectral efficiency is possible by ensuring a narrower allocation of optical channels. Such implementation

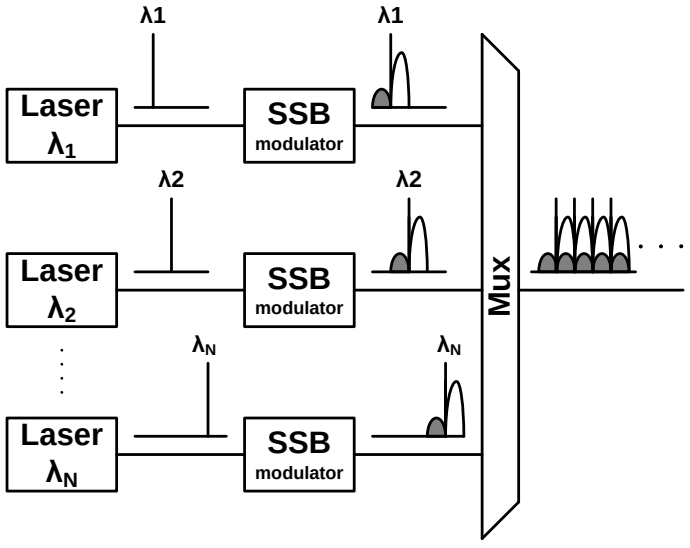

Figure 4.2 Cost and spectrally efficient WDM/SCM/OSSB scheme. Each optical channel composed of one subcarrier. Crosstalk due to the imperfect OSSB signals.

would only be accompanied with optimum system performance when a high value of SSR is ensured at the optical transmitter, as the remnants of the suppressed band will interfere with the subcarriers of the neighbouring optical channel.

In practice, SSR is limited by the imbalances and the extinction ratio of the optical modulators [10]. An SSR of 13 dB was achieved directly with a DD-MZM in [3]. Larger SSR values, up to 28 dB, have been reported but using additional and costly optical filters [11, 12].

A spectrally efficient WDM/SCM/OSSB transmitter is illustrated in Figure 4.2. No additional filters are employed, which translates into a lower cost implementation. The performance of the multichannel system, in comparison with a single wavelength transmission, is impaired due to the crosstalk associated with the imperfect SSR.

4.1.3 Scope

This chapter investigates the viability of the described advanced implementation using state of the art discrete optical IQ modulators. The incurred penalties in performance generated by the residual bands from the neighbouring channel are explored.

As it has been explained in Chapter 2, an all-analogue real-time SCM/QPSK scheme was designed for the experiments. Higher order modulation formats would require demanding signal processing in the receiver [13] with the consequent penalty in the power consumption and latency [14]. The presented all-analogue approach can offer a good trade-off between spectral efficiency and power consumption while using low-cost off-the-shelf microwave components. Simultaneously, moderate-to-medium transmission distances (tens or even hundreds of km) could be achieved due to the combination of SCM and SSB technology [3]. Therefore, the proposed multichannel electro-optical transceiver would be suitable in metro/access networks or in digital radio over fibre systems [15].

4.2 Sideband Suppression Ratio

This section shows that the SSR that is directly achievable with MZM based optical modulators is equal to the Extinction Ratio (ER). For completeness, this is proven for both DD-MZMs and OIQMs. The following analysis is simplified

assuming the only impairment in the modulator is the splitting ratio of the electrical field at the input γ. In all the cases, lossless optical modulators are considered.

4.2.1 Extinction Ratio

In the defined conditions, from section 1.3.2.2, the electric field at the output of a standard MZM can be written as:

$$E_o(t) = E_i\gamma\cos\left(\omega_c t + \frac{\pi\cdot V}{2V_\pi}\right) + E_i(1-\gamma)\cos\left(\omega_c t - \frac{\pi\cdot V}{2V_\pi}\right). \tag{4.1}$$

The peak and null fields will be given by:

$$\begin{aligned} peak &\xrightarrow{V=0} E_{o(peak)} = E_i\cdot\cos(\omega_c t). \\ null &\xrightarrow{V=V_\pi} E_{o(null)} = E_i(1-2\gamma)\cdot\sin(\omega_c t). \end{aligned} \tag{4.2}$$

The ER is given by the power ratio between the peak and the null cases:

$$ER = \frac{1}{(1-2\gamma)^2}. \tag{4.3}$$

It can be easily derived that the same ER would be obtained for a DD-MZM and for an OIQM in which the only impairment is the splitting ratio at the input γ.

4.2.2 Dual-Drive MZM

In the defined conditions, and from section 2.3.2.3, the electrical field at the output of a DD-MZM configured to produce OSSB is given by:

$$E_o(t) = E_i\gamma\cos\left(\omega_c t - \frac{\pi}{2} + \frac{\pi\cdot s(t)}{2V_\pi}\right) + E_i(1-\gamma)\cos\left(\omega_c t - \frac{\pi\cdot \hat{s}(t)}{2V_\pi}\right). \tag{4.4}$$

Following the mathematical procedure described in section 2.3.2.3, and for low amplitude modulating signals, this electric field can be approximated as:

$$E_o(t) \approx E_i\left(\left((1-\gamma)+\gamma\frac{\pi\cdot s(t)}{2V_\pi}\right)\cos(\omega_c t)+\left(\gamma+(1-\gamma)\frac{\pi\cdot \hat{s}(t)}{2V_\pi}\right)\sin(\omega_c t)\right). \quad (4.5)$$

Assuming the modulating signal and its HT are composed of a single tone:

$$\begin{aligned} s(t) &= V_{AC}\cos(\Omega t). \\ \hat{s}(t) &= V_{AC}\sin(\Omega t). \end{aligned} \quad (4.6)$$

Using *cos(A)cos(B)=0.5(cos(A+B)+cos(A-B))* and *sin(A)sin(B)=-0.5(cos(A+B)-cos(A-B))*, the amplitude of the components of interest E_p located at (ω_c+Ω) and (ω_c-Ω) can be obtained. Substituting $m=\pi V_{AC}/2V_\pi$:

$$\begin{aligned} E_p(t) &\xrightarrow{(\omega_c+\Omega)} \left(\gamma\frac{E_i m}{2}-(1-\gamma)\frac{E_i m}{2}\right)=(2\gamma-1)\frac{E_i m}{2}. \\ &\xrightarrow{(\omega_c-\Omega)} \left(\gamma\frac{E_i m}{2}+(1-\gamma)\frac{E_i m}{2}\right)=\frac{E_i m}{2}. \end{aligned} \quad (4.7)$$

Therefore, the SSR defined as the power ratio between the desired and the rejected sidebands, is equal to the extinction ratio:

$$SSR=\frac{1}{(2\gamma-1)^2}=ER. \quad (4.8)$$

4.2.3 Optical IQ Modulator

In the defined conditions, and from section 2.3.2.4, the electrical field at the output of an OIQM configured to produce OSSB is given by:

$$E_o(t)=E_i\left[\begin{array}{l}\gamma\cos\left(-\frac{\pi\cdot V_b}{2V_\pi}+\frac{\pi\cdot s(t)}{2V_\pi}\right)\cos(\omega_c t) \\ +(1-\gamma)\cos\left(-\frac{\pi\cdot V_b}{2V_\pi}+\frac{\pi\cdot \hat{s}(t)}{2V_\pi}\right)\sin(\omega_c t)\end{array}\right]. \quad (4.9)$$

Following the mathematical procedure described in section 2.3.2.4, and for low amplitude modulating signals, this electric field can be approximated as:

$$E_o(t) \approx \frac{E_i}{2}\cos\left(\frac{\pi \cdot V_b}{2V_\pi}\right)\left\{\begin{array}{l}\left[1+\tan\left(\frac{\pi \cdot V_b}{2V_\pi}\right)\cdot\frac{\pi \cdot s(t)}{2V_\pi}\right]\gamma\cos(\omega_c t)+ \\ \left[1+\tan\left(\frac{\pi \cdot V_b}{2V_\pi}\right)\cdot\frac{\pi \cdot \hat{s}(t)}{2V_\pi}\right](1-\gamma)\sin(\omega_c t)\end{array}\right\}. \quad (4.10)$$

With the same analysis developed above from eqs. (4.6) to (4.8), it can be readily seen that the SSR is again equal to the ER, regardless of the bias point V_b.

In the experiments, a state-of-the-art OIQM with a specified ER of >20 dB was employed. Accordingly, the SSR achieved experimentally was ≈20 dB. As it will be shown below, it was possible to verify that the cross-talk associated with the imperfect SSR of a neighbouring optical channel implies a penalty in performance but does not prevent data transmission.

4.3 Multichannel Implementation

The experiment was performed with the setup presented in Figure 4.3, where optical BPFs of 2 nm at the output of every EDFA for ASE suppression have been omitted for simplicity. The setup was largely based on the components detailed in

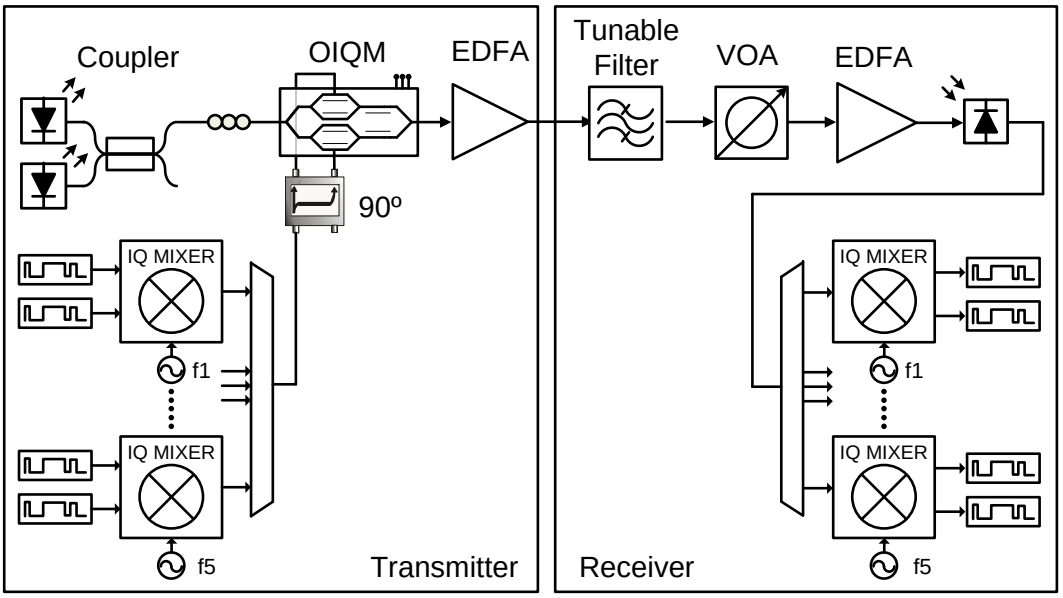

Figure 4.3 Setup to emulate a WDM/SCM/OSSB system consisting of an optical IQ modulator and five QPSK subchannels per wavelength.

section 2.5. The key parameters will be briefly reviewed and the new concepts will be described.

4.3.1 Electrical Features

The RF transmitter consisted of five inexpensive off-the-shelf MMIC IQ mixers that were employed to up-convert ten uncorrelated bit streams. The binary signals had been previously filtered to reduce their spectrum to approximately the first lobe of a sinc function. The performance of the RF IQ mixers was not optimized for spectrally dense broadband signals. As the measurements attempted to isolate the effects of imperfect SSR, short PRBS of 127 bits were employed. The nominal rate of every bit stream was 1.35 Gbit/s making a total rate of 13.5 Gbit/s (2.7 Gbit/s on each RF subcarrier). The local oscillators were located at even harmonics of the data rate (from 5.4 to 16.2 GHz) such that there was no guard band between electrical subchannels. After combining the five subchannels, a 90º hybrid coupler was used to generate the HT pair required by the OIQM to achieve OSSB. The RF receiver performed the splitting and demodulation of the electrical subchannels. The same family of IQ mixers were employed. After applying a LPF to the recovered baseband signals, performance was measured with a BERT.

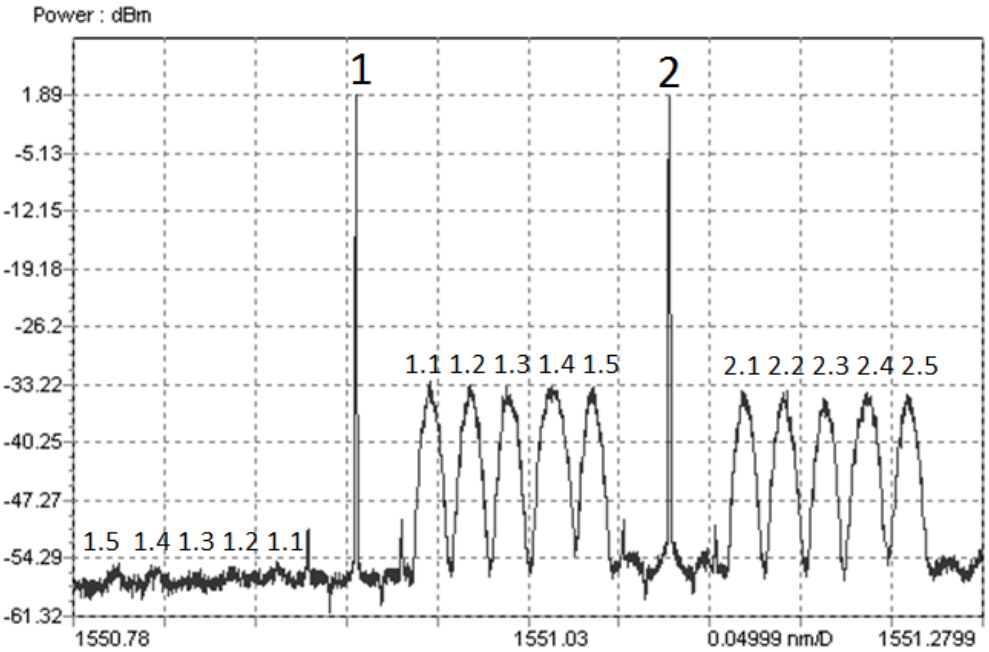

Figure 4.4 Two optical SCM/OSSB channels separated by 20 GHz. An SSR of more than 20 dB can be observed in channel 1.

4.3.2 Optical Features

From the optical perspective, the equipment employed as a light source incorporated two tunable lasers, which were coupled to obtain two wavelengths in the same optical fibre. The electro optical conversion was performed with the previously described state of the art OIQM [16]. Its properties allow the design of a small low-power stable SCM/OSSB transmitter that can achieve a good SSR without the need for additional optical filters in the transmitter. The overall rms OMI employed in the experiments was 7 % with respect to V_π, ensuring negligible NLD. The average optical power at the output of the transmitter EDFA was 5.5 dBm. A tunable filter was used to select one of the optical channels in the receiver. A VOA was employed to emulate additional optical fibre losses. The received EDFA was employed in constant output power mode, ensuring 3 dBm at the input of the photo-receiver regardless the incoming average optical power.

For a separation between optical carriers of 20 GHz, the optical spectrum at the output of the transmitter EDFA is shown in Figure 4.4. Two optical SCM/OSSB channels are present and every channel and subchannel is numbered. On the optical channel 1 it can be seen that an SSR of more than 20 dB was achieved directly with the optical modulator. Simultaneously, that channel was experiencing interference from the imperfectly suppressed sideband of the optical channel 2. Despite the fact that only one transmitter was used in the experiment, data and interference were always uncorrelated regardless of the wavelength separation. This occurred because the interfered data and the interference belonged to opposite sidebands and were modulated by independent lasers, which translated into an arbitrary phase shift between them.

A real WDM system would consist of a number of transmitters with independent optical modulators. Typically, two different SCM channels would be generated in different fibres and then they would be coupled and amplified. The quality of the emulation of a real WDM configuration with the presented setup can be discussed observing Figure 4.4. The peaks of the imperfectly suppressed band were above the noise floor generated by the EDFA. This fact indicates that the described simpler implementation is suitable for the purpose of the experiment: measure the penalty of performance associated with the imperfect SSR.

4.4 Measurements

4.4.1 Overall Performance Degradation

Firstly, the influence of the imperfectly suppressed band on the performance of the neighbouring channel was measured. The two optical channels were separated by 25 GHz to emulate the ITU grid [17] and to relax the selectivity of the optical filter at the receiver. Overall performance was measured for optical channel 1 in two different situations: with and without the interference from the second optical channel. In the second case, instead of switching off the interfering channel, it was moved 100 GHz away so that the gain of the EDFA at the transmitter remained the same for both channels. With this method it was ensured that the average optical power at the input of the pre-amplified receiver P_{IN} did not change in both situations and the measurements with and without interference could be directly compared. For the two optical channel transmission system, Figure 4.5 shows the first channel after the optical filter in the receiver. The optical carrier of the interfering channel was reduced to ≈-40 dBc with respect to the desired optical carrier.

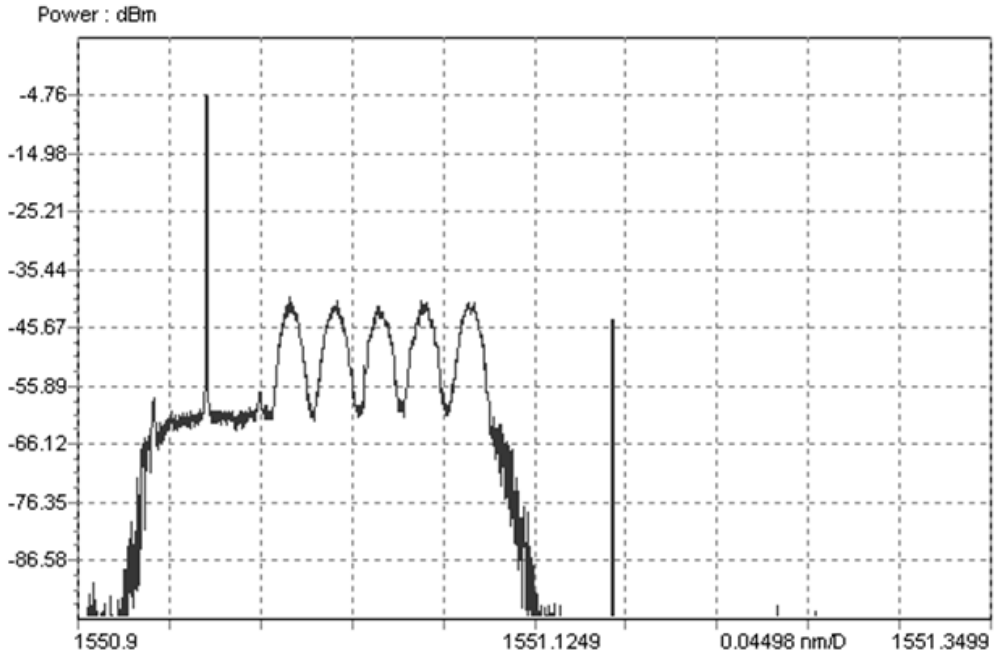

Figure 4.5 Optical spectrum after filtering the two channel SCM/OSSB signal in the receiver. The optical channels were separated 25 GHz.

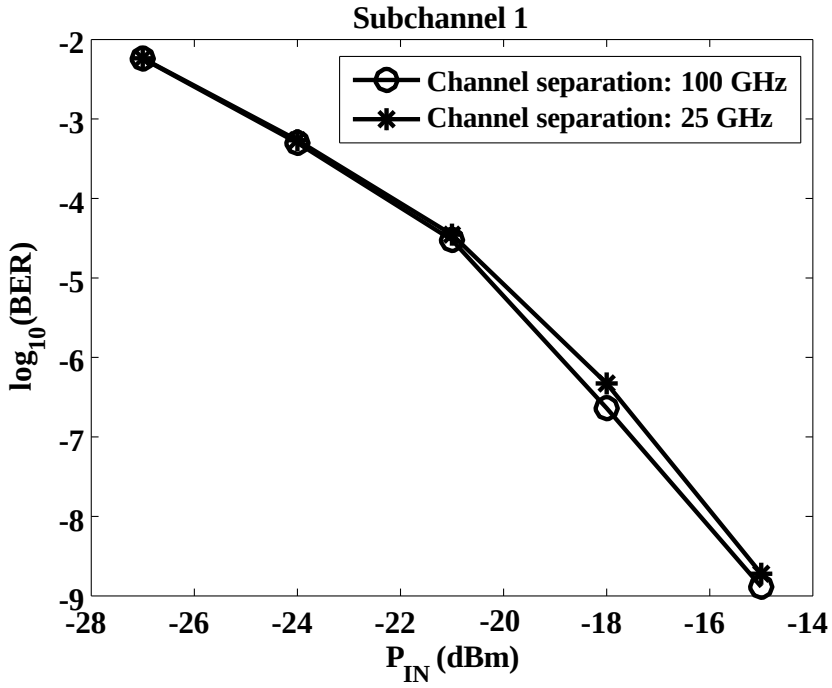

Figure 4.6 Performance measured at subchannel 1.1 when the two transmitted optical channels are separated 25 and 100 GHz.

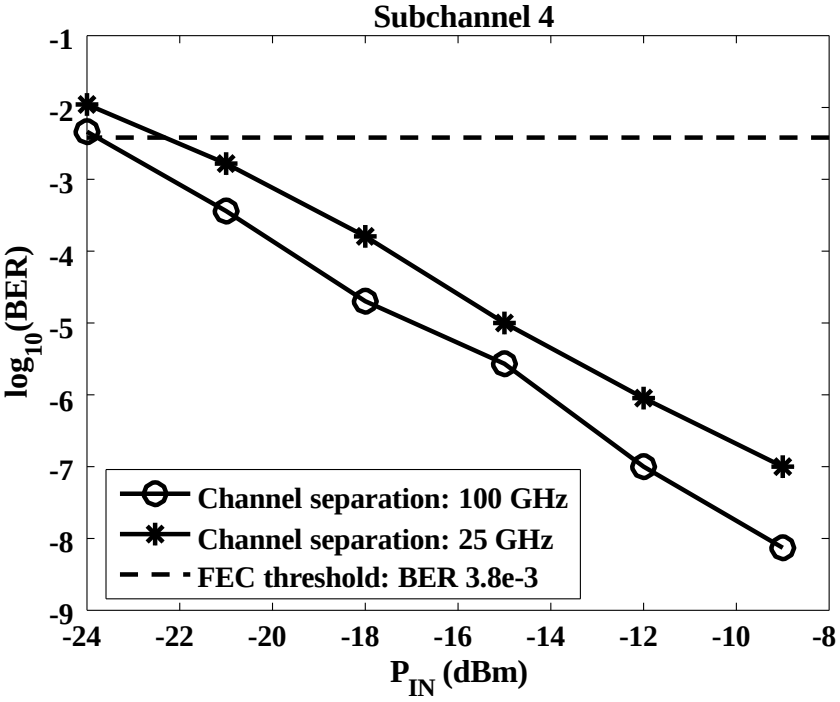

Figure 4.7 Performance measured at subchannel 1.4 when the two transmitted optical channels are separated 25 and 100 GHz. Threshold for a 7% FEC.

Measurements were focused on subchannels 1.1 and 1.4. With the 25 GHz channel separation, subchannel 1.1 was not interfered by any unsuppressed residual image. Consequently, no penalty in performance was expected in comparison to the case where the channel separation was 100 GHz. The expected behaviour was confirmed by the measured BER versus P_{IN} curves which are illustrated in Figure

4.6. In contrast, as it can be observed in Figure 4.7, subchannel 1.4 was interfered by the remnants of the suppressed band of the neighbouring channel with a 25 GHz channel separation. Considering a hard decision FEC with 7% overhead, the penalty due to this interference would be ≈2 dB at the lowest sensitivity. Therefore, there is a trade-off as spectral efficiency can only be maximized at the expense of reducing the maximum reach of the link in at least 10 km. It should be noted that better overall receiver sensitivities would be achieved by applying carrier suppression in the transmitter, as shown in Chapter 3. Relative performance differences between subchannels 1.1 and 1.4 were a consequence of the different behaviour of the IQ mixers in different RF bands.

4.4.2 System Optimization

Another test was performed to study the influence of the frequency position of the unwanted sideband with respect to the desired signal. The optical channels were initially separated by 27.2 GHz and this separation was increased in frequency steps of approximately 300 MHz, changing the relative location of the interference. The maximum additional separation was 2.3 GHz, covering practically one sideband of an up-converted subchannel. The performance of subchannel 1.4 was measured

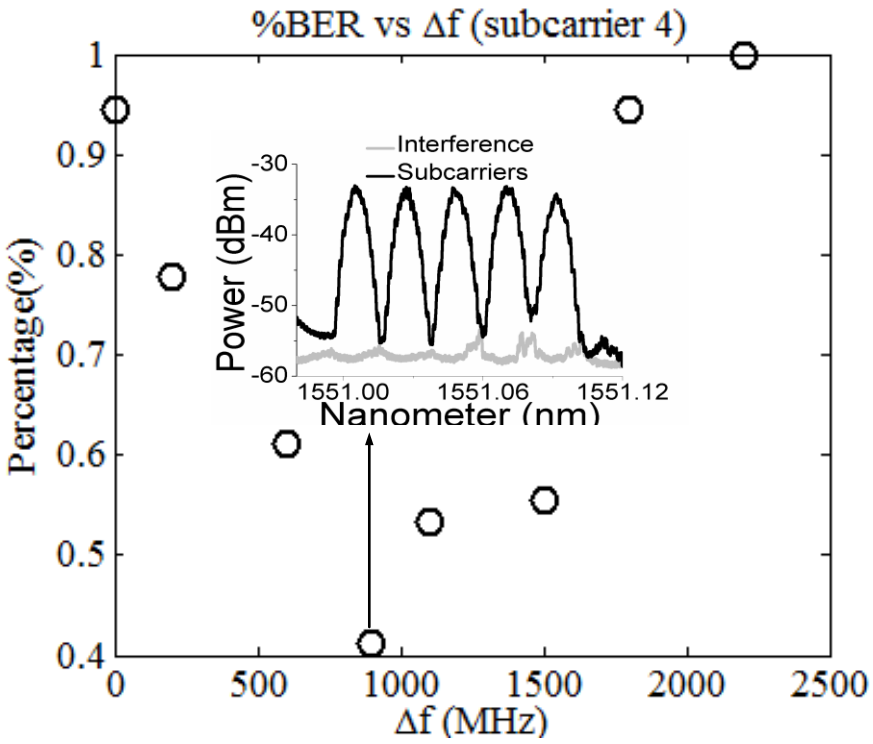

Figure 4.8 Performance measured at subchannel 1.4 when the interfering optical channel is located at different frequencies. Inset shows the optical spectrum of subchannels and interference for the case of minimum BER.

maintaining a P_{IN} of -12 dBm in all the cases. Figure 4.8 illustrates the obtained BER measurements as a percentage with respect to the worst case (BER=9e-8). The minimum BER corresponds to the situation in which the maximum peak of the interference from subchannels 2.4 and 2.5 coincides with the minimum level of the subchannel 1.4, as can also be observed in the inset of Figure 4.8. The maximum values of BER are obtained in the two extremes of the picture, when the maximum residual interference from subchannels 2.4 or 2.5 coincides approximately with the peak of subchannel 1.4.

4.5 Conclusions

SCM is used in many applications employing analogue and digital implementations. The technique can be combined with WDM to increase the flexibility and the capacity of a network. To allocate closer optical channels, achieving improved spectral efficiency, OSSB signals are required but the performance is limited by the sideband suppression ratio obtained at the electro-optic transmitter. This chapter has presented a WDM/SCM/OSSB link, based on a state of the art optical IQ modulator, where the penalty associated with the residual sideband from the neighbouring optical channel was studied. A suppression ratio of more than 20 dB was achieved directly with the optical modulator without requiring additional optical filters, and a penalty of less than 2 dB in overall performance of the WDM/SCM system was measured due to the associated interference. It can be concluded that, despite the imperfect behaviour of optical modulators generating OSSB signals, a close allocation of WDM channels is feasible and viable avoiding expensive optical filters in the transmitter. Additionally, a fine adjustment of the frequency separation between optical channels can also be employed to ensure optimum performance in these systems, making the peaks of the residual interference coincide with the nulls of the desired subchannels.

Moreover, the described direct detection WDM/SCM setup is unique in several senses. Firstly, the use of MMIC IQ mixers demonstrates that a cost effective practical deployment with integrated off-the-shelf analogue components is possible. Secondly, the employment of optical IQ modulators allows the implementation of colourless OSSB transmitters with partial optical carrier suppression without requiring optical filters in the transmitter. Finally, and despite the simplified transmitter lacking optical filters, it has been proven that spectral efficiency is not

compromised by a closer allocation of optical channels. These properties can motivate the application of this solution when flexibility and moderate transmission length are required but cost, power consumption, spectral efficiency and the future scalability determine the technology selected to be deployed. Metro/access networks or digital radio over fibre systems can leverage these features.

4.6 References

[1] P. M. Hill and R. Olshansky, "A 20-channel optical communication system using subcarrier multiplexing for the transmission of digital video signals," *Journal of Lightwave Technology,* vol. 8, pp. 554-560, 1990.

[2] G. H. Smith and D. Novak, "Broad-band millimeter-wave (38 GHz) fiber-wireless transmission system using electrical and optical SSB modulation to overcome dispersion effects," *IEEE Photonics Technology Letters,* vol. 10, pp. 141-143, 1998.

[3] R. Hui, Z. Benyuan, H. Renxing, C. T. Allen, K. Demarest, and D. Richards, "Subcarrier multiplexing for high-speed optical transmission," *Lightwave Technology, Journal of,* vol. 20, pp. 417-427, 2002.

[4] B. Charbonnier, S. Menezo, P. O. Brien, A. Lebreton, J. M. Fedeli, and B. B. Bakir, "Silicon photonics for next generation FDM/FDMA PON," *IEEE/OSA Journal of Optical Communications and Networking,* vol. 4, pp. A29-A37, 2012.

[5] M. Salter, D. Platt, L. Pettersson, L. Aspemyr, and B. Mingquan, "Circuits and system simulations for 100Gb/s optical SCM transmission," in *Electronics, Circuits, and Systems, 2009. ICECS 2009. 16th IEEE International Conference on*, 2009, pp. 960-963.

[6] J. M. Buset, Z. A. El-Sahn, and D. V. Plant, "Experimental demonstration of a 10 Gb/s subcarrier multiplexed WDM PON," *Photonics Technology Letters, IEEE,* vol. 25, pp. 1435-1438, 2013.

[7] W. H. Chen and W. I. Way, "Multichannel single-sideband SCM/DWDM transmission systems," *Lightwave Technology, Journal of,* vol. 22, pp. 1679-1693, 2004.

[8] T. Nakatogawa, M. Maeda, and K. Oyamada, "Optical single sideband modulator for distribution of digital broadcasting signals on millimetre-wave band based on self-heterodyne," *Electron. Lett,* vol. 40, pp. 1369-1370, 2004.

[9] J. Maeda, T. Katoh, and S. Ebisawa, "Effect of Fiber Dispersion on Subcarrier QAM Signal in Radio-Over-Fiber Transmission," *Lightwave Technology, Journal of,* vol. 30, pp. 2625-2632, 2012.

[10] Y. Ogiso, Y. Tsuchiya, S. Shinada, S. Nakajima, T. Kawanishi, and H. Nakajima, "High extinction-ratio integrated Mach–Zehnder modulator with active Y-branch for optical SSB signal generation," *Photonics Technology Letters, IEEE,* vol. 22, pp. 941-943.

[11] T. Fujiwara and K. Kikushima, "140 Carrier, 20GHz SCM signal transmission across 200km SMF by two-step sideband suppression scheme in optical SSB modulation," in *Optical Fiber Communication Conference*, 2007, p. OME2.

[12] X. Shijun and A. M. Weiner, "Optical carrier-suppressed single sideband (O-CS-SSB) Modulation using a hyperfine blocking filter based on a virtually imaged phased-array (VIPA)," *IEEE Photonics Technology Letters,* vol. 17, pp. 1522-1524, 2005.

[13] L. Giorgi, F. Cavaliere, P. Ghiggino, F. Ponzini, A. Bianchi, and A. D'Errico, "Characterization of a High Capacity Multi-User Optical Access Network Using 1 Gb/s 16 QAM Subcarrier Multiplexing," *Lightwave Technology, Journal of,* vol. 27, pp. 1203-1211, 2009.

[14] A. Morea, S. Spadaro, O. Rival, J. Perello, F. Agraz, and D. Verchere, "Power management of optoelectronic interfaces for dynamic optical networks," in *Optical Communication (ECOC), 2011 37th European Conference and Exhibition on*, 2011, pp. 1-3.

[15] R. Almeida, R. Oliveira, N. Moritsuka, C. Frances, A. Teixeira, and J. Costa, "Digital Radio over Fiber transmission based on SCM and WDM system for C-RAN architecture," in *Telecommunications Symposium (ITS), 2014 International*, 2014, pp. 1-5.

[16] Y. Guomin, E. Miller, J. Mallari, W. Cailin, C. Baoquan, C. Hui, *et al.*, "Small form factor thin film polymer modulators for telecom applications," in *Optical Fiber Communication Conference and Exposition (OFC/NFOEC), 2012 and the National Fiber Optic Engineers Conference*, 2012, pp. 1-3.

[17] ITU-T, "G. 694.1: Spectral grids for WDM applications: DWDM frequency grid."

Chapter 5

5 Orthogonal Subcarrier Multiplexing

This chapter studies the key aspects of an optical link which transmits an SCM signal composed of orthogonally overlapping broadband subchannels. The work is presented in the context of creating an all-analogue real-time multi-gigabit orthogonal frequency division multiplexing (OFDM) electro-optical transceiver for short/middle-range high-capacity data networks. Passive microwave filters are used to perform the pulse shaping of the bit streams, allowing orthogonal transmission without the necessity for digital signal processing (DSP). Accordingly, a cyclic prefix that would cause a reduction in the net data rate is not required. An experiment consisting of orthogonally spaced 2.7 Gbaud QPSK subchannels demonstrates that the spectral efficiency of traditional DSP-less SCM links can be potentially doubled. Furthermore, a technique to synchronize the electrical subcarriers employing a lower number of components than previous solutions is demonstrated on a 50 km link.

5.1 Spectrally Efficient Multicarrier Modulation

The increasing demand for capacity in optical links has motivated the development of more spectrally efficient transmission schemes during recent decades. Recently, this tendency has been enhanced with the proliferation of data centres, which have stimulated a growing research effort in optical interconnects and its associated technologies [1]. Multicarrier systems have proved to be relevant solutions, as they divide the available transmission bandwidth into narrower-band RF and optical subsystems that can be processed independently. This section reviews the key multicarrier techniques that have been applied to the design of spectrally-efficient electro-optical transceivers. These schemes can be implemented relying on electrical and/or optical signal processing. Although both options will be described in the text, this work focuses on the configurations based on electrical signal processing as they are more realistic for practical and stable implementations. For those realizations, examples of typical spectra can be found in Figure 5.1.

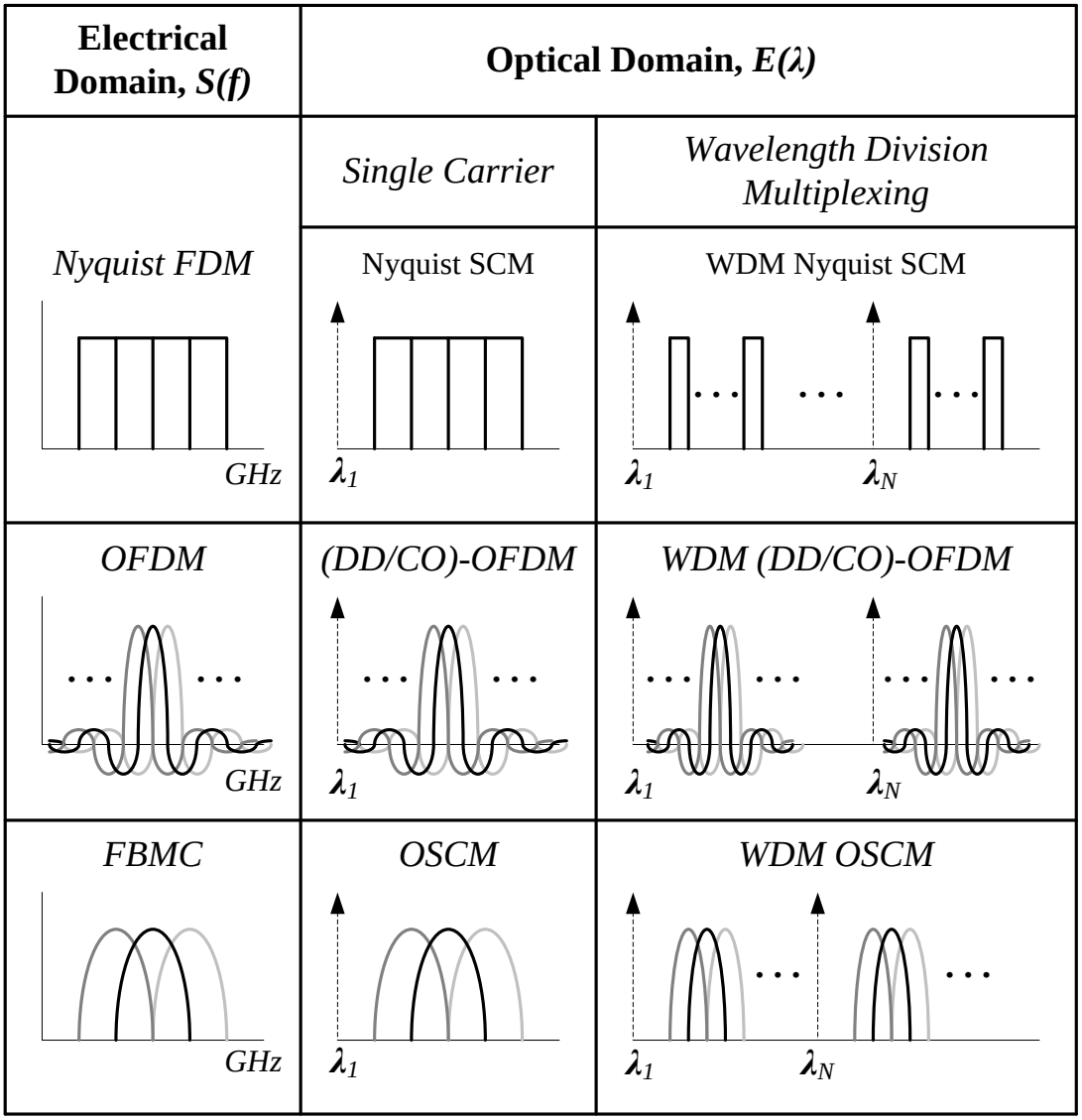

Figure 5.1 Typical electrical and optical spectra obtained in multicarrier spectrally-efficient electro-optical transceivers based on electrical signal processing.

5.1.1 Nyquist Pulse Shape

5.1.1.1 Ideal Filters for Communications

For digital modulation at a symbol rate B Gbaud, a simple square shape pulse translates into a sinc spectrum that is not limited in bandwidth and whose main lobe extends to B Hz. Unavoidably, transmission in a finite bandwidth produces distortion in the spectrum and consequently in the received signal pulses [2]. Nyquist pulses represent shapes that are not limited in time but whose spectra are confined in a certain bandwidth, which allows transmission free from Inter Symbol Interference (ISI) [2]. The most employed Nyquist pulse is called Raised Cosine (RC) and, for a given symbol period T_s (symbol rate $B=1/T_s$), its impulse response $h_{RC}(t)$ and transfer function $H_{RC}(f)$ are given by the following expressions [3]:

$$h_{RC}(t) = \frac{\sin\left(\frac{\pi t}{T_s}\right)}{\frac{\pi t}{T_s}} \frac{\cos\left(\frac{\pi \beta t}{T_s}\right)}{1-\left(\frac{2\beta t}{T_s}\right)^2}. \tag{5.1}$$

$$H_{RC}(f) = \begin{cases} T_s, & 0 \le |f| \le \frac{1}{2T_s}(1-\beta). \\ \frac{T_s}{2}\left\{1-\sin\left[\frac{\pi T_s}{\beta}\left(|f|-\frac{1}{2T_s}\right)\right]\right\}, & \frac{1}{2T_s}(1-\beta) \le |f| \le \frac{1}{2T_s}(1+\beta). \\ 0, & \textit{otherwise.} \end{cases} \tag{5.2}$$

As can be observed in Figure 5.2, the roll-off factor β, defined in the range $0 \le \beta \le 1$, determines the bandwidth of the pulse, f_{BW}, such that $H_{RC}(f)=0$ for $f>f_{BW}$:

$$f_{BW} = \frac{1}{2T_s}(1+\beta) = \frac{B}{2}(1+\beta). \tag{5.3}$$

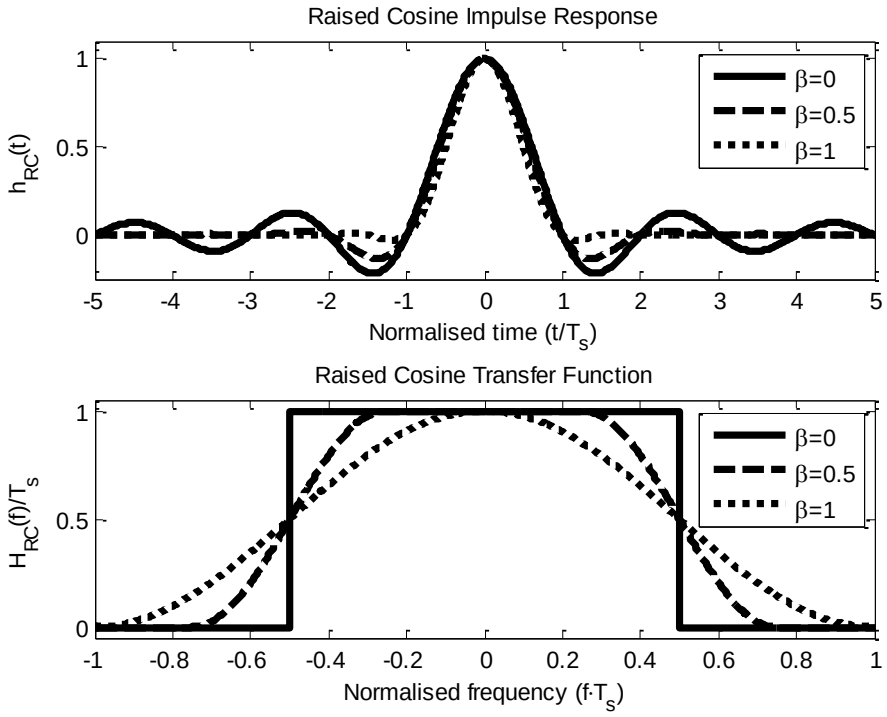

Figure 5.2 Impulse response and transfer function of raised cosine pulse.

The RC represents an individual pulse that can be transmitted in a confined bandwidth. In a communication system, it is typical to transmit symbols with a given shape and filter the received signal to remove the out-of-band interference and noise. For such a scheme, the ideal matched filter that is applied in both the transmitter and the receiver must meet the following properties: confined bandwidth and ISI cancellation in the receiver. It is obvious that an ideal matched filter can be calculated as the square-root of the transfer function of a Nyquist pulse. For the RCs, the associated Square Root Raised Cosine (SRRC) filters are given by [4]:

$$h_{SRRC}(t)=\frac{1}{\sqrt{T_s}}\frac{\sin\left(\frac{\pi t}{T_s}(1-\beta)\right)+\frac{4\beta t}{T_s}\cos\left(\frac{\pi t}{T_s}(1+\beta)\right)}{\frac{\pi t}{T_s}\left[1-\left(\frac{4\beta t}{T_s}\right)^2\right]}. \tag{5.4}$$

$$H_{SRRC}(f)=\sqrt{\left|H_{RC}(f)\right|}. \tag{5.5}$$

The SRRC characteristics are illustrated in Figure 5.3. Note that for the RC and SRRC pulses, the case β=0 represents a sinc pulse in time with a square spectrum.

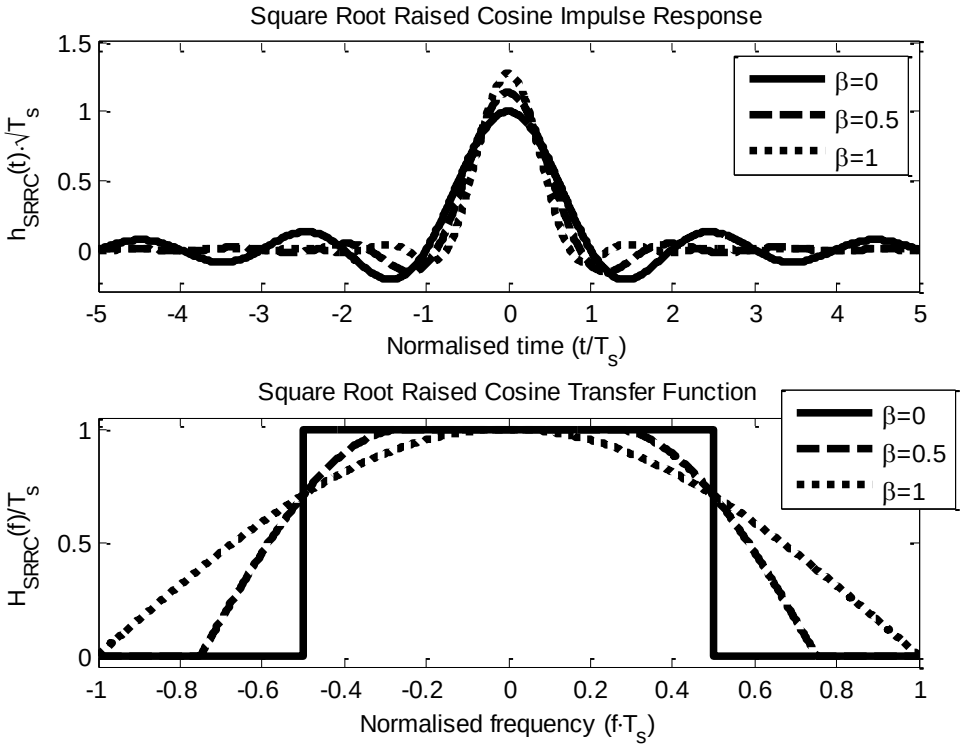

Figure 5.3 Impulse response and transfer function of square root raised cosine pulse.

From the filters described above, it is obvious that the maximum spectral efficiency is achieved by making beta small, ideally β=0. This allows transmitting a baseband signal with a symbol rate *B* Gbaud in a bandwidth equal to *B*/2 Hz. If the signal is transmitted in an RF or an optical carrier, the minimum bandwidth is obviously double, *B* Hz.

5.1.1.2 Nyquist Subcarrier Multiplexing

In Nyquist SCM, an electrical signal composed of one or several tightly allocated subchannels is generated using Nyquist baseband pulses with low beta factors. The electrical signal is then modulated onto an optical carrier, transmitted through fibre, and received with direct detection [4-6] or, potentially, coherent detection [7]. Typical Nyquist SCM/OSSB spectra for the single optical carrier and the WDM cases are illustrated in Figure 5.1, where the presence of the optical carrier is strictly necessary only for direct detection. Focusing on the electrical signal processing, the generation of RCs and SRRCs filters with very low beta factors is not easily achievable with microwave filters, as an abrupt roll-off and constant group delay are not compatible [8]. Accordingly, Nyquist SCM is implemented with DSP [9], with the consequential penalties in power consumption and latency in high-speed systems.

5.1.1.3 Nyquist Wavelength Division Multiplexing

Nyquist implementations based on optical signal processing are also possible. An optical filter with an ideally square Nyquist transfer function can be used to shape the output of an optical modulator [10]. These implementations use high baseband symbol rates in comparison with electrically based multicarrier processing and, accordingly, are less tolerant to dispersion. Lower symbol rates would require a high number of optical modulators. Hence, electrical processing is more realistic for practical Nyquist realizations.

5.1.2 Orthogonal Frequency Division Multiplexing

The term OFDM implies the transmission of orthogonally overlapping subchannels in the frequency domain. While Nyquist SCM relies on transmitting long sinc-shaped time pulses featuring confined non-overlapping square spectra, OFDM follows the opposite approach. Baseband square symbols are employed obtaining a multicarrier spectrum composed of orthogonally overlapping sinc functions.

5.1.2.1 Fast Fourier Transform

The most efficient algorithms for the modulation and demodulation of an OFDM signal are the Inverse Fast Fourier Transform (IFFT) and the Fast Fourier Transform (FFT) respectively. For a realization with *N* subcarriers, if *X[k]* are the *N* complex values to be transmitted in one OFDM symbol and *x[m]* represents the associated electrical signal, the IFFT and the FFT perform the following operations [11]:

$$x[m] = \frac{1}{\sqrt{N}} \sum_{k=0}^{N-1} X[k] \cdot e^{j\frac{2\pi km}{N}}, \quad 0 \le m \le N-1. \tag{5.6}$$

$$X[k] = \frac{1}{\sqrt{N}} \sum_{m=0}^{N-1} x[m] \cdot e^{-j\frac{2\pi km}{N}}, \quad 0 \le k \le N-1. \tag{5.7}$$

5.1.2.2 OFDM Subcarrier Multiplexing

OFDM is a popular multiplexing technique and is mostly implemented relying on DSP. Typically, a high number of narrowband subchannels is employed, enhancing the tolerance to dispersion, e.g. 512 subchannels of ≈5 MHz in [12]. For high-speed systems the signal *x[m]* incorporates high frequency components and high-performance DACs and ADCs are necessary to perform the electrical processing [11]. Note that the signal *x[m]* is complex. The real and the complex parts represent respectively the in-phase and quadrature components that are modulated onto the optical carrier. OFDM can be combined with both direct detection (DD-OFDM) [12] and coherent detection (CO-OFDM) [13]. Typical OFDM/OSSB spectra for single optical carrier and WDM cases are illustrated in Figure 5.1.

Due to transmission over a dispersive medium such as an optical fibre, different subchannels reach the receiver with different relative delays. As a consequence, the duration of each received OFDM symbol is longer than in the original. This effect is illustrated for a simplified case consisting of two subchannels in Figure 5.4(a), and translates into an undesired interference due to time overlapping between different OFDM symbols. To solve this problem, each OFDM symbol is stretched in the transmitter by appending a copy of the last samples at the beginning of the symbol, as illustrated in Figure 5.4(b). This appended portion of the symbol is referred to as *cyclic prefix* and, obviously, implies a penalty in the overall bit rate. The time duration of the cyclic prefix must be equal to or greater than the maximum

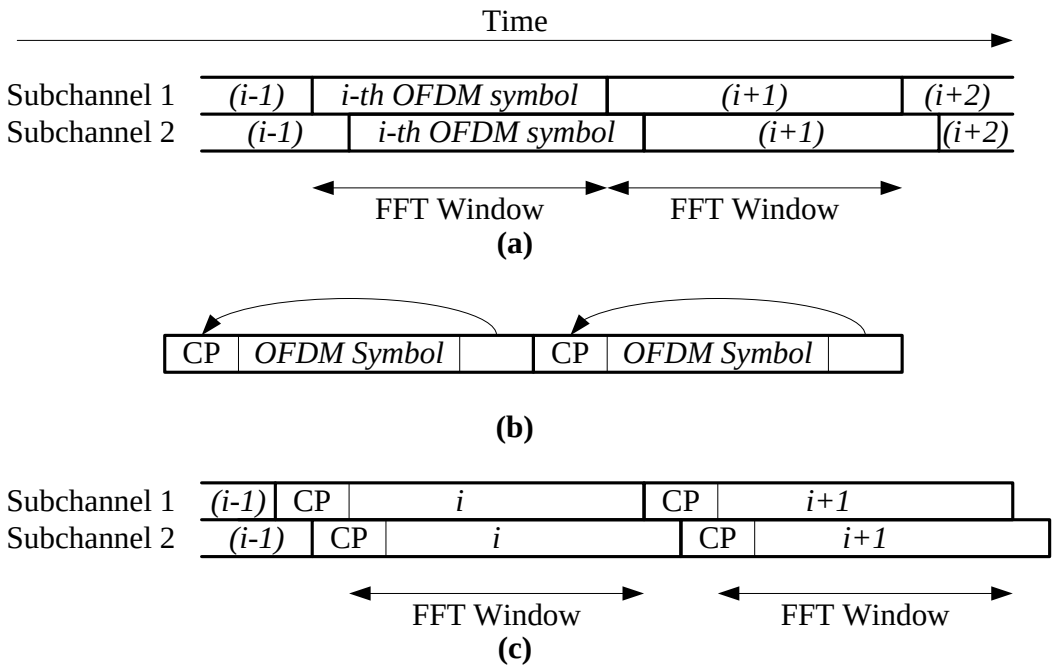

Figure 5.4 OFDM symbol transmission in dispersive media: (a) interference due to dispersion, (b) cyclic prefix (CP) introduction, (c) operation free of interference.

delay spread generated by the optical fibre, which is proportional to the fibre length. With the cyclic prefix, it is ensured that the FFT window only covers components belonging to the same OFDM symbol, as can be observed in Figure 5.4(c).

5.1.2.3 All-optical OFDM / Coherent WDM

OFDM based on optical signal processing has also been demonstrated. One solution consists of implementing the FFT with optical components [14]. This method is known as all-optical OFDM. Another alternative that is equivalent to OFDM but avoids the (I)FFT relies on using banks of filters with square impulse responses in both the transmitter and the receiver [15]. A variant of this technique, referred to as *Filtered OFDM* in signal processing [15], uses time limited impulse responses with smoother transitions than the square pulse. Following this approach, optical OFDM is achieved by a careful selection of the combined effect of optical and electrical filters [16, 17]. This technique has been demonstrated with direct detection and coherent detection [16], and in the second case is usually known as Coherent WDM [18]. The main disadvantage of the described solutions is that the optical carriers cannot be independent. They must be coherent in the sense that the relative phase shifts between them remains constant. While this condition is easily achievable with electrical subcarriers, in the optical domain it is difficult to obtain and requires stable optical frequency combs [14].

5.1.3 Filter Bank Multicarrier

Filter Bank Multicarrier (FBMC) is different to the previous techniques. In FBMC, orthogonal subchannels are modulated and demodulated using SRRC or other Nyquist pulses and filters (see section 5.1.1.1) in the transmitter and the receiver [15]. As a consequence, and unlike OFDM, the associated spectrum is composed of overlapping subchannels that individually occupy a confined bandwidth.

FBMC has been mostly implemented in DSP based systems. The most efficient algorithms use the (I)FFT plus additional filtering to adapt the shape of the spectra [19]. These concepts have been employed in the design of electro-optical FBMC transceivers [20, 21]. Examples of spectra for this solution are also illustrated in Figure 5.1 for the case β=1. Note that FBMC implemented with SRRC shapes of β=0 is equivalent to Nyquist SCM. In FBMC, as subchannels are only overlapped by the neighbouring ones, the tolerance to dispersion is higher and the cyclic prefix can be avoided [20, 21]. To the best of the knowledge of the author, all-optical FBMC implementations have not yet been demonstrated.

Unlike Nyquist SCM and OFDM, FBMC is well-suited for a broadband spectrally-efficient all-analogue electrical implementation. Nyquist SCM requires very abrupt filters. In OFDM, the demodulation of a particular subchannel is influenced by all the others. FBMC presents a good trade-off as the required microwave filters are not as demanding as in Nyquist SCM, and the demodulation of a particular subchannel is only influenced by the adjacent ones. In the rest of the text, the term Orthogonal Subcarrier Multiplexing (OSCM) will be employed to designate broadband electro-optical transceivers consisting of orthogonally overlapping subchannels and based on analogue signal processing. A similar concept was first simulated in [22]. Section 5.2 will describe the advantages of an OSCM transceiver in comparison with a traditional DSP based OFDM scheme. Section 5.3 will detail the implementation of FBMC with microwave components as a method to design an OSCM transceiver. Section 5.4 will demonstrate an experimental broadband OSCM scheme by relying on the excellent stability and low phase noise of microwave oscillators, the frequency selectivity of microwave filters, and the good performance of inexpensive integrated microwave modulators. Finally, section 5.5 will present a novel method to synchronize subcarriers in the receiver, valid for SCM and OSCM, which employs a lower number of components than previous solutions.

5.2 Motivation

Research on all-analogue OSCM transceivers is motivated from two different perspectives. The main weakness of traditional all-analogue SCM [23] is the spectral efficiency. This weakness is overcome with OSCM, while removing the disadvantages of DSP. OSCM also allows higher values of subcarrier spacing, with relevant properties for optical links. These concepts are described in detail below.

5.2.1 Electrical Processing

Traditional DSP-based OFDM has become the most popular spectrally efficient multicarrier technique and, accordingly, it has been proposed for short reach optical networks, including in-building networks, access networks, mobile back-haul/front-haul and data centres [24]. Figure 5.5 illustrates an optical Network Interface Card (NIC) comparing two different implementations: DSP-based OFDM and OSCM. The interface between a computing system and the NIC is called Peripheral Component Interconnect Express (PCI express), which currently supports up to 16 digital lines with peak data rates of 8 Gbit/s per line [25].

OFDM, as shown in Figure 5.5, requires the computation of the (I)FFT. Those operations are complicated and integrated circuits need to parallelize the incoming data to reduce the rate per line from Gbit/s to Mbit/s in the transmitter [26]. Equivalently, the opposite multiplexing, from Mbit/s to Gbit/s, is required in the receiver. High-speed DACs and ADCs are necessary to achieve high transmission rates. Finally, a data driver and an amplifier are required in the transmitter and the receiver before or after the electro-optic and the opto-electronic converters (E/O and O/E). The use of narrowband subchannels is an advantage to compensate high values of accumulated fibre dispersion in long-haul optical communications systems [12], but the implementation of the (I)FFT in short reach systems might be justified only when spectral efficiency has to be maximized regardless of any penalty in resource demand and additional complexity [27]. Even for low modulation orders, there are three limitations in these implementations that cannot be avoided. Firstly, due to the multicarrier sinc spectra, a small amount of dispersion between any two subchannels impairs all subchannels. As a result, a cyclic prefix that reduces the net rate is required for the transmission in any dispersive channel. Secondly, the power consumption is high due to the demanding DSP [28] and increases due to the data interfaces and the ADCs and DACs [29]. Finally, a high number of subchannels

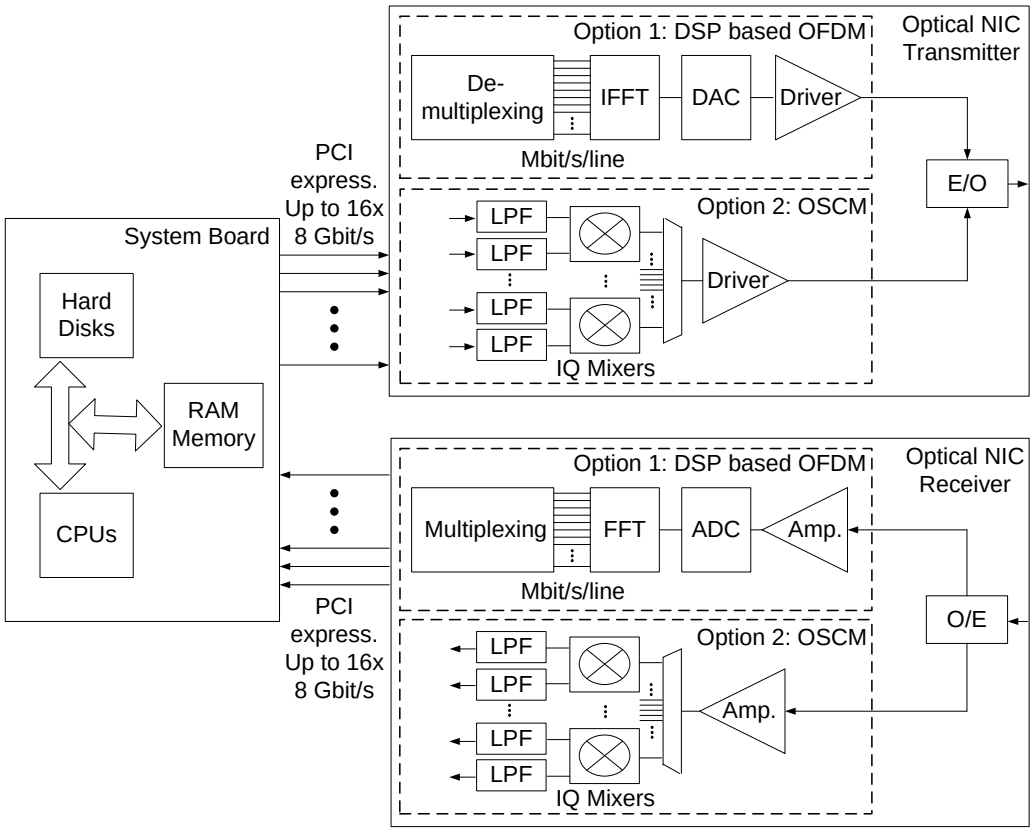

Figure 5.5 Optical NIC showing two different options for an orthogonal transmission: FFT-based OFDM and OSCM

translates into a very high peak to average power ratio, with the corresponding penalty in the dynamic range and the power consumption [30].

In contrast, OSCM can potentially enable a simpler orthogonal implementation with several advantages. Figure 5.5 shows the typical components of a broadband SCM system [23]. Baseband data can be directly processed with a LPF and then used to modulate an RF subcarrier. All the subchannels are combined and multiplexed in a single signal that is amplified and fed to an E/O module. The opposite processing takes place in the receiver. The following section shows the particular conditions that must be met to employ orthogonal subchannels with this analogue implementation, but several advantages can already be deduced. As the number of subchannels is lower, so is the PAPR. No DSP, ADC's, DAC's, or demanding algorithms are required, which emphasizes the low power consumption. As only analogue components are used, latency is reduced to a minimum. In OSCM, unlike OFDM, the dispersion suffered by one subcarrier only impairs the adjacent subchannels, so that the absence of a cyclic prefix maximizes the data rate while the penalty in performance is negligible for short transmission distances. Moreover, the baseband incoming signals have a data rate that is directly compatible with

broadband RF IQ mixers [31], avoiding data rate changes and interfaces. The system architecture used here is based largely on amplifiers and IQ mixers, allowing an integrated low cost, low power implementation with MMIC technology [32, 33].

In general, it can be concluded that, depending on their size and their targeted market, different subsystems inside optical networks can present totally dissimilar requirements of spectral efficiency, power consumption, and latency. A purely analogue OSCM system can potentially offer the best trade-off between those key parameters in certain real-time applications.

5.2.2 Subcarrier Spacing

Long haul coherent communications are limited by fibre nonlinearities [34]. Several independent studies have concluded that the optimum subcarrier spacing for coherent communications is in the range of 2-10 GHz [35-38], and, obviously, increased spectral efficiency would be obtained with orthogonal subchannels. The cost of implementing such subcarrier spacing with all-optical processing is prohibitive as it would require too many optical modulators. Similarly, achieving that subcarrier spacing with DSP is not optimum as the solution would be power hungry and costly, requiring very high-speed DACs and ADCs. In contrast, microwave components and MMIC technology can perfectly (de)modulate broadband subchannels at high frequencies with low cost. It can be concluded that all-analogue OSCM is a potential candidate to implement long-haul coherent systems. This work demonstrates direct detection OSCM and can be seen as a starting point towards coherent OSCM, in line with previous all-analogue coherent SCM implementations [39].

5.3 Microwave FBMC for Electro-Optical Transceivers

This section analyses the key concepts involved in the design of a broadband OSCM electro-optical transceiver based on FBMC theory.

5.3.1 Generic Electrical Scheme

5.3.1.1 Block Diagram

According to FBMC theory, orthogonal QAM transmission can be accomplished when the following three conditions are met [15, 40]. Firstly, every pair of baseband data streams, which will modulate a particular subcarrier, must

present a relative time delay equal to half a bit period. Secondly, the delayed and non-delayed baseband data streams that form a pair must act as the in-phase and the quadrature components alternatively in different subcarriers. Finally, the baseband digital data streams at the transmitter must be filtered in order that every bit has the shape of a SRRC pulse, and the baseband filter at the receiver must present the matched SRRC response. When these conditions are ensured, each received baseband signal will present a sampling point in the middle of the bit period that is free of Inter Symbol Interference (ISI) and Inter Channel interference (ICI). Implementing the described conditions, a back to back FBMC scheme consisting of three QPSK subchannels, where the bit period is T and the angular data frequency is ω_r, can be observed in Figure 5.6(a). The shape of the transmitted spectrum for the case of SRRC filters with β=1 is illustrated in Figure 5.6(b).

5.3.1.2 Component Delays

The delays that can be found in the transmitter in any real microwave implementation are also included in Figure 5.6(a). For the i^{th} frequency band, where i is an integer that can present three consecutive values (k-*1*, k, k+*1*) and whose subcarrier frequency is $i \cdot \omega_r$: the term dA_i accounts for any delay of the baseband pair prior to the IQ mixing, dB_i represents the delay after the mixing and before the overall combination of subchannels, and φ_i is the phase shift in the LO with respect to the ideal case. The LOs at the receiver in Figure 5.6(a) are locked to the incoming signal, as in any FDM transmission system. Without losing generality, the delays in the channel or in the receiver have not been included.

When all the delays (dA_i, dB_i, and φ_i) are zero, as in an ideal case or in a completely digital implementation, the received eye diagrams are free of ISI and ICI, as can be observed in the simulated results obtained with MATLAB and shown in Figure 5.6(c) for the case β=1. Since the central subchannel has more interfering neighbours than the others, the phase margin of its associated eye diagram is reduced, while still remaining perfectly open at the sampling instant. The number of subchannels could be extended to any practical number resulting in equivalent eye diagrams for the extreme and intermediate subchannels, presenting an optimum sample point free of ISI and ICI. In any practical implementation, different IQ mixers and/or PCB tracks can present different values of dA_i and dB_i. Despite these impairments, equivalent perfect system functionality with a sampling instant free of ISI and ICI can be achieved by adjusting only the phases of the LOs φ_i:

$$\varphi_{k-1} = \varphi_k + \frac{\pi}{T}(dA_{k-1} + dA_k + (2k-1)(dB_{k-1} - dB_k)).$$
$$\varphi_{k+1} = \varphi_k + \frac{\pi}{T}(-dA_{k+1} - dA_k + (2k+1)(dB_{k+1} - dB_k)). \quad (5.8)$$

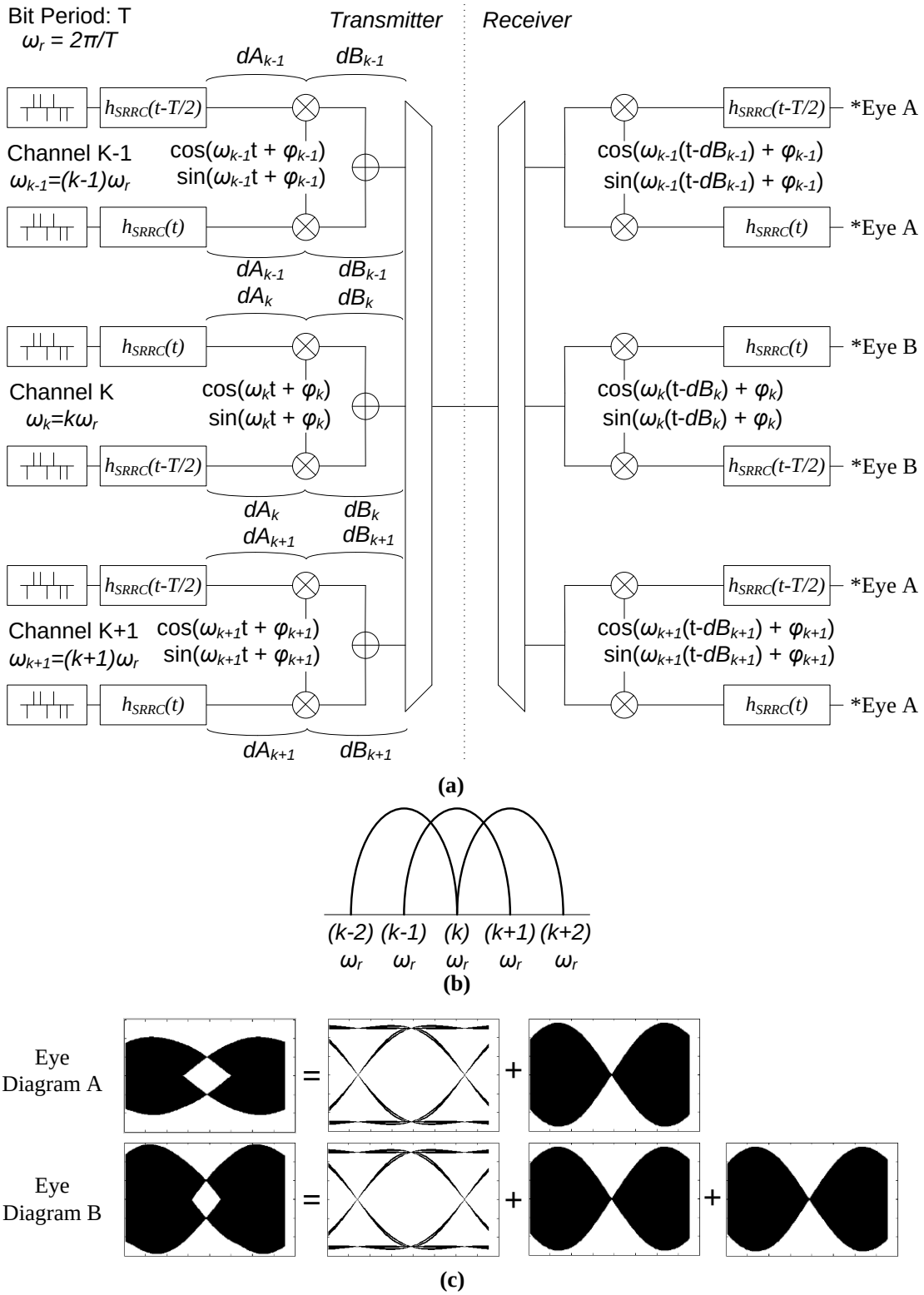

Figure 5.6 (a) FBMC scheme with 3 orthogonal QPSK subchannels and arbitrary delays in every RF band at the transmitter, (b-c) spectrum and received eye diagrams for β=1.

The mathematical derivation of eq. (5.8) is presented in the Appendix C.

5.3.1.3 Practical Implementation

It can be concluded that, in a real implementation, the phases in the transmitter can be aligned by simply inserting appropriate fixed delays in the baseband signals (T/2 shift inside each pair) and in the LOs. In the receiver, the LOs have to be locked to the phase of the incoming signal, as in any SCM link (see section 2.2). This can be accomplished with pilot tones plus PLLs [41]. As all the LOs are harmonically related, the synchronization can be simplified using a single pilot tone plus PLLs [42, 43] or, potentially, a single PLL plus an electrical comb.

In the bench experiments presented in section 5.4 to demonstrate OSCM, variable phase shifters were used in the LOs of the transmitter and the receiver to obtain maximum flexibility. In contrast, section 5.5 elaborates on the synchronization in SCM and OSCM links and proves a novel synchronization technique that requires a lower number of components than previous solutions.

5.3.2 Microwave Orthogonality Filters

This section investigates custom and standard microwave filters that can be employed to implement a microwave FBMC link. A generic schematic of an all-

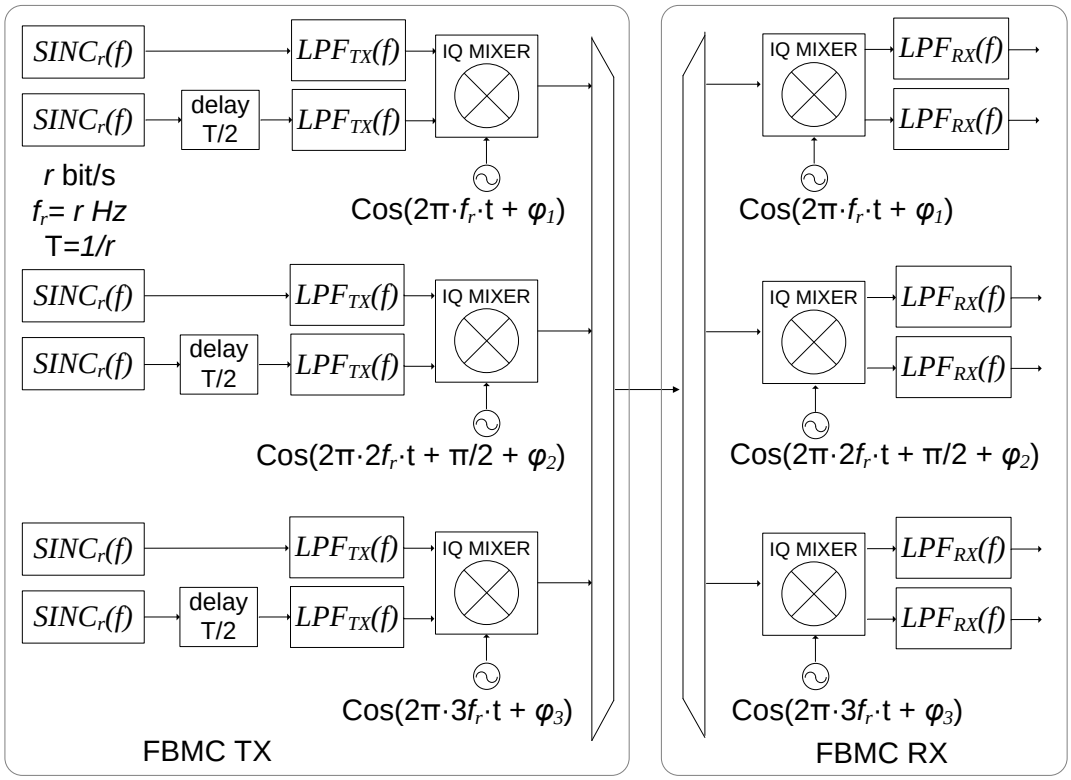

Figure 5.7 Back-to-back microwave FBMC scheme.

analogue FBMC system consisting of three QPSK orthogonal subchannels is illustrated in Figure 5.7. It includes all the conditions described in the previous subsection where the ideal multipliers have been substituted by mixers.

5.3.2.1 Ideal Conditions

Any practical data source produces approximately square shapes instead of impulses, and the generated square bit sequences with rate r Gbit/s (period T s) yield $SINC_r(f)$ baseband spectra over frequency, f. The LPF transfer functions are denoted by $LPF_{TX}(f)$ in the transmitter and $LPF_{RX}(f)$ in the receiver. For every baseband component, the transfer functions of the transmitter, receiver and overall transmitter plus receiver are $H_{TX}(f)$, $H_{RX}(f)$, and $H_{TRX}(f)$ respectively. Ignoring the $T/2$ constant delays, these are:

$$\begin{aligned} H_{TX}(f) &= SINC_r(f) \cdot LPF_{TX}(f). \\ H_{RX}(f) &= LPF_{RX}(f). \\ H_{TRX}(f) &= SINC_r(f) \cdot LPF_{TX}(f) \cdot LPF_{RX}(f). \end{aligned} \tag{5.9}$$

Assuming that the LPF filters have constant group delay, ISI and ICI will cancel at the middle of the bit period in the received baseband signals when the following conditions are met [40]:

$$\begin{aligned} ISI = 0 &\rightarrow |H_{TRX}(f)| \propto |RC_{r,\beta}(f)|, \\ ICI = 0 &\rightarrow |H_{TX}(f)| \propto |H_{RX}(f)|, \end{aligned} \tag{5.10}$$

where $RC_{r,\beta}(f)$ is the raised cosine spectra of rate r GHz with roll-off factor β. Any value of β ($0 \leq \beta \leq 1$) meets the conditions. As this work is dealing with high frequencies and microwave filters, it is important to remark that the ideal performance can only be obtained when the return losses of the filters are also ideal (S_{11}=0 and S_{22}=0). In practice, the transfer functions, the group delay and the return losses are not perfect, and translate into impairments. Three different sets of filters are proposed and analysed below.

5.3.2.2 Pseudo-Ideal Filters

Both conditions stated in eq. (5.10) are perfectly met when $H_{TX}(f)$ and $H_{RX}(f)$ are SRRC filters, with transfer functions represented by $SRRC_{r,\beta}(f)$ where r is the data

rate in GHz and β the roll-off factor. Accordingly, sinc compensated and standard SRRC filters are the LPFs required in the transmitter and the receiver respectively:

$$\begin{aligned} LPF_{TX}(f) &= \frac{SRRC_{r,\beta}(f)}{SINC_r(f)}. \\ LPF_{RX}(f) &= SRRC_{r,\beta}(f). \end{aligned} \tag{5.11}$$

Regardless of the value of β ($0 \leq \beta \leq 1$), perfect system functionality is obtained in FBMC. However, restrictions arise due to limitations in a microwave implementation. As shown in eq. (5.3), the frequency response of the associated SRRC filter extends from DC to $f_{BW}=0.5 \cdot r(1+\beta)$ GHz. If β was very low, the filter

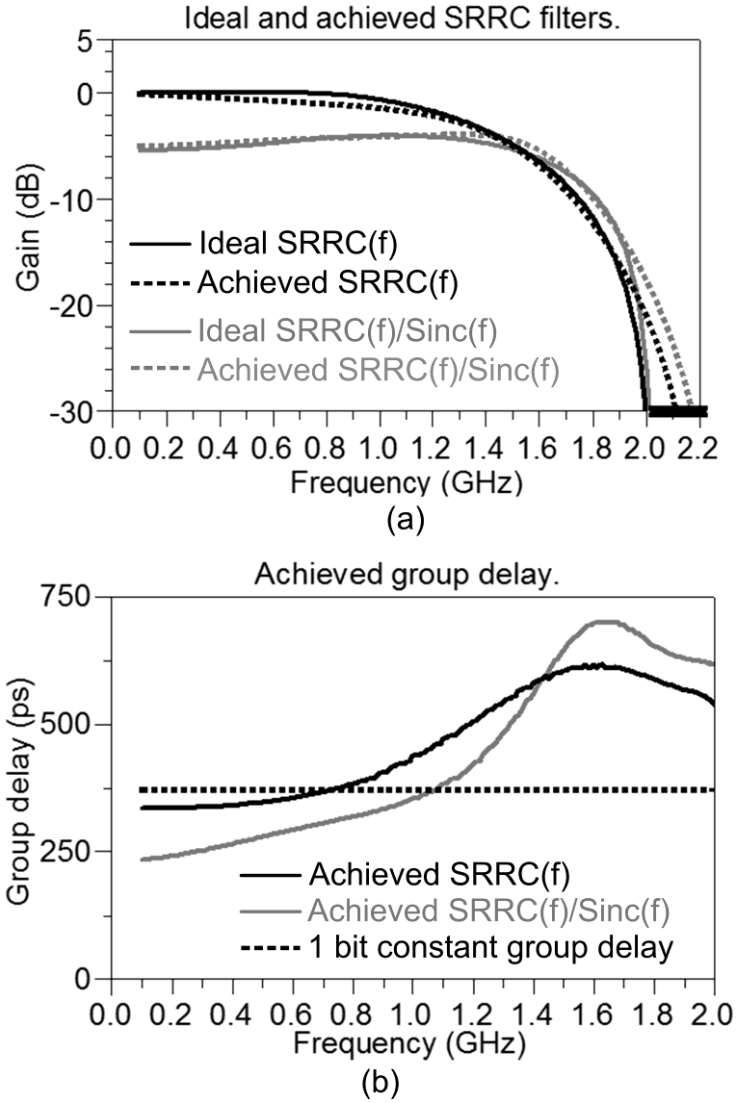

Figure 5.8 Ideal and achieved microwave SRRC filters for a rate of 2.7 Gbit/s where β=0.5 with and without sinc compensation: (a) amplitude response and (b) group delay compared with an ideal case where it is constant and equal to 1 bit interval.

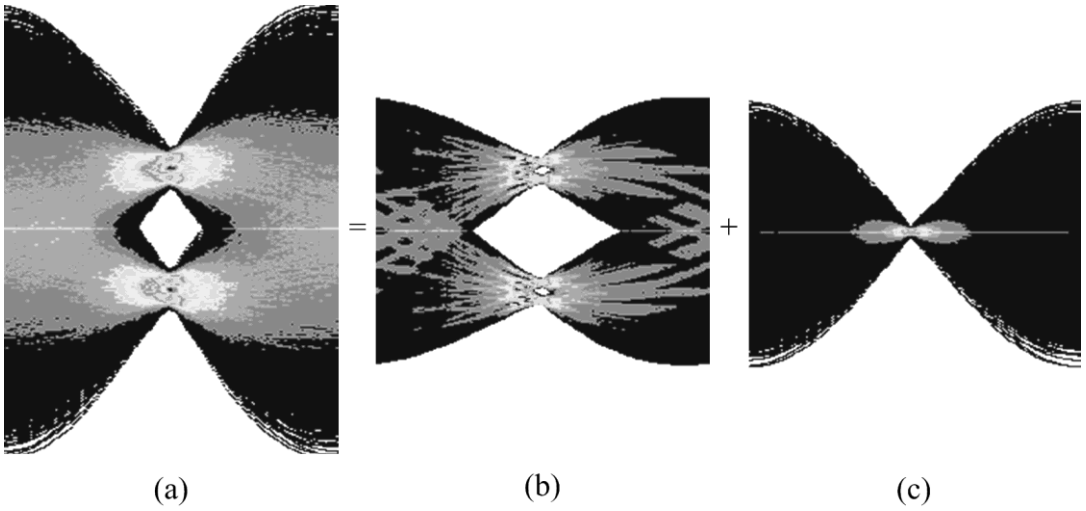

Figure 5.9 (a) Simulated received eye diagram with the achieved SRRC filters for intermediate subchannel and contributions from (b) desired signal and (c) ICI.

would be very abrupt, making it more difficult to compensate group delay [8]. If β was very high, the compensation of the sinc response at the transmitter would be more difficult because the sinc function evaluated at r GHz is equal to zero. For this work, microwave $SRRC_{2.7,0.5}(f)$ and $SRRC_{2.7,0.5}(f)/SINC_{2.7}(f)$ filters were designed for a rate of 2.7 Gbit/s. In practice, during the filter design process, a value of β=0.5 was found to be suitable, as it was conducive to physically realizable filters with almost perfect frequency response, while the impairments in the group delay did not compromise the achievable eye diagrams. The frequency response and the group delay of the developed filters is shown and compared with ideal implementations in Figure 5.8. Although the theory of controlled group delay filter design has been understood for several decades, the ability to manufacture these filters over the bandwidth required here (2.7 GHz) has only become possible more recently with high quality, low tolerance lumped components and skilful use of Computer Aided Design (CAD) environments. For this work, these designs were outsourced to a professional filter design company, BSC Filters Ltd.

The microwave FBMC system of Figure 5.7 was simulated with the software "Advance Design System (ADS)" including: the achieved $SRRC_{2.7,0.5}(f)/SINC_{2.7}(f)$ filters in the transmitter, the achieved $SRRC_{2.7,0.5}(f)$ filters in the receiver, ideal devices for the rest of the components (IQ mixers, power combiners and splitters), and binary signals employing square shapes and PRBS of 2^{15}-1 bits. The six PRBSs were decorrelated by adding different delays at the output of each data source. The received eye diagram obtained for one component allocated in the intermediate subchannel can be observed in Figure 5.9. The contributions coming from the desired

signal and the ICI are also illustrated. It can be concluded that a good ICI cancellation is obtained while the imperfections of the filters, mainly associated with the non-flat group delay, translate into ISI. The physical filters were also tested experimentally as described in section 5.4.1.

With β=0.5, these filters constrain the bandwidth of a 2.7 Gbaud baseband signal to ≈2 GHz, instead of the typical 2.7 GHz of the main lobe of a sinc function. Moreover, after modulating an RF carrier, the resultant bandwidth is ≈4 GHz instead of 5.4 GHz. Therefore, this solution employs custom filters, but it relaxes the specifications required from the microwave IQ mixers.

5.3.2.3 Bessel Filters

As the SRRC filters are difficult to design in the microwave domain, FBMC implementations with standard filters are interesting. Typically, microwave wired communications links make use of Bessel filters because of the maximally flat group delay [44]. The transfer function of a Bessel filter with a 3 dB cut-off frequency of f_c GHz and order n is denoted as $B_{fc,n}(f)$. A solution based on off-the-shelf Bessel filters was investigated. For a baseband rate, r, of 2.7 Gbit/s, the proposed solution consists of using a filter that passes the first lobe of the sinc in the transmitter and two cascaded Bessel filters of fourth order with f_c located at ≈75% of the data rate, $B_{2,4}(f)$, in the receiver:

$$\begin{aligned} \left|H_{TX}(f)\right| &= \left|SINC_{2.7}(f)\right|. \\ \left|H_{RX}(f)\right| &= \left|B_{2,4}(f)\cdot B_{2,4}(f)\right|. \\ \left|H_{TRX}(f)\right| &= \left|SINC_{2.7}(f)\cdot B_{2,4}(f)\cdot B_{2,4}(f)\right|. \end{aligned} \tag{5.12}$$

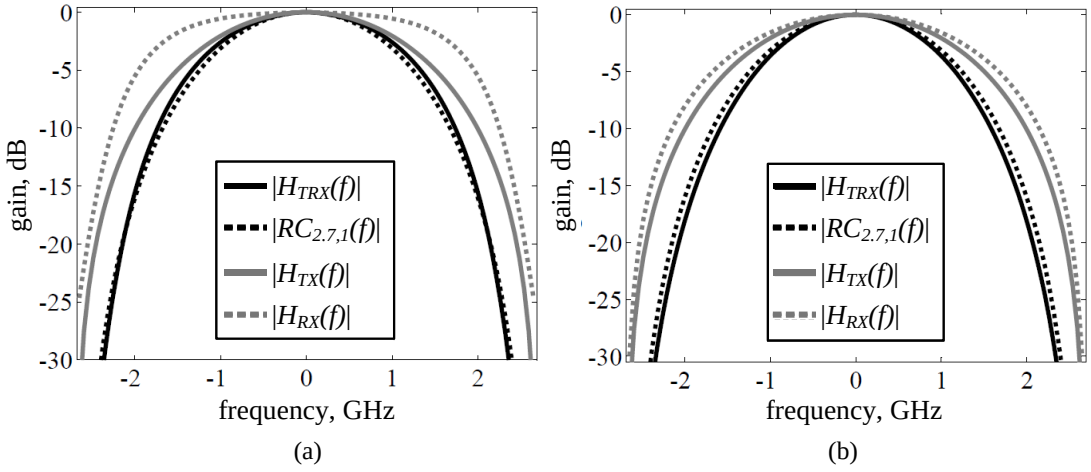

Figure 5.10 Normalized responses of transfer functions and comparison with the ideal for 2.7 Gbit/s and solutions based on (a) Bessel filters and (b) FIR filters.

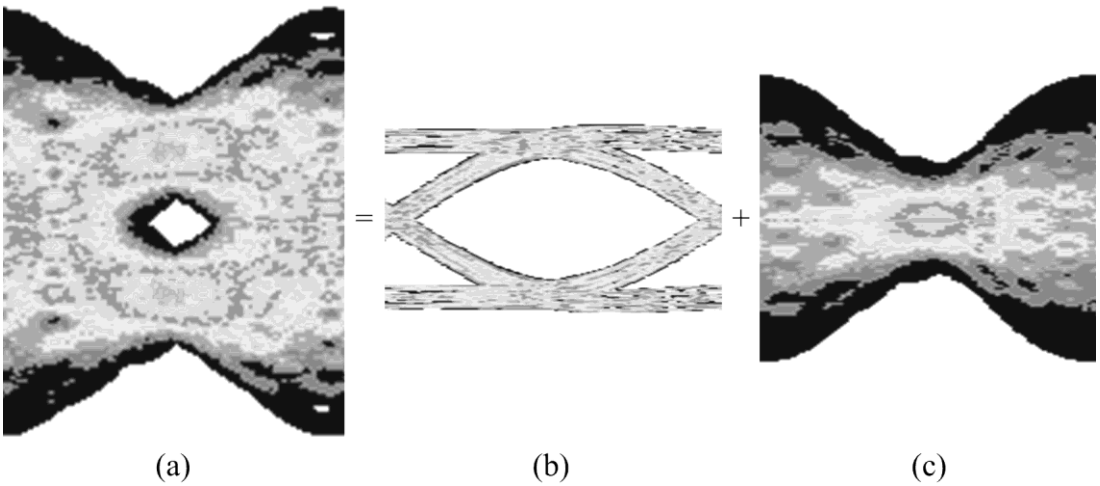

Figure 5.11(a) Simulated received eye diagrams with the available Bessel filters for intermediate subchannel and contributions from (b) desired signal and (c) ICI.

The previous transfer functions are illustrated in Figure 5.10(a), where they are also compared with the conditions stated in eq (5.10). The overall transfer function $H_{TRX}(f)$ is similar to a raised cosine spectrum $RC_{2.7,1}(f)$. In contrast, the baseband transfer functions in the transmitter and the receiver are different. It can be concluded that good ISI cancelation would be achieved while the main source of distortion would be generated by ICI.

The expected behaviour was confirmed with a simulation performed as described in the previous subsection. In the receiver, the model of a commercially available absorptive Bessel filter was employed. It matched the $B_{2,4}(f)$ response with an error smaller than 1 dB till 3 GHz and its group delay ripple was $\leq$ 20 ps till 2.3 GHz. In the transmitter, there are many filters that could be used as the proposed solution relies on passing the first lobe of the sinc. For consistency with the experimental results presented in section 5.4.1, the simulation made use of the filter Minicircuits model VLF-2500. This filter has the 3 dB cut-off frequency at 3.075 GHz and a group delay ripple of 100 ps till 2 GHz. The received eye diagram and the contributions from the desired signal and the ICI for one component of the middle subchannel are shown in Figure 5.11. As expected, a good cancellation of ISI is obtained and the main impairments are generated by ICI. It should be noted that the use of Bessel filters in the transmitter (namely $B_{4,4}(f)$) was also tested achieving similar performance. Although this solution can use standard commercially available filters, it occupies more bandwidth than the custom designs and performance is limited by ICI.

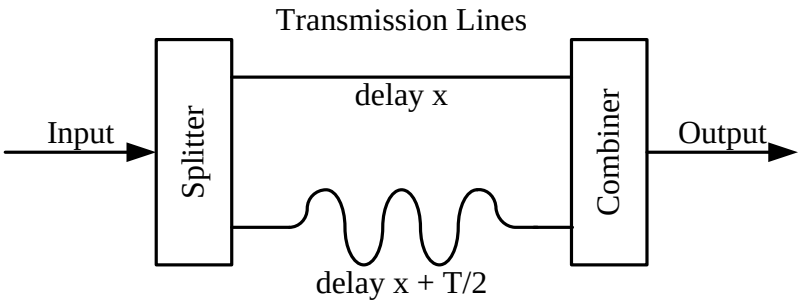

Figure 5.12 Simple microwave FIR filter.

5.3.2.4 Finite Impulse Response Filter

This solution uses a simple transmission-line based Finite Impulse Response (FIR) filter in the receiver. This FIR filter can be implemented using only a resistive splitter, two transmission lines that differ in length and a resistive combiner, as shown in Figure 5.12. The transfer function can be calculated as:

$$LPF_{RX}(f) \propto 1 + e^{-j\omega\frac{T}{2}} = e^{-j\omega\frac{T}{4}}\left(e^{j\omega\frac{T}{4}} + e^{-j\omega\frac{T}{4}}\right) = 2\cos\left(\omega\frac{T}{4}\right)e^{-j\omega\frac{T}{4}}. \quad (5.13)$$

Note that the filter presents constant group delay equal to T/4.

For the $LPF_{TX}(f)$, the same requirement as in the previous case, passing the first lobe of the sinc, is employed. Therefore, the baseband transfer functions for this solution for the rate of 2.7 Gbit/s are:

$$\begin{aligned} \left|H_{TX}(f)\right| &= \left|SINC_{2.7}(f)\right|. \\ \left|H_{RX}(f)\right| &= \left|\cos\left(2\pi f\frac{T}{4}\right)\right|. \\ \left|H_{TRX}(f)\right| &= \left|SINC_{2.7}(f)\cdot\cos\left(2\pi f\frac{T}{4}\right)\right|. \end{aligned} \quad (5.14)$$

The normalized transfer functions are illustrated in Figure 5.10(b), where they are also compared with the conditions stated in eq. (5.10). In this case, FBMC is potentially achieved with a good cancellation of both ISI and ICI. An important disadvantage is that the transfer function of the filter employed in the receiver is periodic in frequency, and an additional filter is required in practice to attenuate or ideally cancel all the frequencies higher than 2.7 GHz.

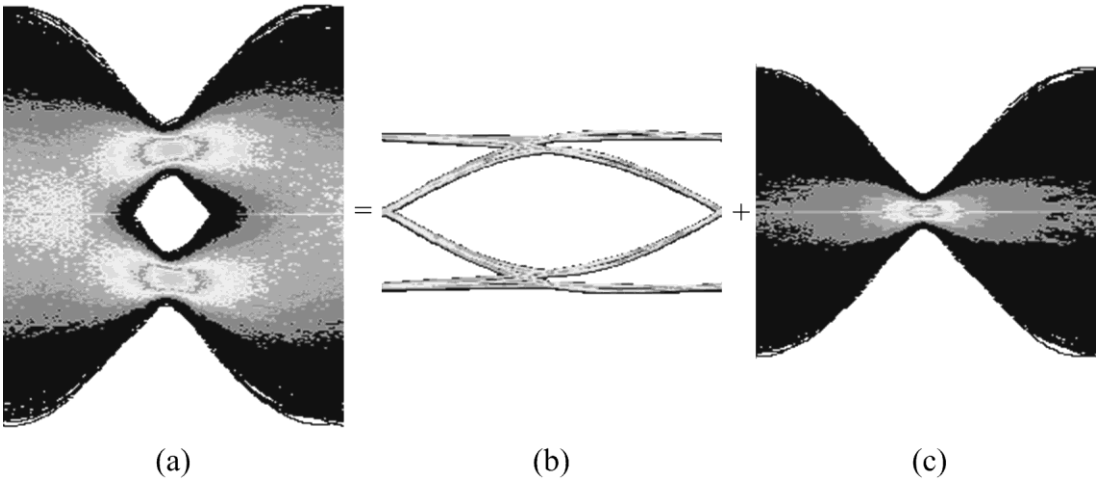

Figure 5.13 (a) Simulated received eye diagrams with the available Bessel filters for intermediate subchannel and contributions from (b) desired signal and (c) ICI.

A simulation was performed in the same conditions explained above. In this case the filter Minicircuits model VLF-2500 was again used in the transmitter, and also in the receiver cascaded with an ideal implementation of the proposed FIR filter. The filter VLF-2500 was employed for consistency with the experiments presented in section 5.4.1. The simulated results are illustrated in Figure 5.13 and agree with the theoretical prediction. This solution achieves good ISI and ICI cancellation but any passive implementation of the FIR filter will introduce a loss of at least 6 dB.

5.3.3 Optical Link

The configuration of the microwave FBMC transmitter and receiver has been explained. This section focuses on the implementation of the optical link discussing the general scheme, the achievable optical sensitivity in the receiver and the tolerance to dispersion.

5.3.3.1 Generic Electro-Optical Scheme

The electrical FBMC signal generated in the transmitter must be modulated onto an optical carrier. An OSSB modulation is preferred as it increases tolerance to

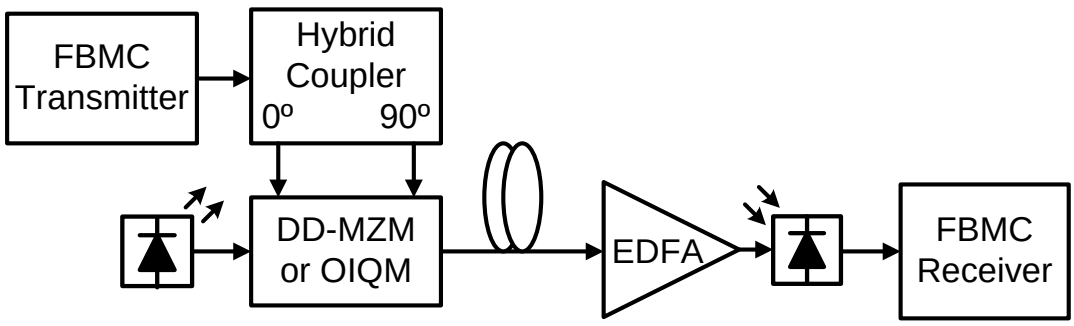

Figure 5.14 Generic OSCM/OSSB link with a pre-amplified optical receiver.

dispersion and allows a WDM implementation with closer optical channels. As explained in section 2.3.2, dual-drive Mach-Zehnder modulators (DD-MZM) and optical IQ modulators (OIQM) can achieve OSSB directly, without requiring additional optical filters. The block diagram of a generic direct detection OSCM/OSSB scheme with a pre-amplified optical receiver is illustrated in Figure 5.14. The optical modulator has two electrical inputs; one needs to be fed with the desired microwave signal, and the other with its Hilbert transform (HT) (the original signal with all the frequencies shifted 90 degrees). In the microwave domain, the HT is obtained with a microwave 90 degrees hybrid coupler.

5.3.3.2 Optical Sensitivity

A mathematical model to calculate sensitivities in SCM/OSSB links based on OIQMs was presented in Chapter 3. This model is not directly applicable to the case of OSCM/OSSB for several reasons. Firstly, due to the overlapping spectra in FBMC, an intermodulation product produces cross-talk with up to three subchannels instead of one. Second, the received eye diagrams in FBMC present a reduced margin with respect to the typical case. Finally, different beta factors could also have an impact on the system.

However, for the cases where optical noise is dominant over nonlinearities, the developed model provides an approximation of the theoretical limit for the potentially achievable optical sensitivities in OSCM/OSSB. Such a situation

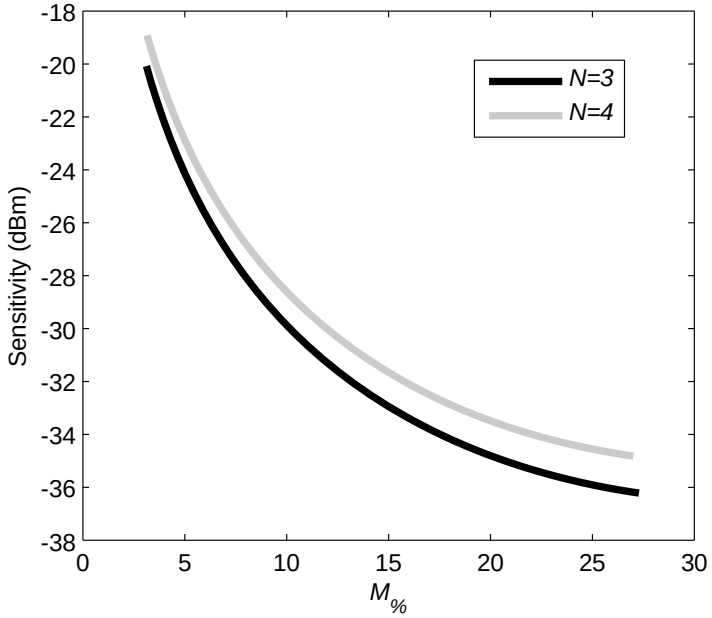

Figure 5.15 Calculated best achievable sensitivities for OSCM/OSSB links based on OIQMs biased at quadrature. Derived from eq. (3.14) with the following parameters: Q_F=2.36, B_e=2.7 GHz, F=5 dB, ν=193.4 THz, N_{CSO}=0, N_{CTB}=0.

typically occurs when an optical link uses an FEC code with a high BER threshold in the receiver, for example a hard decision FEC with a 7% overhead and a BER threshold of $3.8 \cdot 10^{-3}$ (Quality factor Q_F=2.67 from eq. (2.39)) [45]. For that case, sensitivities were calculated considering three and four orthogonal QPSK 2.7 Gbaud subchannels, as in the experiments that were performed. These sensitivities are provided in Figure 5.15 as a function of the total overall OMI with respect to V_π, $M_{\%}$ (defined in section 3.3.1).

5.3.3.3 Tolerance to Dispersion

When transmitting over fibre, dispersion can affect the orthogonality that is established in the transmitter. The distortion generated in the received signals, due to dispersive media in FBMC links, was theoretically analysed in [40], concluding that a value of β=0.5 translates into lower distortion than β=1. When SRRC shapes with β=0.5 are used, the distortion per km, γ, measured as a percentage of the absolute value of the desired received signal is [40]:

$$\gamma = 1.1 \cdot \frac{D}{T^2} \cdot 100 \quad (\% / km) \tag{5.15}$$

where D is the dispersion of the channel in (s/Hz)/km. The dispersion of SSMF is 17 (ps/nm)/km at 1550 nm, being $D \approx 1.3614 \cdot 10^{-22}$ (s/Hz)/km. Therefore, from eq. (5.15), and for the employed rate of 2.7 Gbaud, the distortion in a received FBMC signal transmitted through SSMF is $\gamma \approx 0.1$ %/km. It can be concluded that the effect of dispersion in short range OSCM links over SSMF is negligible. The experimental results described in section 5.4 present a good agreement with the theoretical prediction.

OSCM/OSSB is also suitable for longer transmission distances according to the following perspectives. Firstly, OSSB was originally developed as a method to overcome dispersive fading [46, 47]. With that technique, SCM/OSSB signals have been transmitted over hundreds of km with no penalty due to chromatic dispersion [48]. Secondly, several independent studies have concluded that the optimum subcarrier spacing for long transmission distance over SSMF is within the range of 2-10 Gbaud [35-38]. While that spacing is prohibitive for single-carrier dense WDM links, it is ideal for WDM/SCM or WDM/OSCM, as closer electrical subchannels can be allocated in the electrical domain with a lower cost and complexity. Finally,

according to eq. (5.15), the penalty generated by fibre dispersion is small in OSCM even for long transmission distances. For example, with a rate of 2.7 Gbaud, the distortion after 100 km of SSMF fibre would be ≈10 %. An analogy can be made with all-optical filtered OFDM or coherent WDM, where orthogonally overlapping subchannels are also multiplexed adjusting the phases at the transmitter [49], and dispersion penalties are small even for high speed rates transmitted over tens of km [50]. In section 5.5, an OSCM/OSSB link of 50 km will be demonstrated.

Finally, it should be noted that under the effect of dispersion, the optimum electrical subcarrier phase offset in the receiver LO is not the ideal 0º with respect to the incoming subcarrier phase [40]. Furthermore, in absence of dispersion there is a symmetric margin of ≈±7.5 degrees in the LO phase offset with associated peak power distortions below 3 dB. However, with dispersive media, the margin of phase error is not symmetric with respect to the optimum [40].

5.4 Proof of Concept

This section proves experimentally that the OSCM technique discussed on the previous section is feasible and can be successfully implemented with physical components. The demonstration is performed in two stages, only with microwave components and in a full electro-optical system.

5.4.1 Microwave Domain

5.4.1.1 Experimental Scheme

A microwave FBMC system, equivalent to the one illustrated in Figure 5.7, was physically implemented. In the experimental scheme there are two differences

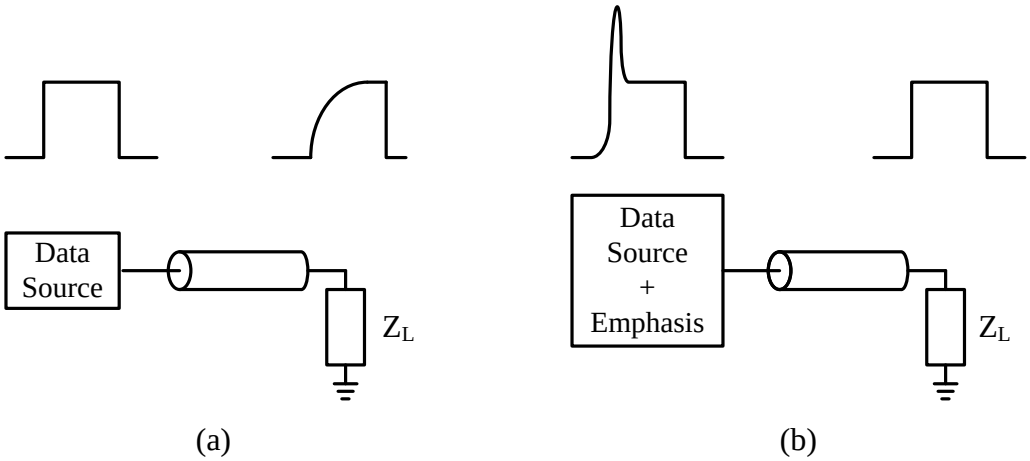

Figure 5.16 Square bit propagation (a) without emphasis and (b) with emphasis.

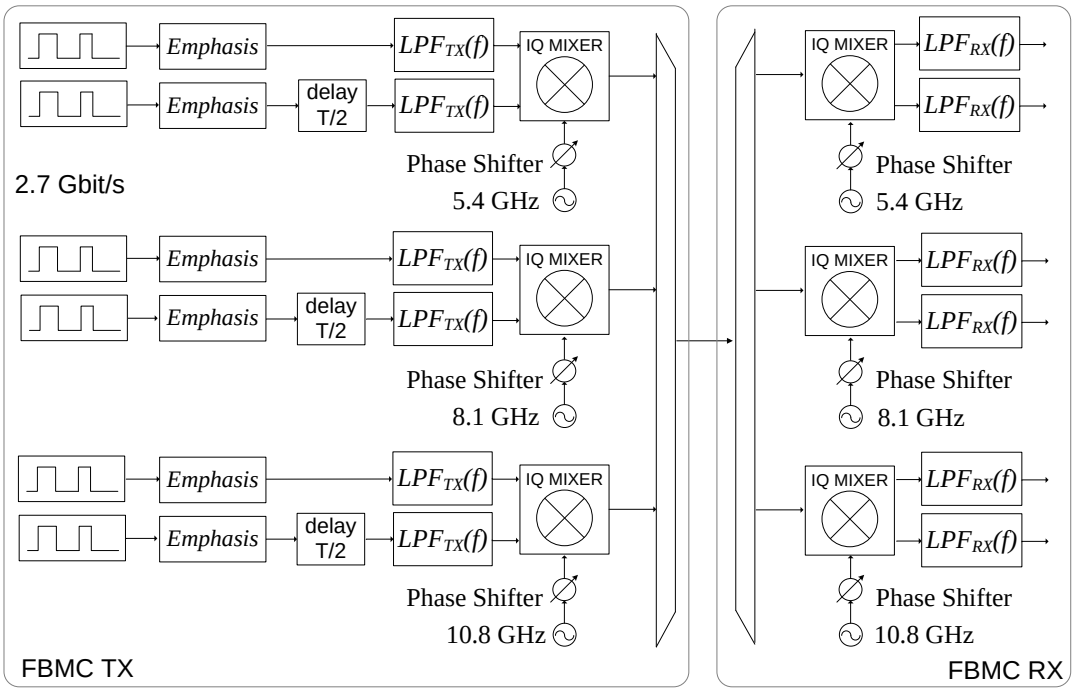

Figure 5.17 Back-to-back microwave FBMC implementation.

with respect to the figure. Firstly, in the theoretical analysis provided in section 5.3.2, the performance of the microwave orthogonality filters is based in the pulse shape of every bit. Thus, it is important to ensure that quasi-square signals arrive to the input of the orthogonality filters in the transmitter. Although the attenuation of high frequency components is common in any circuit, these effects can be compensated using pre-emphasis in the analogue source [51], as shown in Figure 5.16. Secondly, as has been explained in section 5.3.1, a particular phase alignment is required in the transmitter to achieve orthogonality, and a PLL is required in the receiver to achieve phase locking. For flexibility, phase shifters were employed in the transmitter and the receiver and the required phases were established manually.

The practical block diagram that incorporates the two previous concepts can be observed in Figure 5.17. It was implemented relying largely on the components described in section 2.5. Inexpensive off-the-shelf MMIC IQ mixers were used to generate and demodulate a signal composed of three orthogonal QPSK subchannels modulated at 2.7 Gbaud, making an overall data rate of 16.2 Gbit/s. A master reference of 2.7 GHz was fed to the input of an electrical comb generator that provided the orthogonal LOs. A multi-port microwave filter was used to demultiplex the desired tones, namely the second, third and fourth harmonics of the data rate (5.4, 8.1 and 10.8 GHz). In the FBMC transmitter, six bit streams were sourced from an FPGA with integrated analogue transceivers. The FPGA data clock was frequency

locked to the master reference. PRBSs of 2^{31}-1 bits, uncorrelated with different relative delays, were employed. In every pair of baseband signals, a T/2 relative phase shift was introduced using adjustable phase trimmers. Subsequently, both signals were pulse shaped with the low pass orthogonality filters, and, finally, connected to the baseband input ports of the IQ mixers. As explained above, the best performance was obtained when quasi-square signals arrived to the input of the orthogonality filters. This was achieved using the emphasis functionality that modern FPGAs incorporate in the analogue transceivers [52]. The broadband outputs of the IQ mixers were equalized in amplitude with attenuators and multiplexed with a passive combiner. The phases of the LOs that feed the IQ mixers in the transmitter were adjusted with variable phase shifters. In the back to back electrical FBMC configuration, subchannels were included progressively, and the phase shifters were adjusted ensuring a maximum eye opening in the receiver. After these phases had been adjusted, they remained constant and fixed for the whole set of the measurements. In the FBMC receiver, the incoming RF signal was passively split, before IQ mixers were used to perform the demodulation. The resultant output signals were fed to the matched orthogonality filters. The LOs of the IQ mixers were locked to the incoming phase of the desired subcarrier, using variable phase shifters that emulated the functionality of a PLL. In the received baseband signals, there was an optimum sampling point with minimum ISI and ICI. Final performance was measured in real time with a BERT.

5.4.1.2 Experimental Results

Using the same average power of ≈-5 dBm at the input of the FBMC receiver, the three filter solutions proposed in section 5.3.2 were tested.

The first solution employed a sinc compensated SRRC filter in the transmitter and a SRRC filter in the receiver, using β=0.5 in both cases. The received eye diagrams for the middle subchannel, showing the contributions of the desired signal and the ICI, are illustrated in Figure 5.18. As expected, a good ICI cancellation was obtained while the main impairments associated to the imperfect group delay translated into ISI.

The second solution employed the LPF Minicircuits model VLF2500 in the transmitter and two cascaded Bessel filters in the receiver. The obtained eye diagrams in the middle subchannel for this case are showed in Figure 5.19. As

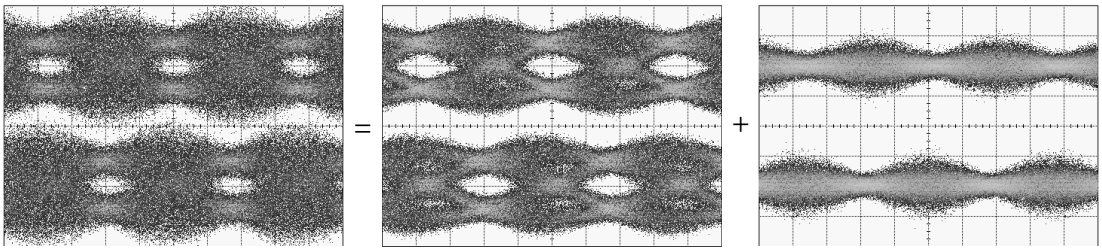

(a) (b) (c)

Figure 5.18 (a) Received eye diagram with the achieved SRRC filters for the middle subchannel and contributions from (b) desired signal and (c) ICI. In all the cases 60 mV per amplitude division and 100 ps per time division.

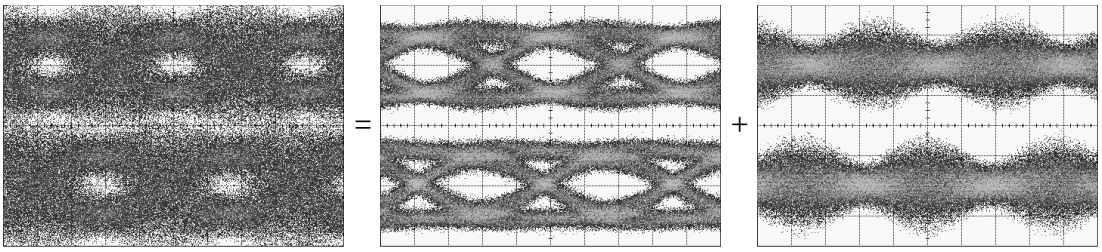

(a) (b) (c)

Figure 5.19 (a) Received eye diagram with the Bessel filters for the middle subchannel and contributions from (b) desired signal and (c) ICI. In all the cases 60 mV per amplitude division and 100 ps per time division.

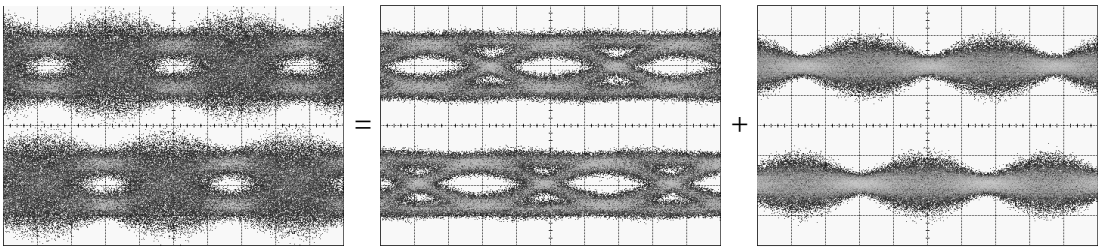

(a) (b) (c)

Figure 5.20 (a) Received eye diagram with the FIR filter for the middle subchannel and contributions from (b) desired signal and (c) ICI. In all the cases 30 mV per amplitude division and 100 ps per time division.

predicted, a good ISI cancelation was achieved but the performance of the solution was limited by ICI.

Finally, the third solution employed the LPF Minicircuits model VLF2500 in the transmitter, and also in the receiver cascaded with the FIR filter shown in Figure 5.12. The FIR filter was implemented with power splitters and with a phase shifter to establish the T/2 relative delay between the two paths. As predicted, the received eye diagrams, which are illustrated in Figure 5.20, presented good ISI and ICI cancellation, although the amplitude was lower than in the previous solutions due to the attenuation of the FIR filter.

Table 5-1 Average BER of in-phase and quadrature components.

Solution	*Subchannel 1*	*Subchannel 2*	*Subchannel 3*
SRRC	$2.45 \cdot 10^{-6}$	$5.85 \cdot 10^{-5}$	$2.05 \cdot 10^{-8}$
Bessel	$1.52 \cdot 10^{-5}$	$6.65 \cdot 10^{-4}$	$2.33 \cdot 10^{-7}$
FIR	$4.05 \cdot 10^{-4}$	$8.9 \cdot 10^{-5}$	$6 \cdot 10^{-7}$

The received eye diagrams are open in all the cases showing the feasibility of the solutions. Performance was measured in real-time with a BERT and the BER measurements are showed in Table 5-1 for all the subchannels averaging the BER of the I and the Q components. In all the solutions, the different performance between subchannels 1 and 3 was associated with the different loss and group delay characteristics of the IQ mixers. Subchannel 2 had two adjacent subchannels and, accordingly, was more impaired by ICI tending to present a worse BER than subchannels 1 and 3 (with the exception of solution 3, as explained below). Solution 1 achieved the best performance because the bandwidth of the RF signal was constrained (4 GHz instead of 5.4 GHz), reducing the impairments produced by the imperfect IQ mixers. The differences between solutions 2 and 3 were due to two different effects. First, solution 3 generated a lower ICI, which translated into lower BER for the second subchannel. Second, solution 3 introduced extra losses due to the FIR filter, which generated a higher BER for subchannels 3 and 1. For subchannel 1 this effect was more pronounced due to the higher conversion loss of the IQ mixers employed in the first RF band. These results suggest that all these solutions can be used in electro-optical systems, where the typical 7% hard-decision FEC codes set the operative threshold at a BER equal to $3.8 \cdot 10^{-3}$.

5.4.2 Electro-Optical Domain

5.4.2.1 Experimental Scheme

An OSCM system was demonstrated with the experiment illustrated in Figure 5.21. The microwave FBMC transmitter and receiver described in the previous subsection performed the electrical processing. The SRRC filters were used for this experiment, as it is obvious that they achieved the best results of the proposed solutions. The multichannel RF signal in the transmitter was amplified before a 90º hybrid coupler provided the HT that is required to achieve OSSB. Another RF amplifier was employed after the photo-receiver and before the electrical demodulation. PRBSs of 2^{15}-1 bits were transmitted.

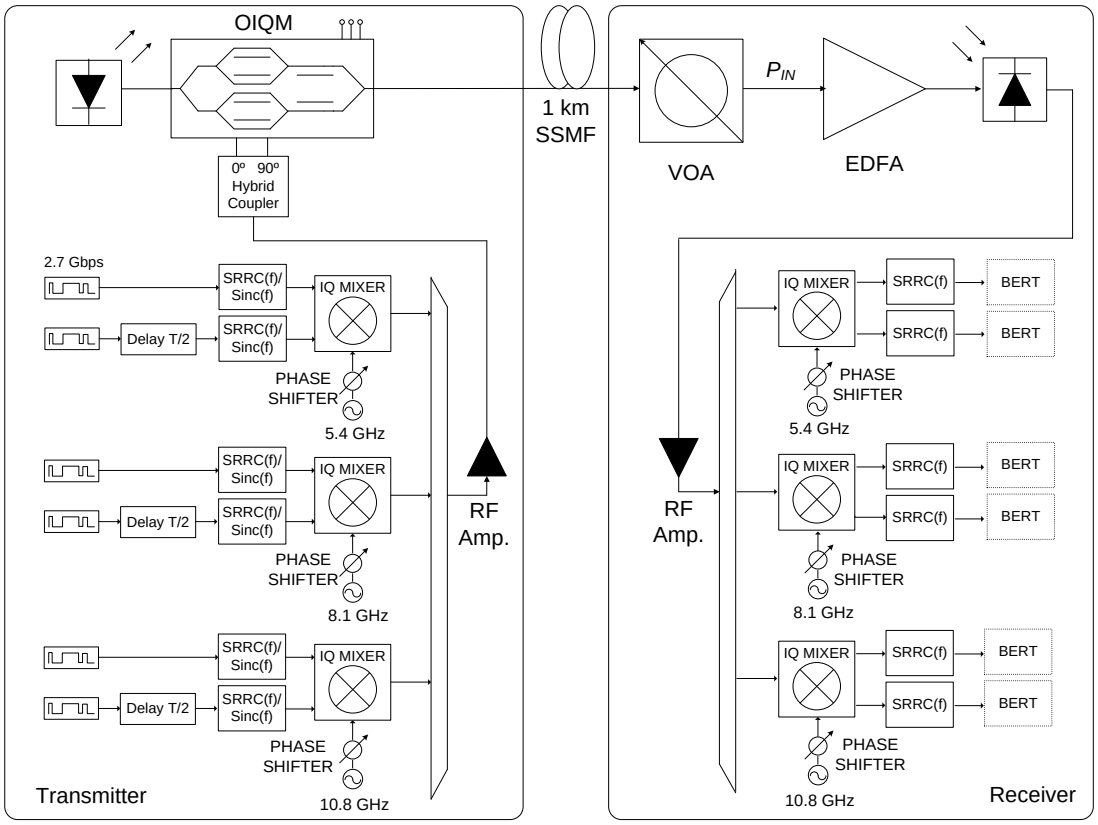

Figure 5.21 Direct Detection OSCM/OSSB link consisting of three orthogonal 2.7 Gbaud QPSK subchannels.

The optical link was established with an external cavity laser and a polymer based OIQM [53] with a half-wave voltage V_π=2.5V and a bandwidth of 20 GHz. The parallel MZMs inside the OIQM were biased at *quadrature*, and driven by the RF FBMC signal and its HT, achieving OSSB, with a total rms OMI, $M_{\%}$, of ≈20%, or ≈500 mV_{RMS}. From Figure 5.15, a sensitivity of -35 dBm for a BER of $3.8 \cdot 10^{-3}$ would be potentially achievable with ideal components. A higher OMI was avoided as the peak to peak voltage signal would be higher than the V_π value, and more undesirable nonlinear effects would occur in the modulator. The optical signal was transmitted over 1 km of SSMF. At its output, a variable optical attenuator was used to emulate more fibre losses. A pre-amplified receiver, consisting of an EDFA and a photo-receiver with a 20 GHz bandwidth, was used at the end of the optical link. The EDFA worked in constant power mode, ensuring 3.5 dBm at its output regardless of the average received optical power, P_{IN}. An optical BPF of 2 nm removed ASE at the output of the EDFA, but it is omitted in Figure 5.21 for simplicity. The optical signal was down-converted to its original microwave frequencies, using direct detection with a single photodiode.

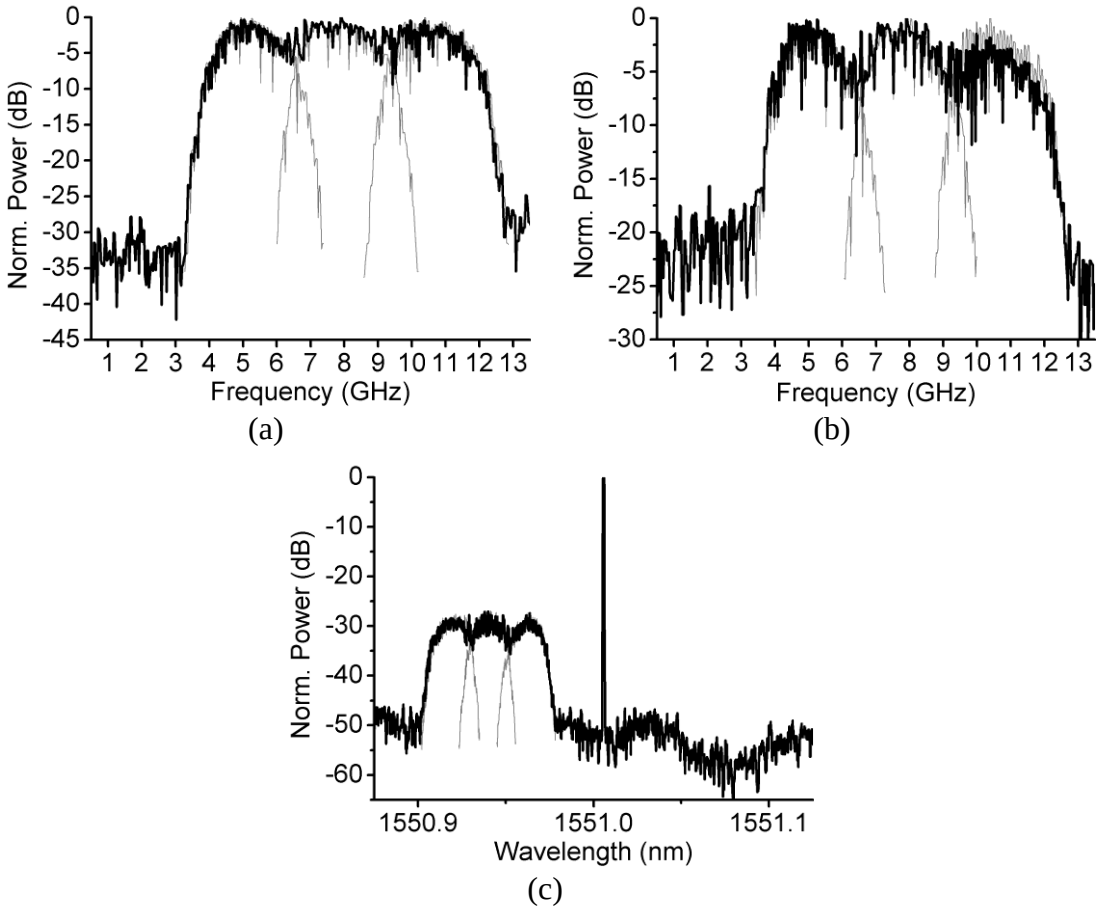

Figure 5.22 Optical and electrical spectra at: (a) the output of the RF FBMC transmitter, (b) the output of the photo-receiver and (c) the output of the optical modulator (resolution 180 MHz). In all the spectra, the black line shows the overall spectrum, while the grey lines show individual subchannels measured when they are transmitted alone.

5.4.2.2 Experimental Results

With the frequency plan consisting of three orthogonal QPSK subchannels, the overall data rate was 16.2 Gbit/s over a bandwidth of 12.8 GHz (1.265 bit/s/Hz) including the optical carrier or 9.4 GHz (1.72 bit/s/Hz) excluding the optical carrier. Note that the calculation of the spectral efficiency has taken into account that the SRRC filters reduce the bandwidth of the RF subchannels to 4 GHz. The transmitted electrical spectrum at the input of the hybrid coupler and the received electrical spectrum at the output of the photo-receiver are illustrated in Figure 5.22. The spectrum of the OSSB signal, which presents a sideband suppression ratio of 20 dB, is also shown in Figure 5.22. In all the cases, the contributions from individual subchannels can be observed.

BER as a function of P_{IN} was measured for the three subchannels, and it is illustrated averaging the I and the Q components in Figure 5.23. Measurements were

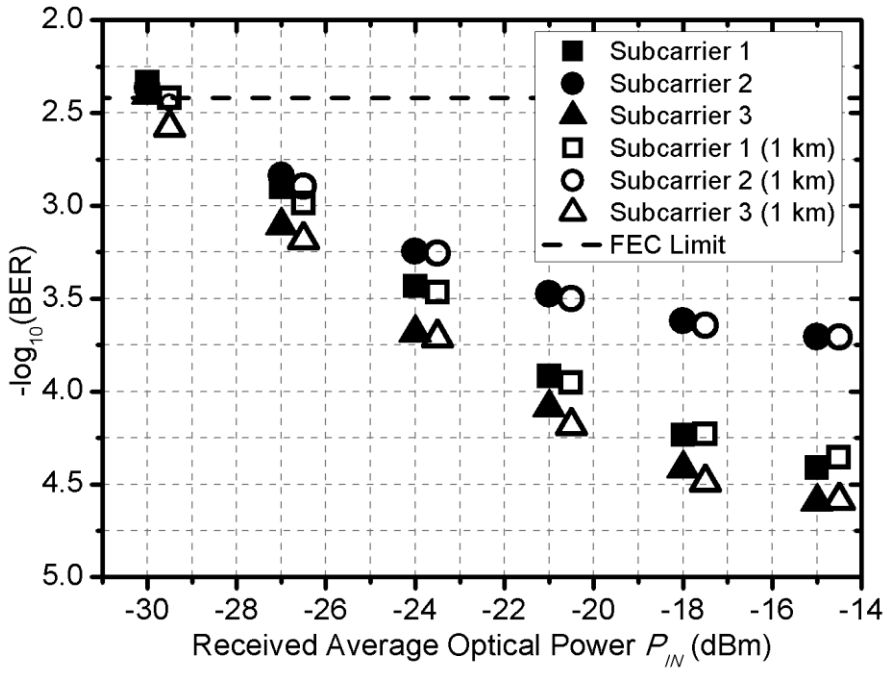

Figure 5.23 Average BER as a function of P_{IN} for the I and Q components transmitted in the first, second, and third subchannels for optical back to back and transmission over 1 km of SSMF. FEC limit for a 7 % overhead.

taken with an optical Back to Back (BTB) link, and transmitting over 1 km of SSMF. Considering a hard-decision FEC code with a 7% overhead, the threshold of acceptable BER is $3.8 \cdot 10^{-3}$. The results show a good agreement with the theoretical predictions. Firstly, the middle subchannel is more impaired than the ones in the extremes, as can be observed at P_{IN}=-14.5 dBm, when the optical noise is low. Secondly, the sensitivity is close to -30 dBm for all the subchannels. When P_{IN} is very low, the optical noise at the output of the EDFA is dominant and determines the Q_F of the system. This experimental result is 5 dB worse than the theoretical limit. Finally, the dispersion generated by the fibre does not have any influence on the performance. As predicted, OSCM achieves orthogonal transmission without requiring a cyclic prefix.

The presented results indicate that purely analogue broadband OSCM links are feasible. Neglecting the optical carrier, and assuming that all the multicarrier schemes can be implemented in an OSSB configuration, traditional all-analogue SCM/QPSK links achieve a spectral efficiency of 1 bit/s/Hz. In the same conditions, the spectral efficiency of OSCM/QPSK is at least 1.5 bit/s/Hz for a three subchannel configuration, and approaches to 2 bit/s/Hz when a higher number of subchannels is employed. Broadband SCM/16-QAM links have been reported, but DSP has been required to overcome the limitations of the microwave IQ mixers [54]. In that sense,

it is noteworthy that the results presented here have been achieved using off-the-shelf IQ mixers and long PRBS sequences of 2^{15}-1 bits. The spectral efficiency achieved with OSCM/QPSK can be close to the one obtained with SCM/16-QAM, with the advantage of employing a simpler front-end interface in the baseband receiver, a bi-level comparator.

5.5 Synchronization

5.5.1 Relevance

Synchronization in SCM systems consists of ensuring that the receiver LOs are phase and frequency locked to the incoming subcarriers, as explained in section 2.2. In practice, any realistic communication transceiver requires a sophisticated synchronization scheme based on PLLs [55].

In contrast, research SCM experiments often simplify the synchronization and employ a unique LO source that is split to generate the transmitter and receiver LOs, obtaining immediate frequency locking. The phase locking is then achieved employing phase shifters. This approach presents several drawbacks.

Firstly, as explained below, any realistic synchronization scheme implies the introduction of new elements that typically translate into additional impairments and a loss of sensitivity. In other words, by avoiding a realistic synchronization scheme, sensitivities that might not be achieved in practice are obtained.

Secondly, fibre is very sensitive to environmental fluctuations. Namely, temperature changes both the length of the fibre, with a coefficient of thermal expansion equal to $4 \cdot 10^{-7}$/ºC, and also the refractive index, with a coefficient of $1.2 \cdot 10^{-5}$/ºC [56, 57]. Considering both values, a subcarrier transmitted over fibre suffers a phase shift with temperature that is equal to 15^{o} $^{o}C^{-1}$ GHz^{-1} km^{-1} [58]. As an example, if a QPSK subchannel is transmitted at 10.8 GHz over 10 kms of fibre, a change in fibre temperature of only $\Delta T=0.027$ ºC translates into a phase shift of 45º, closing completely the received eye diagrams. This effect, which is more pronounced over longer distances and at higher subcarrier frequencies, can be easily observed in SCM transmission experiments where phase locking is performed manually. It is manifested as a continuous and random closing and opening of the received eye diagrams. In practice, for the BER measurements that are performed in real-time broadband SCM experiments over long distances, it can be concluded that any

manual phase locking only ensures an accurate measurement for a small fraction of time. As a result, the quality of the measurements obtained without realistic synchronization can be disputed.

This section reviews typical synchronization schemes that have been used in SCM systems, and proposes and demonstrates a new method that requires a lower number of components and can be employed in both SCM and OSCM schemes.

5.5.2 Review of Typical Methods

5.5.2.1 Carrier Recovery

An interesting method consists of generating the subcarrier directly from the received subchannel. This is potentially achievable with a particular PLL called a Costas loop [59], or elevating the subchannel to the power of *N* [60]. If a BPSK subchannel is squared, the subcarrier is obtained at two times the original frequency. Similarly, if a QPSK subchannel is elevated to the fourth, the subcarrier is obtained at four times the original frequency. In both cases, the modulation is removed and a PLL with a division factor (2 for BPSK and 4 for QPSK) is used to recover the nominal frequency required by the receiver mixer.

This method was employed in an SCM link in [61] and is conceptually illustrated in Figure 5.24. The main advantage of this procedure is that no power is wasted in the transmission of pilot tones. It also presents several disadvantages. Firstly, it requires that high frequencies are generated and, secondly, one nonlinear block plus one PLL are necessary per each subchannel.

5.5.2.2 Pilot Tones

Another option relies on transmitting pilot tones that are locked to the subchannels. These pilot tones follow the phase fluctuations that the signal

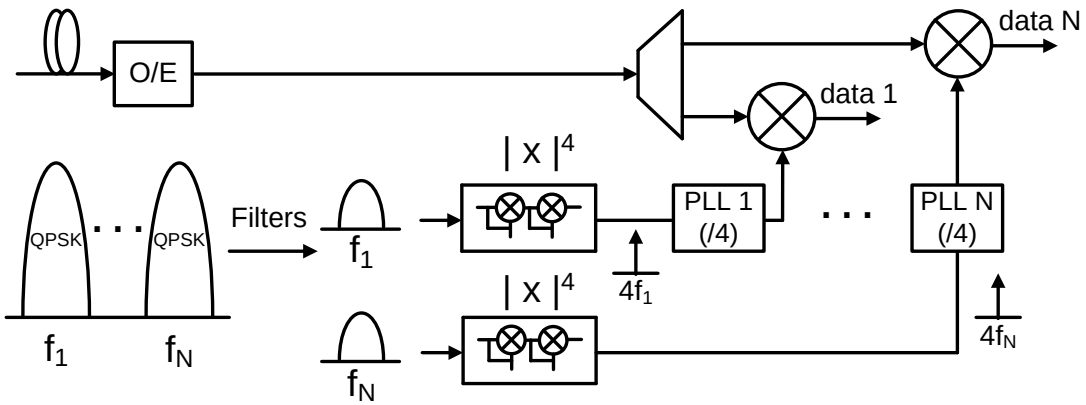

Figure 5.24 Carrier recovery of QPSK subchannels elevating to the 4th in the receiver.

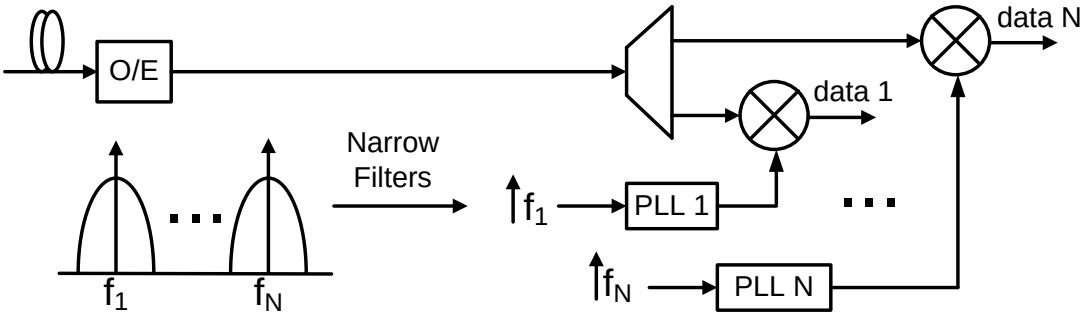

Figure 5.25 SCM receiver using a pilot tone per subchannel to synchronize.

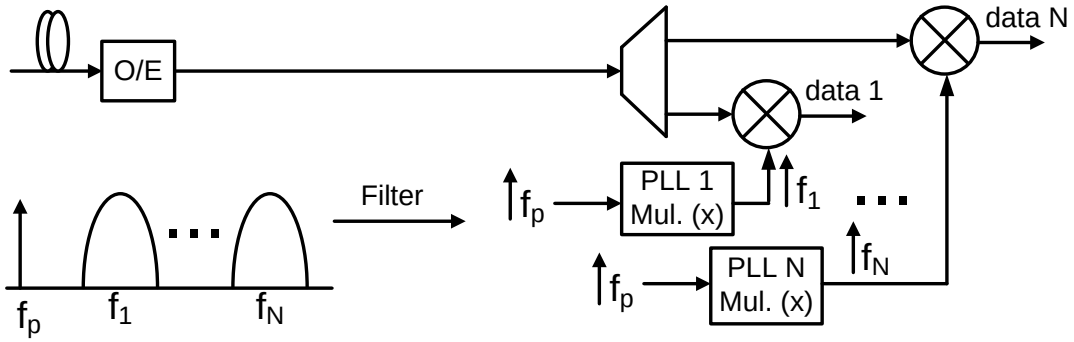

Figure 5.26 SCM receiver using one pilot tone to synchronize all the subchannels.

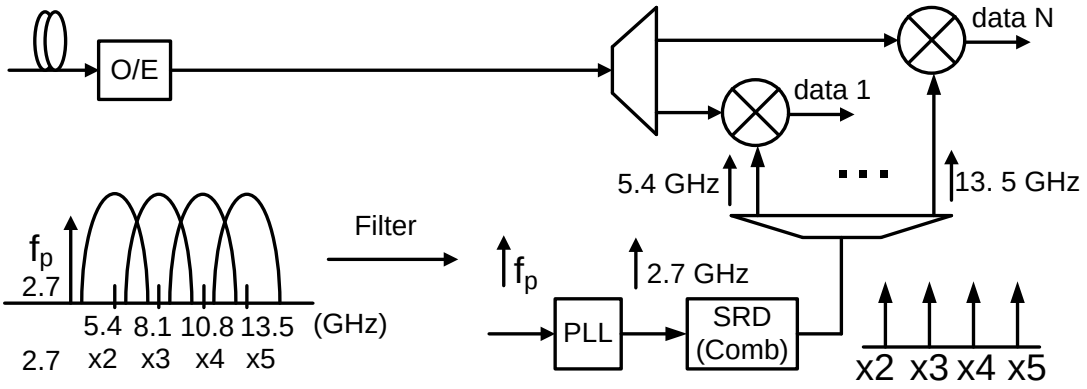

Figure 5.27 SCM receiver using one SRD to synchronize all the subchannels.

experiences during the transmission over fibre. PLLs are used in the receiver to obtain the locked subcarriers from the pilot tones. There are two possibilities to implement this method.

The first alternative is to transmit one pilot tone with every subchannel, as was proposed in [41] and is conceptually illustrated in Figure 5.25. This method is simpler than the previous solution as no higher frequencies are generated. However, it also presents several disadvantages. Namely, there is a power penalty due to the transmission of the pilots, and one pilot tone and one PLL per subchannel are necessary.

The second alternative only transmits one low frequency pilot tone that is used to generate all the locked subcarriers in the receiver. This method was employed in [42] and is illustrated in Figure 5.26. As the dependency of chromatic dispersion with temperature is very small [62], the phase variations due to temperature are practically the same for the pilot tone and the subchannels, which ensures the stability of this technique [42]. Although this approach presents a simpler configuration, one PLL per subchannel is still required. Apart from that, the phase noise of the receiver LOs is proportional to the multiplication factors of the PLLs, which are high when the pilot tone is located at a low frequency [42].

5.5.3 Novel Technique

5.5.3.1 Concept

The proposed method is illustrated in Figure 5.27 for the case of four overlapping subchannels and a symbol rate of 2.7 Gbaud. The use of SRRC shapes reduces the bandwidth of the subchannels so that it is possible to allocate the pilot tone at the data rate frequency, 2.7 GHz. This method exploits the fact that the subcarriers frequencies are harmonics of the data rate. The pilot tone is filtered and locked to the receiver reference with a PLL. Then, all the subcarriers are generated employing an electrical comb based on a Step Recovery Diode (SRD). These LOs are then fed to the corresponding mixers.

Despite the small power penalty due to the transmission of one pilot tone, the method presents several advantages. Firstly, the number of components is lower than in any of the previous techniques. Secondly, only one pilot tone and one PLL are required regardless of the number of subchannels. Finally, the pilot tone is allocated at a high frequency so that the maximum multiplication factor is small, only five in this case, ensuring low phase noise in the generated LOs.

5.5.3.2 Experimental Setup

This technique was demonstrated in an OSCM/OSSB link equivalent to the one illustrated in Figure 5.28. Four 2.7 Gbaud QPSK overlapping subchannels were transmitted employing the SRRC filters with β=0.5. As a result, the electrical data signal had an overall data rate of 21.6 Gbit/s and a spectral efficiency of 1.78 bit/s/Hz. The optical link presented in the schematic has been described in section 5.4.2.1, but it employed 50 km of SSMF for this experiment. Similarly, the

implementation of the microwave FBMC transmitter and receiver was equivalent to the one described in section 5.4.1.1, but including four subchannels instead of three.

The proposed synchronization scheme can also be observed in Figure 5.28. A 2.7 GHz reference was employed in the transmitter to generate the LOs. That reference was also multiplexed with the transmitted signal as a pilot tone. In the receiver, the pilot tone was filtered and fed to a PLL that locked a 2.7 GHz reference. Finally, this reference was employed by an SRD to generate the receiver LOs. A PLL with a 2.7 GHz reference input can be implemented with discrete components [41], but in this case an off-the-shelf MMIC PLL with an integrated oscillator was

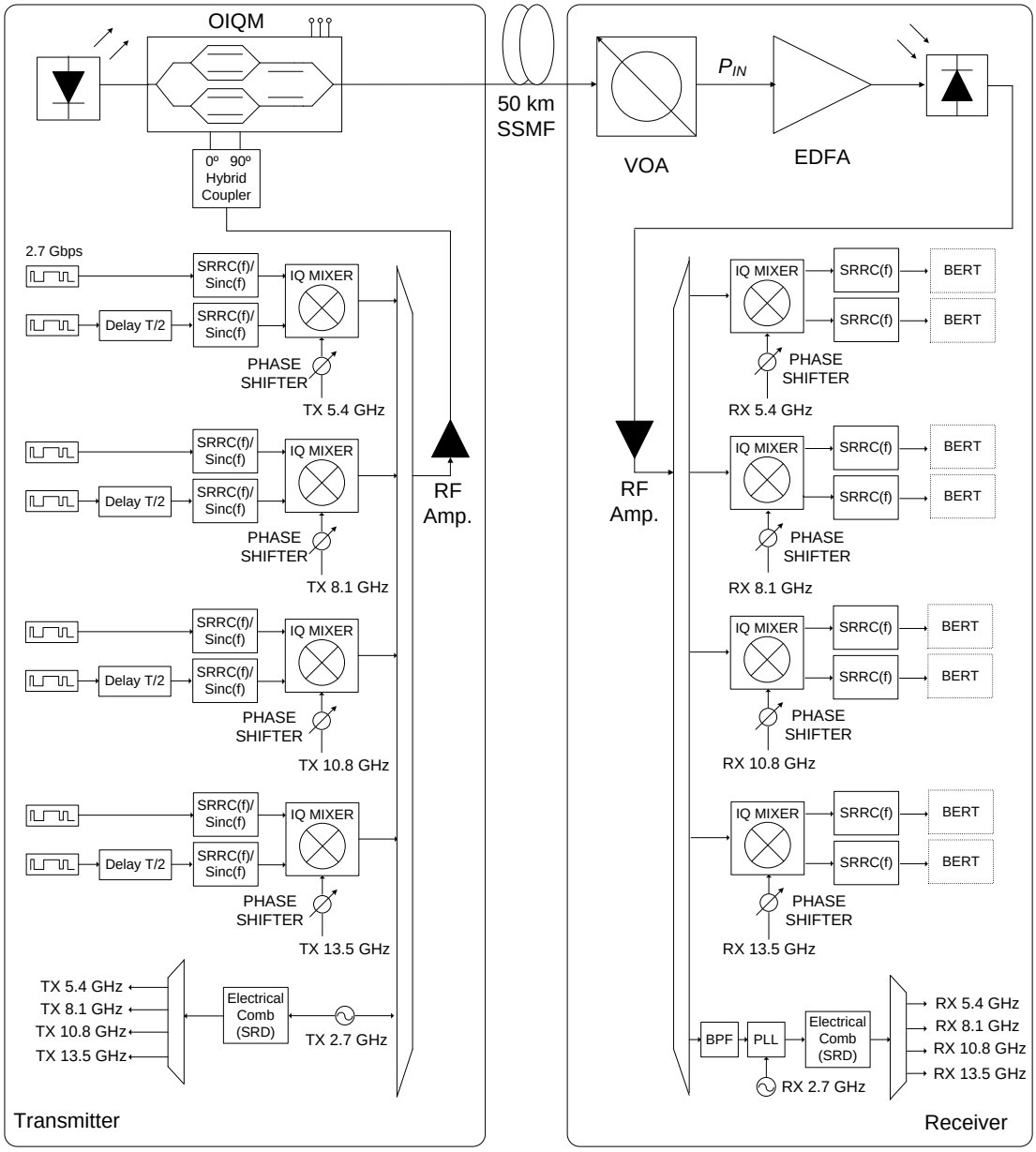

Figure 5.28 Direct detection OSCM/OSSB link with four orthogonal 2.7 Gbaud subchannels. Synchronization achieved with only one PLL for all the subcarriers.

employed, namely the device Hittite model HMC840LP6CE. These commercially available devices typically require low frequencies in the reference input. For that reason the recovered 2.7 GHz pilot tone was passed through two frequency dividers, namely the Hittite models HMC363 (/8) and HMC361 (/2), obtaining an overall division ratio of 16 and a tone at 168.75 MHz that was appropriate for the PLL input. The output of the PLL was the nominal 2.7 GHz.

5.5.3.3 Results

The transmitted and received electrical spectra can be observed in Figure 5.29(a-b). With the SRRC shapes, the bandwidth of the first subchannel is reduced to the range between 3.4 GHz and 7.4 GHz so that there is wide margin of 700 MHz to filter and recover the pilot tone in the receiver. The optical spectrum at the output of the optical modulator is illustrated in Figure 5.29(c). An OSCM/OSSB signal with a sideband suppression ratio of 20 dB can be observed. For all these figures, the overall OMI was $M_{\%}\approx 11\%$. It should be noted that due to the synchronization scheme more reliable BER measurements over longer time scales could be obtained.

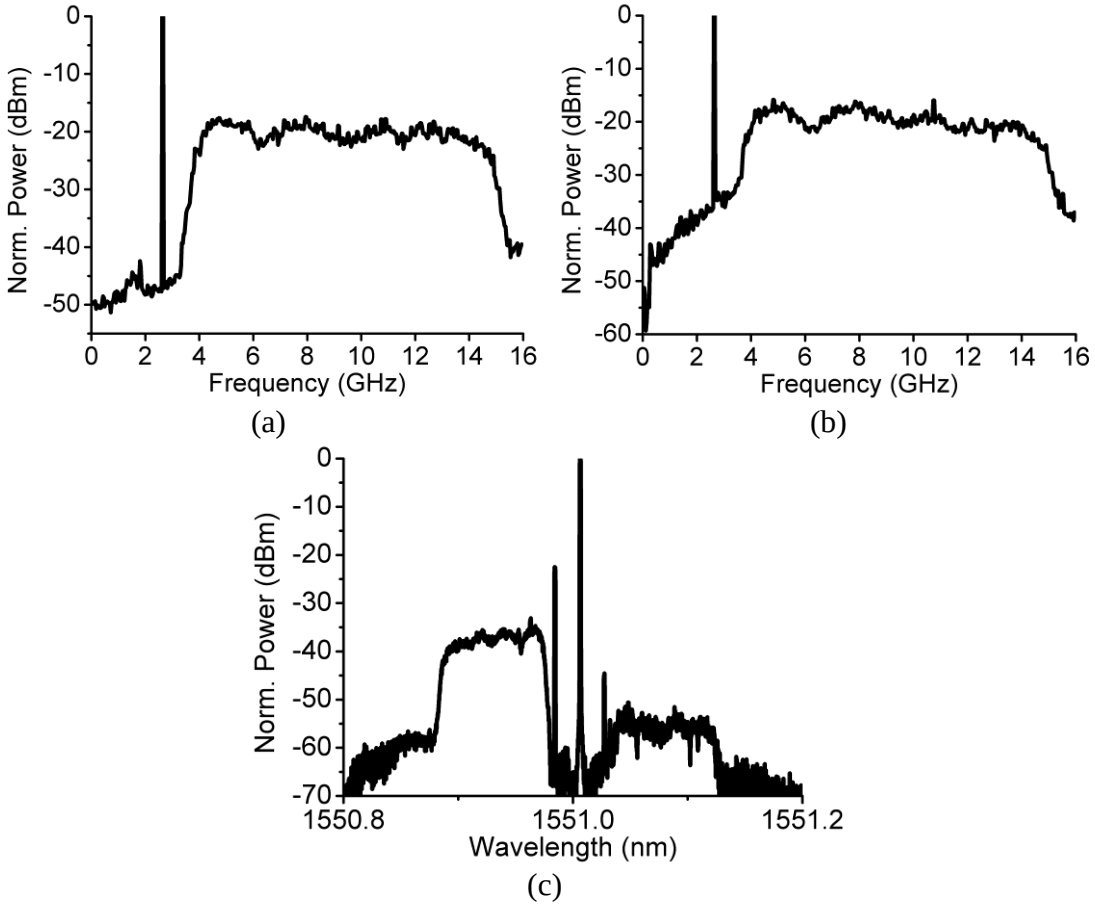

Figure 5.29 Electrical and optical spectra at (a) the output of the RF transmitter, (b) the input of the RF receiver, and (c) the output of the optical modulator for a synchronized OSCM/OSSB scheme with overall OMI of 11%.

With the described setup, there are several trade-offs in the selection of the OMI. To begin with, the trade-off between the CSPR and NLD that was thoroughly analysed in Chapter 3 is present. Additionally, the inclusion of the pilot tone and the synchronization scheme also has an influence [42]. A high CNR in the received pilot tone is desired to diminish the phase noise at the output of the PLL. In other words, the level of the received pilot tone must be much higher than the noise sources (ASE, RIN, shot noise, thermal). However, a high level of the pilot tone in the transmitter translates into a higher OMI and higher nonlinearities, which are enhanced during the fibre transmission [63, 64], and from a certain level the carrier to noise ratio of the pilot tone decreases.

The experiments were conducted in the following way. The OIQM was biased at *quadrature* and the power of the electrical signal at the input was varied in steps of 3 dB (from a CSPR of ≈24 dB to ≈12 dB). The power of the pilot tone was 10 dB below the power of the rest of the electrical signal. Figure 5.30 illustrates the BER measurements for the different values of OMI. Considering all the subchannels,

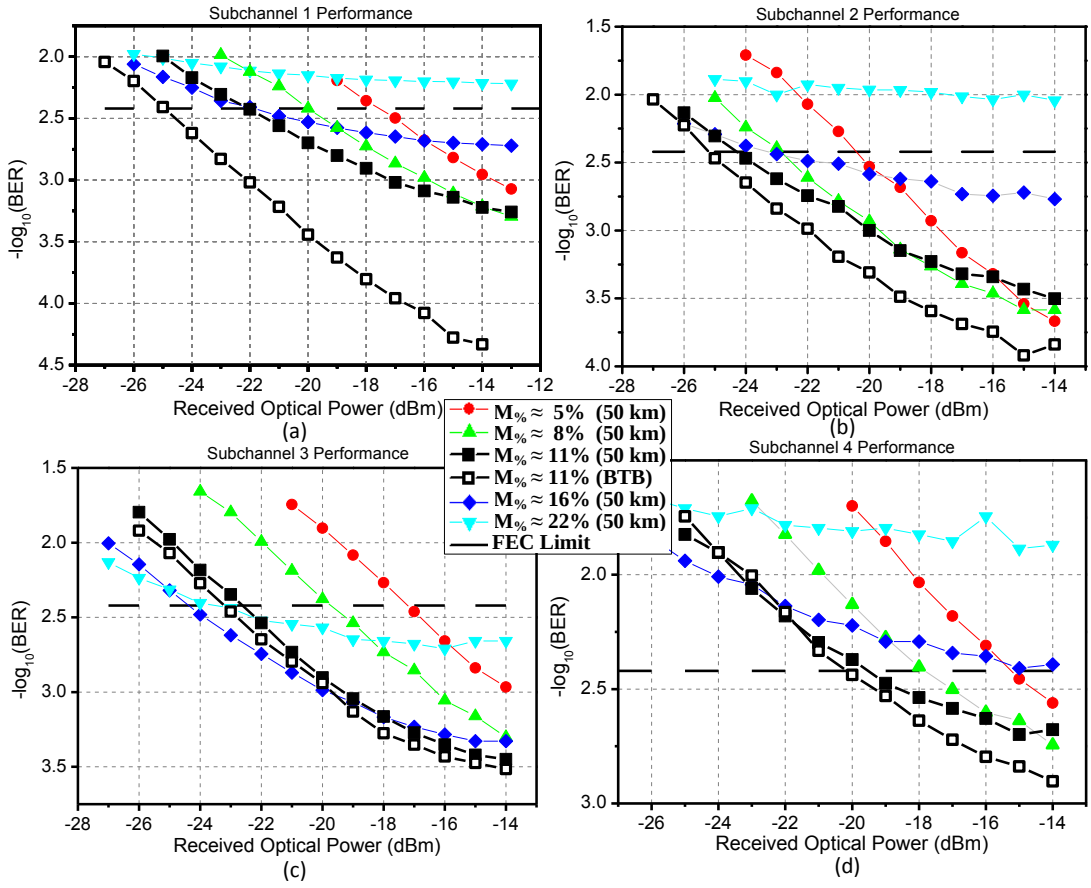

Figure 5.30 Performance versus average optical input power as a function of OMI for subchannels: (a) 1, (b) 2, (c) 3 and (d) 4.

the best OMI was $M_{\%}\approx 11\%$. Sensitivities were in the range of -20 to -24 dBm due to the different behaviour of the RF components in the RF bands. The values of sensitivity are much higher than the theoretical ideal limit of -29 dBm (obtained from Figure 5.15) due to the imperfect components and the additional nonlinearities produced by the pilot tone and the fibre transmission.

For the case of best OMI, Figure 5.30 also compares the measurements of the 50 km transmission case with the back to back configuration. From eq. (5.15), a distortion of 5% after 50 km transmission is expected. Accordingly, a small impact on the BER can be anticipated. However, the fibre transmission increases the CSO [63, 64], which is zero at *quadrature* for low transmission distances (see Chapter 3), and affects the subchannels with a higher $N_{CSO.}$ With the presented frequency plan, and including the pilot tone, N_{CSO}=3 for subchannel 1, N_{CSO}=2 for subchannel 2, N_{CSO}=1 for subchannel 3, and N_{CSO}=0 for subchannel 4. This effect explains that the highest penalties in sensitivities due to fibre transmission occur in subchannel 1 (3 dB) followed by subchannel 2 (1 dB), while there is practically no penalty in subchannels 3 and 4.

5.6 Conclusions

SCM allows the implementation of reliable electro-optical transceivers, as it leverages the performance of the more mature microwave components. The main disadvantage of SCM systems is the low spectral efficiency, especially when it is compared with DSP based implementations.

This chapter has presented a novel technique, referred to as OSCM, which can potentially double the spectral efficiency of traditional all-analogue SCM links by transmitting orthogonally overlapping subchannels. The concept has been demonstrated in real-time experiments employing 2.7 Gbaud QPSK orthogonal subchannels and relying largely on off-the-shelf components. The technique requires the implementation of FBMC schemes with broadband microwave circuits. With the appropriate microwave filtering, bits sourced at multi-gigabit rates can be pulse shaped, and modulated and demodulated orthogonally without requiring DSP. It has been demonstrated that standard filters can be employed, although the best performance is achieved with custom implementations that match the ideal Nyquist shapes. Additionally, the combination of FBMC signals and SCM permits the transmission of orthogonal subchannels over fibre without requiring a cyclic prefix.

The expected tolerance to dispersion of OSCM/OSSB has also been confirmed. The highest penalty occurs in the subchannel that is most affected by the nonlinearities associated with the combined effect of the optical modulator and the fibre dispersion. A novel synchronization scheme, applicable to both traditional SCM and OSCM, has been introduced. It allows the synchronization of any number of practical subchannels requiring only one PLL. As a consequence, this synchronization method presents the lowest number of components of any analogue solution presented to date.

5.7 References

[1] Z. Li, I. Shubin, and X. Zhou, "Optical interconnects: recent advances and future challenges," *Optics Express*, vol. 23, pp. 3717-3720, 2015/02/09 2015.

[2] H. Nyquist, "Certain topics in telegraph transmission theory," 1928.

[3] J. G. Proakis, "Digital Communications, 4th edition," ed: McGraw-Hill Companies, Inc., New York, NY, 1998.

[4] W. I. Way, *Broadband Hybrid Fiber Coax Access System Technologies*: Academic Press, Inc., 1998.

[5] F. A. Flood, "A 20 Gb/s per wavelength subcarrier multiplexed optical transmission system," in *Optical Fiber Communication Conference and Exhibit, 2002. OFC 2002*, 2002, pp. 145-146.

[6] J. C. Cartledge and A. S. Karar, "100 Gb/s Intensity Modulation and Direct Detection," *Journal of Lightwave Technology*, vol. 32, pp. 2809-2814, 2014/08/15 2014.

[7] D. Hillerkuss, R. Schmogrow, M. Meyer, S. Wolf, M. Jordan, P. Kleinow, *et al.*, "Single-laser 32.5 Tbit/s Nyquist WDM transmission," *IEEE/OSA Journal of Optical Communications and Networking*, vol. 4, pp. 715-723, 2012.

[8] L. Young, "Microwave Filters - 1965," *IEEE Transactions on Microwave Theory and Techniques*, vol. 13, pp. 489-508, 1965.

[9] J. Wang, C. Xie, and Z. Pan, "Generation of Spectrally Efficient Nyquist-WDM QPSK Signals Using Digital FIR or FDE Filters at Transmitters," *Journal of Lightwave Technology*, vol. 30, pp. 3679-3686, 2012.

[10] Z. Dong, J. Yu, Z. Jia, H. C. Chien, X. Li, and G. K. Chang, "7x224 Gb/s/ch Nyquist-WDM Transmission Over 1600-km SMF-28 Using PDM-CSRZ-QPSK Modulation," *IEEE Photonics Technology Letters*, vol. 24, pp. 1157-1159, 2012.

[11] J. Armstrong, "OFDM for Optical Communications," *Lightwave Technology, Journal of*, vol. 27, pp. 189-204, 2009.

[12] B. J. C. Schmidt, A. J. Lowery, and J. Armstrong, "Experimental Demonstrations of Electronic Dispersion Compensation for Long-Haul Transmission Using Direct-Detection Optical OFDM," *Journal of Lightwave Technology*, vol. 26, pp. 196-203, 2008.

[13] W. Shieh, H. Bao, and Y. Tang, "Coherent optical OFDM: theory and design," *Optics Express*, vol. 16, pp. 841-859, 2008/01/21 2008.

[14] D. Hillerkuss, R. Schmogrow, T. Schellinger, M. Jordan, M. Winter, G. Huber, *et al.*, "26 Tbit s-1 line-rate super-channel transmission utilizing all-optical fast Fourier transform processing," *Nature Photonics*, vol. 5, pp. 364-371, 2011.

[15] B. Farhang-Boroujeny, "OFDM Versus Filter Bank Multicarrier," *IEEE Signal Processing Magazine*, vol. 28, pp. 92-112, 2011.

[16] J. Zhao and A. Ellis, "Electronic impairment mitigation in optically multiplexed multicarrier systems," *Lightwave Technology, Journal of*, vol. 29, pp. 278-290, 2011.
[17] J. Zhao and A. D. Ellis, "Offset-QAM based coherent WDM for spectral efficiency enhancement," *Optics express*, vol. 19, pp. 14617-14631, 2011.
[18] A. D. Ellis and F. C. G. Gunning, "Spectral density enhancement using coherent WDM," *IEEE Photonics Technology Letters*, vol. 17, pp. 504-506, 2005.
[19] B. Farhang-Boroujeny, *Signal processing techniques for software radios*: Lulu publishing house, 2008.
[20] J. Zhao, "DFT-based offset-QAM OFDM for optical communications," *Optics Express*, vol. 22, pp. 1114-1126, 2014/01/13 2014.
[21] S. Y. Jung, S. M. Jung, and S. K. Han, "AMO-FBMC for Asynchronous Heterogeneous Signal Integrated Optical Transmission," *IEEE Photonics Technology Letters*, vol. 27, pp. 133-136, 2015.
[22] K. P. Benterud, W. A. Krzymien, and W. D. Grover, "Quasi-orthogonal subcarrier multiplexing for high-capacity optical data links," *Canadian Journal of Electrical and Computer Engineering*, vol. 18, pp. 159-169, 1993.
[23] R. Hui, Z. Benyuan, H. Renxing, C. T. Allen, K. Demarest, and D. Richards, "Subcarrier multiplexing for high-speed optical transmission," *Lightwave Technology, Journal of*, vol. 20, pp. 417-427, 2002.
[24] N. Cvijetic, "OFDM for short-reach optical networks," in *2014 IEEE Photonics Conference*, 2014, pp. 86-86.
[25] PCI-SIG, "PCI Express Base Specification Revision 3.0," ed, 2010.
[26] R. Bouziane, P. Milder, R. Koutsoyannis, Y. Benlachtar, C. R. Berger, J. C. Hoe, *et al.*, "Design studies for an ASIC implementation of an optical OFDM transceiver," in *36th European Conference and Exhibition on Optical Communication*, 2010, pp. 1-3.
[27] R. P. Giddings, X. Q. Jin, E. Hugues-Salas, E. Giacoumidis, J. L. Wei, and J. M. Tang, "Experimental demonstration of a record high 11.25Gb/s real-time optical OFDM transceiver supporting 25km SMF end-to-end transmission in simple IMDD systems," *Optics Express*, vol. 18, pp. 5541-5555, 2010/03/15 2010.
[28] R. Giddings, "Real-time Digital Signal Processing for Optical OFDM-Based Future Optical Access Networks," *Journal of Lightwave Technology*, vol. 32, pp. 553-570, 2014.
[29] I. Dedic, "56Gs/s ADC : Enabling 100GbE," in *Optical Fiber Communication (OFC), collocated National Fiber Optic Engineers Conference, 2010 Conference on (OFC/NFOEC)*, 2010, pp. 1-3.
[30] I. Orovi, x, N, x017D, ari, x, *et al.*, "Analysis of power consumption in OFDM systems," in *MIPRO, 2011 Proceedings of the 34th International Convention*, 2011, pp. 653-657.
[31] B. Olsson, J. Martensson, and A. Alping, "RF-assisted transmitter and receiver for 100G optical transmission," in *Microwave Photonics, 2011 International Topical Meeting on & Microwave Photonics Conference, 2011 Asia-Pacific, MWP/APMP*, 2011, pp. 180-183.
[32] M. Salter, D. Platt, L. Pettersson, L. Aspemyr, and B. Mingquan, "Circuits and system simulations for 100Gb/s optical SCM transmission," in *Electronics, Circuits, and Systems, 2009. ICECS 2009. 16th IEEE International Conference on*, 2009, pp. 960-963.
[33] J. Hubert, "MMIC design techniques for low-cost high-volume commercial modules," in *Microwave Conference, 2003. 33rd European*, 2003, pp. 887-890 Vol.3.
[34] A. D. Ellis, Z. Jian, and D. Cotter, "Approaching the Non-Linear Shannon Limit," *Lightwave Technology, Journal of*, vol. 28, pp. 423-433, 2010.

[35] A. D. Ellis, I. Tomkos, A. K. Mishra, J. Zhao, S. K. Ibrahim, P. Frascella, *et al.*, "Adaptive modulation schemes," in *2009 IEEE/LEOS Summer Topical Meeting*, 2009, pp. 141-142.

[36] Y. Tang, W. Shieh, and B. S. Krongold, "DFT-Spread OFDM for Fiber Nonlinearity Mitigation," *IEEE Photonics Technology Letters*, vol. 22, pp. 1250-1252, 2010.

[37] L. B. Du and A. J. Lowery, "Optimizing the subcarrier granularity of coherent optical communications systems," *Optics Express*, vol. 19, pp. 8079-8084, 2011/04/25 2011.

[38] P. Poggiolini, Y. Jiang, A. Carena, G. Bosco, and F. Forghieri, "Analytical results on system maximum reach increase through symbol rate optimization," in *Optical Fiber Communications Conference and Exhibition (OFC), 2015*, 2015, pp. 1-3.

[39] P. M. Hill and R. Olshansky, "Multigigabit subcarrier multiplexed coherent lightwave system," *Journal of Lightwave Technology*, vol. 10, pp. 1656-1664, 1992.

[40] B. Saltzberg, "Performance of an Efficient Parallel Data Transmission System," *IEEE Transactions on Communication Technology*, vol. 15, pp. 805-811, 1967.

[41] P. Kourtessis and S. D. Walker, "A Complete 8-GHz QPSK-MODEM Featuring Novel Subcarrier and Data Synchronization for Optical Communications," *IEEE Transactions on Communications*, vol. 55, pp. 987-995, 2007.

[42] I. Seto, H. Shoki, and S. Ohshima, "Optical subcarrier multiplexing transmission for base station with adaptive array antenna," *IEEE Transactions on Microwave Theory and Techniques*, vol. 49, pp. 2036-2041, 2001.

[43] A. Hilto, A. Zolomy, T. Berceli, G. Jaro, and E. Udvary, "Millimeter Wave Synthesizer Locked To An Optically Transmitted Reference Using Harmonic Mixing," in *Microwave Photonics, 1997. MWP '97. International Topical Meeting on*, 1997, pp. 91-94.

[44] J. R. Andrews, "Low-pass risetime filters for time domain applications," *Picosecond Pulse Labs, Application Note AN-7a*, 1999.

[45] ITU-T, "G. 975.1," *Forward error correction for high bit-rate DWDM submarine systems*, 2004.

[46] G. H. Smith, D. Novak, and Z. Ahmed, "Overcoming chromatic-dispersion effects in fiber-wireless systems incorporating external modulators," *Microwave Theory and Techniques, IEEE Transactions on*, vol. 45, pp. 1410-1415, 1997.

[47] J. Maeda, T. Katoh, and S. Ebisawa, "Effect of Fiber Dispersion on Subcarrier QAM Signal in Radio-Over-Fiber Transmission," *Lightwave Technology, Journal of*, vol. 30, pp. 2625-2632, 2012.

[48] T. Fujiwara and K. Kikushima, "140 Carrier, 20GHz SCM signal transmission across 200km SMF by two-step sideband suppression scheme in optical SSB modulation," in *Optical Fiber Communication Conference*, 2007, p. OME2.

[49] A. D. Ellis, F. C. G. Gunning, and T. Healy, "Coherent WDM: the achievement of high information spectral density through phase control within the transmitter," in *2006 Optical Fiber Communication Conference and the National Fiber Optic Engineers Conference*, 2006, p. 3 pp.

[50] F. C. G. Gunning, T. Healy, and A. D. Ellis, "Dispersion tolerance of coherent WDM," *IEEE Photonics Technology Letters*, vol. 18, pp. 1338-1340, 2006.

[51] H. Fu, "Equalization for high-speed serial interfaces in Xilinx 7 series FPGA transceivers," *Xilinx white paper*, vol. 419, 2012.

[52] Xilinx. (2011), Virtex-6 FPGA GTX Transceivers User Guide UG366. Available: http://www.xilinx.com/support/documentation/user_guides/ug366.pdf

[53] Y. Guomin, E. Miller, J. Mallari, W. Cailin, C. Baoquan, C. Hui, *et al.*, "Small form factor thin film polymer modulators for telecom applications," in *Optical Fiber Communication Conference and Exposition (OFC/NFOEC), 2012 and the National Fiber Optic Engineers Conference*, 2012, pp. 1-3.

[54] B. Olsson, J. Martensson, A. Kristiansson, and A. Alping, "RF-assisted optical dual-carrier 112 Gbit/s polarization-multiplexed 16-QAM transmitter," in *Optical Fiber*

Communication (OFC), collocated National Fiber Optic Engineers Conference, 2010 Conference on (OFC/NFOEC), 2010, pp. 1-3.

[55] F. M. Gardner, *Phaselock techniques*: John Wiley & Sons, 2005.

[56] A. Hartog, A. Conduit, and D. Payne, "Variation of pulse delay with stress and temperature in jacketed and unjacketed optical fibres," *Optical and Quantum Electronics,* vol. 11, pp. 265-273, 1979.

[57] J. Carr, S. Saikkonen, and D. Williams, "Refractive index measurements on single-mode fiber as functions of product parameters, tensile stress, and temperature," *Fiber & Integrated Optics,* vol. 9, pp. 393-396, 1990.

[58] M. Shadaram, J. Medrano, S. A. Pappert, M. H. Berry, and D. M. Gookin, "Technique for stabilizing the phase of the reference signals in analog fiber-optic links," *Applied optics,* vol. 34, pp. 8283-8288, 1995.

[59] J. P. Costas, "Synchronous communications," *Proceedings of the IRE,* vol. 44, pp. 1713-1718, 1956.

[60] J. R. Barry, E. A. Lee, and D. G. Messerschmitt, *Digital communication*: Springer Science & Business Media, 2004.

[61] P. Hill and R. Olshansky, "Bandwidth efficient transmission of 4 Gb/s on two microwave QPSK subcarriers over a 48 km optical link," *Photonics Technology Letters, IEEE,* vol. 2, pp. 510-512, 1990.

[62] T. Kato, Y. Koyano, and M. Nishimura, "Temperature dependence of chromatic dispersion in various types of optical fiber," *Optics letters,* vol. 25, pp. 1156-1158, 2000.

[63] W. H. Chen and W. I. Way, "Multichannel single-sideband SCM/DWDM transmission systems," *Lightwave Technology, Journal of,* vol. 22, pp. 1679-1693, 2004.

[64] P. Laurencio, S. O. Simoes, and M. C. R. Medeiros, "Impact of the Combined Effect of RIN and Intermodulation Distortion on OSSB/SCM Systems," *Lightwave Technology, Journal of,* vol. 24, pp. 4250-4262, 2006.

Chapter 6

6 Multichannel WDM/OSCM based on Optical Frequency Combs

Electro-optical transceivers can be implemented employing all-analogue signal processing in order to achieve low values of power consumption and latency. Simultaneously, the spectral efficiency of an optical channel can be increased by employing orthogonal multicarrier techniques. Overall capacity can then be multiplied by combining a number of WDM optical channels. For the generation of the optical carriers, Optical Frequency Combs (OFC) are a promising technique because they can generate multiple optical carriers from ideally a single laser. Unlike independent lasers, OFCs can achieve a stable optical carrier spacing and potentially lower cost. Real-time OSCM experiments with data rates of up to 400 Gbit/s were performed emulating a WDM system composed of multiple optical channels. The optical carriers were provided by different types of OFCs, namely Gain Switched Lasers (GSL) and Mode Locked Lasers (MLL). The use of orthogonally overlapping subchannels and tightly allocated optical carriers achieves an unprecedented spectral efficiency in all-analogue real-time broadband WDM/SCM links.

6.1 Motivation

The increasing demand for capacity in optical networks has translated into a growing interest and research effort in high-speed short-reach optical interconnects and its associated technologies [1]. For practical and real-time applications, electro-optical transceivers are preferred due to the stability and maturity of electronic circuits and microwave components, in contrast with their optical counterparts. The broad range of possible electronic implementations presents a trade-off between three major figures of merit in communications systems: spectral efficiency, power consumption and latency. In recent years, the majority of advances in the area have been supported by DSP due to its ability to increase spectral efficiency and mitigate impairments [2]. However, a high number of computational operations also brings about disadvantages such as increased power consumption and latency [3]. This fact

motivates the investigation of electro-optical transceivers that rely on all-analogue signal processing to maximize power efficiency and minimize latency [4].

Nowadays, there is a proliferation of data centres addressing a variety of services. Most data centre subsystems need moderate total capacity but a high capacity per interface while reducing power consumption and latency to a minimum. For such applications, a purely analogue implementation potentially presents the best trade-off between those key parameters. In addition to these fundamental features, there are several important performance requirements which may determine the most appropriate scheme. Firstly, tolerance to dispersion allows compatibility between inter and intra data centre distances, simplifying inventory. Secondly, direct compatibility with parallel Gbit/s electrical interfaces would simplify the buffering and (de)multiplexing of data at different symbol rates. Finally, integration with WDM systems multiplies the overall capacity and potentially allows the same transponders to be employed in the wide area network.

As explained in previous chapters, a purely analogue SCM/OSSB scheme is possible and compatible with the desired baseband rates using microwave filters, mixers, combiners and splitters [5]. It achieves high interface capacity per port, its power consumption is determined solely by the drive amplifiers common to all solutions, and the latency is low as it is given by the group delay of the microwave components. Apart from that, the overall electrical transceiver can be integrated using MMIC technology [6], widely employed in the front ends of commercial and consumer communication devices. Furthermore, SCM/OSSB meets all the additional requirements. Firstly, high tolerance to dispersion is achieved [7]. Secondly, an appropriate subcarrier symbol rate also allows direct termination of parallel Gbit/s electrical interfaces avoiding data rate converters. Finally, as shown in chapter 4, cost and spectrally efficient WDM implementations consisting of tightly allocated optical channels are viable.

The main weakness of previously reported all-analogue SCM and WDM/SCM solutions is the spectral efficiency as they make use of traditional QPSK subchannels [8, 9]. However, as explained in the previous chapter, OSCM overcomes this weakness by multiplexing orthogonally overlapping subchannels according to FBMC theory [10, 11]. This chapter demonstrates WDM/OSCM schemes employing optical frequency combs (OFC) to generate the optical carriers for the WDM signal. An OFC obtains multiple optical carriers from ideally a single laser, ensuring a more

stable carrier spacing and potentially a lower cost compared with independent lasers. As a result, WDM/OSCM links with tightly allocated optical channels were implemented, enhancing further the increased spectral efficiency with respect to previous all-analogue WDM/SCM solutions.

6.2 Generic Scheme

A WDM/OSCM transmission scheme composed of *N* OSSB channels and based on an OFC is shown in Figure 6.1. The use of an OFC instead of individual lasers reduces the number of required components and ensures the maintenance of constant frequency spacing, referred to from now on as Free Spectral Range (FSR), between the optical channels.

The optical carriers at the output of the OFC are demultiplexed and each one is modulated producing an OSSB signal. As explained in chapter 2, this can be achieved with dual drive Mach Zehnder (DD-MZM) modulators or with optical IQ modulators (OIQM) whose electrical inputs are fed with the desired signal and its Hilbert transformed (HT) pair. The HT of an electrical signal can be obtained directly in the analogue domain by employing a microwave hybrid splitter. The modulating electrical signal is generated with an all-analogue FBMC transmitter and is composed of orthogonally overlapping subchannels carrying digital data. The *N* optical channels are combined and transmitted over fibre. In the receiver, the optical channels are demultiplexed and direct detection is used to recover the FBMC electrical signals. Finally, all-analogue FBMC receivers demodulate the orthogonal electrical subchannels. The realization of the all-analogue FBMC blocks has been thoroughly explained in chapter 5.

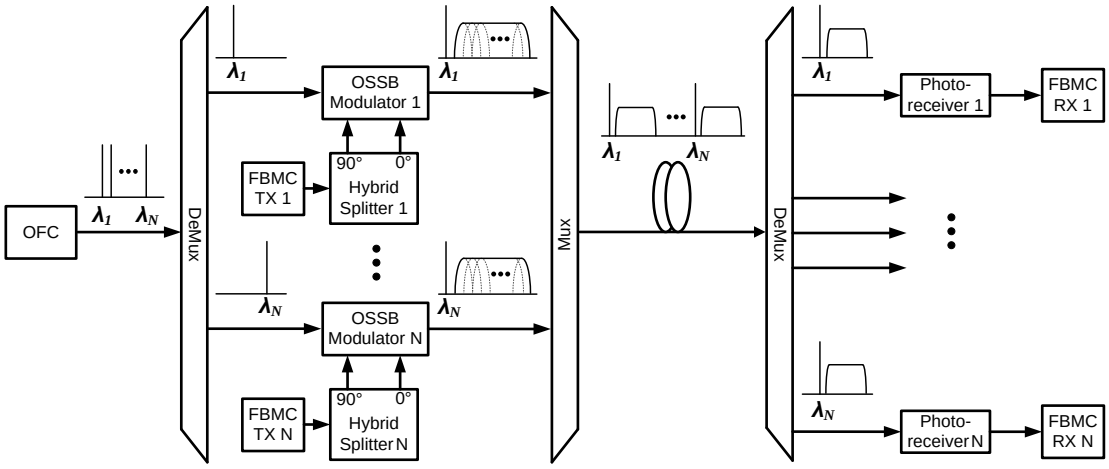

Figure 6.1 WDM/OSCM transmission scheme with *N* OSSB channels based on OFC.

6.3 Optical Frequency Combs

Unlike independent lasers, OFCs offer constant frequency spacing or FSR between the optical carriers, allowing the reduction of inter-channel guard bands and the spacing between optical channels. However, an OFC needs to exhibit a number of properties such as excellent spectral flatness, high frequency stability, and high optical carrier to noise ratio (CNR). For direct detection links OFCs also require low RIN while low linewidth is necessary for coherent systems. Additionally, for flexible networks a tunable FSR is also a requisite. Different OFC technologies are briefly reviewed below.

Typically, mode-locked lasers (MLL) are popular candidates for the generation of OFCs in electro-optical transceivers [12, 13]. The term mode-locking indicates the phase locking between multiple longitudinal modes in a laser cavity [14]. If the cavity modes oscillate with comparable amplitudes and locked phases, mode-locking occurs and a periodical pulsed radiation, which is equivalent to a multicarrier signal in the optical domain, is generated. The different mechanisms to obtain mode-locking can be classified into active, when phase synchronization requires an external periodic source, or passive, when the synchronization is obtained directly in the laser cavity [14]. MLLs can generate a high number of optical carriers in a wide bandwidth. The main disadvantages are cavity complexity, high linewidth and RIN per individual comb line, and fixed FSR. Apart from that, from a practical perspective, they present difficulties to maintain stable mode locking.

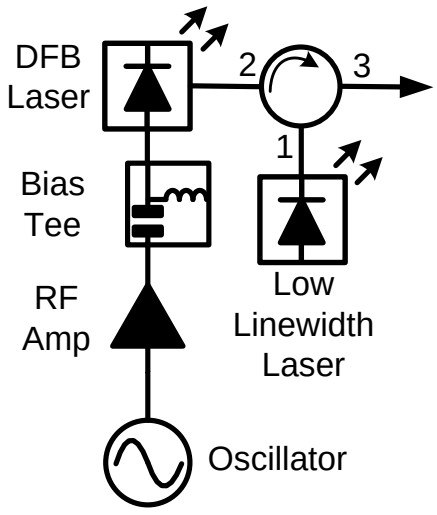

Figure 6.2 Schematic of an OFC based on an externally injected gain-switched laser.

OFC generation with gain switched lasers (GSL), typically DFBs, is another simple and cost efficient alternative [15]. Gain switching is achieved by driving the laser diode with a large RF signal at the desired frequency or FSR. The associated abrupt periodic optical pulse is equivalent to a multicarrier signal in frequency. The GSL is usually combined with external injection obtaining beneficial properties, such as an increase in the number of comb tones, improved spectral flatness, enhanced CNR, and reduced RIN and linewidth on each of the comb tones [16]. Optical external injection is a complicated procedure in which a laser "locks" to an external laser, partially acquiring the properties of the second. A typical set-up diagram of an externally-injected GSL can be observed in Figure 6.2. In practice, the main advantages of this technique are the stability and the tunable FSR, while the main disadvantage is the lower number of comb tones that are obtained when compared with MLLs.

OFCs can also be obtained by cascading a number of optical modulators driven by a large voltage RF tone, exploiting the non-linear behaviour of the modulators to obtain multiple carrier frequencies at the output [17, 18]. Inherent modulator properties such as bias drift and high insertion loss make this technique less attractive for network deployment. Finally, parametric OFCs that make use of highly nonlinear fibre to excite multiple optical carriers have also been demonstrated [19], but this solution is difficult to integrate in a realistic network.

Table 6-1 Summary of the WDM/OSCM Experiments.

Properties	*Experiment 1*	*Experiment 2*
Section	6.4.1	6.4.2
OFC Technology	Externally-Injected GSL	Quantum-Dash MLL
FSR	20 GHz	37 GHz
Optical Channels	5	20
Electrical Subchannels per Optical Channel	4	4
Total Electrical Subchannels	20	80
Electrical Modulation	Orthogonal QPSK	Orthogonal QPSK
Orthogonality Filters	Bessel (section 5.3.2.3)	SRRC (section 5.3.2.2)
Baseband Data Rate	2.7 Gbit/s	2.7 Gbit/s
Baseband Patterns	PRBS7	PRBS7
Data Rate per Optical Channel	21.6 Gbit/s	21.6 Gbit/s
Overall Gross Data Rate	108 Gbit/s	432 Gbit/s
Net Data Rate after 7% FEC	100.44 Gbit/s	401.76 Gbit/s
Subcarrier Synchronization	Same LOs in TX/RX	PLL+SRD in RX (as section 5.5.3.2)
Fibre Length	Back to Back	2 km SSMF

6.4 Experiments

For a practical electro-optical transceiver, MLLs represent the most straightforward solution to integrate an OFC in an industrial product. GSLs are also promising because of their simplicity and stability. For those reasons, both technologies were employed in the real-time WDM/OSCM experiments described in this section. The parameters of the two experiments are summarized in Table 6-1. For this kind of direct detection system, the performance of different optical channels depends on the RIN and the CNR of the optical lines in the OFC, as it has been demonstrated for OFDM signals [20].

6.4.1 WDM/OSCM based on Gain-Switched Laser

6.4.1.1 Scheme and Spectra

A real-time direct detection WDM/OSCM system equivalent to that shown in Figure 6.1 was emulated for the case of five optical channels separated by 20 GHz, as illustrated in Figure 6.3. The physical implementation of the basic electrical scheme has been thoroughly described in section 5.4.2. In this case, the microwave FBMC scheme (de)modulated four QPSK 2.7 Gbaud orthogonal subchannels employing the solution based on Bessel filters described in section 5.3.2.3. Typical transmitted and received electrical spectra can be observed in Figure 6.4.

The OFC was generated with an externally injected gain-switched DFB laser. The spectrum of the OFC is illustrated in Figure 6.5(a). The FSR was 20 GHz, set by the radio frequency synthesizer used to drive the laser. Five lines of similar amplitude (≈3 dB flatness) were filtered and amplified, as can be observed in Figure 6.5(b). During the experiments, the OFC was also substituted with an ECL to compare the performance of the system with a single optical carrier case.

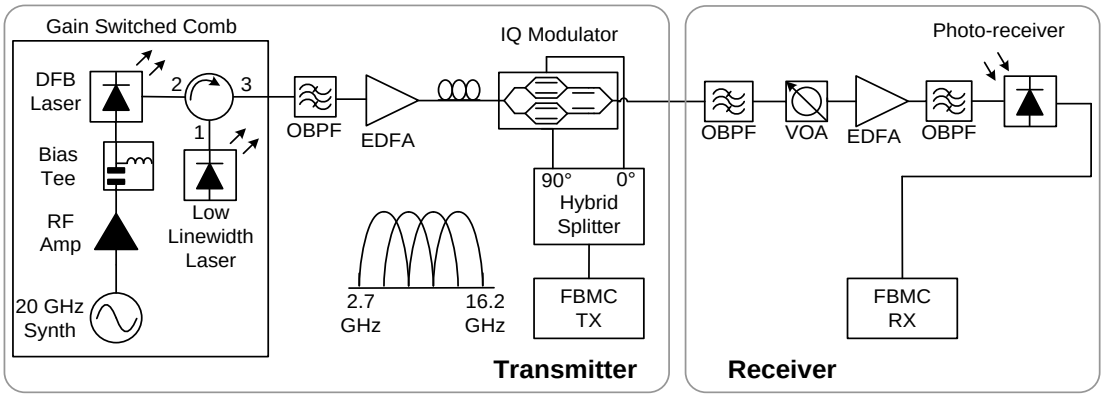

Figure 6.3 Schematic of the WDM/OSCM experiment based on a GSL.

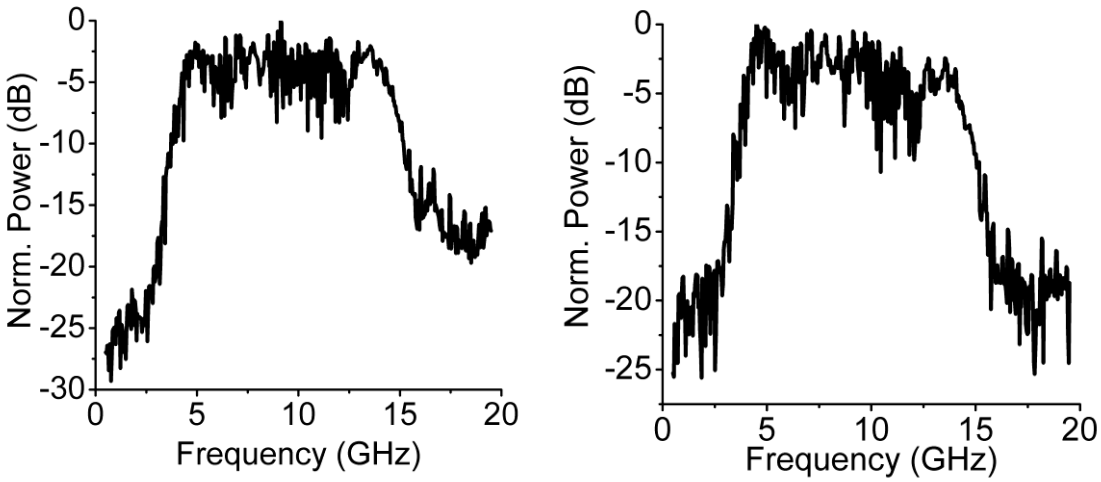

Figure 6.4 Typical electrical spectra composed of four orthogonal QPSK 2.7 Gbaud subchannels at the output of the (a) FBMC transmitter and (b) photo-receiver.

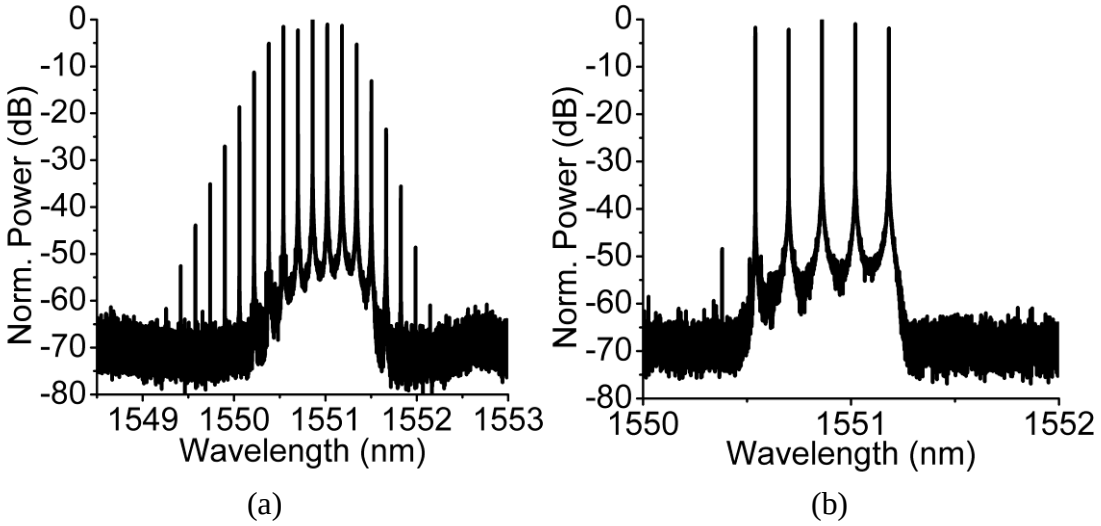

Figure 6.5 (a) OFC at the output of the externally-injected GSL and (b) after filtering and amplifying five comb lines.

The optical link was established with a polymer based OIQM that presented a half-wave voltage V_π=2.5V and a bandwidth of 20 GHz. Every optical carrier was modulated generating an OSSB channel. A sideband suppression ratio of 20 dB was achieved. The optical spectrum of the WDM/OSCM signal at the output of the OIQM can be observed in Figure 6.6. The parallel MZMs inside the OIQM were biased at *quadrature*, and driven by the RF FBMC signal and its HT, with a total rms OMI of M≈20%, or ≈500 mV_{RMS}. From Figure 5.15, a sensitivity of ≈-33 dBm for a BER of $3.8 \cdot 10^{-3}$ would be the theoretical limit achievable with perfect components. The desired optical channel was then selected with a tunable optical BPF, as shown in Figure 6.7. The rejection ratio of the adjacent optical carrier was 22 dB. A VOA

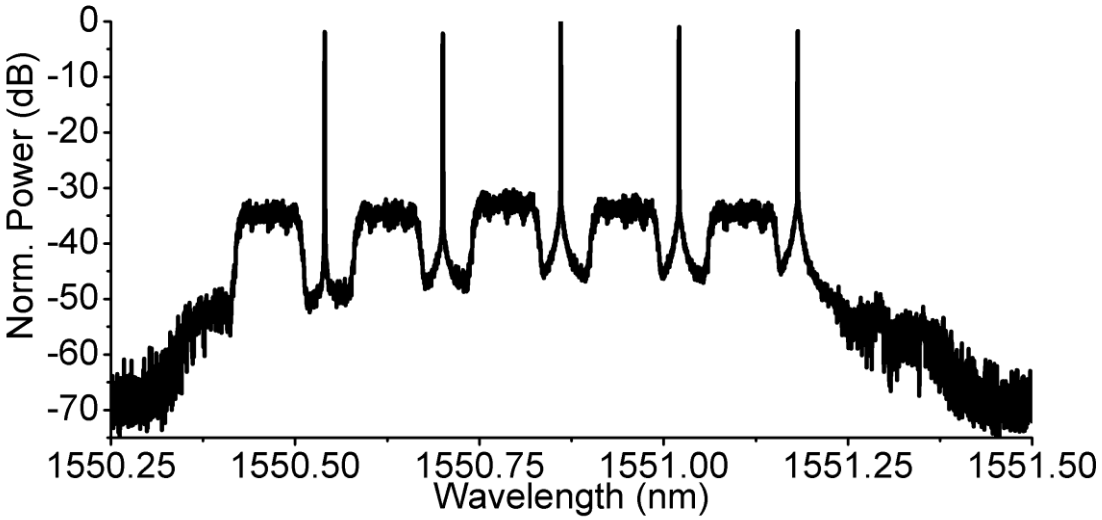

Figure 6.6 Spectrum of the 5x21.6 Gbit/s WDM/OSCM signal.

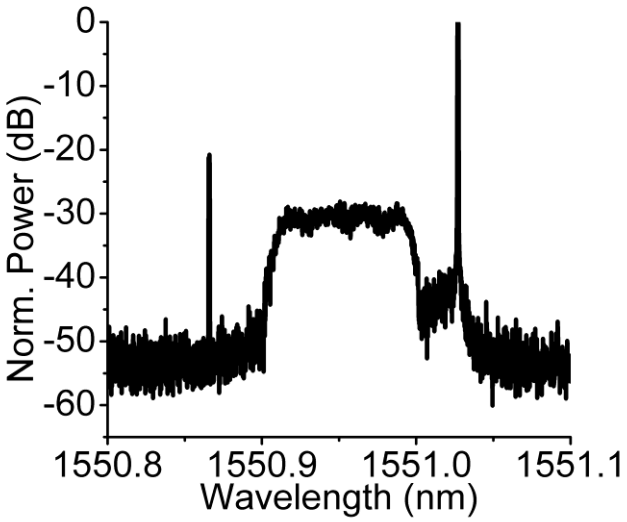

Figure 6.7 Spectrum of the fourth channel after being selected and filtered.

was used to simulate fibre losses. The resultant signal was introduced into a pre-amplified optical receiver consisting of an EDFA and a photo-receiver with 20 GHz bandwidth. The EDFA was operated in constant power mode to ensure an average optical power of 5 dBm was fed to the photo-receiver regardless of the average received optical power, P_{IN}.

Given the close allocation of optical channels, there are two contributions that set the minimum distortion of the system. Firstly, the imperfectly suppressed side bands from the neighbouring OSSB channel, as explained in chapter 4. Secondly, the optical carrier of the adjacent optical channel could not be perfectly suppressed in the receiver (see Figure 6.7), adding cross-talk due to the beating in the photo-detector. As the transmitted baseband streams are uncorrelated, and with the selected

frequency plan, it can be deduced that in all the cases both distortions are uncorrelated with the desired signal. Therefore, no further decorrelation of the WDM signal is required.

6.4.1.2 Results

The optical carriers were modulated generating OSSB subchannels (see Figure 6.6). As it can be observed in Figure 6.5(b), the fifth optical channel presented the lowest CNR for this modulation, ≈50 dB, and, accordingly, the worst performance. For this channel, Figure 6.8 shows the average BER of the two components (I and Q) transmitted in every electrical subchannel, as a function of the average optical power at the input of the pre-amplified optical receiver, P_{IN}. Measurements were taken with an optical back to back link. The performance of all the electrical subchannels was similar and the sensitivity for the 7% HD-FEC code was ≈-23 dBm. Under the same conditions, performance was measured using only one optical channel whose optical carrier was coming from a high-performance ECL. The RIN of the ECL was ≈-155 dB/Hz, in contrast with ≈-130 dB/Hz in the OFC [16]. The CNR of the ECL was >80 dB, in contrast with the ≈50 dB in the worst case of the OFC. As it can also be observed in Figure 6.8, the sensitivity achieved with the ECL was ≈-28 dBm for all the electrical subchannels, closer to the estimated ideal

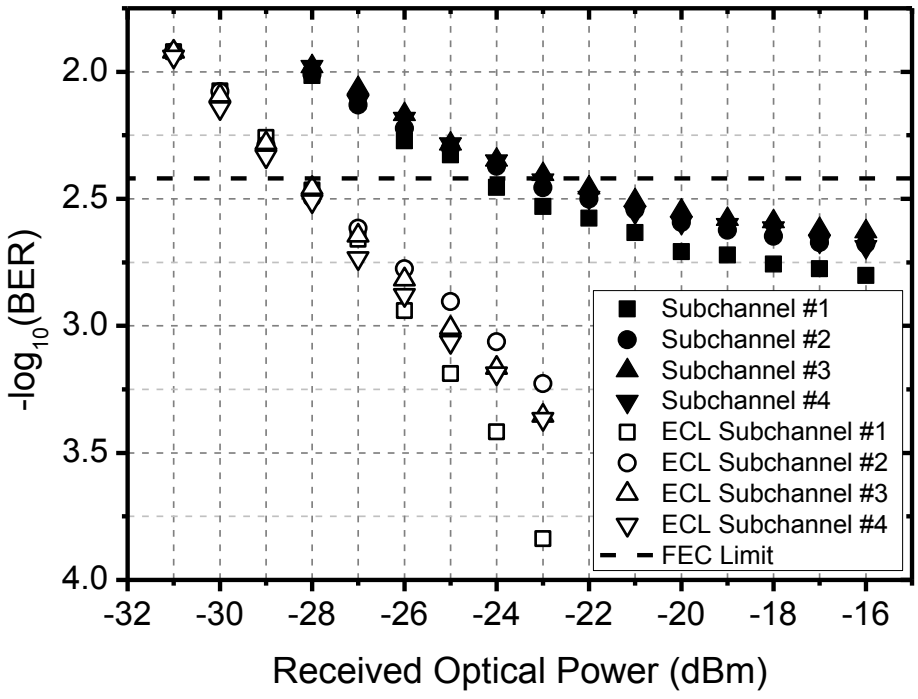

Figure 6.8 Comparison of performance between the worst optical channel in the WDM signal based on a GSL, and a single channel based on one low-RIN high-CNR ECL. FEC limit for a 7 % overhead.

value of -33 dBm. It should be noted that in the WDM case, the optical channel 5 experienced interference from the imperfectly suppressed sideband of channel 4, as can be deduced from chapter 4. It can be concluded that the maximum penalty generated by the tightly allocated WDM solution based on an externally-injected gain switched DFB laser was 5 dB with respect to a high performance individual channel. The penalty was due to the higher RIN and lower CNR of the OFC, and the interference generated by the adjacent optical channel. In Figure 6.8, it can also be observed that the WDM case, in comparison with the ECL case, establishes a higher noise floor that limits the best performance that can be obtained regardless the value of P_{IN}.

A more comprehensive approach requires individually analysing the 40 components (5x4x2, 5 optical carriers, 4 electrical subcarriers, and 2 due to the quadrature modulation on each subcarrier). Another realization of the measurements was carried out obtaining the sensitivity for a 7% FEC for the 40 electrical components. The results are illustrated in Figure 6.9. Components 1 to 8 belong to the first optical channel and components 33 to 40 belong to the fifth one. There are several points that can be discussed. Firstly, some subchannels presented a disparity between the I and Q components (up to 5.5 dB). This IQ imbalance was mainly attributed to the limited performance of the electrical IQ mixers with broadband

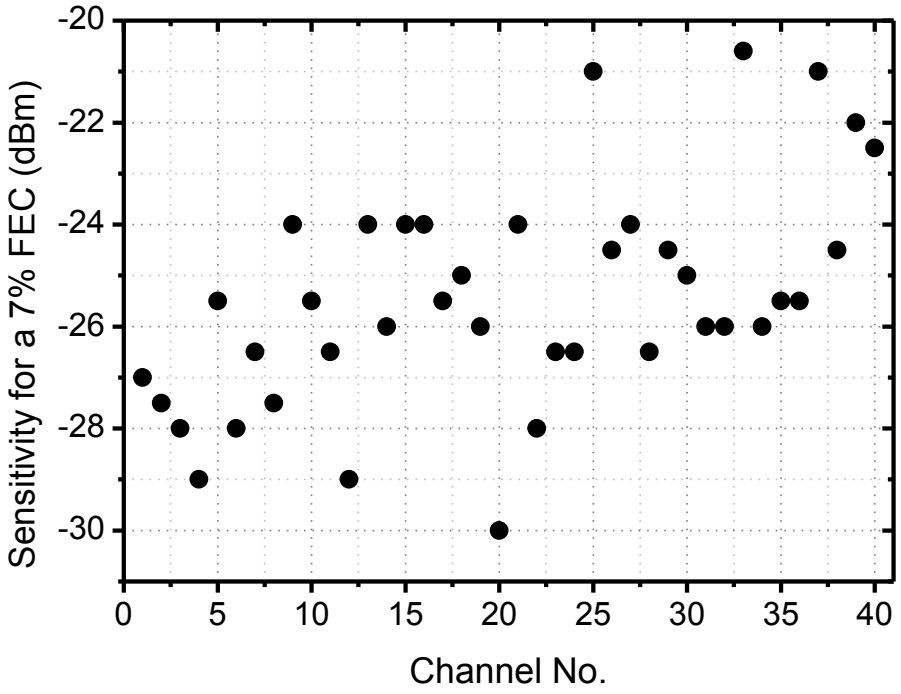

Figure 6.9 Individual sensitivities for all the baseband components in the WDM/OSCM link based on a GSL.

signals. Secondly, it can be confirmed that the CNR of the optical lines in the OFC determines the final performance of the optical channels. In this case the best CNR value corresponds to optical channel 1, ≈65 dB (see Figure 6.5(b)), and it presents the best performance. Moreover, optical channel 5 presents the worst performance with a CNR of ≈50 dB. Finally, all the components were able to achieve BER values below the FEC limit, with the sensitivity of the worst case at -20.5 dBm.

The overall data rate is 108 Gbit/s (5x21.6) which after a 7% overhead FEC would be reduced to 101.44 Gbit/s. The presented results achieve a higher spectral efficiency than any previously reported broadband real-time DSP-less WDM/SCM link, as they made use of traditional non-orthogonal QPSK modulation that is limited to 1 bit/s/Hz in the electrical signal [8, 9]. Neglecting the optical carriers, the spectral efficiency of the presented OSCM scheme is 1.6 bit/s/Hz (21.6 Gbit/s in a bandwidth of 13.5 GHz), approaching 2 bit/s/Hz for a higher number of subcarriers. Additionally, the presented experiment has employed reduced guard bands with an optical channel separation of 20 GHz. This reduction has been supported by the use of an OFC, which ensures a fixed FSR, in contrast with independent lasers whose frequency separation drifts with time.

6.4.2 WDM/OSCM based on Mode-Locked Laser

6.4.2.1 Scheme and Spectra

A real-time direct detection WDM/OSCM system equivalent to that shown in Figure 6.1 was also emulated employing a MLL as illustrated in Figure 6.10. The key differences with respect to the previous experiment will be listed.

The electrical scheme was the one described in section 5.5.3.2. It consisted of four 2.7 Gbaud QPSK orthogonal subchannels. The SRRC orthogonality filters

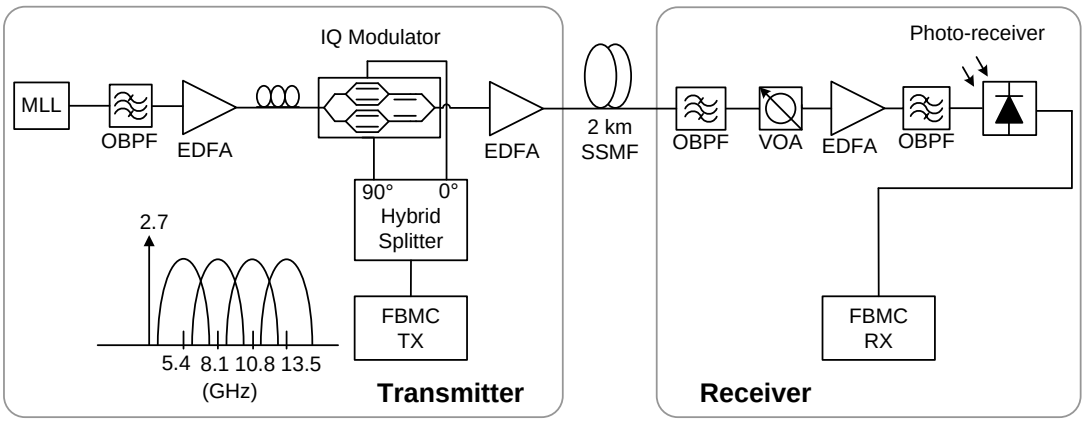

Figure 6.10 Schematic of the WDM/OSCM experiment based on a MLL.

described in chapter 5 were employed. A pilot tone at 2.7 GHz was multiplexed in the transmitted signal and used in the receiver to synchronize all the subcarriers. Examples of transmitted and received electrical spectra are shown in Figure 6.11.

The OFC was generated with a passively locked Quantum-Dash MLL [21] biased at 200 mA and with an FSR of 37 GHz. The spectrum of the OFC is illustrated in Figure 6.12(a). Twenty lines of similar amplitude were filtered and amplified, as can be observed in Figure 6.12(b). During the experiments, the MLL was also substituted with a high-performance ECL to compare the performance of the system with a single optical carrier case.

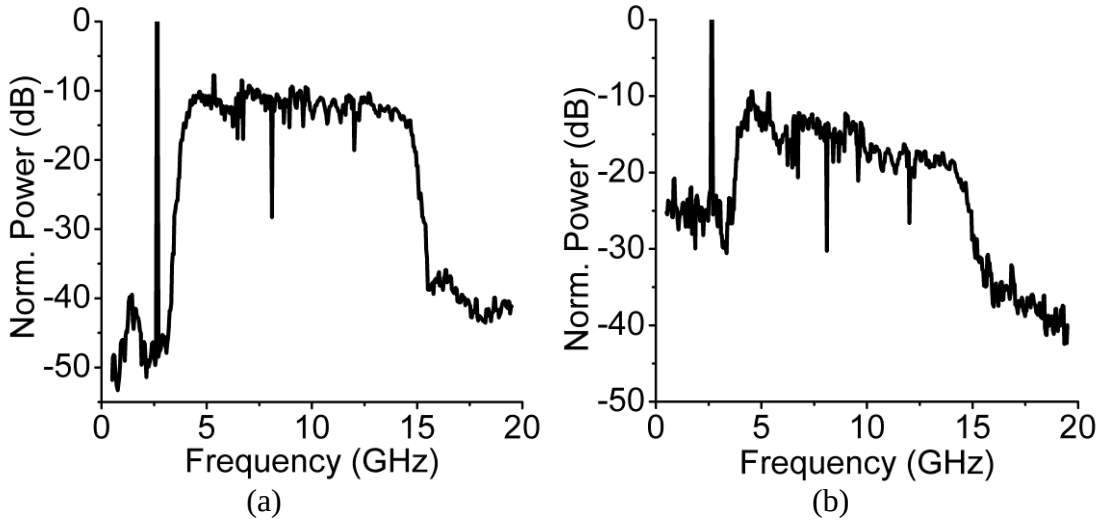

Figure 6.11 Typical electrical spectra composed of four orthogonal subchannels and pilot tone at the output of the (a) FBMC transmitter and (b) photo-receiver.

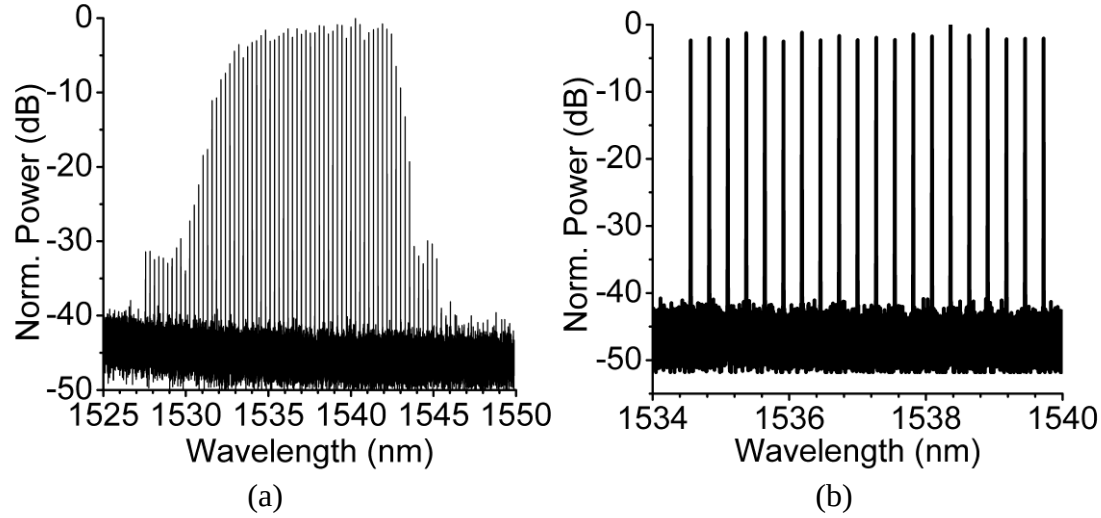

Figure 6.12 (a) OFC at the output of the Quantum-Dash MLL and (b) after filtering and amplifying twenty comb lines.

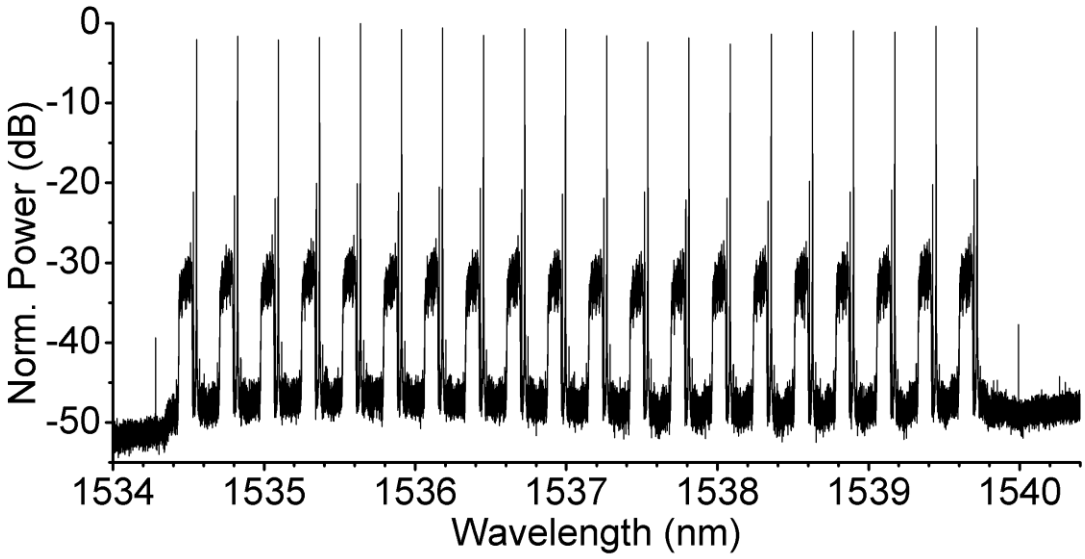

Figure 6.13 Spectrum of the 20x21.6 Gbit/s WDM/OSCM signal.

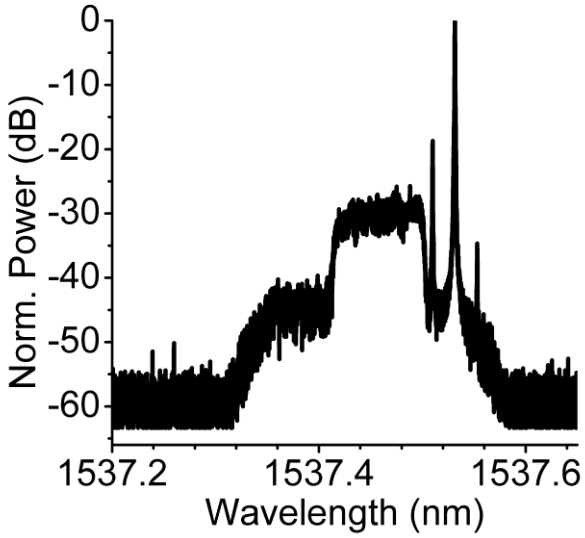

Figure 6.14 Spectrum of the twelfth channel after being selected and filtered.

The resultant comb was optically modulated emulating a 20x21.6 Gbit/s WDM scheme (see Figure 6.13). The OIQM produced the OSSB signal with an OMI of M=20%. The optical signal was amplified and transmitted through 2 km of SSMF. The desired optical channel was then selected with a tunable optical BPF in the receiver (see Figure 6.14). A VOA was used to simulate additional fibre losses. The resultant signal was introduced into a pre-amplified receiver consisting of an EDFA and a 20 GHz photo-receiver. The EDFA was operated in constant power mode to ensure an average optical power of -4 dBm was fed to the photo-receiver.

6.4.2.2 Results

The performance of the system was measured obtaining the BER as a function of the average optical power at the input of the receiver EDFA, P_{IN}. From Figure 6.13, one of the worst optical channels was the 12th channel, as it had lower optical CNR, ≈45 dB. The BER measured for its four electrical subchannels (averaging the I and Q components) is shown in Figure 6.15. Measurements were taken with a link of 2 km of SSMF. The performance of all the electrical subchannels was similar and the sensitivity for the 7% HD-FEC code was ≈-25 dBm. Under the same conditions, the performance was measured using only one optical channel whose optical carrier was coming from a high-performance ECL. The RIN of the ECL was ≈-155 dB/Hz, in contrast with ≈-130 dB/Hz in the MLL [21]. The CNR of the ECL was >80 dB, in contrast with the ≈45 dB in the worst case of the MLL. As it can also be observed in Figure 6.15, the sensitivity achieved with the ECL was ≈-29.5 dBm for all the electrical subchannels, closer to the estimated ideal value of ≈-33 dBm. The achieved sensitivities are ≈2 dB better than with the GSL because this experiment employed the pseudo-ideal SRRC orthogonality filters. Apart from that, in the MLL case, due to the FSR of 37 GHz, the optical channels did not experience interference from the imperfectly suppressed sideband of the adjacent

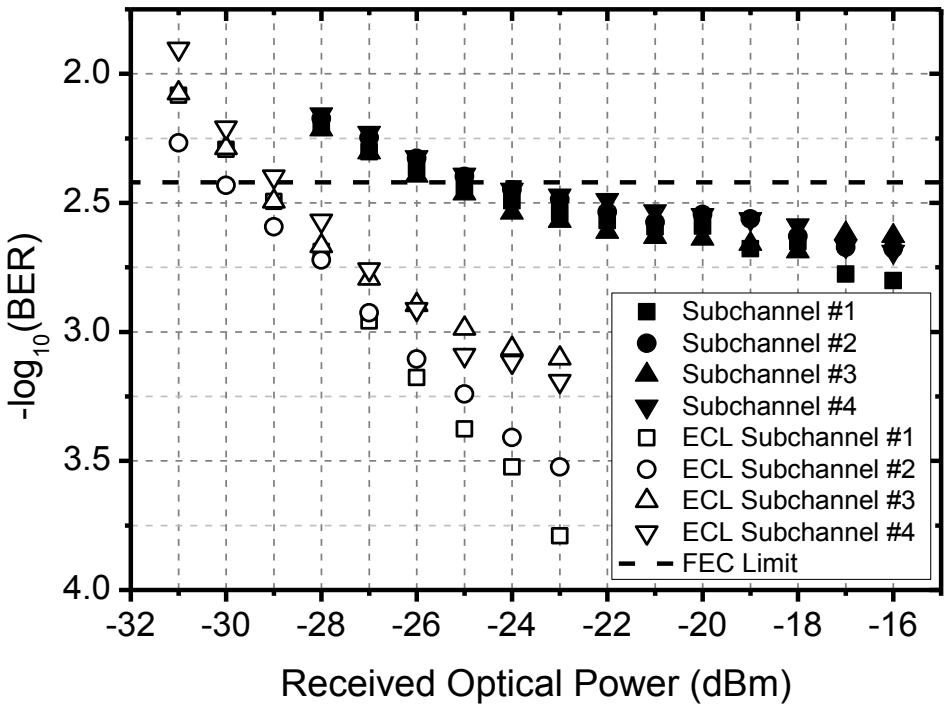

Figure 6.15 Comparison of performance between the worst optical channel in the WDM signal based on a MLL, and a single channel based on one low-RIN high-CNR ECL. FEC limit for a 7 % overhead.

channel. It can be concluded that the maximum penalty generated by the WDM solution based on a MLL was ≈4.5 dB with respect to a high performance individual channel. The penalty was due to the higher RIN and lower CNR of the OFC. Again, in Figure 6.15, it can also be observed that the WDM case, in comparison with the ECL case, establishes a higher noise floor that limits the best performance that can be obtained regardless the value of P_{IN}.

A more thorough measurement individually analysed the 160 baseband signals (20x4x2, 20 optical channels, 4 subchannels, and 2 due to the QPSK modulation). All the sensitivities, considering a hard decision 7% FEC code, are illustrated in Figure 6.16. Components 1 to 8 belong to the first optical channel and components 153 to 160 belong to the twentieth one. All the sensitivities are in the range of -22 to -28.5 dBm. Performance differences can be attributed to the amplitude asymmetry of the optical carriers, and the varying behaviour of the IQ mixers in each of the frequency bands. In comparison with the GSL based case, all the optical channels present a more uniform behaviour due to the more similar CNR in the different comb lines.

The overall data rate was 432 Gbit/s (20x21.6) that, after a 7% overhead FEC, would be reduced to 401.76 Gbit/s. The spectral efficiency of the electrical signals was 1.78 bit/s/Hz, (21.6 Gbit/s in a bandwidth of 12.1 GHz), slightly higher than in

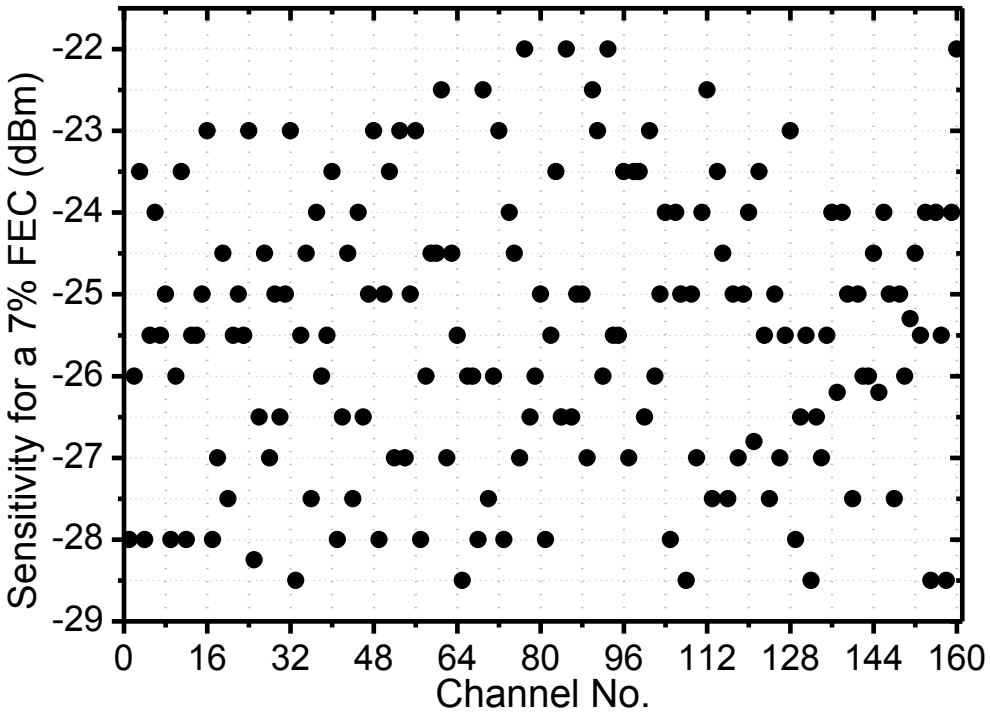

Figure 6.16 Individual sensitivities for all the baseband components in the WDM/OSCM link based on a MLL.

the previous experiment with the GSL due to the use of the SRRC filters. In contrast, considering the optical carriers, the overall spectrally efficiency was reduced because of the higher FSR of 37 GHz of the MLL in comparison to that of the GSL.

6.5 Conclusions

SCM can leverage the maturity of microwave components to implement reliable real-time electro-optical transceivers. Purely analogue SCM implementations have the potential to achieve good performance in terms of power consumption, latency and tolerance to dispersion, but have been traditionally limited to low values of spectral efficiency. The previous weakness has been overcome by the transmission of orthogonal electrical subchannels following FBMC theory.

For the first time, broadband real-time all-analogue WDM/OSCM schemes have been demonstrated, achieving a higher spectral efficiency than any previously reported equivalent link. The most relevant features of the described experiments are emphasized below. Firstly, net rates higher than 100 Gbit/s and 400 Gbit/s would be achieved after applying a 7% FEC. Secondly, the compatibility and suitability of OSCM and two different types of OFCs has been proved. GSLs are simple and stable solutions, can be implemented with off-the-shelf components, and achieve a tight allocation of optical channels. MLLs are custom solutions and have stability issues but they generate a high number of comb lines obtaining higher overall data rates. Finally, the baseband rate used in the experiment was 2.7 Gbit/s, directly compatible with the typical electrical interfaces employed in computing and electro-optical transceivers. The described features ensure that OSCM is a feasible and promising technique to be considered in the design of future WDM electro-optical transceivers.

6.6 References

[1] Z. Li, I. Shubin, and X. Zhou, "Optical interconnects: recent advances and future challenges," *Optics Express*, vol. 23, pp. 3717-3720, 2015/02/09 2015.

[2] J. C. Rasmussen, T. Takahara, T. Tanaka, Y. Kai, M. Nishihara, T. Drenski, *et al.*, "Digital signal processing for short reach optical links," in *2014 The European Conference on Optical Communication (ECOC)*, 2014.

[3] A. Morea, S. Spadaro, O. Rival, J. Perello, F. Agraz, and D. Verchere, "Power management of optoelectronic interfaces for dynamic optical networks," in *Optical Communication (ECOC), 2011 37th European Conference and Exhibition on*, 2011, pp. 1-3.

[4] N. Nambath, R. K. Raveendranath, D. Banerjee, A. Sharma, A. Sankar, and S. Gupta, "Analog domain signal processing-based low-power 100-Gb/s DP-QPSK receiver," *Journal of Lightwave Technology*, vol. 33, pp. 3189-3197, 2015.

[5] R. Hui, Z. Benyuan, H. Renxing, C. T. Allen, K. Demarest, and D. Richards, "Subcarrier multiplexing for high-speed optical transmission," *Lightwave Technology, Journal of*, vol. 20, pp. 417-427, 2002.

[6] M. Salter, D. Platt, L. Pettersson, L. Aspemyr, and B. Mingquan, "Circuits and system simulations for 100Gb/s optical SCM transmission," in *Electronics, Circuits, and Systems, 2009. ICECS 2009. 16th IEEE International Conference on*, 2009, pp. 960-963.

[7] G. H. Smith, D. Novak, and Z. Ahmed, "Overcoming chromatic-dispersion effects in fiber-wireless systems incorporating external modulators," *IEEE transactions on microwave theory and techniques*, vol. 45, pp. 1410-1415, 1997.

[8] E. Rochat, P. Kourtessis, M. Webster, T. Quinlan, S. Dudley, S. D. Walker, *et al.*, "Ultra-high capacity transmission over 3 km of legacy 50µm multimode-fibre using C-band HDWDM and quadrature-subcarrier multiplexing," in *Proc. ECOC 2002*, 2002, p. 8.2.

[9] P. M. Anandarajah, Z. Rui, V. Vujicic, M. Deseada Gutierrez Pascual, E. Martin, and L. P. Barry, "Long reach UDWDM PON with SCM-QPSK modulation and direct detection," in *Optical Fiber Communications Conference and Exhibition (OFC), 2014*, 2014, pp. 1-3.

[10] B. Saltzberg, "Performance of an Efficient Parallel Data Transmission System," *IEEE Transactions on Communication Technology*, vol. 15, pp. 805-811, 1967.

[11] B. Farhang-Boroujeny, "OFDM Versus Filter Bank Multicarrier," *IEEE Signal Processing Magazine*, vol. 28, pp. 92-112, 2011.

[12] V. Vujicic, P. M. Anandarajah, C. Browning, and L. P. Barry, "WDM-OFDM-PON Based on Compatible SSB Technique Using a Mode Locked Comb Source," *IEEE Photonics Technology Letters*, vol. 25, pp. 2058-2061, 2013.

[13] Y. B. M'Sallem, Q. T. Le, L. Bramerie, Q. T. Nguyen, E. Borgne, P. Besnard, *et al.*, "Quantum-Dash Mode-Locked Laser as a Source for 56-Gb/s DQPSK Modulation in WDM Multicast Applications," *IEEE Photonics Technology Letters*, vol. 23, pp. 453-455, 2011.

[14] H. A. Haus, "Mode-locking of lasers," *IEEE Journal of Selected Topics in Quantum Electronics*, vol. 6, pp. 1173-1185, 2000.

[15] P. M. Anandarajah, R. Maher, Y. Q. Xu, S. Latkowski, J. O. Carroll, S. G. Murdoch, *et al.*, "Generation of Coherent Multicarrier Signals by Gain Switching of Discrete Mode Lasers," *IEEE Photonics Journal*, vol. 3, pp. 112-122, 2011.

[16] R. Zhou, S. Latkowski, J. O'Carroll, R. Phelan, L. P. Barry, and P. Anandarajah, "40nm wavelength tunable gain-switched optical comb source," *Optics Express*, vol. 19, pp. B415-B420, 2011.

[17] R. Wu, V. Supradeepa, C. M. Long, D. E. Leaird, and A. M. Weiner, "Generation of very flat optical frequency combs from continuous-wave lasers using cascaded intensity and phase modulators driven by tailored radio frequency waveforms," *Optics letters*, vol. 35, pp. 3234-3236, 2010.

[18] T. Sakamoto, T. Kawanishi, and M. Izutsu, "Widely wavelength-tunable ultra-flat frequency comb generation using conventional dual-drive Mach-Zehnder modulator," *Electronics Letters*, vol. 43, p. 1, 2007.

[19] B. P.-P. Kuo, E. Myslivets, V. Ataie, E. G. Temprana, N. Alic, and S. Radic, "Wideband parametric frequency comb as coherent optical carrier," *Journal of Lightwave Technology*, vol. 31, pp. 3414-3419, 2013.

[20] V. Vujicic, P. Anandarajah, R. Zhou, C. Browning, and L. Barry, "Performance investigation of IM/DD Compatible SSB-OFDM systems based on optical multicarrier sources," *IEEE Photonics Journal*, vol. 6, pp. 1-10, 2014.

[21] V. Vujicic, C. Caló, R. Watts, F. Lelarge, C. Browning, K. Merghem, *et al.*, "Quantum Dash Mode-Locked Lasers for Data Centre Applications," *IEEE Journal of Selected Topics in Quantum Electronics*, vol. 21, pp. 53-60, 2015.

Chapter 7

7 Conclusions and Future Work

Optical communications overcame the limited data rates of electrical systems and made possible the development of the Internet. Currently, all high-capacity networks employ optical systems regardless of their reach and purpose. The devices that carry out the interface between the electrical and optical domains are called electro-optical transceivers. These key components can adopt a number of forms and characteristics depending on the network where they are deployed. The signals, modulations, and processing techniques that they employ, must be carefully selected to meet the requirements of a given subsystem.

SCM is a well-known and reliable technique that can be employed in the design of electro-optical transceivers. It divides the available bandwidth into narrower subchannels obtaining high-speed transmission with relevant advantages: baseband signals with reduced bit rate and increased tolerance to dispersion. From an electronics perspective, ASP is preferred to ensure low power consumption and low latency, but a practical industrial implementation would only be possible employing MMIC technology. Accordingly, an SCM electro-optical transceiver relying on off-the-shelf MMIC components has been presented. The key electrical devices, namely the microwave IQ mixers, have been characterized. Off-the-shelf components are designed for radio applications, which do not employ broadband multi-gigabit signals as in optical transmission. As a result, their group delay is not optimized for broadband communications and the highest modulation order that can be reliably achieved is QPSK. In the presented SCM transceiver, five 1.35 Gbaud QPSK subchannels were employed, obtaining 13.5 Gbit/s and a spectral efficiency of 1 bit/s/Hz in the electrical signal. Higher modulation orders would require custom ICs for this particular and demanding application.

Best SCM performance is achieved when it is combined with two techniques: OSSB and carrier suppression. OSSB avoids dispersive fading and allows a closer allocation of WDM channels. Carrier suppression potentially achieves better sensitivities in the receiver. The mathematical study of SCM has been extended by analysing the OIQM, an ideal choice in the transmitter because, unlike other

alternatives, both OSSB and carrier suppression can be obtained directly, without external components, by adjusting the bias points. When the frequency plan ensures that the subchannels are only affected by CTB, CSPR can be modified without adding any additional impairment in the subchannels. When at least one of the subchannels is interfered by CSO, a trade-off between CSPR and NLD is present. A mathematical model has been developed and can be applied to any frequency plan. It can be used to determine the optimum bias point and predict the gains in sensitivity that can be achieved for every subchannel. Experiments have been conducted with a scheme and components that ensure subcarriers are located at multiples of the data rate, which makes it ideal for an accurate study of the effects of intermodulation distortion. The theoretical predictions have been validated measuring CSPR, NLD, and their effect on the performance of channels. The sensitivity gains that can be directly achieved with OIQMs prove the suitability of this device to improve the power budget of SCM/OSSB links without incurring additional costs.

SCM can be combined with WDM to increase the flexibility and the capacity of a network. To allocate closer optical channels, achieving improved spectral efficiency, OSSB signals are required but the performance is limited by the sideband suppression ratio obtained at the electro-optic transmitter. A WDM/SCM link consisting of OSSB signals has been presented. It was based on a state of the art OIQM, and the penalty associated with the residual sideband from the neighbouring optical channel was studied. A suppression ratio of more than 20 dB was achieved directly with the optical modulator without requiring additional optical filters, and a penalty of less than 2 dB in overall performance of the WDM/SCM system was measured due to the associated interference. It can be concluded that, despite the imperfect behaviour of optical modulators generating OSSB signals, a close allocation of WDM channels, which gives rise to a spectrally efficient solution, is feasible and viable avoiding expensive optical filters in the transmitter. Additionally, a fine adjustment of the frequency separation between optical channels can also be employed to ensure optimum performance in these systems, making the peaks of the residual interference coincide with the nulls of the desired subchannels.

The main disadvantage of SCM systems is the low spectral efficiency, especially when it is compared with DSP based implementations. This thesis has proposed a novel technique, referred to as OSCM, which can potentially double the spectral efficiency of traditional all-analogue SCM links by transmitting orthogonally

overlapping subchannels. The concept has been demonstrated in real-time experiments employing up to four 2.7 Gbaud QPSK orthogonal subchannels, with a total rate per optical channel of up to 21.6 Gbit/s and spectral efficiencies of up to 1.78 bit/s/Hz, and relying largely on off-the-shelf components. The technique requires the implementation of FBMC schemes with broadband microwave circuits. With the appropriate microwave filtering, bits sourced at multi-gigabit rates can be pulse shaped, and modulated and demodulated orthogonally without requiring DSP. It has been demonstrated that standard filters can be employed, although the best performance is achieved with custom implementations that match the ideal Nyquist shapes. Additionally, the combination of FBMC signals and SCM permits the transmission of orthogonal subchannels over fibre without requiring a cyclic prefix.

The expected tolerance to dispersion of OSCM/OSSB has also been confirmed. The highest penalty occurs in the subchannel that is most affected by the nonlinearities associated to the combined effect of the optical modulator and the fibre dispersion. A novel synchronization scheme, applicable to both traditional SCM and OSCM, has been introduced. By locating all the subcarriers at harmonics of the data rate, they can be generated with a single device, an electrical comb or SRD. As a consequence, the technique allows the synchronization of any number of practical subchannels requiring only one PLL. Accordingly, this synchronization method presents the lowest number of components of any analogue solution presented to date.

Broadband real-time all-analogue WDM/OSCM schemes have also been demonstrated, achieving a higher spectral efficiency than any previously reported equivalent link. The most relevant features of the described experiments are emphasized below. Firstly, net rates higher than 100 Gbit/s and 400 Gbit/s would be achieved after applying a 7% FEC. Secondly, the compatibility and suitability of OSCM and two different types of OFCs has been proved. GSLs are simple and stable solutions, can be implemented with off-the-shelf components, and achieve a tight allocation of optical channels. MLLs are custom solutions and have stability issues, but they generate a high number of comb lines obtaining higher overall data rates. Finally, the baseband rate used in the experiment was 2.7 Gbit/s, directly compatible with the typical electrical interfaces employed in computing and electro-optical transceivers. The described features ensure that OSCM is a feasible and promising technique to be considered in the design of future WDM electro-optical transceivers.

This section also describes several ideas to extend the concepts that have been studied:

- The thesis has presented a real-time all-analogue broadband SCM link. Off-the-shelf microwave IQ mixers limit the higher modulation order achieved in the system, as detailed in chapter 2. A possible solution consists of employing off-the-shelf microwave low-pass FIR filters to compensate the impairments of these devices. Potentially, the same FIR filters could achieve pulse shaping, IQ mixer equalization and dispersion compensation, obtaining a high-performance SCM/OSCM link with a high modulation order and low power consumption.

- Chapter 3 analysed the case of SCM/OSSB with OIQMs at any bias point, which implies different levels of optical carrier suppression and nonlinear distortion. This study could be extended by comparing thoroughly the OIQM with the DD-MZM in terms of CSPR, NLDs and best achievable sensitivities.

- In chapter 3, a technique to measure accurate CSPR from the photocurrent of the intensity modulated optical signals was provided. In the area of accuracy, this method improves traditional approximations that rely on estimating the area inside the spectrum that can be observed in any optical spectrum analyser. Potentially, a generalized accurate mathematical expression of the CSPR could be provided for FDM, OFDM and FBMC signals as a function of the bandwidth of each subchannel, the optical subchannel to noise ratio, the roll-off factor, and the level of the optical carrier. The validity of the expression could be confirmed experimentally using the technique shown in this project consisting of measuring the photocurrent.

- Spectrally efficient WDM/SCM schemes have been presented in chapter 4. When a closer allocation of OSSB channels is implemented, a source of distortion is the imperfect SSR achieved directly with the optical modulator. An interesting task consists of studying mathematically the impairments in performance as a function of the SSR, the bandwidth of every subchannel and the modulation order. Such a study, if verified with experimental results, would potentially be used to predict

the minimum suppression ratio required in any future WDM/SCM system consisting of OSSB channels. Experimentally, the analysis could be verified obtaining different SSRs with the optical modulator and then measuring performance. These different SSRs could be achieved by biasing some of the optical modulators with phase shifts deviated from the theoretical 90 degrees.

- The OSCM study presented in chapter 5 can be extended. Theoretically, the distortions associated with dispersion for any beta factor and for any microwave filter could be studied obtaining optimum filters for an electro-optical link. A digital implementation with an arbitrary waveform generator and a high speed digital scope could be used to verify the predictions emulating any microwave filter.

- The WDM/OSCM technique has been demonstrated in chapter 6 relying on OFCs, achieving up to 400 Gbit/s transmissions. In practice, MLLs produce a high number of comb lines. Optimizing all the components in the systems, it is possible to use more lines and increase the overall data rate. According to the number of lines generated by semiconductor MLLs, it should be possible to reach 1 Tbit/s with real-time WDM/OSCM implementations.

- All the experiments presented in the thesis have been conducted with direct detection. Coherent OSCM and the associated long-reach transceivers are potentially possible. An option consists of transmitting a pilot tone that is used in the receiver to implement an RF-assisted optical PLL. The same pilot tone could also be used to perform subcarrier synchronization.

- The proposed OSCM scheme can also be applied to radio over fibre systems in the 60 GHz band or beyond. A possible study consists of finding the highest bandwidth per subchannel that can be implemented in such a radio-wireless link. The advantages of microwave FBMC in terms of power consumption and latency would be potentially obtained.

APPENDIX

Appendix A

LO Management and Distribution PCB

This appendix shows the schematics of the PCB that was designed to split, equalize and phase shift the LO signals coming from the electrical comb. All those tasks were performed with MMIC phase shifters, attenuators and amplifiers. The board was supplied with three different voltages: +15V, +8V and -8V.

A.1 Block Diagram

The board splits an incoming LO and performs variable phase shift and variable gain amplification according to the following diagram of blocks:

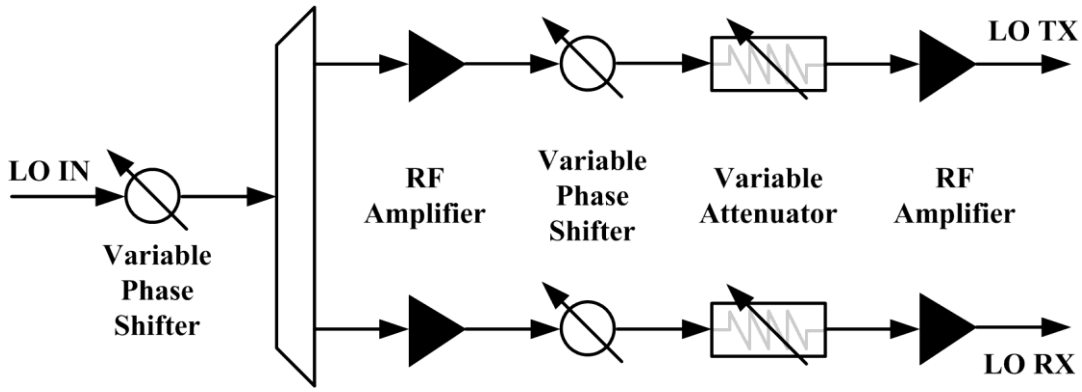

A.2 Schematics

The schematics with all the components of the board are illustrated below.

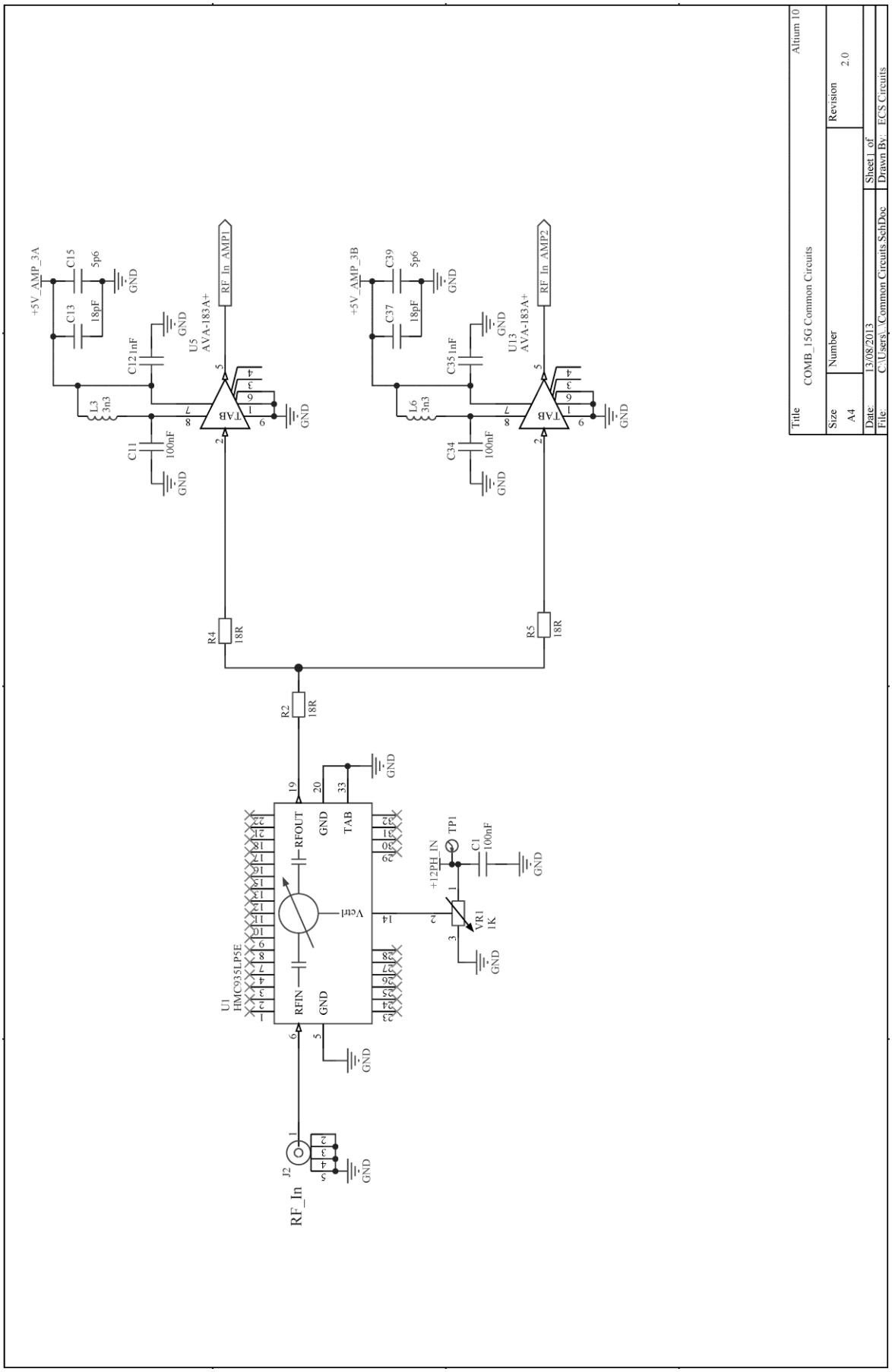
Title
COMB_15G Common Circuits
Altium 10
Size
A4
Number
Revision
2.0
Date
13/08/2013
Sheet 1 of
File
C:\Users\...\Common Circuits.SchDoc
Drawn By:
EC'S Circuits
+5V_AMP_3A
C15
5p6
C13
18pF
C12 1nF
U5
AVA-183A+
RF_In_AMP1
L3
3n3
C11
100nF
+5V_AMP_3B
C39
5p6
C37
18pF
C35 1nF
U13
AVA-183A+
RF_In_AMP2
L6
3n3
C34
100nF
TAB
GND
R4
18R
R5
18R
R2
18R
U1
HMC935LP5E
RFOUT
RFIN
Vctrl
TAB
TP1
+12PH_IN
C1
100nF
VR1
1K
J2
RF_In

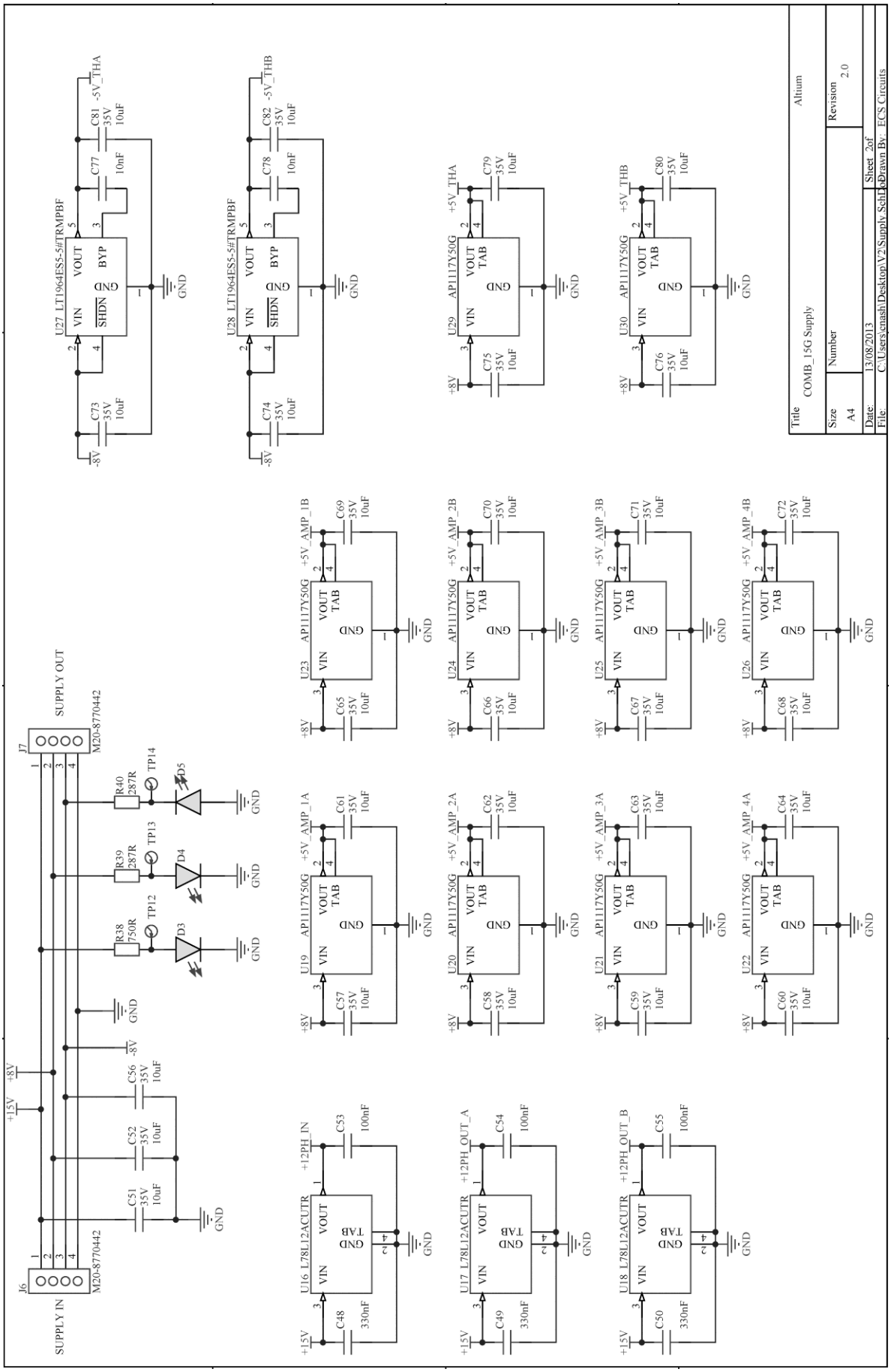
Title
COMB_15G Supply
Altium
Size
A4
Number
Revision
2.0
Date:
13/08/2013
Sheet 2of
File:
C:\Users\cnash\Desktop\V2\Supply Sch.
Drawn By:
ECS Circuits
SUPPLY IN
SUPPLY OUT
J6
J7
M20-8770442
+15V
+8V
-8V
GND
U16 L78L12ACUTR
U17 L78L12ACUTR
U18 L78L12ACUTR
+12PH_IN
+12PH_OUT_A
+12PH_OUT_B
U19 AP1117Y50G
U20 AP1117Y50G
U21 AP1117Y50G
U22 AP1117Y50G
U23 AP1117Y50G
U24 AP1117Y50G
U25 AP1117Y50G
U26 AP1117Y50G
+5V_AMP_1A
+5V_AMP_2A
+5V_AMP_3A
+5V_AMP_4A
+5V_AMP_1B
+5V_AMP_2B
+5V_AMP_3B
+5V_AMP_4B
U27 LT1964ES5-5#TRMPBF
U28 LT1964ES5-5#TRMPBF
-5V_THA
-5V_THB
U29 AP1117Y50G
U30 AP1117Y50G
+5V_THA
+5V_THB
R38 750R
R39 287R
R40 287R
TP12
TP13
TP14
D3
D4
D5

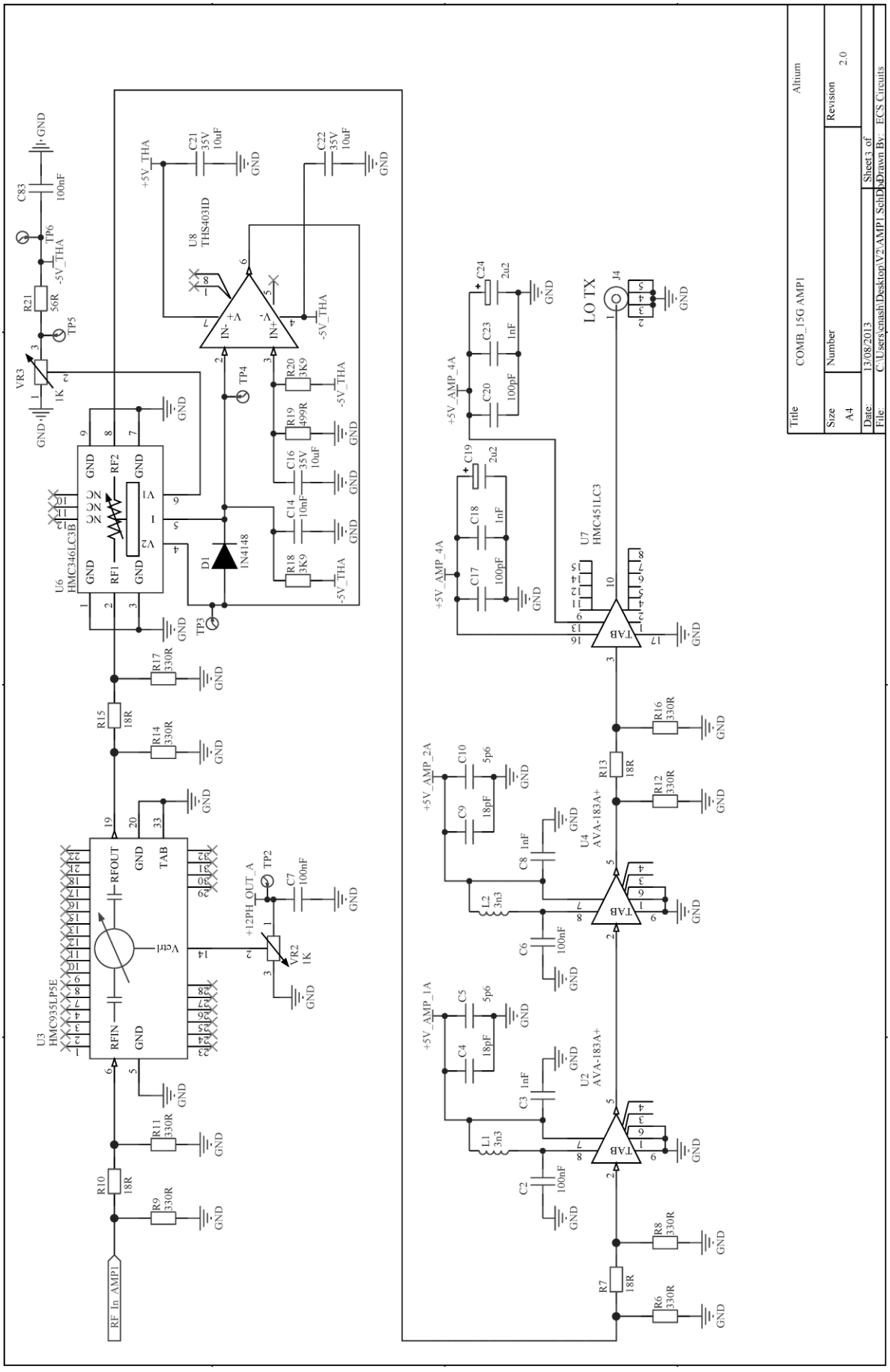
Title COMB_15G AMP1
Altium
Size A4
Number
Revision 2.0
Date: 13/08/2013
Sheet 3 of
File: C:\Users\cnash\Desktop\V2\AMP1.SchDoc
Drawn By: EC'S Circuits
RF_In_AMP1
LO TX
U3 HMC935LP5E
U6 HMC346LC3B
U7 HMC451LC3
U8 THS4031D
U2 AVA-183A+
U4 AVA-183A+
+5V_THA
-5V_THA
+5V_AMP_1A
+5V_AMP_2A
+5V_AMP_4A
+12PH_OUT_A
VR1 1K
VR2 1K
VR3 1K
D1 1N4148

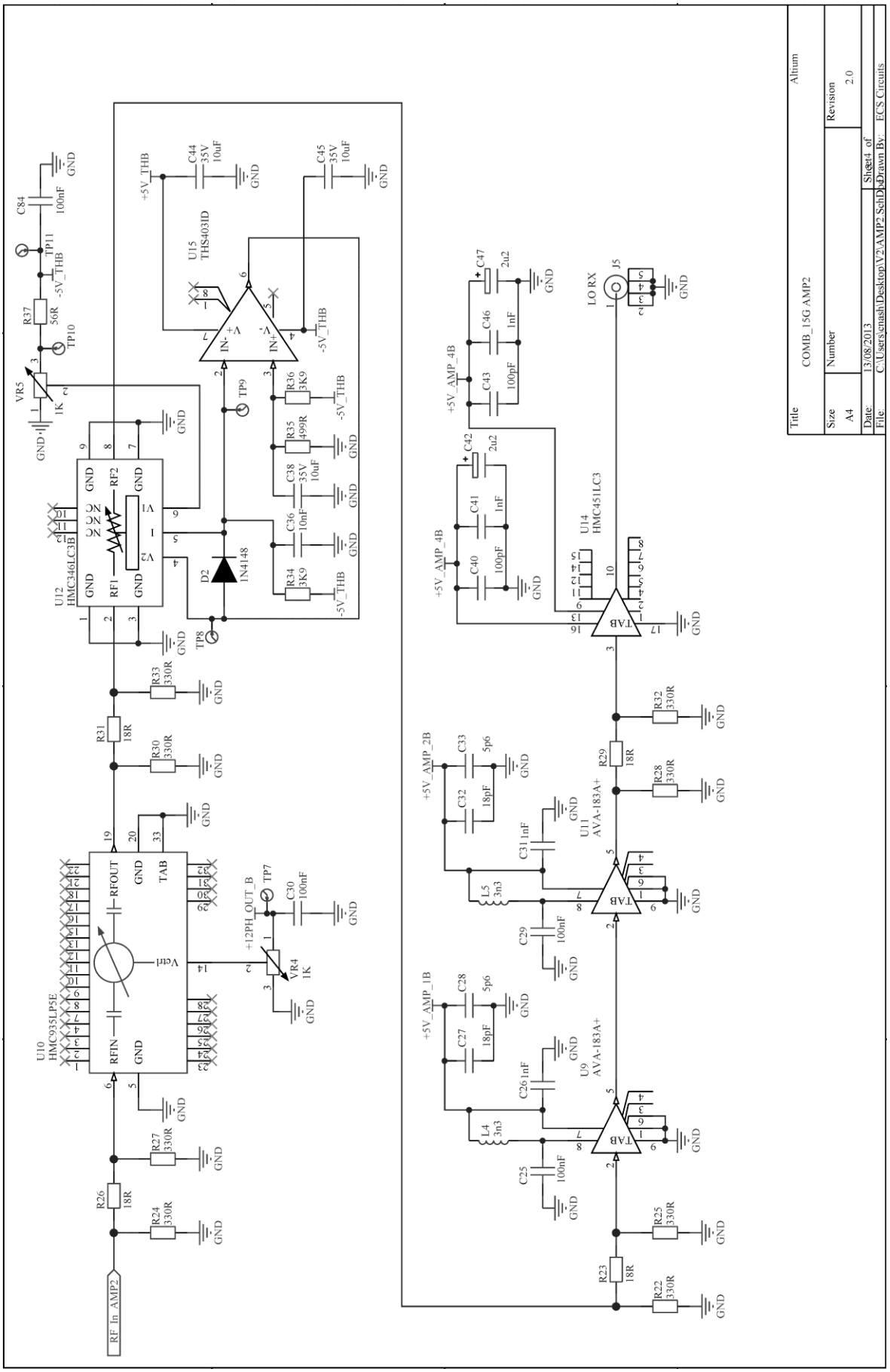
Title
COMB_15G AMP2
Size
A4
Number
Revision
2.0
Date:
13/08/2013
Sheet 4 of
File:
C:\Users\enash\Desktop\V2\AMP2.SchDoc
Drawn By:
ECS Circuits
Altium
RF In AMP2
LO RX
J5
U10 HMC935LP5E
U11 AVA-183A+
U12 HMC346LC3B
U14 HMC451LC3
U15 THS4031D
D2 1N4148
+5V_AMP_1B
+5V_AMP_2B
+5V_AMP_4B
+5V_THB
-5V_THB
+12PH_OUT_B
GND

A.3 Top PCB Print

This is the top layer of the PCB before being populated with components:

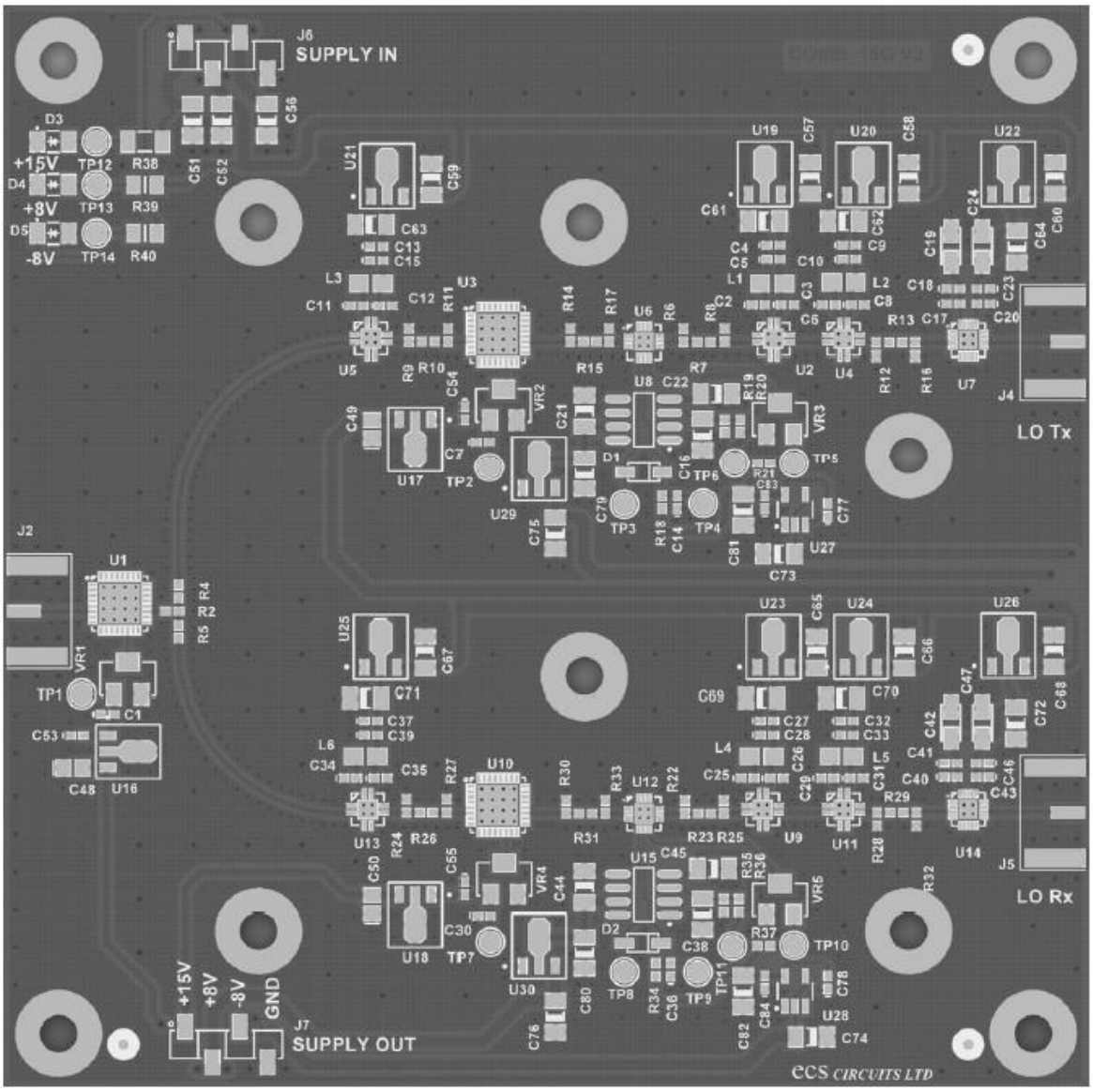

Appendix B

Optical IQ Modulator Equations

This section shows the derivation of the mathematical expressions that are required for the analysis of the trade-off between CSPR and NLD that occurs in an SCM/OSSB link based on an OIQM.

B.1 Output Electrical Field $E_o(t)$

An OIQM is composed of two parallel MZMs whose inputs are fed by the same optical field which is split at the input of the device, and whose outputs go through a third MZM that introduces an additional relative phase shift before recombination. To generate OSSB, the electrical ports of the two parallel MZMs are fed with the desired RF signal and its Hilbert transform (HT) pair respectively. Additionally, the third MZM must introduce a relative phase shift of 90 degrees.

The analysis of the electrical field $E_o(t)$ at the output of the OIQM can be simplified using phasors. The optical carrier at the input is $E_i \cdot e^{j\omega t}$ and the associated phasor is then E_i. For a lossless OIQM, it can considered that the incoming phasor is split into four phasors with equal amplitudes $E_i/4$ and each one goes through a different path as it can be observed in the following picture:

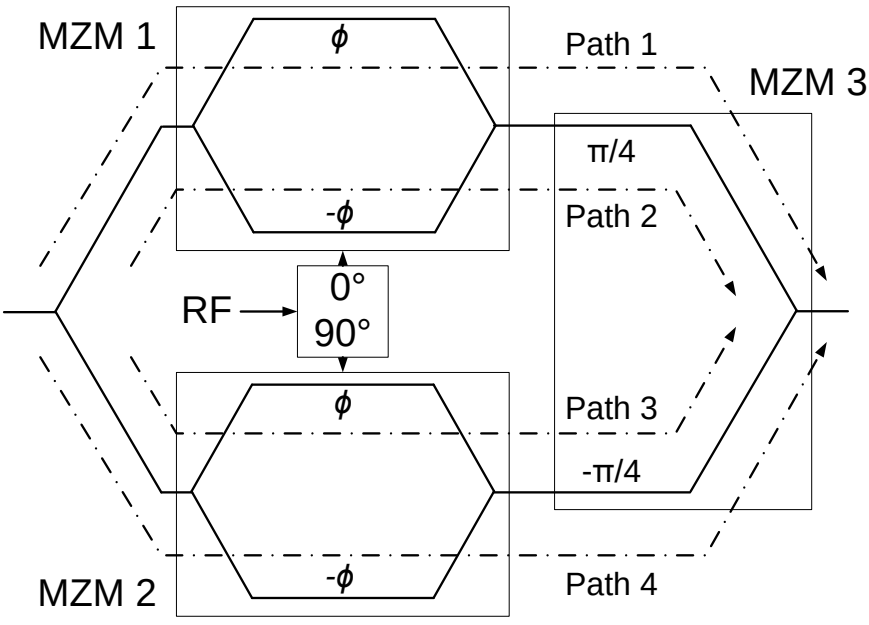

In each arm a different phase is applied. In all the cases a push-pull internal configuration has been considered. The overall relative phase shifts performed by the parallel MZMs, 2ϕ, are determined by the bias voltage V_b with the following expression:

$$\phi = \frac{\pi \cdot V_b}{2V_\pi} \tag{B.1}$$

The overall phase shift of the third modulator must be π/2 for an OSSB configuration. The RF modulating signals are composed of N tones of amplitude V_{AC} and whose frequencies and phases are arbitrary and denoted as Ω_i and θ_i for the i^{th} tone. Thus, the desired signal $s(t)$ and its HT pair $\hat{s}(t)$ are:

$$s(t) = \sum_{i=1}^{N} V_{AC} \cdot \cos\left(\Omega_i t + \theta_i\right). \tag{B.2}$$

$$\hat{s}(t) = \sum_{i=1}^{N} V_{AC} \cdot \cos\left(\Omega_i t + \theta_i - \frac{\pi}{2}\right). \tag{B.3}$$

Thus, the OMI per subcarrier m is defined as:

$$m = \frac{\pi \cdot V_{AC}}{2V_\pi}. \tag{B.4}$$

The contribution of the first path E_1 is:

$$\begin{aligned} E_1 e^{j\omega_c t} &= \frac{E_i}{4} e^{j\left[\omega_c t + \left(\sum_{i=1}^{N} m\cos\left(\Omega_i t + \theta_i\right)\right) + \phi + \frac{\pi}{4}\right]} = \\ &= \frac{E_i}{4}\left(\prod_{i=1}^{N} e^{jm\cos\left(\Omega_i t + \theta_i\right)}\right) \cdot e^{j\left(\phi + \frac{\pi}{4}\right)} \cdot e^{j\omega_c t}. \end{aligned} \tag{B.5}$$

Similarly, the contribution of every phasor at the end of every path can be written as:

$$E_1 = \frac{E_i}{4}\left(\prod_{i=1}^{N} e^{jm\cos\left(\Omega_i t+\theta_i\right)}\right)\cdot e^{j\left(\phi+\frac{\pi}{4}\right)}. \tag{B.6}$$

$$\begin{aligned} E_2 &= \frac{E_i}{4}\left(\prod_{i=1}^{N} e^{-jm\cos\left(\Omega_i t+\theta_i\right)}\right)\cdot e^{j\left(-\phi+\frac{\pi}{4}\right)} = \\ &= \frac{E_i}{4}\left(\prod_{i=1}^{N} e^{jm\cos\left(\Omega_i t+\theta_i-\pi\right)}\right)\cdot e^{j\left(-\phi+\frac{\pi}{4}\right)}. \end{aligned} \tag{B.7}$$

$$E_3 = \frac{E_i}{4}\left(\prod_{i=1}^{N} e^{jm\cos\left(\Omega_i t+\theta_i-\frac{\pi}{2}\right)}\right)\cdot e^{j\left(+\phi-\frac{\pi}{4}\right)}. \tag{B.8}$$

$$\begin{aligned} E_4 &= \frac{E_i}{4}\left(\prod_{i=1}^{N} e^{-jm\cos\left(\Omega_i t+\theta_i-\frac{\pi}{2}\right)}\right)\cdot e^{j\left(-\phi-\frac{\pi}{4}\right)} = \\ &= \frac{E_i}{4}\left(\prod_{i=1}^{N} e^{jm\cos\left(\Omega_i t+\theta_i-\frac{3\pi}{2}\right)}\right)\cdot e^{j\left(-\phi-\frac{\pi}{4}\right)}. \end{aligned} \tag{B.9}$$

The resultant phasor at the output is:

$$E = E_1 + E_2 + E_3 + E_4. \tag{B.10}$$

The terms inside the products can be expanded with Bessel functions according to the Jacobi-Anger expansion:

$$e^{jm\cos\left(\Omega t+\varphi\right)} = \sum_{r=-\infty}^{+\infty} e^{jr\frac{\pi}{2}} J_r\left(m\right) e^{jr\Omega t} e^{jr\varphi}, \tag{B.11}$$

where $J_r(m)$ stands for the r^{th} order Bessel function of the first kind.

Adding all the terms required to obtain the total contribution of any fundamental tone, harmonic or intermodulation product $E_{k1,k2...kN}$ whose frequency is $(\omega_c+k_1\Omega_1+k_2\Omega_2+\ldots+k_N\Omega_N)$, where $k_1,k_2,\ldots,k_N$ are arbitrary integer numbers reflecting the nature of the signal in question, the total contribution from the four paths is given by the following expression:

$$E_{k_1,k_2,\ldots k_N} = \frac{E_i}{4}\cdot\left(\prod_{i=1}^{N} J_{k_i}(m)\right)\cdot e^{j\left(\sum_{i=1}^{N} k_i\theta_i\right)}\cdot \left(\begin{array}{l} e^{j\left(\phi+\frac{\pi}{4}+\frac{\pi}{2}\cdot\sum_{i=1}^{N}k_i\right)}+e^{j\left(-\phi+\frac{\pi}{4}-\frac{\pi}{2}\cdot\sum_{i=1}^{N}k_i\right)}+e^{j\left(\phi-\frac{\pi}{4}\right)}+e^{j\left(-\phi-\frac{\pi}{4}-\pi\cdot\sum_{i=1}^{N}k_i\right)} \end{array}\right). \quad \text{(B.12)}$$

Extracting a common factor:

$$E_{k_1,k_2,\ldots k_N} = \frac{E_i}{4}\cdot\left(\prod_{i=1}^{N} J_{k_i}(m)\right)\cdot e^{j\left(\sum_{i=1}^{N} k_i\theta_i\right)} e^{-j\left(\frac{\pi}{4}\cdot\sum_{i=1}^{N}k_i\right)}\cdot \left(\begin{array}{l} e^{j\left(\phi+\frac{\pi}{4}+\frac{3\pi}{4}\cdot\sum_{i=1}^{N}k_i\right)}+e^{j\left(-\phi+\frac{\pi}{4}-\frac{\pi}{4}\cdot\sum_{i=1}^{N}k_i\right)}+ \\ e^{j\left(\phi-\frac{\pi}{4}+\frac{\pi}{4}\cdot\sum_{i=1}^{N}k_i\right)}+e^{j\left(-\phi-\frac{\pi}{4}-\frac{3\pi}{4}\cdot\sum_{i=1}^{N}k_i\right)} \end{array}\right). \quad \text{(B.13)}$$

According to Euler's formula, the previous equation becomes:

$$E_{k_1,k_2,\ldots k_N} = \frac{E_i}{4}\cdot\left(\prod_{i=1}^{N} J_{k_i}(m)\right)\cdot e^{j\left(\sum_{i=1}^{N} k_i\left(\theta_i-\frac{\pi}{4}\right)\right)}\cdot \left(2\cos\left(\phi+\frac{\pi}{4}+\frac{3\pi}{4}\cdot\sum_{i=1}^{N}k_i\right)+2\cos\left(\phi-\frac{\pi}{4}+\frac{\pi}{4}\cdot\sum_{i=1}^{N}k_i\right)\right). \quad \text{(B.14)}$$

Applying the identity cos(u)+cos(v)=2cos((u+v)/2)cos((u-v)/2):

$$E_{k_1,k_2,\ldots,k_n} = E_i \cdot \left(\prod_{i=1}^{N} J_{k_i}(m) \right) \cdot \cos\left(\frac{\pi}{4} \left(1 + \sum_{i=1}^{N} k_i \right) \right) \cdot \cos\left(\phi + \frac{\pi}{2} \left(\sum_{i=1}^{N} k_i \right) \right) \cdot \prod_{i=1}^{N} e^{j\left(k_i \left(\theta_i - \frac{\pi}{4} \right) \right)}. \quad \text{(B.15)}$$

As the development has dealt with phasors, the final contribution of any frequency component $E_{o\_k1,k2\ldots kN}(t)$ can be written as:

$$E_{o\_k_1,k_2,\ldots k_N}(t) = \mathrm{Re}\left\{ E_{k_1,k_2,\ldots k_N} \cdot e^{j\left(\omega_c + \sum_{i=1}^{N} k_i \Omega_i \right) t} \right\} = E_i \cdot \left(\prod_{i=1}^{N} J_{k_i}(m) \right) \cdot \cos\left(\frac{\pi}{4} \left(1 + \sum_{i=1}^{N} k_i \right) \right) \cdot \cos\left(\phi + \frac{\pi}{2} \left(\sum_{i=1}^{N} k_i \right) \right) \cdot \cos\left(\left(\omega_c + \sum_{i=1}^{N} k_i \Omega_i \right) t + \sum_{i=1}^{N} k_i \left(\theta_i - \frac{\pi}{4} \right) \right). \quad \text{(B.16)}$$

Note that the configuration of the phases in the origin gives rise to a lower single side band signal. Also, the value of *m* usually meets the following property: $m << 1$.

Any fundamental tone, harmonic product, or intermodulation product can be derived from eq. (B.16). The nonlinear distortion can be obtained as the power ratio between any harmonic or intermodulation product and a desired tone. The most meaningful values are presented in Table 3-2.

B.2 Output Photo-Current $I_o(t)$

B.2.1 Analytical Expression

To calculate the associated photo-current at the output of the OIQM, $I_o(t)$, an analytical expression for the electrical field $E_o(t)$ must firstly be obtained. NLD in $I_o(t)$ will be the same regardless the OSSB configuration that it is employed, upper side band or lower side band.

The parameters defined in the previous subsection are employed. Without losing generality, it will be considered that the electrical field at the input of the OIQM is $E_i \cdot \cos(\omega_c t - \pi/4)$. The electrical fields at the output of the parallel MZMs, $E_{MZM\_I}(t)$ and $E_{MZM\_Q}(t)$, when they are biased at the same point can be expressed as:

$$E_{MZM_I}(t) = \frac{E_i}{\sqrt{2}}\left(\cos\left(m \cdot s(t) + \phi\right)\right)\cos\left(\omega_c t - \frac{\pi}{4}\right). \quad \text{(B.17)}$$

$$E_{MZM_Q}(t) = \frac{E_i}{\sqrt{2}}\left(\cos\left(m \cdot \hat{s}(t) + \phi\right)\right)\cos\left(\omega_c t - \frac{\pi}{4}\right). \quad \text{(B.18)}$$

The third MZM induces a relative phase shift of 90 degrees (+π/4,-π/4) before recombination. Therefore, the total field at the output of the OIQM is given by:

$$E_o(t) = \frac{E_i}{2}\left(\left(\cos(m \cdot s(t) + \phi)\right) \cdot \cos\left(\omega_c t\right) + \left(\cos(m \cdot \hat{s}(t) + \phi)\right) \cdot \sin\left(\omega_c t\right)\right). \quad \text{(B.19)}$$

Now the following equality will be applied:

$$A\cos\left(\omega_c t\right) + B\sin\left(\omega_c t\right) = \sqrt{A^2 + B^2}\,\cos\left(\omega_c t - \tan^{-1}\left(\frac{B}{A}\right)\right). \quad \text{(B.20)}$$

Resulting in:

$$E_o(t) = \frac{E_i}{2}\left(\sqrt{\left(\cos(m \cdot s(t) + \phi)\right)^2 + \left(\cos(m \cdot \hat{s}(t) + \phi)\right)^2} \cdot \cos\left(\omega_c t - \tan^{-1}\left(\varphi\right)\right)\right). \quad \text{(B.21)}$$

The phase φ depends on *m*, *s(t)* and ϕ, but it has not been written out because it will not have any influence in the photocurrent. The associated photocurrent is equal to the mean square value of the electric field. This can be obtained squaring $E_o(t)$ and removing the frequency terms at $2\omega_c$:

$$I_o(t) = \left\langle E_o^2(t) \right\rangle = \frac{E_i^2}{8}\left(\left(\cos(m \cdot s(t) + \phi)\right)^2 + \left(\cos(m \cdot \hat{s}(t) + \phi)\right)^2\right). \quad \text{(B.22)}$$

After a basic manipulation, the final result is:

$$I_o(t) = \frac{E_i^2}{8}\left(1 + \frac{1}{2}\cos(2m \cdot s(t) + 2\phi) + \frac{1}{2}\cos(2m \cdot \hat{s}(t) + 2\phi)\right). \quad \text{(B.23)}$$

B.2.2 Bessel Expansion

B.2.2.1 Global Expression

To calculate the frequency components and NLD at the output photocurrent of an OIQM that is generating OSSB, it is necessary to process the Bessel expansion of the sinusoidal terms in eq. (B.23). The expression to expand can be reduced to:

$$I_o^{'}(t)=\cos\left(2m\cdot\sum_{i=1}^{N}\left(\cos\left(\Omega_i t+\theta_i\right)\right)+2\phi\right)+\cos\left(2m\cdot\sum_{i=1}^{N}\cos\left(\Omega_i t+\theta_i-\frac{\pi}{2}\right)+2\phi\right). \quad \text{(B.24)}$$

Applying the equality cos(u+v)=cos(u)cos(v)-sin(u)sin(v), the result is:

$$\begin{aligned} I_o^{'}(t)=&\cos\left(2m\cdot\sum_{i=1}^{N}\cos\left(\Omega_i t+\theta_i\right)\right)\cdot\cos\left(2\phi\right)\\ &-\sin\left(2m\cdot\sum_{i=1}^{N}\cos\left(\Omega_i t+\theta_i\right)\right)\cdot\sin\left(2\phi\right)\\ &+\cos\left(2m\cdot\sum_{i=1}^{N}\cos\left(\Omega_i t+\theta_i-\frac{\pi}{2}\right)\right)\cdot\cos\left(2\phi\right)\\ &-\sin\left(2m\cdot\sum_{i=1}^{N}\cos\left(\Omega_i t+\theta_i-\frac{\pi}{2}\right)\right)\cdot\sin\left(2\phi\right). \end{aligned} \quad \text{(B.25)}$$

Applying Euler's formulas:

$$\begin{aligned} I_o^{'}(t)=&\frac{e^{j2m\sum_{i=1}^{N}\cos\left(\Omega_i t+\theta_i\right)}+e^{-j2m\sum_{i=1}^{N}\cos\left(\Omega_i t+\theta_i\right)}}{2}\cdot\cos\left(2\phi\right)\\ &-\frac{e^{j2m\sum_{i=1}^{N}\cos\left(\Omega_i t+\theta_i\right)}-e^{-j2m\sum_{i=1}^{N}\cos\left(\Omega_i t+\theta_i\right)}}{2j}\cdot\sin\left(2\phi\right)\\ &+\frac{e^{j2m\sum_{i=1}^{N}\cos\left(\Omega_i t+\theta_i-\frac{\pi}{2}\right)}+e^{-j2m\sum_{i=1}^{N}\cos\left(\Omega_i t+\theta_i-\frac{\pi}{2}\right)}}{2}\cdot\cos\left(2\phi\right)\\ &-\frac{e^{j2m\sum_{i=1}^{N}\cos\left(\Omega_i t+\theta_i-\frac{\pi}{2}\right)}-e^{-j2m\sum_{i=1}^{N}\cos\left(\Omega_i t+\theta_i-\frac{\pi}{2}\right)}}{2j}\cdot\sin\left(2\phi\right). \end{aligned} \quad \text{(B.26)}$$

After some manipulation, previous equation becomes:

$$
\begin{aligned}
I_o^{'}(t) = & \frac{\prod_{i=1}^{N} e^{j2m\cdot\cos\left(\Omega_i t+\theta_i\right)} + \prod_{i=1}^{N} e^{j2m\cdot\cos\left(\Omega_i t+\theta_i+\pi\right)}}{2}\cdot\cos\left(2\phi\right) \\
& - \frac{\prod_{i=1}^{N} e^{j2m\cdot\cos\left(\Omega_i t+\theta_i\right)} - \prod_{i=1}^{N} e^{j2m\cdot\cos\left(\Omega_i t+\theta_i+\pi\right)}}{2j}\cdot\sin\left(2\phi\right) \\
& + \frac{\prod_{i=1}^{N} e^{j2m\cdot\cos\left(\Omega_i t+\theta_i-\frac{\pi}{2}\right)} + \prod_{i=1}^{N} e^{j2m\cdot\cos\left(\Omega_i t+\theta_i+\frac{\pi}{2}\right)}}{2}\cdot\cos\left(2\phi\right) \\
& - \frac{\prod_{i=1}^{N} e^{j2m\cdot\cos\left(\Omega_i t+\theta_i-\frac{\pi}{2}\right)} - \prod_{i=1}^{N} e^{j2m\cdot\cos\left(\Omega_i t+\theta_i+\frac{\pi}{2}\right)}}{2j}\cdot\sin\left(2\phi\right).
\end{aligned}
\tag{B.27}
$$

With the previous equation, the Bessel expansion is reduced to analyse one expression and then substitute for the different frequencies and phases in eq. (B.27). Such an expression is the Jacobi-Anger expansion, shown in eq. (B.11).

B.2.2.2 Individual Terms Deduction

The important terms will be derived in this subsection. Every term inside the products in eq. (B.27) is expanded with Bessel functions according to eq. (B.11). Initially, the analysis focuses on the first product. That product is expanded as follows (for a case with $N > 3$):

$$
\begin{aligned}
\prod_{i=1}^{N} e^{j2m\cdot\cos\left(\Omega_i t+\theta_i\right)} = & \left(\sum_{p=-\infty}^{+\infty} e^{jp\frac{\pi}{2}} J_p\left(2m\right) e^{jp\Omega_1 t} e^{jp\theta_1}\right)\cdot \\
& \cdot\left(\sum_{q=-\infty}^{+\infty} e^{jq\frac{\pi}{2}} J_q\left(2m\right) e^{jq\Omega_2 t} e^{jq\theta_2}\right)\cdot \\
& \cdots\cdots \\
& \cdot\left(\sum_{r=-\infty}^{+\infty} e^{jr\frac{\pi}{2}} J_r\left(2m\right) e^{jr\Omega_N t} e^{jr\theta_N}\right).
\end{aligned}
\tag{B.28}
$$

To obtain the first harmonic of the first subcarrier, only the following sub-indexes must be considered: p=+1 and p=-1, and the rest of the sub-indexes equal to zero. The partial solution for the first harmonic would be:

$$\begin{aligned} I''_{1st\_harmonic}(t) = \\ = \left(e^{-j\frac{\pi}{2}} J_{-1}(2m) e^{-j\Omega_1 t} e^{-j\theta_1} + e^{j\frac{\pi}{2}} J_1(2m) e^{j\Omega_1 t} e^{j\theta_1} \right) \cdot J_0^{N-1}(2m) = \\ = j2 J_0^{N-1}(2m) J_1(2m) \cos(\Omega_1 t + \theta_1). \end{aligned} \quad \text{(B.29)}$$

For the previous derivation, and for the subsequent that take place in this section, the following relation is required:

$$J_{-n}(z) = (-1)^n \cdot J_n(z). \quad \text{(B.30)}$$

The result obtained in equation (B.29) is the most general, but it can be immediately modified to obtain all the terms that are required in eq. (B.27), just substituting θ_1 with the required phases. Substituting all these terms and resolving eq. (B.27), the value of the first harmonic in the output photocurrent of the OIQM is obtained. All the constant multipliers that were shown in eq. (B.23) are now taken into account and the final result is:

$$I_{1st\_harmonic}(t) = -E_i^2 \frac{\sqrt{2}}{8} J_o^{N-1}(2m) J_1(2m) \sin(2\phi) \cos\left(\Omega_1 t + \theta_1 - \frac{\pi}{4} \right). \quad \text{(B.31)}$$

For the second harmonic, only the following sub-indexes must be considered: p=+2 and p=-2, and the rest of the sub-indexes equal to zero. The partial and the final solutions for the second harmonic are:

$$\begin{aligned} I''_{2nd\_harmonic}(t) &= -2 J_0^{N-1}(2m) J_2(2m) \cos(2\Omega_1 t + 2\theta_1). \\ I_{2nd\_harmonic}(t) &= 0. \end{aligned} \quad \text{(B.32)}$$

For the third harmonic, only the following sub-indexes must be considered: p=+3 and p=-3, and the rest of the sub-indexes equal to zero. The partial and the final solutions for the third harmonic are:

$$\begin{aligned} &I''_{3rd\_harmonic}(t) = -j2J_0^{N-1}(2m)J_3(2m)\cos(3\Omega_1 t + 3\theta_1). \\ &I_{3rd\_harmonic}(t) = E_i^2\frac{\sqrt{2}}{8}J_o^{N-1}(2m)J_3(2m)\sin(2\phi)\cos\left(3\Omega_1 t + 3\theta_1 + \frac{\pi}{4}\right). \end{aligned} \tag{B.33}$$

For the second order intermodulation, only the following sub-indexes must be considered: p=+1 and p=-1, q=+1 and q=-1, and the rest of the sub-indexes equal to zero. The partial and the final solutions for the second order intermodulation are:

$$\begin{aligned} &I''_{2nd\_IMD}(t) = -2J_0^{N-2}(2m)J_1^2(2m)\begin{bmatrix}\cos\left((\Omega_1+\Omega_2)t+\theta_1+\theta_2\right)\\ +\cos\left((\Omega_1-\Omega_2)t+\theta_1-\theta_2\right)\end{bmatrix}. \\ &I_{2nd\_IMD\_(\Omega_1+\Omega_2)}(t) = 0. \\ &I_{2nd\_IMD\_(\Omega_1-\Omega_2)}(t) = \\ &\qquad = -E_i^2\frac{1}{4}J_o^{N-2}(2m)J_1^2(2m)\cos(2\phi)\cos\left((\Omega_1-\Omega_2)t+\theta_1-\theta_2\right). \end{aligned} \tag{B.34}$$

For the third order intermodulation, only the following sub-indexes must be considered: p=+1 and p=-1, q=+2 and q=-2, and the rest of the sub-indexes equal to zero. The partial and the final solutions for the third order intermodulation are:

$$\begin{aligned} &I''_{3rd\_IMD}(t) = -j2J_0^{N-2}(2m)J_1(2m)J_2(2m)\begin{bmatrix}\cos\left((\Omega_1+2\Omega_2)t+\theta_1+2\theta_2\right)\\ +\cos\left((\Omega_1-2\Omega_2)t+\theta_1-2\theta_2\right)\end{bmatrix}. \\ &I_{3rd\_IMD\_(\Omega_1+2\Omega_2)}(t) = \\ &E_i^2\frac{\sqrt{2}}{8}J_0^{N-2}(2m)J_1(2m)J_2(2m)\sin(2\phi)\cos\left((\Omega_1+2\Omega_2)t+\theta_1+2\theta_2+\frac{\pi}{4}\right). \\ &I_{3rd\_IMD\_(\Omega_1-2\Omega_2)}(t) = \\ &E_i^2\frac{\sqrt{2}}{8}J_0^{N-2}(2m)J_1(2m)J_2(2m)\sin(2\phi)\cos\left((\Omega_1-2\Omega_2)t+\theta_1-2\theta_2+\frac{\pi}{4}\right). \end{aligned} \tag{B.35}$$

Finally, for the triple beat, only the following sub-indexes must be considered: p=+1 and p=-1, q=+1 and q=-1, r=+1 and r=-1, and the rest of the sub-indexes equal to zero. The partial and the final solutions for the third order intermodulation products are:

$$I''_{triple\_beat}(t) = -j2J_0^{N-3}(2m)J_1^3(2m)\begin{bmatrix}\cos\left((\Omega_1+\Omega_2+\Omega_3)t+\theta_1+\theta_2+\theta_3\right)\\+\cos\left((\Omega_1-\Omega_2+\Omega_3)t+\theta_1-\theta_2+\theta_3\right)\\+\cos\left((\Omega_1-\Omega_2-\Omega_3)t+\theta_1-\theta_2-\theta_3\right)\\+\cos\left((\Omega_1+\Omega_2-\Omega_3)t+\theta_1+\theta_2-\theta_3\right)\end{bmatrix}.$$

$$I_{triple\_beat\_(\Omega_1+\Omega_2+\Omega_3)}(t) =$$

$$E_i^2\frac{\sqrt{2}}{8}J_0^{N-3}(2m)J_1^3(2m)\sin(2\phi)\cos\left((\Omega_1+\Omega_2+\Omega_3)t+\theta_1+\theta_2+\theta_3+\frac{\pi}{4}\right).$$

$$I_{triple\_beat\_(\Omega_1-\Omega_2+\Omega_3)}(t) =$$

$$-E_i^2\frac{\sqrt{2}}{8}J_0^{N-3}(2m)J_1^3(2m)\sin(2\phi)\cos\left((\Omega_1-\Omega_2+\Omega_3)t+\theta_1-\theta_2+\theta_3-\frac{\pi}{4}\right).$$

$$I_{triple\_beat\_(\Omega_1-\Omega_2-\Omega_3)}(t) =$$

$$E_i^2\frac{\sqrt{2}}{8}J_0^{N-3}(2m)J_1^3(2m)\sin(2\phi)\cos\left((\Omega_1-\Omega_2-\Omega_3)t+\theta_1-\theta_2-\theta_3+\frac{\pi}{4}\right).$$

$$I_{triple\_beat\_(\Omega_1+\Omega_2-\Omega_3)}(t) =$$

$$-E_i^2\frac{\sqrt{2}}{8}J_0^{N-3}(2m)J_1^3(2m)\sin(2\phi)\cos\left((\Omega_1+\Omega_2-\Omega_3)t+\theta_1+\theta_2-\theta_3-\frac{\pi}{4}\right). \quad \text{(B.36)}$$

When all the terms are derived, the nonlinear distortion can be obtained as the power ratio between any harmonic or intermodulation product and a desired tone. The most meaningful values of nonlinear distortion are shown in Table 3-3. In the calculations of the intermodulation products contributions, it should be noted that only one of every two potential combinations of frequencies is obtained. As an example, focusing on triple beat in eq. (B.36), the mixing of 3 frequencies generate 8 potential combinations, but only 4 are present in the output. The eight possibilities are represented by four pairs, and each pair is formed by a set of mixing frequencies and the opposite one. Only one of the realizations of every pair appears in the output. This fact must be taken into account when counting intermodulation product numbers like N_{CSO} and N_{CTB} (see Table 3-1).

Another important component that can be obtained with the previous analysis is the DC term in the photocurrent. With that purpose, and from eq. (B.28), all the sub-indexes must be equal to zero: p=0, q=0, …. and r=0. The partial result must be introduced in eq. (B.27) and then in eq. (B.23) to obtain the final value:

$$I_{DC} = \frac{E_i^2}{8}\left(1 + J_0^N(2m)\cos(2\phi)\right). \tag{B.37}$$

The previous value is the DC term that arises when the electric field is squared and the optical carrier and the fundamental tones are multiplied by themselves. However, more terms can fall at DC, but those would be the result of NLD and, in general, will be small in comparison with the DC component obtained as a consequence of the optical carrier.

B.3 Optimum Bias Point

This subsection shows the mathematical derivation of the minimum achievable sensitivity for a desired quality factor Q_F in a SCM/OSSB link based on an optical IQ modulator, a pre-amplified receiver (see Figure 3.5) and N QPSK subchannels.

The receiver consists of an EDFA whose gain is G, a photo-detector whose responsivity is R and an RF demodulator. The average optical power at the input of the receiver can be obtained as the DC component of the associated photocurrent for responsivity equal to 1. From eq. (B.37), and normalizing E_i=1:

$$P_{IN} = \frac{1}{8}\left(1 + J_0^N(2m)\cos(2\phi)\right). \tag{B.38}$$

The amplitude of the kth electrical subcarrier at the detected photocurrent can be obtained from eq. (B.31):

$$A_k = RG\frac{\sqrt{2}}{8} J_0^{N-1}(2m) J_1(2m)\sin(2\phi). \tag{B.39}$$

To calculate the sensitivity of the link, the detected photocurrent must be written making P_{IN} an independent variable:

$$I = RGP_{IN}\left(1+\sum_{k=1}^{N} I_{\phi}\cos(\Omega_k t+\theta_k)+NLD\right) \tag{B.40}$$

where Ω_k and θ_k is the frequency and phase of the k^{th} subcarrier and I_ϕ represents the dependency of the amplitude of the subcarrier on the bias point:

$$I_{\phi} = \frac{\sqrt{2}J_0^{N-1}(2m)J_1(2m)\sin(2\phi)}{1+J_0^N(2m)\cos(2\phi)}. \tag{B.41}$$

Thus, the amplitude of the k^{th} subcarrier can be written as:

$$I_k = RGP_{IN}I_{\phi}. \tag{B.42}$$

In the described link, neglecting NLD, the main source of noise will be amplified spontaneous emission (ASE) coming from the EDFA. After demodulation the contribution of this noise will be [1]:

$$\sigma_{ASE}^2 = 2R^2P_{IN}G(G-1)Fh\nu B_e \tag{B.43}$$

where F is the noise figure of the EDFA, h is Planck's constant, ν is the optical frequency and B_e is the electrical bandwidth of the baseband channel at the receiver. Under a Gaussian approximation the time averaged second and third order intermodulation current power [2, 3] is added like noise as in [4]. Thus, from eq. (3.7), the absolute contribution of NLD is:

$$\sigma_{NLD}^2 = \sigma_{CSO}^2+\sigma_{CTB}^2 = \left(N_{CSO}\frac{IMD_2}{2}+N_{CTB}\frac{IMD_{3B}}{2}\right)I_K^2. \tag{B.44}$$

The quality factor Q_F after the RF demodulator for a SCM/QPSK system is obtained substituting in eq. (2.38):

$$Q_F = \frac{\sqrt{2}I_K}{2(\sqrt{\sigma_{ASE}^2 + \sigma_{NLD}^2})}. \tag{B.45}$$

After some manipulations and for G>>1, the minimum achievable sensitivity for a desired value of Q_F can be deduced as:

$$P_{IN} = \frac{4Q_F^2 FhvB_e}{I_\phi^2\left(1 - Q_F^2\left(N_{CSO}IMD_2 + N_{CTB}IMD_{3B}\right)\right)}. \tag{B.46}$$

B.4 References

[1] R. Hui, Z. Benyuan, H. Renxing, C.T. Allen, K. Demarest, D. Richards, Subcarrier multiplexing for high-speed optical transmission, Lightwave Technology, Journal of, 20 (2002) 417-427.

[2] R. Olshansky, "Optimal design of subcarrier multiplexed lightwave systems employing linearized external modulators," J. Lightw. Technol., vol. 10, no. 3, pp. 378–382, Mar. 1992.

[3] F. Ramos and J. Marti, "Compensation for fiber-induced composite second-order distortion in externally modulated lightwave AM-SCM systems using optical-phase conjugation," J. Lightw. Technol., vol. 16, no. 8, pp. 1387–1392, Aug. 1998.

[4] P. Laurencio, S. O. Simoes, and M. C. R. Medeiros, "Impact of the combined effect of RIN and intermodulation distortion on OSSB/SCM systems," J. Lightw. Tech., vol. 24, no. 11, pp. 4250–4262, Nov. 2006.

Appendix C

Phase Alignment in Microwave FBMC

This section details a simplified technique to achieve the orthogonal phase alignment in a microwave FBMC transmission system, equivalent to the one presented in Chapter 5.

C.1 FBMC Scheme

The original FBMC scheme developed in [1], where the bit period is T and the angular data frequency is ω_r, is shown below:

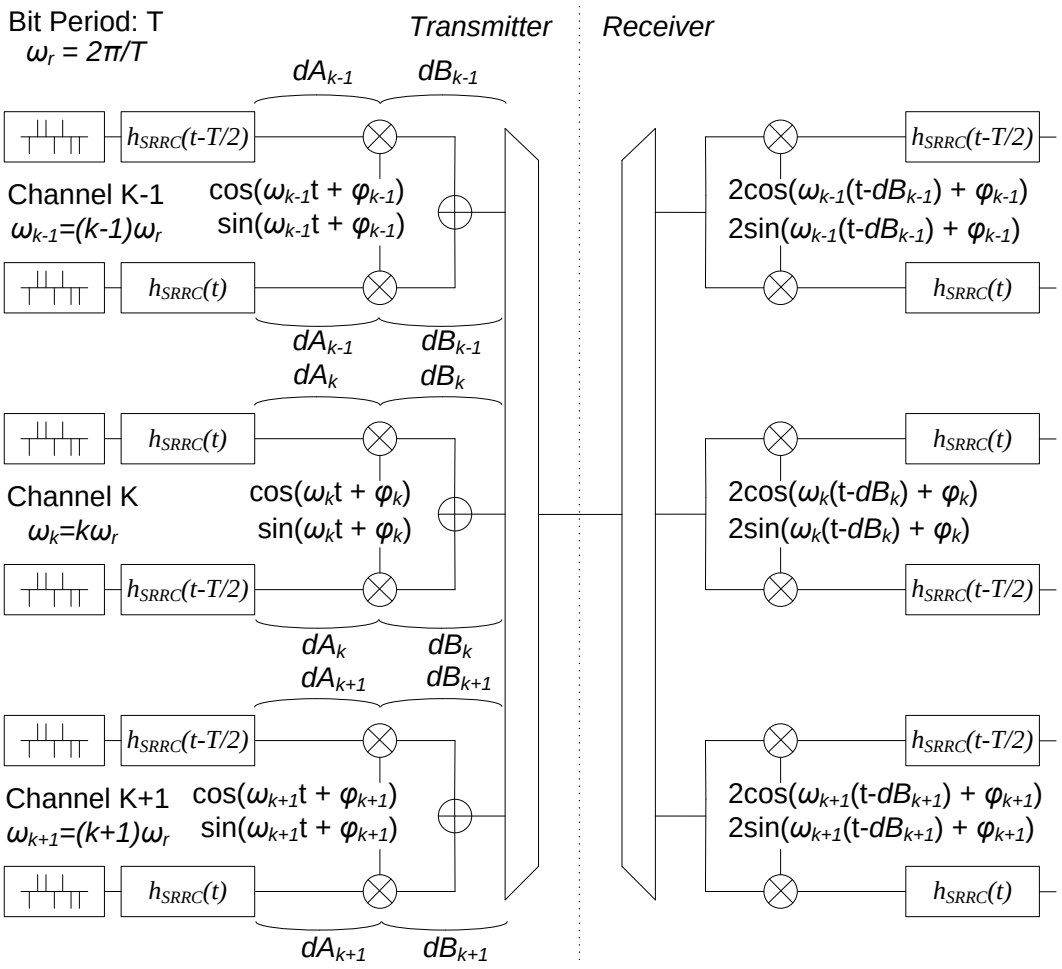

The delays that can be found in the transmitter in any real microwave implementation are also included in the figure. For the i^{th} frequency band, where i is an integer that can present three consecutive values (k-1, k, k+1) and whose subcarrier frequency is $i \cdot \omega_r$: the term dA_i accounts for any delay of the baseband pair

prior to the IQ mixing, dB_i represents the delay after the mixing and before the overall combination of subchannels, and φ_i is the phase shift in the LO with respect to the ideal case. The LOs at the receiver are locked to the incoming signal, as in any FDM transmission system. Without losing generality, the delays in the channel or in the receiver have not been included.

The real physical implementation using IQ mixers, as illustrated in Figure 5.7, includes extra phase shifts of 180 degrees in some of the LOs, but it can be readily seen that those shifts do not have any influence in the final results. Considering any phase shift between different pairs of baseband data, and any difference in the delay introduced by the IQ mixers at the different RF frequencies, orthogonal phase alignment can be accomplished by adjusting only the phase of the transmitting LOs. This ensures that there is a sampling point free of ISI and ICI in the received baseband signals. The required phase shifts in the transmitting LOs will be derived mathematically. In the derivation, a full roll-off $H_{SRRC}(\omega)$ extending till ω_r (β=1) is used.

C.2 Transmitted Spectrum

When a single pulse is transmitted, the spectrum of the generated signal, $S(\omega)$, is equal to the sum of the I and Q contributions in each frequency band, $S_{i,I}(\omega)$ and $S_{i,Q}(\omega)$. Considering the three orthogonal subchannels:

$$S(\omega)=S_{k-1,I}(\omega)+S_{k-1,Q}(\omega)+S_{k,I}(\omega)+S_{k,Q}(\omega)+S_{k+1,I}(\omega)+S_{k+1,Q}(\omega). \quad \text{(C.1)}$$

The individual contributions are:

$$S_{k-1,I}(\omega)=\frac{1}{2}\begin{bmatrix} H_{SRRC}(\omega-\omega_{k-1})\cdot e^{-j(\omega-\omega_{k-1})\left(\frac{T}{2}+dA_{k-1}\right)}\cdot e^{j\varphi_{k-1}}\cdot e^{-j\omega\cdot dB_{k-1}}+ \\ H_{SRRC}(\omega+\omega_{k-1})\cdot e^{-j(\omega+\omega_{k-1})\left(\frac{T}{2}+dA_{k-1}\right)}\cdot e^{-j\varphi_{k-1}}\cdot e^{-j\omega\cdot dB_{k-1}} \end{bmatrix}.$$

$$S_{k-1,Q}(\omega)=\frac{1}{2}\begin{bmatrix} H_{SRRC}(\omega-\omega_{k-1})\cdot e^{-j(\omega-\omega_{k-1})dA_{k-1}}\cdot e^{-j\frac{\pi}{2}}\cdot e^{j\varphi_{k-1}}\cdot e^{-j\omega\cdot dB_{k-1}}+ \\ H_{SRRC}(\omega+\omega_{k-1})\cdot e^{-j(\omega+\omega_{k-1})dA_{k-1}}\cdot e^{j\frac{\pi}{2}}\cdot e^{-j\varphi_{k-1}}\cdot e^{-j\omega\cdot dB_{k-1}} \end{bmatrix}. \quad \text{(C.2)}$$

$$S_{k,I}(\omega)=\frac{1}{2}\begin{bmatrix} H_{SRRC}(\omega-\omega_k)\cdot e^{-j(\omega-\omega_k)dA_k}\cdot e^{j\varphi_k}\cdot e^{-j\omega\cdot dB_k}+ \\ H_{SRRC}(\omega+\omega_k)\cdot e^{-j(\omega+\omega_k)dA_k}\cdot e^{-j\varphi_k}\cdot e^{-j\omega\cdot dB_k} \end{bmatrix}.$$

$$S_{k,Q}(\omega)=\frac{1}{2}\begin{bmatrix} H_{SRRC}(\omega-\omega_k)\cdot e^{-j(\omega-\omega_k)\left(\frac{T}{2}+dA_k\right)}\cdot e^{-j\frac{\pi}{2}}\cdot e^{j\varphi_k}\cdot e^{-j\omega\cdot dB_k}+ \\ H_{SRRC}(\omega+\omega_k)\cdot e^{-j(\omega+\omega_k)\left(\frac{T}{2}+dA_k\right)}\cdot e^{j\frac{\pi}{2}}\cdot e^{-j\varphi_k}\cdot e^{-j\omega\cdot dB_k} \end{bmatrix}. \quad \text{(C.3)}$$

$$S_{k+1,I}(\omega)=\frac{1}{2}\begin{bmatrix} H_{SRRC}(\omega-\omega_{k+1})\cdot e^{-j(\omega-\omega_{k+1})\left(\frac{T}{2}+dA_{k+1}\right)}\cdot e^{j\varphi_{k+1}}\cdot e^{-j\omega\cdot dB_{k+1}}+ \\ H_{SRRC}(\omega+\omega_{k+1})\cdot e^{-j(\omega+\omega_{k+1})\left(\frac{T}{2}+dA_{k+1}\right)}\cdot e^{-j\varphi_{k+1}}\cdot e^{-j\omega\cdot dB_{k+1}} \end{bmatrix}.$$

$$S_{k+1,Q}(\omega)=\frac{1}{2}\begin{bmatrix} H_{SRRC}(\omega-\omega_{k+1})\cdot e^{-j(\omega-\omega_{k+1})dA_{k+1}}\cdot e^{-j\frac{\pi}{2}}\cdot e^{j\varphi_{k+1}}\cdot e^{-j\omega\cdot dB_{k+1}}+ \\ H_{SRRC}(\omega+\omega_{k+1})\cdot e^{-j(\omega+\omega_{k+1})dA_{k+1}}\cdot e^{j\frac{\pi}{2}}\cdot e^{-j\varphi_{k+1}}\cdot e^{-j\omega\cdot dB_{k+1}} \end{bmatrix}. \quad \text{(C.4)}$$

C.3 Interference

Initially, the I component of the k^{th} subchannel is analysed. As matched $H_{SRRC}(\omega)$ filters are used in the transmitter and the receiver, ISI will be zero at:

$$t_{(ISI=0)k,I}=nT+dA_k+dB_k, \quad \text{(C.5)}$$

where n denotes the bit number.

C.3.1 Interaction with (k-1)th Subchannel

The ICI coming from the $(k\text{-}1)^{th}$ subchannel can be derived as follows. In the receiver, the interfering spectrum generated by the I component of the $(k\text{-}1)^{th}$ subchannel, over the I component of the k^{th} subchannel is:

$$R_{k,I}^{(k-1),I}(\omega)=\frac{1}{2}H_{SRRC}(\omega)\cdot \left[\begin{array}{c} H_{SRRC}(\omega-\omega_{k-1}+\omega_k)\cdot \\ e^{-j\left(\omega-\omega_{k-1}+\omega_k\right)\left(\frac{T}{2}+dA_{k-1}\right)}\cdot e^{j\varphi_{k-1}}\cdot e^{-j(\omega+\omega_k)dB_{k-1}}\cdot e^{-j\varphi_k}\cdot e^{j\omega_k dB_k} \\ + \\ H_{SRRC}(\omega+\omega_{k-1}-\omega_k)\cdot \\ e^{-j\left(\omega+\omega_{k-1}-\omega_k\right)\left(\frac{T}{2}+dA_{k-1}\right)}\cdot e^{-j\varphi_{k-1}}\cdot e^{-j(\omega-\omega_k)dB_{k-1}}\cdot e^{j\varphi_k}\cdot e^{-j\omega_k dB_k} \end{array}\right]. \quad \text{(C.6)}$$

Note that:

$$\omega_k-\omega_{k-1}=k\cdot\omega_r-(k-1)\omega_r=\omega_r=\frac{2\pi}{T}. \quad \text{(C.7)}$$

Therefore, eq. (C.6) can be written as:

$$R_{k,I}^{(k-1),I}(\omega)=$$
$$\frac{1}{2}H_{SRRC}(\omega)\left[H_{SRRC}\left(\omega-\frac{2\pi}{T}\right)e^{j\psi}+H_{SRRC}\left(\omega+\frac{2\pi}{T}\right)e^{-j\psi}\right]e^{j\omega\tau},$$
$$where: \quad \text{(C.8)}$$
$$\tau=-\frac{T}{2}-dA_{k-1}-dB_{k-1}.$$
$$\psi=\pi+\frac{2\pi}{T}dA_{k-1}-\varphi_{k-1}+\omega_k dB_{k-1}+\varphi_k-\omega_k dB_k.$$

The temporal contribution can be calculated as in section C.4.1. From eq. (C.32) it can be deduced that the ICI coming from the I component of the *(k-1)*th subchannel, over the I component of the k^{th} subchannel, cancels when:

$$t_{(ICI=0),k,I}^{(k-1),I}-dA_{k-1}-dB_{k-1}+\frac{T}{\pi}\left(\frac{2\pi}{T}dA_{k-1}-\varphi_{k-1}+\omega_k dB_{k-1}+\varphi_k-\omega_k dB_k\right)=nT. \quad \text{(C.9)}$$

Similarly, the interfering spectrum generated by the Q component of the *(k-1)*th subchannel, over the I component of the k^{th} subchannel is:

$$R_{k,I}^{(k-1),Q}(\omega)=\frac{1}{2}H_{SRRC}(\omega)\cdot \left[\begin{array}{c} H_{SRRC}(\omega-\omega_{k-1}+\omega_k)\cdot \\ e^{-j\left(\omega-\omega_{k-1}+\omega_k\right)dA_{k-1}}\cdot e^{-j\frac{\pi}{2}}\cdot e^{j\varphi_{k-1}}\cdot e^{-j(\omega+\omega_k)dB_{k-1}}\cdot e^{-j\varphi_k}\cdot e^{j\omega_k dB_k} \\ + \\ H_{SRRC}(\omega+\omega_{k-1}-\omega_k)\cdot \\ e^{-j\left(\omega+\omega_{k-1}-\omega_k\right)dA_{k-1}}\cdot e^{j\frac{\pi}{2}}\cdot e^{-j\varphi_{k-1}}\cdot e^{-j(\omega-\omega_k)dB_{k-1}}\cdot e^{j\varphi_k}\cdot e^{-j\omega_k dB_k} \end{array}\right]. \quad \text{(C.10)}$$

After some manipulation, the previous equation becomes:

$$R_{k,I}^{(k-1),Q}(\omega)=$$
$$-\frac{j}{2}H_{SRRC}(\omega)\left[H_{SRRC}\left(\omega+\frac{2\pi}{T}\right)e^{-j\psi}-H_{SRRC}\left(\omega-\frac{2\pi}{T}\right)e^{j\psi}\right]e^{j\omega\tau},$$
$$where: \quad \text{(C.11)}$$
$$\tau=-dA_{k-1}-dB_{k-1}.$$
$$\psi=\frac{2\pi}{T}dA_{k-1}-\varphi_{k-1}+\omega_k dB_{k-1}+\varphi_k-\omega_k dB_k.$$

The temporal contribution can be calculated as in section C.4.2. From eq. (C.38) it can be deduced that the ICI coming from the Q component of the *(k-1)*th subchannel, over the I component of the k^{th} subchannel, cancels when:

$$t_{(ICI=0),k,I}^{(k-1),Q}-dA_{k-1}-dB_{k-1}+\frac{T}{\pi}\left(\frac{2\pi}{T}dA_{k-1}-\varphi_{k-1}+\omega_k dB_{k-1}+\varphi_k-\omega_k dB_k\right)=nT. \quad \text{(C.12)}$$

As this is the same condition as that in eq. (C.9), it can be generalized that the ICI coming from the *(k-1)*th subchannel, over the I component of the k^{th} subchannel, cancels at:

$$t_{(ICI=0),k,I}^{(k-1)}=t_{(ICI=0),k,I}^{(k-1),I}=t_{(ICI=0),k,I}^{(k-1),Q}. \quad \text{(C.13)}$$

From eqs. (C.9) and (C.12), it becomes clear that varying the phase of the *(k-1)*th subcarrier φ_{k-1}, the sampling point at which the ICI is equal to zero moves. It must coincide with the sampling point free of ISI, from eq. (C.5), such that:

$$t_{(ICI=0),k,I}^{(k-1)} = t_{(ISI=0)k,I}. \tag{C.14}$$

Substituting, the desired value of φ_{k-1} is derived:

$$\varphi_{k-1} = \varphi_k + \frac{\pi}{T}(dA_{k-1} + dA_k + (2k-1)(dB_{k-1} - dB_k)). \tag{C.15}$$

With the previous value of phase, the ICI coming from the I component of the k^{th} subchannel, over the I and Q components of the *(k-1)*$^{\text{th}}$ subchannel, can also be analysed yielding the desired results, as it cancels at $t=(2n+1)(T/2)+dA_{k-1}+dB_{k-1}$ and $t=nT+dA_{k-1}+dB_{k-1}$ respectively.

C.3.2 Interaction with (k+1)th Subchannel

Similarly, in the receiver, the interfering spectrum generated by the I component of the *(k+1)*th subchannel, over the I component of the k^{th} subchannel is:

$$R_{k,I}^{(k+1),I}(\omega) = \frac{1}{2} H_{SRRC}(\omega) \cdot \left[\begin{array}{c} H_{SRRC}(\omega - \omega_{k+1} + \omega_k) \cdot \\ e^{-j(\omega-\omega_{k+1}+\omega_k)\left(\frac{T}{2}+dA_{k+1}\right)} \cdot e^{j\varphi_{k+1}} \cdot e^{-j(\omega+\omega_k)dB_{k+1}} \cdot e^{-j\varphi_k} \cdot e^{j\omega_k dB_k} \\ + \\ H_{SRRC}(\omega + \omega_{k+1} - \omega_k) \cdot \\ e^{-j(\omega+\omega_{k+1}-\omega_k)\left(\frac{T}{2}+dA_{k+1}\right)} \cdot e^{-j\varphi_{k+1}} \cdot e^{-j(\omega-\omega_k)dB_{k+1}} \cdot e^{j\varphi_k} \cdot e^{-j\omega_k dB_k} \end{array} \right]. \tag{C.16}$$

Note that:

$$\omega_{k+1} - \omega_k = (k+1)\omega_r - k \cdot \omega_r = \omega_r = \frac{2\pi}{T}. \tag{C.17}$$

Therefore, eq. (C.16) can be written as:

$$R_{k,I}^{(k+1),I}(\omega) = \frac{1}{2}H_{SRRC}(\omega)\left[H_{SRRC}\left(\omega-\frac{2\pi}{T}\right)e^{j\psi}+H_{SRRC}\left(\omega+\frac{2\pi}{T}\right)e^{-j\psi}\right]e^{j\omega\tau},$$
$$where: \quad \tau = -\frac{T}{2}-dA_{k-1}-dB_{k-1}. \quad \psi = \pi+\frac{2\pi}{T}dA_{k-1}+\varphi_{k+1}-\omega_k dB_{k+1}-\varphi_k+\omega_k dB_k. \quad (C.18)$$

The temporal contribution can be calculated as in section C.4.1. From eq. (C.32) it can be deduced that the ICI coming from the I component of the $(k+1)^{th}$ subchannel, over the I component of the k^{th} subchannel, cancels when:

$$t_{(ICI=0),k,I}^{(k+1),I}-dA_{k+1}-dB_{k+1}+\frac{T}{\pi}\left(\frac{2\pi}{T}dA_{k+1}+\varphi_{k+1}-\omega_k dB_{k+1}-\varphi_k+\omega_k dB_k\right)=nT. \quad (C.19)$$

Similarly, the interfering spectrum generated by the Q component of the $(k+1)^{th}$ subchannel, over the I component of the k^{th} subchannel is:

$$R_{k,I}^{(k+1),Q}(\omega)=\frac{1}{2}H_{SRRC}(\omega)\cdot \left[\begin{array}{c} H_{SRRC}(\omega-\omega_{k+1}+\omega_k)\cdot \\ e^{-j(\omega-\omega_{k+1}+\omega_k)dA_{k+1}}\cdot e^{-j\frac{\pi}{2}}\cdot e^{j\varphi_{k+1}}\cdot e^{-j(\omega+\omega_k)dB_{k+1}}\cdot e^{-j\varphi_k}\cdot e^{j\omega_k dB_k} \\ + \\ H_{SRRC}(\omega+\omega_{k+1}-\omega_k)\cdot \\ e^{-j(\omega+\omega_{k+1}-\omega_k)dA_{k+1}}\cdot e^{j\frac{\pi}{2}}\cdot e^{-j\varphi_{k+1}}\cdot e^{-j(\omega-\omega_k)dB_{k+1}}\cdot e^{j\varphi_k}\cdot e^{-j\omega_k dB_k} \end{array}\right]. \quad (C.20)$$

After some manipulation, the previous equation becomes:

$$R_{k,I}^{(k+1),Q}(\omega) =$$
$$\frac{j}{2}H_{SRRC}(\omega)\left[H_{SRRC}\left(\omega+\frac{2\pi}{T}\right)e^{-j\psi}-H_{SRRC}\left(\omega-\frac{2\pi}{T}\right)e^{j\psi}\right]e^{j\omega\tau},$$
$$where: \quad \text{(C.21)}$$
$$\tau = -dA_{k+1} - dB_{k+1}.$$
$$\psi = \frac{2\pi}{T}dA_{k+1} + \varphi_{k+1} - \omega_k dB_{k+1} - \varphi_k + \omega_k dB_k.$$

The temporal contribution can be calculated as in section C.4.2. From eq. (C.38) it can be deduced that the ICI coming from the Q component of the $(k+1)^{th}$ subchannel, over the I component of the k^{th} subchannel, cancels when:

$$t_{(ICI=0),k,I}^{(k+1),Q} - dA_{k+1} - dB_{k+1} + \frac{T}{\pi}\left(\frac{2\pi}{T}dA_{k+1} + \varphi_{k+1} - \omega_k dB_{k+1} - \varphi_k + \omega_k dB_k\right) = nT. \quad \text{(C.22)}$$

As this is the same condition as that in eq. (C.19), it can be generalized that the ICI coming from the $(k+1)^{th}$ subchannel, over the I component of the k^{th} subchannel, cancels at:

$$t_{(ICI=0),k,I}^{(k+1)} = t_{(ICI=0),k,I}^{(k+1),I} = t_{(ICI=0),k,I}^{(k+1),Q}. \quad \text{(C.23)}$$

From eqs. (C.19) and (C.22), it becomes clear that varying the phase of the $(k+1)^{th}$ subcarrier φ_{k+1}, the sampling point at which the ICI is equal to zero moves. It must coincide with the sampling point free of ISI, from eq. (C.5), such that:

$$t_{(ICI=0),k,I}^{(k+1)} = t_{(ISI=0)k,I}. \quad \text{(C.24)}$$

Substituting, the desired value of φ_{k+1} is derived:

$$\varphi_{k+1} = \varphi_k + \frac{\pi}{T}(-dA_{k+1} - dA_k + (2k+1)(dB_{k+1} - dB_k)). \quad \text{(C.25)}$$

With the previous value of phase, the ICI coming from the I component of the k^{th} subchannel, over the I and Q components of the $(k+1)^{th}$ subchannel, can also be

analysed yielding the desired results, as it cancels at $t=(2n+1)(T/2)+dA_{k+1}+dB_{k+1}$ and $t=nT+dA_{k+1}+dB_{k+1}$ respectively.

Due to the symmetry of the system, the same values of φ_{k-1} and φ_{k+1} are obtained if the Q component of the k^{th} subchannel is analysed. The functionality of these values was verified by simulation.

C.4 Temporal Solutions

During the mathematical developments described above, two generic spectra are obtained. This subsection shows the temporal signals associated with the spectra and their resolution.

C.4.1 Case 1

For a spectrum defined with the following equation:

$$R(\omega)=\frac{1}{2}F(\omega)\left[F\left(\omega-\frac{2\pi}{T}\right)e^{j\psi}+F\left(\omega+\frac{2\pi}{T}\right)e^{-j\psi}\right]e^{j\omega\tau}, \qquad \text{(C.26)}$$

where $F(\omega)$ is an even function defined in the range (-2π/T, 2π/T), equivalent to an $H_{SRRC}(\omega)$ (see Figure 5.3).

The associated temporal signal is given by:

$$\begin{aligned} r(t)=\frac{1}{2\pi}\int_{-\frac{2\pi}{T}}^{\frac{2\pi}{T}} R(\omega)\cdot e^{j\omega t}\cdot d\omega = \\ \frac{1}{2\pi}\int_{0}^{\frac{2\pi}{T}}\frac{1}{2}F(\omega)\cdot F\left(\omega-\frac{2\pi}{T}\right)\cdot\cos\left(\omega(t+\tau)+\psi\right)\cdot d\omega+ \\ \frac{1}{2\pi}\int_{-\frac{2\pi}{T}}^{0}\frac{1}{2}F(\omega)\cdot F\left(\omega+\frac{2\pi}{T}\right)\cdot\cos\left(\omega(t+\tau)-\psi\right)\cdot d\omega+ \\ \frac{j}{2\pi}\int_{0}^{\frac{2\pi}{T}}\frac{1}{2}F(\omega)\cdot F\left(\omega-\frac{2\pi}{T}\right)\cdot\sin\left(\omega(t+\tau)+\psi\right)\cdot d\omega+ \\ \frac{j}{2\pi}\int_{-\frac{2\pi}{T}}^{0}\frac{1}{2}F(\omega)\cdot F\left(\omega+\frac{2\pi}{T}\right)\cdot\sin\left(\omega(t+\tau)-\psi\right)\cdot d\omega. \end{aligned} \qquad \text{(C.27)}$$

As *F(ω)* is an even function, the two first terms in the equation are equal, while the sum of the third term and the fourth term cancels. The previous statement is illustrated below showing an example of the shape of the functions:

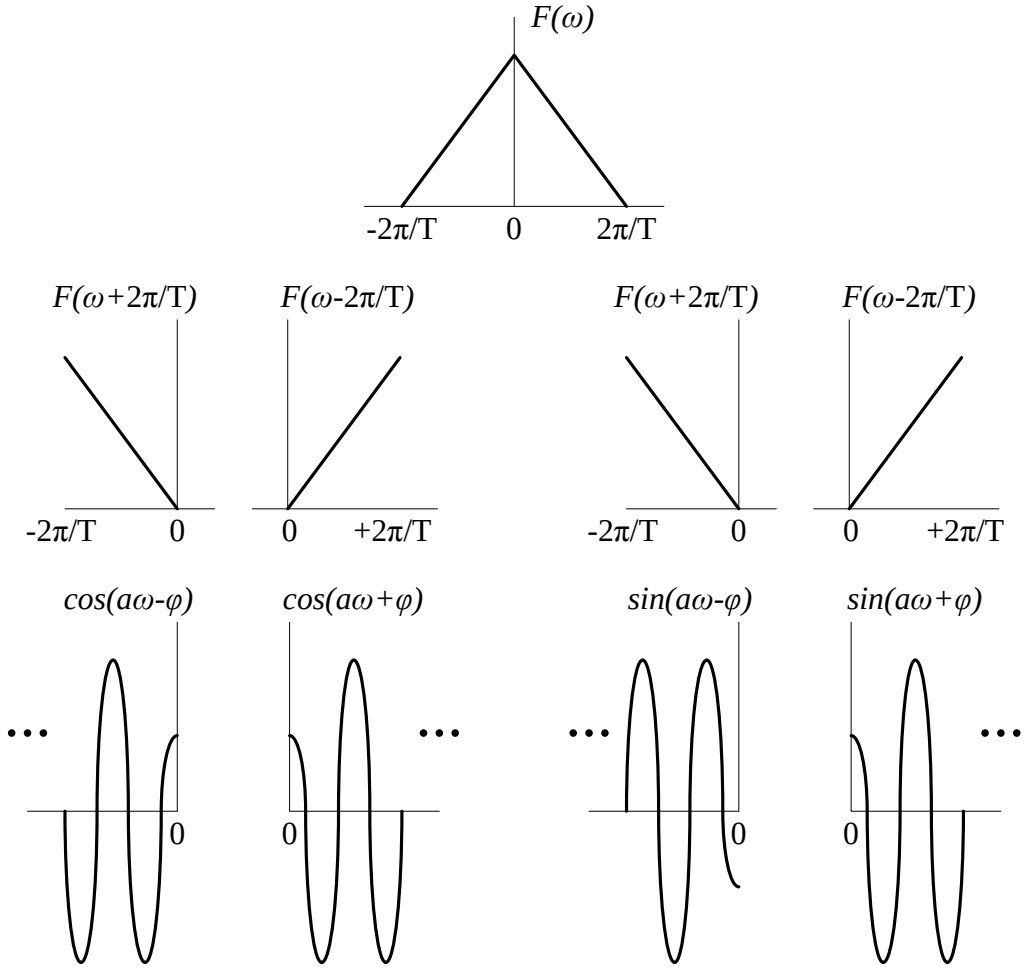

As a result, eq. (C.27) becomes:

$$r(t)=\frac{1}{2\pi}\int_{0}^{\frac{2\pi}{T}} F(\omega)\cdot F\left(\omega-\frac{2\pi}{T}\right)\cdot\cos\left(\omega(t+\tau)+\psi\right)\cdot d\omega. \qquad \text{(C.28)}$$

With a change of variable $u = \omega - \pi/T$:

$$r(t)=\frac{1}{2\pi}\int_{-\frac{\pi}{T}}^{\frac{\pi}{T}} F\left(u+\frac{\pi}{T}\right)\cdot F\left(u-\frac{\pi}{T}\right)\cdot\cos\left(\left(u+\frac{\pi}{T}\right)(t+\tau)+\psi\right)\cdot du. \qquad \text{(C.29)}$$

After some manipulations:

$$r(t)=\frac{1}{2\pi}\int_{-\frac{\pi}{T}}^{\frac{\pi}{T}} F\left(u+\frac{\pi}{T}\right)\cdot F\left(u-\frac{\pi}{T}\right)\cdot\cos\left(u(t+\tau)+\frac{\pi}{T}\left(t+\tau+\psi\frac{T}{\pi}\right)\right)\cdot du. \qquad \text{(C.30)}$$

When the integrand of the previous equation is an odd function, *r(t)* cancels, as it can be deduced from the following picture:

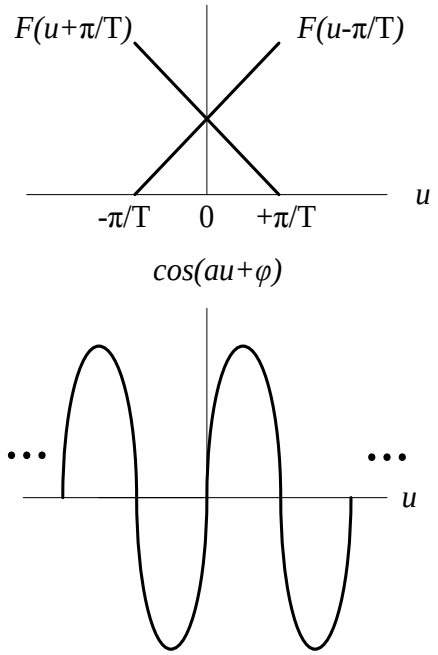

Hence, from eq. (C.30), *r(t)*=0 when:

$$\frac{\pi}{T}\left(t+\tau+\psi\frac{T}{\pi}\right)=(2n+1)\frac{\pi}{2}\rightarrow t+\tau+\psi\frac{T}{\pi}=(2n+1)\frac{T}{2}. \qquad \text{(C.31)}$$

Note that if τ can be expressed in the form $\tau=\pm\frac{T}{2}+\tau'$, the previous condition becomes:

$$t+\tau'+\psi\frac{T}{\pi}=nT. \qquad \text{(C.32)}$$

C.4.2 Case 2

For a spectrum defined with the following equation:

$$R(\omega)=\frac{j}{2}F(\omega)\left[F\left(\omega+\frac{2\pi}{T}\right)e^{-j\psi}-F\left(\omega-\frac{2\pi}{T}\right)e^{j\psi}\right]e^{j\omega\tau}, \qquad \text{(C.33)}$$

where $F(\omega)$ is an even function defined in the range (-2π/T, 2π/T), equivalent to an $H_{SRRC}(\omega)$ (see Figure 5.3).

The associated temporal signal is given by:

$$\begin{aligned} r(t)=\frac{1}{2\pi}\int_{-\frac{2\pi}{T}}^{\frac{2\pi}{T}} R(\omega)\cdot e^{j\omega t}\cdot d\omega = \\ -\frac{j}{2\pi}\int_{0}^{\frac{2\pi}{T}}\frac{1}{2}F(\omega)\cdot F\left(\omega-\frac{2\pi}{T}\right)\cdot\cos\left(\omega(t+\tau)+\psi\right)\cdot d\omega+ \\ \frac{j}{2\pi}\int_{-\frac{2\pi}{T}}^{0}\frac{1}{2}F(\omega)\cdot F\left(\omega+\frac{2\pi}{T}\right)\cdot\cos\left(\omega(t+\tau)-\psi\right)\cdot d\omega+ \\ -\frac{j\cdot j}{2\pi}\int_{0}^{\frac{2\pi}{T}}\frac{1}{2}F(\omega)\cdot F\left(\omega-\frac{2\pi}{T}\right)\cdot\sin\left(\omega(t+\tau)+\psi\right)\cdot d\omega+ \\ \frac{j\cdot j}{2\pi}\int_{-\frac{2\pi}{T}}^{0}\frac{1}{2}F(\omega)\cdot F\left(\omega+\frac{2\pi}{T}\right)\cdot\sin\left(\omega(t+\tau)-\psi\right)\cdot d\omega. \end{aligned} \qquad \text{(C.34)}$$

As $F(\omega)$ is an even function, the two first terms in the equation cancel, while the third and fourth terms are equal. As a result, the previous equation can be expressed as:

$$r(t)=\frac{1}{2\pi}\int_{0}^{\frac{2\pi}{T}}F(\omega)\cdot F\left(\omega-\frac{2\pi}{T}\right)\cdot\sin\left(\omega(t+\tau)+\psi\right)\cdot d\omega. \qquad \text{(C.35)}$$

With a change of variable $u = \omega - \pi/T$:

$$r(t)=\frac{1}{2\pi}\int_{-\frac{\pi}{T}}^{\frac{\pi}{T}} F\left(u+\frac{\pi}{T}\right)\cdot F\left(u-\frac{\pi}{T}\right)\cdot\sin\left(\left(u+\frac{\pi}{T}\right)(t+\tau)+\psi\right)\cdot du. \qquad \text{(C.36)}$$

After some manipulations:

$$r(t)=\frac{1}{2\pi}\int_{-\frac{\pi}{T}}^{\frac{\pi}{T}} F\left(u+\frac{\pi}{T}\right)\cdot F\left(u-\frac{\pi}{T}\right)\cdot\sin\left(u(t+\tau)+\frac{\pi}{T}\left(t+\tau+\psi\frac{T}{\pi}\right)\right)\cdot du. \qquad \text{(C.37)}$$

When the integrand of the previous equation is an odd function, *r(t)* cancels. This happens when:

$$\frac{\pi}{T}\left(t+\tau+\psi\frac{T}{\pi}\right)=n\pi\rightarrow t+\tau+\psi\frac{T}{\pi}=nT. \qquad \text{(C.38)}$$

Note that if τ can be expressed in the form $\tau=\pm\frac{T}{2}+\tau'$, the previous condition becomes:

$$t+\tau'+\psi\frac{T}{\pi}=(2n+1)\frac{T}{2}. \qquad \text{(C.39)}$$

C.5 Conclusions

It can be concluded that, aligning only the T/2 shift inside every baseband pair, any number of practical subchannels can be orthogonally aggregated by adjusting the phase shift of every new transmitting LO. This phase moves the time at which the new ICI over the baseband components transmitted in the neighbouring subchannels is cancelled, until it coincides with the sampling point, where ISI is also zero. Knowing all the delays of the components, the required phase shifts can be directly introduced in the tracks of a hypothetical integrated circuit or printed circuit board.

C.6 References

[1] B. Saltzberg, "Performance of an Efficient Parallel Data Transmission System," IEEE Transactions on Communication Technology, vol. 15, pp. 805-811, 1967.

Appendix D
List of Publications

The following is the list of publications arising from this work:

- F. A. Gutiérrez, P. Perry, F. Smyth, A. D. Ellis and L. P. Barry, "Optimum Bias Point in Broadband Subcarrier Multiplexing With Optical IQ Modulators," in Journal of Lightwave Technology, vol. 33, no. 1, pp. 258-266, January 2015.

- F. A. Gutiérrez, P. Perry, F. Smyth, A. D. Ellis and L. P. Barry, "Impact of band rejection in multichannel broadband subcarrier multiplexing," in IEEE/OSA Journal of Optical Communications and Networking, vol. 7, no. 4, pp. 248-252, April 2015.

- F. A. Gutiérrez, E. P. Martin, P. Perry, A. D. Ellis, P. Anandarajah, F. Smyth, and L. P. Barry, "100 Gbit/s real-time all-analogue filter bank OFDM based on a gain-switched optical comb," European Conference on Optical Communication (ECOC), Valencia, October 2015.

- F. A. Gutiérrez, P. Perry, E. P. Martin, A. D. Ellis, F. Smyth and L. P. Barry, "All-Analogue Real-Time Broadband Filter Bank Multicarrier Optical Communications System," in Journal of Lightwave Technology, vol. 33, no. 24, pp. 5073-5083, December 2015.

- F. A. Gutiérrez, E. P. Martin, P. Perry, A. D. Ellis, and L. Barry, "All-Analogue Real-Time Filter Bank OFDM over 50 Km of SSMF using a Novel Synchronization Technique," in Optical Fiber Communication Conference (OFC), Anaheim, March 2016, paper W1G.7.

- F. A. Gutiérrez, E. P. Martin, P. Perry, A. D. Ellis, P. M. Anandarajah and L. P. Barry, "WDM Orthogonal Subcarrier Multiplexing," in Journal of Lightwave Technology, vol. 34, no. 8, pp. 1815-1823, April 2016 (Invited).

- F. A. Gutiérrez, E. P. Martin, P. Perry, A. D. Ellis, A. Anthur, V. Panapakkam, Q. Gaimard, K. Merghem, F. Lelarge, A. Ramdane and L. P. Barry, " 400 Gbit/s Real-Time All-Analogue FBMC/OFDM based on a Mode Locked Laser," European Conference on Optical Communication (ECOC), Dusseldorf, September 2016.